

การเกิดของเนินทรายบริเวณอ่าวบางเบิด ตำบลปากคลอง อำเภอปะทิว จังหวัดชุมพร



นางสาววีรยา เลิศนอก

ศูนย์วิทยทรัพยากร

วิทยานิพนธ์นี้เป็นส่วนหนึ่งของการศึกษาตามหลักสูตรปริญญาวิทยาศาสตรมหาบัณฑิต

สาขาวิชาธรณีวิทยา ภาควิชาธรณีวิทยา

คณะวิทยาศาสตร์ จุฬาลงกรณ์มหาวิทยาลัย

ปีการศึกษา 2552

ลิขสิทธิ์ของจุฬาลงกรณ์มหาวิทยาลัย

FORMATION OF SAND DUNE AT AO BANG BERD, TAMBON PAKKHLONG,
AMPHOE PATHIO, CHANGWAT CHUMPHON



Miss Weeraya Lertnok

A Thesis Submitted in Partial Fulfillment of the Requirements
for the Degree of Master of Science Program in Geology

Department of Geology

Faculty of Science

Chulalongkorn University

Academic Year 2009

Copyright of Chulalongkorn University

Thesis Title FORMATION OF SAND DUNE AT AO BANG BERD,
TAMBON PAKKHLONG, AMPHOE PATHIO,
CHANGWAT CHUMPHON


By Miss Weeraya Lertnok

Field of Study Geology


Thesis Advisor Associate Professor Montri Choowong, Ph.D.

Thesis Co-Advisor Thanop Thitimakorn, Ph.D.


Accepted by the Faculty of Science, Chulalongkorn University in Partial
Fulfillment of the requirements for the Master's Degree


 Dean of the Faculty of Science
(Professor Supot Hannongbua, Dr.rer.nat)


THESIS EXAMINER

 Chairman
(Assistant Professor Thasinee Charoentitirat, Ph.D.)

 Thesis Advisor
(Associate Professor Montri Choowong, Ph.D.)

 Thesis Co-Advisor
(Thanop Thitimakorn, Ph.D.)

 Examiner
(Vichai Chutakositkanon, Ph.D.)

 External Examiner
(Assanee Meesook, Ph.D.)

วิชา เลิศนอก : การเกิดของเนินทรายบริเวณอ่าวบางเบิด ตำบลปากคลอง อำเภอปะทิว จังหวัดชุมพร. (FORMATION OF SAND DUNE AT AO BANG BERD, TAMBOL PAKKHLONG, AMPHOE PATHIO, CHANGWAT CHUMPHON) อ. ที่ปรึกษา
 วิทยานิพนธ์หลัก : รองศาสตราจารย์ ดร.มนตรี ชูวงศ์, อ. ที่ปรึกษาวิทยานิพนธ์ร่วม :
 อาจารย์ ดร.ฐานภ ธิติมากร, 169 หน้า.

สันทรายบางเบิดทอดตัวเป็นแนวยาวขนานกับแนวหาด โดยมีความสูงจากระดับน้ำทะเลปานกลางประมาณ 20 เมตร ในการศึกษาครั้งนี้มีวัตถุประสงค์เพื่อศึกษาลักษณะพื้นฐานและลักษณะตะกอนวิทยาของสันทราย เพื่ออธิบายการเกิดของสันทรายในบริเวณนี้

ผลจากการแปลภาพถ่ายทางอากาศ พบว่า สันทรายในบริเวณนี้ส่วนใหญ่มีลักษณะเป็นรูปพาราโบลา (parabola dune) และสันเนินทรายแนวโค้ง (transverse dune) พบสันทรายรูปดาว (star dune) บ้างเล็กน้อย รูปทรงของสันทรายสามารถบ่งชี้ทิศทางลมว่าส่วนใหญ่พัดจากทิศตะวันออกเฉียงใต้มาทางทิศตะวันตก เม็ดทรายที่ก่อตัวเป็นสันทรายมีขนาดละเอียดถึงปานกลาง พบโครงสร้างขนาดเล็กในชั้นตะกอนบ้าง เมื่อตัดหน้าตัดของสันทรายเพื่อศึกษาลักษณะทางตะกอนวิทยา แต่ไม่มากนัก อย่างไรก็ตาม ผลการสำรวจด้วยเครื่องหยั่งธรณีฟิสิกส์ด้วยเรดาร์ (Ground Penetrating Radar, GPR) พบลักษณะของโครงสร้างของตะกอนที่แสดงขอบเขตการสะสมตัวของสันทรายที่ปิดทับอยู่บนการสะสมตัวของแนวชายหาด ผลจากการสำรวจ GPR สามารถแบ่งสภาพแวดล้อมในการสะสมตัวของตะกอนในบริเวณนี้ได้เป็นการสะสมตัวของสันทราย (การสะสมตัวของสันทรายชายหาด (D1) และการสะสมตัวของสันทรายบริเวณกว้าง (D2)) การสะสมตัวโดยทะเล (การพอกสะสมตัว (B1) และการสะสมตัวโดยทะเลบริเวณชายหาด (B2)) และลักษณะของคลองที่ตัดเข้ามาชั้นตะกอนที่สะสมตัวโดยทะเล จากลักษณะของโครงสร้างที่พบและลักษณะของสันทราย บ่งชี้ว่าทิศทางการพัดพาของลมมีทิศทางหลักพัดพาจากทางด้านตะวันออกเฉียงใต้มาสะสมตัวทางด้านตะวันตกของพื้นที่ ซึ่งผลจากการสำรวจ GPR นับว่าสัมพันธ์กับลักษณะพื้นฐานของสันทรายและผลจากการแปลภาพถ่ายทางอากาศ

จากลักษณะธรณีฐานวิทยา ธรณีวิทยา และลักษณะของตะกอนทรายของสันทราย บ่งชี้ว่าตะกอนทรายที่มาสะสมตัวเป็นสันทรายในบริเวณนี้น่าจะมาจากหินตะกอนที่พบเป็นพื้นที่สูงทางด้านตะวันตกและทางทิศเหนือของพื้นที่ ผลจากระดับน้ำทะเลที่รูก้าขึ้นมาในช่วงต้นของยุคโฮโลซีน ทำให้หินผุพังได้ง่ายและมีการพัดพาสะสมตัวเป็นตะกอนน้ำพามาสะสมตัวในทะเลตลอดแนวชายฝั่ง หลังจากนั้นตะกอนน้ำพามาที่จมตัวจึงถูกพัดพาขึ้นมาสะสมตัวเป็นสันทรายในช่วงตอนกลางของยุคโฮโลซีนที่มีสภาพแวดล้อมอากาศแห้งแล้ง จากผลการหาอายุด้วยวิธี OSL พบว่าการสะสมตัวของสันทรายเกิดขึ้นอย่างต่อเนื่องมาจนถึงช่วงปลายของยุคโฮโลซีน

ภาควิชา ธรณีวิทยา

ลายมือชื่อนิติศ

สาขาวิชา ธรณีวิทยา

ลายมือชื่อ อ.ที่ปรึกษาวิทยานิพนธ์หลัก

ปีการศึกษา 2552

ลายมือชื่อ อ.ที่ปรึกษาวิทยานิพนธ์ร่วม

4972490623 : MAJOR GEOLOGY

KEYWORDS : COASTAL DUNE / DUNE FORMATION / HOLOCENE / GPR

WEERAYA LERTNOK : FORMATION OF SAND DUNE AT AO BANG BERD,
TAMBON PAKKHLONG, AMPHOE PATHIO, CHANGWAT CHUMPHON.
THESIS ADVISOR : ASSOC. PROF. MONTRI CHOOWONG, Ph.D., THESIS
CO-ADVISOR : THANOP THITIMAKORN, Ph.D, 169 pp.

At Bang Berd Bay, a remarkable wind blown sand dune lies almost parallel to the present coastline with its highest elevation about 20 m above the present mean sea level. This study is aimed to characterize sand dune morphology and sedimentology for explaining its formation.

As a result from aerial photograph interpretation, dune morphology shows a majority of parabolic and transverse pattern; whereas star shapes were rarely and locally recognized. Most of dune shapes indicated the direction of wind blown mainly from the east to the west. Dune texture is very homogenous and characterized by fine- to medium-grained sand mainly. Very rare micro-scale sedimentary structures have been observed from dune profiles. However, result from Ground Penetrating Radar (GPR) showed some obvious macro-scale sedimentary patterns, clear boundary of dune and the underlain prograded beach ridge plain. Reflecting configuration from GPR divided the depositional environment in this area into dune deposition (coastal sand dune (D1), cover sand (D2), marine deposition (beach ridge (B1), littoral deposits (B2) and channel filled (C). Based on macro-scale sedimentary patterns, lee and stoss angles of some burial dunes ascribed mainly major directions of wind from the east to the west. This result in analyzing wind direction based on GPR signals is corresponded well with dune morphology interpreted from aerial photographs.

According to the morphology, geology and texture of dune, the possible sources of sand supply are thought to come from the sedimentary rocks formed as highland locating at the western part of the area. These rocks were eroded and transported to deposit and formed as alluvium substrate throughout the offshore during the early-Holocene transgression. The majority of dune started to deposit during dry condition of the middle Holocene and continued its formation to the late Holocene based on OSL datings.

Department : Geology

Field of Study : Geology

Academic Year : 2009

Student's Signature *W. Lertnok*

Advisor's Signature *M. Choowong*

Co-Advisor's Signature *T.F.*

ACKNOWLEDGEMENTS

The author would like to thank Associate Professor Dr. Montri Choowong, advisor and Dr. Thanop Thitimakorn, co-advisor for their advices. Thanks also extend to the Department of Mineral Resources for providing geological data, maps, aerial photographs and GPR instrument. Staffs from the Department of Mineral Resources are thanked for field assistance.

Special appreciation is given to Dr. Vichai Chutakositkanon, Assistant Professor Dr. Thasinee Charoentitirat and Mr. Akkaneewut Chabangbon for their helps and constructive suggestions in collecting samples in the field. Dr. Santi Pailoplee is thanked for OSL dating.

This research was partially funded from the Thailand Research Fund (TRF) through Dr. Montri Choowong. Special thanks go to Dr. Assanee Meesook, thesis committee who gave valuable suggestions of the thesis.



ศูนย์วิทยทรัพยากร
จุฬาลงกรณ์มหาวิทยาลัย

CONTENTS

	Page
Abstract (Thai).....	IV
Abstract (English).....	V
Acknowledgements.....	VI
Contents.....	VII
List of Figures.....	IX
List of Tables.....	XV
CHAPTER	
I Introduction.....	1
1.1 General statement.....	1
1.2 Objectives.....	1
1.3 Scope of work.....	2
1.4 Location and accessibility.....	3
1.5 Previous work.....	4
1.6 Theoretical background.....	9
1.7 Background of study area.....	15
II Regional setting.....	16
2.1 General Geology.....	16
2.2 Structural Geology.....	16
2.3 Geomorphology of the study area.....	19
2.4 Stratigraphy.....	19
III Methodology.....	26
3.1 Office work.....	27
3.2 Field investigation.....	29
3.3 Laboratory analysis.....	32
3.4 Discussion and conclusion.....	39

CHAPTER	Page
IV	Result of study..... 44
	4.1 Arial photo interpretation 44
	4.2 Topography survey..... 47
	4.3 Ground penetrating radar survey..... 47
	4.4 Sedimentary structure..... 75
	4.5 Grain size analysis..... 75
	4.6 Optically stimulated luminescence..... 79
V	Discussion and conclusion..... 80
	5.1 Discussion..... 80
	5.2 Conclusion..... 95
	REFERENCE..... 97
	APPENDICES..... 106
	APPENDIX A (Location of Ground penetrating survey)..... 107
	APPENDIX B (Grain size analysis)..... 119
	APPENDIX C (Petrology)..... 163
	APPENDIX D (Rare earth element analysis, REE)..... 166
	APPENDIX E (Frequency distribution plot of the wind direction between 1981-2009)..... 167
	BIOGRAPHY..... 169

ศูนย์วิทยทรัพยากร
 จุฬาลงกรณ์มหาวิทยาลัย

LIST OF FIGURES

Figure	Page
1.1 Distribution of wind-blown sand dune in the western coastal plain of the Gulf of Thailand at Khao Tao, Prachuap Khiri Khan (top), Bang Berd, Chumphon (middle) and Thepha, Songkhla (bottom).....	2
1.2 The study area is located at Ban Bang Berd, Amphoe Pathio, Changwat Chumphon, in the western coast of the Gulf of Thailand.....	3
1.3 The three basic modes of sand movement by wind. Grains in saltation bounce across the desert. Surface creep is the jerky forward movement of the larger grains impacted by saltating grains. The finest grains of silt and dust travel in suspension and are commonly removed from a basin over time, unless trapped in sheltered zones within the dunefield and buried by dune advance or other processes (Available from: http://www.guaddunes.com).....	10
1.4 Relation between wind-velocity, friction velocity, grain size and various eolian transport modes for homogeneous groups of spherical quartz grains (Eisma, 1965).....	11
1.5 Dune growth and movement are the result of sand flow on and around during periods when the wind is strong enough to move sand (about 15 km/hr) (Available from: http://www.indiana.edu).....	12
1.6 Classifies individual dunes in terms of the number and position of slip-faces, under the assumption that the number of slip-faces corresponds to the number of dominant wind directions in the local wind regime. (A-D available from: http://www.indiana.edu.com , E available from: http://cartage.org and, F available from: http://digital-desert.com).....	14
1.7 Main factors control dune type.....	14
2.1 Geological map at the western coastal plain of the Gulf of Thailand (modified after Suphawadee Vimuktanandana, Assanee Meesook and Suvapak Imsamut., 2007) (see explanation on the next page). The study area, Bang Berd sand dune is located in blue inset.....	17

Figure	Page
2.2 Photograph showing highland in the southern part of the study area and beach sand in the eastern part.....	20
2.3 Massive limestone, locally chert nodules at Khao Berd, northern part of the study area.....	21
2.4 The red bed cliff near the coast in the northern part of the study area. Rocks are composed of basal conglomerate, pebbles of limestone, subangular to angular, sandstone and quartz, sub-rounded to rounded with calcareous matrix and cement.....	22
2.5 Reddish brown sandstone interbedded with conglomerate at highway no.3114, northern part of the study area.....	23
2.6 Rock fragments of quartzite, sandstone, siltstone, granite, sand and silt matrixes of colluvial and residual deposits in the northern part of the study area.....	24
2.7 Yellowish brown sand of old beach ridge deposit occurs beside beach deposits. Sand's color represents oxidation, distinction with present beach deposits.....	25
2.8 Beach sediments of sand, gravel and fragment of mollusk are deposited in the northern part of the study area.....	25
3.1 Flow chart showing the methodology in this study.....	27
3.2 Aerial photograph covering the study area.....	28
3.3 Topographic survey for profiling dune morphology along GPR lines.....	29
3.4 Application of ground penetrating radar consists of transmitter antenna and receiver antenna. Where the transmitter antenna generates an EM pulse that travels into the subsurface and then reflect off an interface or scatters off point sources, where it is recorded by receiver antenna (Available from: http://www.emrl.byu.edu).....	31
3.5 GPR model SIR 2000 of DMR used to study subsurface structure of dune with transmitter antenna 200 MHz and depth of penetration is 5 m.....	32

Figure	Page
3.6 Methodology used to collect sample for analysis grain size to define environment deposits, by pitting and auguring.....	33
3.7 Methodology used to collect sample for define absolute age by optically stimulated luminescence (OSL) dating. Collecting the samples from the top of profile dune is every 0.15 m.....	33
3.8 Example of graphs to shows distribution of grain size.....	29
3.9 Graphs show plot of standard deviation & skewness of grain size distribution to analyzed environment deposition (after Pettijohn, 1975).....	35
3.10 Generalized processes that produce the luminescence signal (steps 1 and 2), and the sampling and analytical procedure to determine the age of deposition (steps 3 through 6) (Available from: http://core.ecu.edu).....	36
3.11 Equipment that comprises the “reader”, which is necessary for measuring the paleodose, irradiating the sample, heating the sample, and deriving a “growth” curve (from Lian, 2007) (Available from: http://core.ecu.edu).....	38
3.12 Terminology to define and describe radar surfaces, radar packages and radar facies (Neal, 2004).....	41
3.13 Radar facies chart of characteristic reflection patterns from various sedimentary environments (Overmeeren, 1998).....	42
3.14 Radar facies chart of characteristic reflection patterns from various sedimentary environments (Overmeeren, 1998).....	42
4.1 Geomorphological units in this area overlain on aerial photograph (details in text).....	45
4.2 Patterns of sand dune with their distributions, parabolic shape dominates in the outer part of dune field close to shore; star pattern is locally recognized in the southern portion and transverse morphology is localized in the western end of dune field. The major direction of wind blown was from the east to the west.....	48

Figure	Page
4.3 Topographic profiles of dune field in the outer part of dune field close to shore at different portions. The highest elevation of dune crest is recognized at line E with about 25 m above the present mean sea level, southern part of dune field.....	49
4.4 Parabolic shape dominates in the outer part of dune field close to shore, transverse morphology is localized in the western end of dune field; star pattern is locally recognized in the southern portion.....	50
4.5 GPR lines survey was conducted along – transects oriented parallel to the prevailing wind are labeled as GPR 4, GPR 5, GPR 7, GPR 9, GPR 10, GPR 11, and GPR 12 perpendicular to the prevailing wind, on the top of dune are labeled GPR 3, GPR 6, GPR 8, GPR 13, and GPR.....	51
4.6 Processed GPR profile in E-W direction, the characteristic reflection patterns of radar signal related to eolian deposits on top (reflection continuous and horizontal or slightly undulating), marine deposits on bottom (reflection oblique dipping seaward of beach ridge), and channel fill is overlain by beach ridge (reflection trough).....	52
4.7 Characteristic reflection patterns of eolian environment can be divided into 2 units as the coastal sand dune (D1) with cross bedding in forests and bounding planes, and covered sand (D2) with parallel, continuous reflections overlying.....	53
4.8 Event depositions of dune can be divided into 3 events (subunits d1, d2 and d3) by third order bounding surface (mark 1, 2 and 3): mark 1- individual forest, mark 2-interface separating different dune generations or second bounding surface, and mark 3-third order bounding surface. The water table represents a surface of beach ridge deposit (B1), underneath dune deposits.....	55
4.9 GPR profile oriented parallel to the dune’s downwind axis show the slip face at the western part of dune.....	56

Figure	Page
4.10 Characteristic reflection patterns of marine environment can be divided into 2 units, including beach ridge (B1) with oblique (low angle slope) reflection configuration, and littoral deposits (B2) with parallel stratified reflection configuration.....	64
4.11 Characteristic reflection patterns of channel filled (C) with trough- or channel- shaped reflections.....	64
4.12 GPR profile oriented perpendiculars to the dune's downwind axis.....	67
4.13 Characteristics of radar signals recognized in GPR profile.....	72
4.14 The reflection parallel stratified of littoral deposit from GPR signal correlate with the profile of sand sheet at the coastal, northern part of the study area.....	73
4.15 The difference between sediments of dune deposits and old beach ridge deposits.....	74
4.16 Event boundaries of dune deposition are clearly seen from outcrop, southern part of dune field. Within 5 m thick of dune, at least 3 depositional events were identified.....	76
4.17 Rare micro-scale sedimentary structures of parallel and inclined lamination persisted in dune. Some rootlets as one bioturbation are also preserved.....	77
4.18 Map showing locations of sediment samples for grain size analysis.....	77
4.19 Graphs showing distribution of grain size analyzed by Malvern, Mastersizer laser granulometry.....	78
4.20 Histogram plot showing distribution of statistic parameters and their assemblages in interpreting depositional environment.....	78
4.21 OSL dating defined age on top of dune deposition.....	79
5.1 Dune morphology correlated with GPR signal can separated dune deposits with seaward prograded beach ridge by characteristic of clearly reflection configuration to represent environment deposition.....	84

Figure	Page
5.2 The Stratigraphical profile along west-east transects (Data modified from DMR logs, 2006) divided the stratigraphy to 4 units; as dune deposits, swamp deposits, beach ridge and alluvial deposits.....	85
5.3 The events separated from depositional break of dune in GPR profile and core logs no. BB 5 (DMR, 2006). Dune stratigraphy represents at least 3 events.....	86
5.4 The events break deposition of dune in GPR profile and core logs no. BB 5 (DMR, 2006) at dune stratigraphy, represents at least 3 events deposition.....	86
5.5 Idealized cross section of Bang Berd sand dune. Morphology of dune regionally shows wind blown from the east to the west.....	87
5.6 The schematic model for the formation stage of Bang Berd sand dune.....	90
5.7 Possible time of dune formation correlated with the sea-level envelop for Thailand during Holocene (Choowong et al., 2004) and OSL dating in the top-half of parabolic dune profile reveal that the formation of formation of sand dune Bang Berd may have occurred during a dry condition probably during and after the mid-Holocene regression.....	94
5.8 The present morphological features of Bang Berd sand dune.....	96

LIST OF TABLES

Table	Page
3.1 Calculation of statistic parameters by using result of grain size analysis (after Folk, 1968).....	34
3.2 Range of standard deviation, using to indicated degree of sorting (after Folk, 1968).....	34
3.3 Classification of skewness (after Folk, 1968).....	34
3.4 Radar facies element of different sedimentary depositional environment (Overmeeren, 1998).....	43
4.1 Result of OSL dating sand dune sediments.....	79



ศูนย์วิทยทรัพยากร
จุฬาลงกรณ์มหาวิทยาลัย

CHAPTER I

INTRODUCTION

1.1 General statement

The accumulation of windblown sand marks the beginning of one of nature's most interesting and beautiful phenomena. Sand dunes occur throughout the world, from coastal and lakeshore plains to arid desert regions. In addition to the remarkable structures and patterns of sand dunes, they also provide habitats for a variety of life, which is marvelously adapted to this unique environment.

At Bang Berd Bay, a remarkable wind blown sand dune lies almost parallel to the present coastline with its highest elevation about 20 m above the present mean sea level. The highest elevation of dune is generally located in the south of Bang Berd Bay and decreases both altitude and extension to the north ending at the northern headland.

The distribution of wind blown sand dune in the western coastal plain of the Gulf of Thailand (Figure 1.1) is very limited and left behind some significant geological challenges for the explanation of its formation in relation with the paleoclimate condition. Thus, this study is aimed to characterize sand dune morphology and sedimentology as the basic geological clues for explaining its formation. The work started with aerial photographs interpretation along with the descriptive field survey. Fieldwork included a regional geological mapping to delineate boundary between dune and underlying beach ridge deposits, pitting for stratigraphical correlation. Shallow geophysical survey (i.e. Ground Penetrating Radar or GPR) was also conducted.

1.2 Objectives

The objectives of this study are (1) to characterize sedimentology of sand dune in the study area, (2) to evaluate possible sources of dune and (3) to model dune formation.

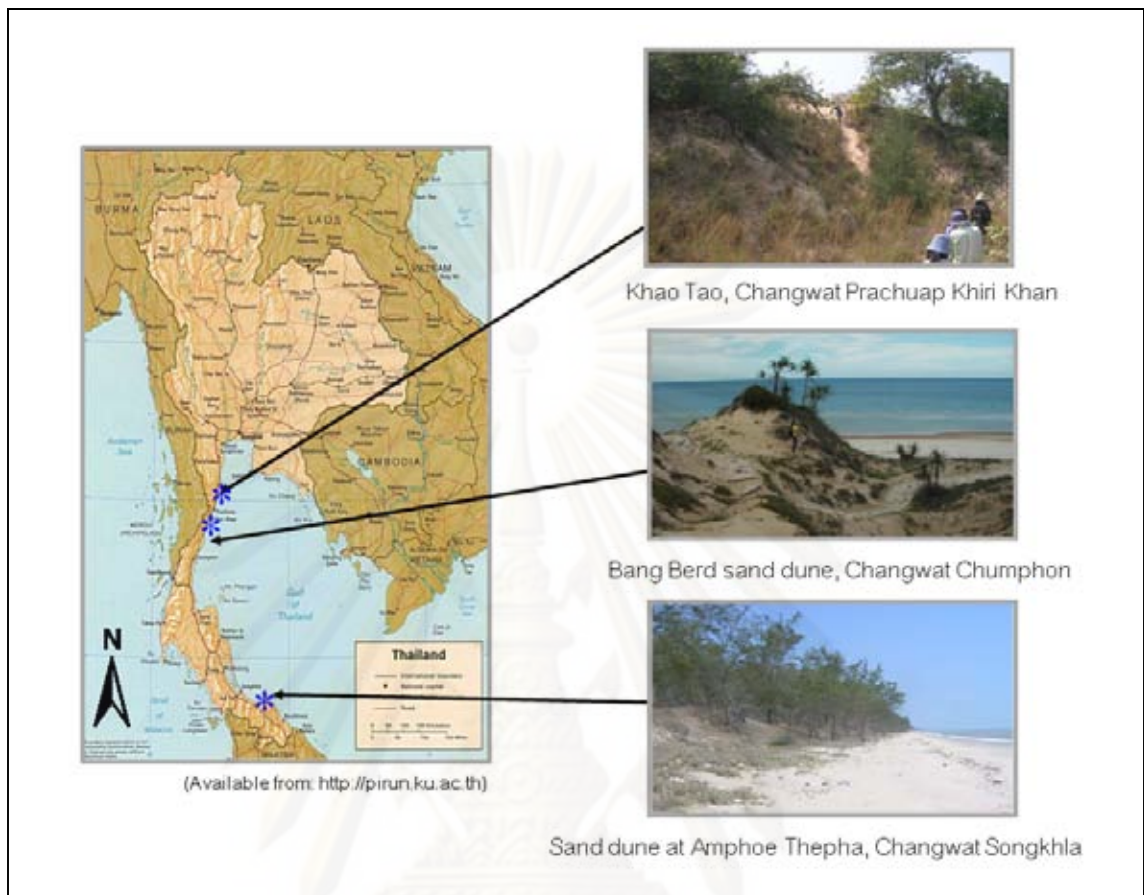


Figure 1.1. Distribution of wind-blown sand dune in the western coastal plain of the Gulf of Thailand at Khao Tao, Prachuap Khiri Khan (top), Bang Berd, Chumphon (middle) and Thepha, Songkhla (bottom).

1.3 Scope of work

The scope of this work is limited to the characterization of sand dune morphology from aerial photographs and the explanation of dune formation based solely on sedimentological characteristics. Macro-scale sedimentary structures were interpreted from GPR facies to which they can presumably be inferred the ancient wind directions. Additional age dating was carried out from optically stimulated luminescence (OSL) dating and literatures. Laboratory work includes grain size analysis by laser granulometry.

1.4 Location and accessibility

The study area is located at Ban Bang Berd, Amphoe Pathio, Changwat Chumphon, in the western coast of the Gulf of Thailand (Figure 1.2). Ban Bang Berd is about 430 km south of Bangkok at the border between Changwat Prachuap Khiri Khan and Changwat Chumphon, and covers about 25 km².

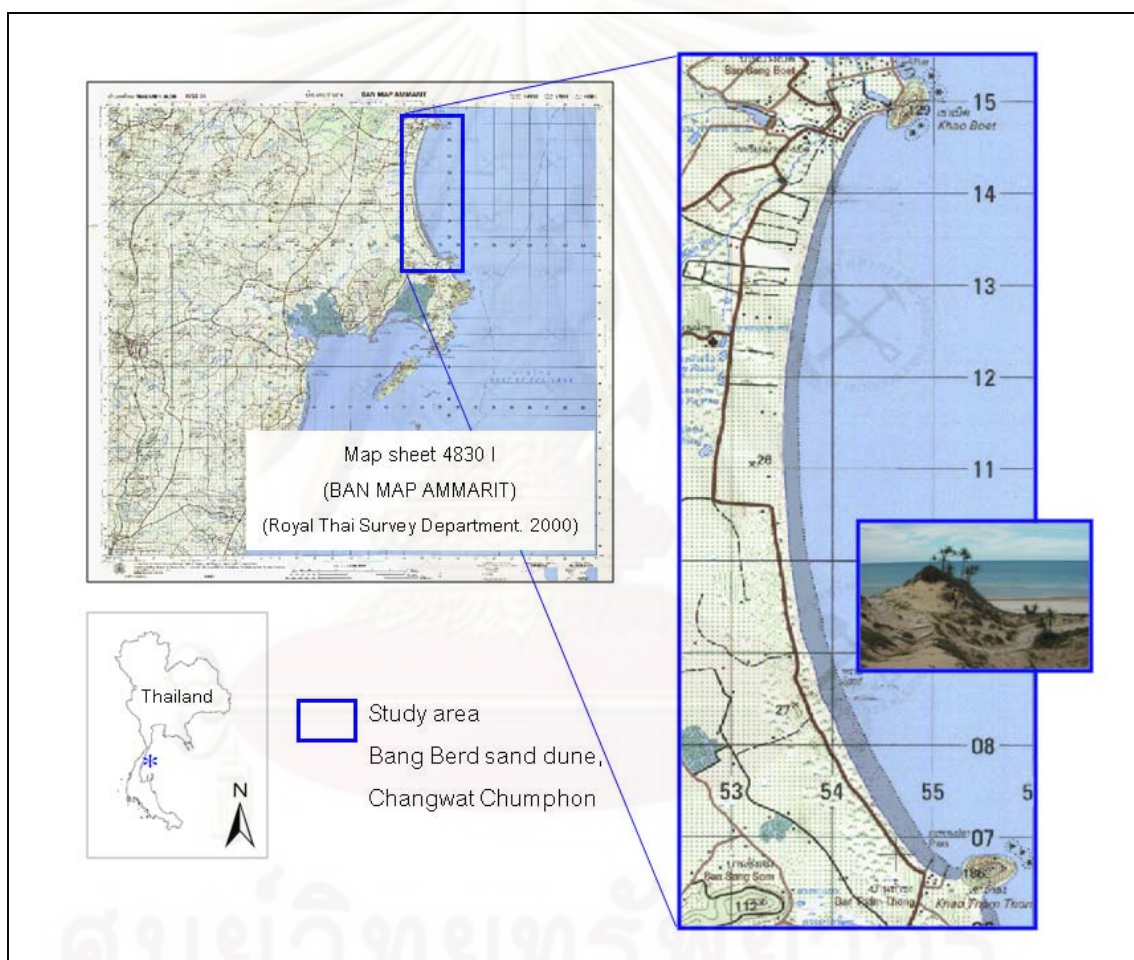


Figure 1.2. The study area is located at Ban Bang Berd, Amphoe Pathio, Changwat Chumphon, in the western coast of the Gulf of Thailand.

The climate of Changwat Chumphon is classified as a tropical monsoon type and can generally be sub-divided into 2 main seasons. The first is the wet season, which starts from May and lasts in January. This season is influenced by a southwest monsoon between May and September. And northwest monsoon between October and January is

characterized by heavy rainfall. The second is dry season that occurs between February and April. This period is under the influence of the humid and hot southeast monsoon. In the past 4 decades, this area was occasionally affected by typhoons and tropical storms.

1.5 Previous works

Friedman (1961) analyzed grain-size distribution of sand dune to the recognition and reconstruction of the depositional environment. Dune sands, commonly, can be distinguished from beach sands on the basis of such grain-size parameter plots. The distinction between the sand types can be numerically stated by computing the third moment (skewness) of the distribution curve. On the phi scale the third moment (skewness) for dune sands is generally positive, whereas that of beach sands is generally negative.

Eisma (1965) studied about the difference in roundness of beach and dune sands, and concluded that angular grains are more easily picked up from the beach by the wind and angular grains are carried further inland in suspension. The relative importance of these processes will depend on the size of the grains and on wind velocity.

Smith and Whalley (1981) used scanning electron microscopy (SEM) to study the character of individual grain and compare with adjacent fixed dunes and present-day pedi-sediment. Results indicate that the drift is well sorted and has the textural characteristics of loess. SEM micrographs showed that the drift contains grains with a wide variety of morphologies, although they are predominantly angular to subangular with only limited evidence of abrasion by aeolian and/or fluvial transport and some overgrowths of secondary silica.

Isla and Espinosa (1995) used geomorphological features and radiocarbon dating to study the Holocene sea level fluctuation events during 6,000 years ago when a sea level was at 2 m higher than present. This fluctuation has caused several

environmental changes. During the latter stages of the Holocene transgression, sand dunes were developed as a result of high wave energy and a plentiful sand supply. The subsequent regressive phase produced lagoons, tidal flats, marshes and cheniers. These processes occurred before the drift reversal mentioned above.

Clemmensen et al. (1996) built up the 3D structure of the dunefield deposits. They studied the geomorphological analysis, sedimentological facies analysis of borings, trenches and natural exposures, and most importantly by georadar mapping. The dune deposits are locally composed of up to four depositional sub-units separated by immature soils. The base of the lower aeolian unit formed around 300 A.D., the upper aeolian unit has been dated to ca. 1000 A.D. Present dunefield was primarily formed between 1,550 and 1,850 A.D.

Overmeeren (1998) analyzed the radar data in order to know the reflection characteristic patterns of different depositional environments. This paper presents typical examples of radar patterns for most sedimentary environments.

O'Neal and McGeary (2002) used ground penetrating radar (GPR) and lithologic data and they revealed the six Pleistocene sea-level highstand sequences, forming two composite terraces along the northern margin of Delaware Bay in southern New Jersey, USA. GPR analysis of coastal drainage modification revealed a contrasting lowstand sequence of incised paleo-valleys, supporting the interpretation that these bay-margin deposits contain one of the most complete sections of late Quaternary highstand stratigraphy in the Mid-Atlantic region.

Orford et al. (2003) studied the mechanisms and timescales of fine and coarse beach sediment decoupling and deposition of prograded Holocene beach ridges with superimposed dunes in north-east Ireland. Considered in the light of infrared-stimulated luminescence ages of sand units within beach ridges, and ¹⁴C ages from organic horizons in dunes, sediment volume entering the beach is thought to have fluctuated as a function of a forced regression associated with the falling sea level from the mid-

Holocene highstand (ca. 6,000 cal. yr BP) identified in north-east Ireland. The prograded beach ridges dated at ca. 3,000 to 2,000 cal. yr BP indicate that the Holocene highstand's regressive phase may have lasted longer than previously specified.

Buynevich et al. (2004) used coastal-morphological, geophysical (ground-penetrating radar: GPR), and sedimentological data documented extreme storm events along the sandy barriers. Stratigraphy suggested the bog varied in size through time, contracting during overwash events and aeolian deposition and expanding across washover sheets during extended periods of barrier stability.

Dawson et al. (2004) investigated the coastal marshes along the Atlantic coast of the Outer Hebrides, the majority of the sand units were produced during episodes of climate deterioration both prior to and after the period of medieval warmth (MWP). Many were produced after ca. AD 1,400. It is argued that the episodes of sand blow indicated by the deposits may reflect periods of increased cyclogenesis in the Atlantic associated with increased sea ice cover and an increase in the thermal gradient.

Pederson and Clemmensen (2005) used GPR and ^{14}C dating to study Holocene coastal dune field system from Denmark, interpretation of the accumulation history of the eolian system since about 2,200 BC.

Saye et al. (2005) used LIDAR data, conventional topographic and bathymetric surveys to investigate morphological of beach and dune, presence of a general relationship between beach morphology, dune morphology and erosion/accretion. Eroding dunes were found to be associated with narrower, steeper beaches whilst accreting dunes were associated with wider, low-angle beaches.

Switzer et al. (2006) used GPR to investigate the sedimentary structures and contacts of the barrier and back-barrier lagoonal sequences of the Killalea barrier system on the southeast Australia. GPR profiles show the presence of erosion surfaces within the Holocene dune deposits and provide more information on the sandsheet and erosion surface. A late Holocene sandsheet dominated by marine sand has been

identified in the upper fill of a back barrier lagoonal, event during the last 200–800 years based on AMS radiocarbon and optically stimulated luminescence (OSL) dates.

Baddock et al. (2007) studied about airflow patterns in transverse dune and interdunes. Patterns of flow in interdunes can be characterized into two groups. The first group covers sandy interdunes with closely-spaced dunes where the near-surface velocity pattern, interdune topography and the close relationship between these two variables supports a flow response model. The second covers interdunes that are identifiably long and flat ('extended' interdunes) where the interdune is considerably longer than the separation length. These interdunes show an overall wind speed distribution within them that is different to velocity patterns established by flow response.

Giannini et al. (2007) studied about late Quaternary relative sea level changes controlling eolian depositional coast by TL and OSL dating from Brazilian coast. Two eolian depositional sequences are separated by an unconformity. The older eolian sequence is correlated to the relative sea level rise of the last interglacial period. The younger eolian sequence was initiated during the relative sea level rise in the post-glacial.

Moura et al. (2007) interpreted based on morphological and sedimentological similarities between older geomorphic features (cemented beach and dune rocks) and present to study about environment changes during the Holocene. Sea level rose between about 8,800 and 6,600 yrs, then the transgressive dunes formed, and massive dune accumulation started at 3,200 yrs, due to a regression of sea level.

Aagaard et al. (2007) considered the origin and development of older dune fields on a barrier spit complex and chrono-stratigraphy based on OSL-dating. Older dune can be temporally correlated with a phase of relative sea level rise and with a high frequency of storm surges along the coast. Dune formation started at a relatively late stage of the Little Ice Age (LIA). Onshore sand supply was caused by marine, rather than aeolian, agents; this supply provided the basis for subsequent dune formation.

Tamura et al. (2008) used ground-penetrating radar (GPR) to study Holocene beach deposits to examine a marker of past sea level recognized in beach profiles. A GPR survey was performed on a modern aeolian dune and beach ridges of the strand plain using a PulseEKKO100 system with 100-MHz antennae. The profiles obtained contain five vertically stacked radar units (R1–R5) with characteristic reflections. Ground truthing using sediment cores and the morphology of the modern beach suggest that these radar units correspond to aeolian dune (R1), small-scale swale (R2), backshore and foreshore (R3), upper shoreface (R4) and lower shoreface (R5) deposits, in descending order.

Santalla et al. (2009) used GPR support data from topographic DGPS analyzed dune field dynamics of El Fangar spit, Ebro Delta, Spain. Topographic data shows that zones with low heights have migration rates higher than zones with higher dune height and internal structure shows accretion and progradation sequences of dunes over beach deposits, relationship with the dune height, suggesting that low height involves significant migratory activity, while a height increase leads to a decrease in dune migration.

Clemmensen et al. (2009) studied about the evolution of Holocene coastal dunefields. Dunefield development was characterized by repeated periods of transgressive dune formation punctuated by periods of dune stabilization and soil formation. The chronology of dunefield evolution is based on Accelerator Mass Spectrometry (AMS) radiocarbon dating and Optically Stimulated Luminescence (OSL) dating, aeolian activity occurred around 2,200 BC, 800 BC, AD 100, AD 1,050–1,200, and between AD 1,550 and 1,650.

Girardi and Davis (2010) observed dune patterns from series of map since the 19th century and aerial imagery since 1930. They studied changes in the aeolian geomorphology of coastal parabolic dunes over the last ~170 years. This study has concentrated on a dune with a particularly complex history of stabilization, by correlated that dune's surface evolution, as revealed by aerial imagery, with its internal structures

imaged using 200 MHz and 500 MHz Ground Penetrating Radar (GPR) surveys. Both 2D (transect) and high-resolution 3D GPR imagery. Unique mode of blowout deposition that is alternate on a decadal scale between opposite sides of a parabolic dune during reactivation and migration.

1.6 Theoretical background

The accumulation of wind blown sand dune commonly marks as the beginning of one of nature's most interesting and beautiful landform. Sand dunes can be formed from coastal and lakeshore plains to arid desert regions. In addition to the remarkable structure and patterns, sand dunes also provide habitats for a variety of life which is marvelously adapted to this unique environment.

1.6.1 Origin of Sand Dunes

The origin of sand dunes is very complex, but there are three essential prerequisites: (1) an abundant supply of loose sand in a region generally devoid of vegetation (such as an ancient lake bed or river delta); (2) a wind energy source sufficient to move the sand grains; and (3) a topography whereby the sand particles lose their momentum and settle out. Any number of objects, such as shrubs, rocks or fence posts can obstruct the wind force causing sand to pile up in drifts and ultimately large dunes. There are even reports of ant hills forming the nucleus upon which sand dunes are built. The direction and velocity of winds, in addition to the local supply of sand, result in a variety of dune shapes and sizes. The wind moves individual grains along the inclined windward surface until they reach the crest and cascade down the steep leeward side or "slip face," piling up at the base and slowly encroaching on new territory.

1.6.2 Sand movement

Sand movement by wind is a complex process involving several styles of grain movement by wind that occur more or less simultaneously (Bagnold, 1941). The

process most easily observed is saltation, the bouncing of sand grains near the sand surface, sometimes in streamers (Figure 1.3). A second component of the sand drift process is surface creep. Surface creep is the jerky forward movement of larger grains that are too heavy to be lifted by the wind, but are jolted forward when struck by smaller flying grains. The third manner in which sand moves is by suspension. Suspended grains are so small that they are carried along without returning to the ground once they are thrown into the air by saltating grains or direct wind scour. Some of the suspension population is merely dust, which is carried into the atmosphere and far away from the dunes. One of the reasons dune sand is so well sorted is the narrow size range of sand that wind can move under most conditions usually grains up to .5 mm or so in size. Larger grains are too heavy to be moved by wind and are soon left behind, while the silt and clay size fractions are either removed to the atmosphere or settle into sheltered places such interdunes.

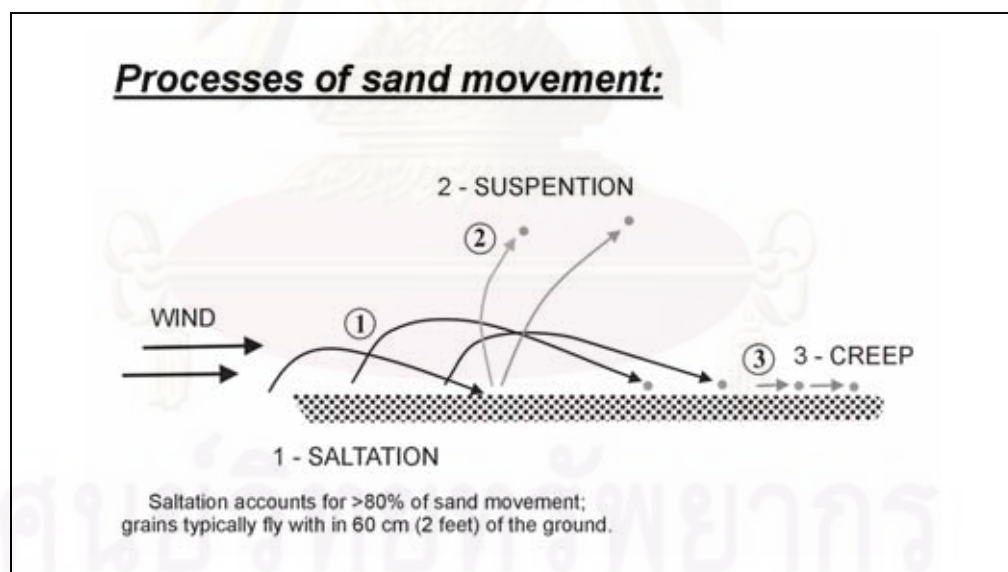


Figure 1.3. The three basic modes of sand movement by wind. Grains in saltation bounce across the desert. Surface creep is the jerky forward movement of the larger grains impacted by saltating grains. The finest grains of silt and dust travel in suspension and are commonly removed from a basin over time, unless trapped in sheltered zones within the dunefield and buried by dune advance or other processes (Available from: <http://www.guaddunes.com>).

The relative importance of these processes will depend on the size of the grains and on wind velocity (Figure 1.4). Thus, the fact that the fine dune sands are generally rounder than the fine beach sands can adequately be explained by assuming removal of the more angular grains from the dunes in suspension. That the fine sand of the dunes contains more heavy minerals and less mica than the corresponding beach sands: the fine sands in the dunes have the character of lag deposits (Eisma, 1965).

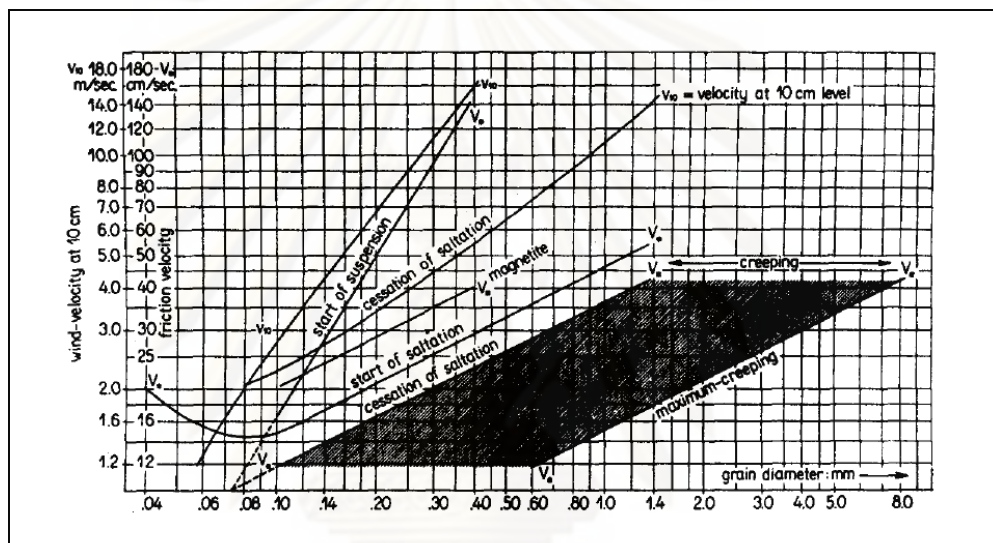


Figure 1.4. Relation between wind-velocity, friction velocity, grain size and various eolian transport modes for homogeneous groups of spherical quartz grains (Eisma, 1965).

1.6.3 Dune Growth and movement

Dune growth and movement is the result of sand flow on and around a dune during periods when the wind is strong enough to move sand (for dry sand this threshold is about 15 mph). Dunes are constantly changing shape in response to changes in wind velocity or direction. Dunes grow when more sand drifts onto them from surrounding areas than is removed downwind. Figure 1.5 shows a small barchan (horseshoe-shaped) dune near the Heart of the Dunes loop road. The small dune shown in Figure 1.5 has grown by trapping sand drifting from the right side of the

picture toward the left. During storms, sand flows over all parts of the dune. Sand that flows over the center parts of the dune settles on the upper part of the slip face as grain-fall deposits. When the sand accumulates to a certain thickness and angle (the angle of repose: about 32 degrees) it becomes unstable and slides down the slip face. This process, known as avalanching is the basic mechanism of forward advance of most of the bedforms at the Monument. Note also the arms of the dune in Figure 1.5. It is clear that some sand that drifts onto the dune from upwind can move past this dune and not become trapped in the slip face. Thus, this dune lives in a continual balance between sand loss at the arms and sand entrapment on the slip face.

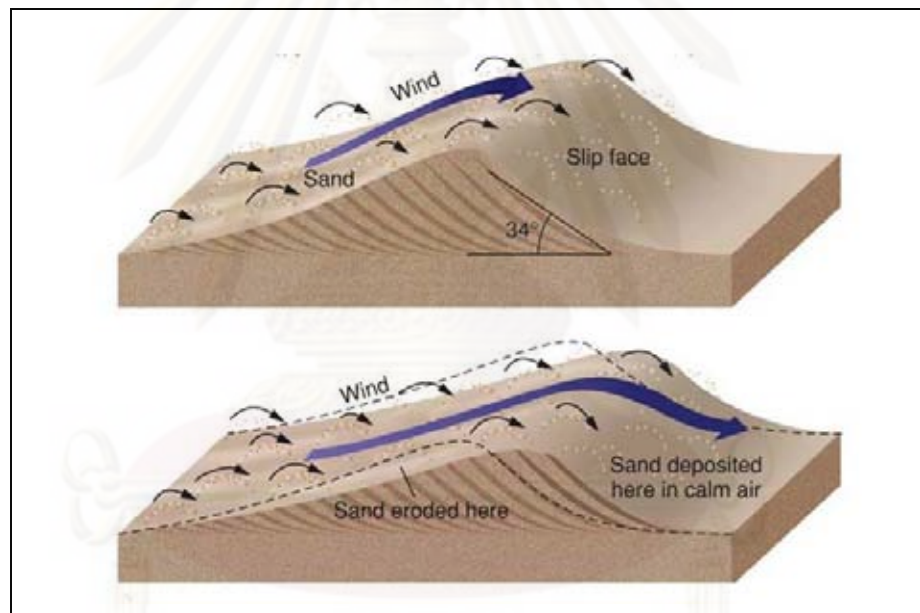


Figure 1.5. Dune growth and movement are the result of sand flow on and around during periods when the wind is strong enough to move sand (about 15 km/hr) (Available from: <http://www.indiana.edu>).

1.6.4 Dune types

Dunes occur in different forms and sizes, formed by interaction with the wind. Most kinds of dunes are longer on the windward side where the sand is pushed up the dune and have a shorter "slip face" in the lee of the wind.

The most common dune form on Earth is the crescentic. Crescent-shaped mounds generally are wider than long. The slip face is on the dune's concave side. These dunes form under winds that blow from one direction, and they also are known as barchans (Figure 1.6-A), or transverse dunes (Figure 1.6-B). Some types of crescentic dunes move faster over desert surfaces than any other type of dune.

U-shaped mounds of sand with convex noses trailed by elongated arms are parabolic dunes (Figure 1.6-C). Sometimes these dunes are called U-shaped, blowout, or hairpin dunes, and they are well known in coastal deserts.

Straight or slightly sinuous sand ridges typically much longer than they are wide are known as linear dunes (Figure 1.6-D). They may be more than 160 kilometers long. Linear dunes may occur as isolated ridges, but they generally form sets of parallel ridges separated by miles of sand, gravel, or rocky interdune corridors. Some linear dunes merge to form Y-shaped compound dunes. Many form in bidirectional wind regimes. The long axes of these dunes extend in the resultant direction of sand movement.

Radially symmetrical, star dunes (Figure 1.6-E) are pyramidal sand mounds with slip faces on three or more arms that radiate from the high center of the mound. They tend to accumulate in areas with multidirectional wind regimes. Star dunes grow upward rather than laterally. They dominate the Grand Erg Oriental of the Sahara. In other deserts, they occur around the margins of the sand seas, particularly near topographic barriers. In the southeast Badain Jaran Desert of China, the star dunes are up to 500 meters tall and may be the tallest dunes on Earth.

Oval or circular mounds that generally lack a slip face, dome dunes are rare and occur at the far upwind margins of sand seas.

Reversing dunes (Figure 1.6-F) occurring wherever winds periodically reverse direction, reversing dunes are varieties of any of the above shapes. These dunes typically have major and minor slip faces oriented in opposite directions.

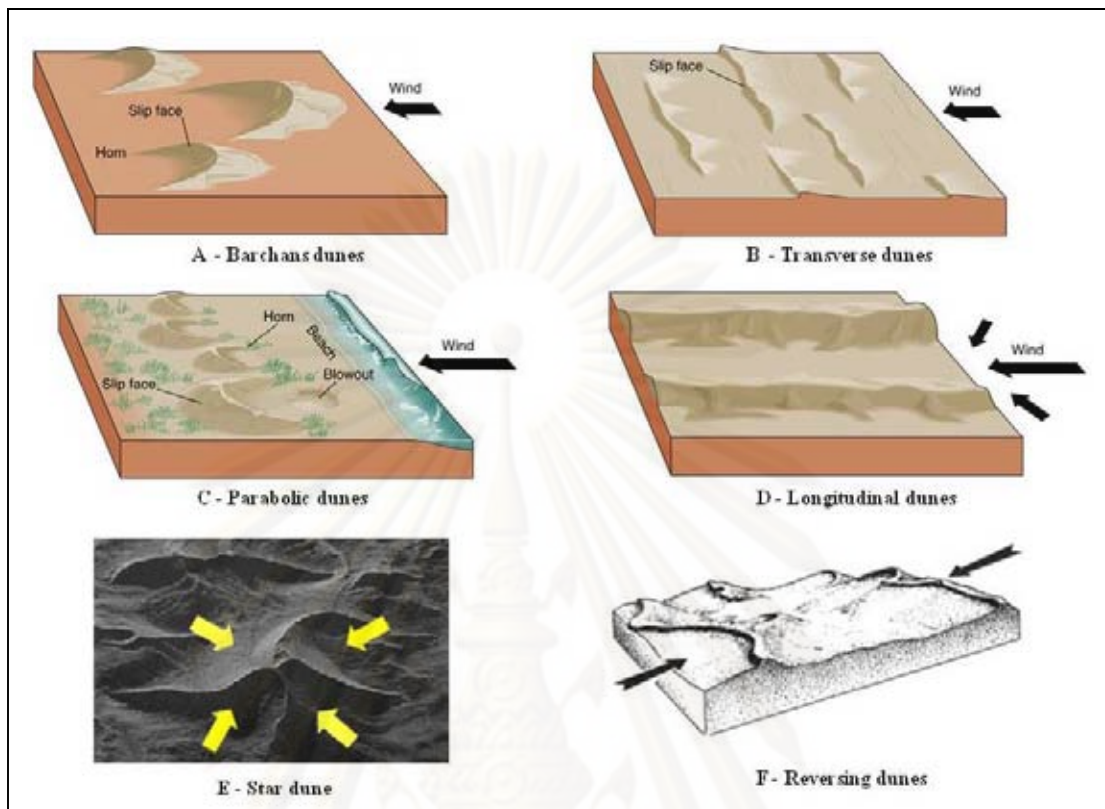


Figure 1.6. Classifies individual dunes in terms of the number and position of slip-faces, under the assumption that the number of slip-faces corresponds to the number of dominant wind directions in the local wind regime. (A-D available from: <http://www.indiana.edu.com>, E available from: <http://cartage.org> and, F available from: <http://digital-desert.com>)

All these dune types may occur in three forms: simple, compound, and complex. Simple dunes are basic forms with a minimum number of slip faces that define the geometric type. Compound dunes are large dunes on which smaller dunes of similar type and slip face orientation are superimposed, and complex dunes are combinations of two or more dune types. A crescentic dune with a star dune superimposed on its crest is the most common complex dune. Simple dunes represent a wind regime that has not changed in intensity or direction since the formation of the dune, while compound and complex dunes suggest that the intensity and direction of the wind has changed.

1.7 Background of study area

Economic Geology Division, Department of Mineral Resources (DMR) (1990) surveyed the economic geology of Changwat Prachuap Khiri Khan and Changwat Chumphon (location of area 2A and 2B). Bang Berd sand dune is located in southern part of area 2B. Methodology used included shallow marine seismic reflection profiling systems, Echo-sounding systems and magnetic systems, collected samples by gravity corer, dredger and sand pump. Heavy minerals are observed extensively in the south of the bay, represent to long shore current in the study area flows from north to south along semi-enclosed bay.

Nattawut Prachantasen et al. (2008) studied the characteristics of sand dune from Bang Berd, Changwat Chumphon. The morphological feature can divided into 3 units, outer dunes, middle dunes and inner dunes. The deposition of washover covers the outer dunes that are aligned in east-west direction. The stratigraphy and sedimentary structures suggested a geological history of the topmost part of dune that includes the effect from paleo-storm deposits. OSL dating results in washover sediments showed the deposition by unusual storm at the age between 93 ± 18 yrs and 126 ± 14 yrs.

Environmental Geology Division, DMR (2006) surveyed and made the bunga coring and hand auger to collect sand samples from the dune and swamp at Bang Berd sand dune for grain size analysis. The stratigraphy of Bang Berd can be divided into 4 units, eolian sand dune, beach deposits, gravel bed and fine sand and silt.

ศูนย์วิทยทรัพยากร
จุฬาลงกรณ์มหาวิทยาลัย

CHAPTER II

REGIONAL SETTING

2.1 Regional Geology

Rocks and sediments within the western coastal plain of the Gulf of Thailand at the border between Amphoe Pathio, Changwat Chumphon and Amphoe Bangsaphan Noi, Changwat Prachuap Khiri Khan are composed mainly of Quaternary deposits and some sedimentary rocks. Igneous rock is locally exposed in the western part (Figure 2.1), ranging in age from Carboniferous-Permian to Quaternary. The oldest rocks are found in the western part of the study area displaying as highland mountainous areas, which are composed of granite (K_{gr}), pebbly sandstone and pebbly mudstone in the Koh He Formation (CP_{kh}), mudstone in the Khao Phra Formation (CP_{kp}) and arkosic sandstone in the Khao Chao Formation (CP_{kc}). The central plain is colluvial and residual deposits (Q_c), alluvial deposits (Q_a) and terrace deposits (Q_t). In the southern part of the study area is mountain of sandstone interbedded with conglomeratic sandstone in the Lam Thap formation (JK_{lt}). Massive limestone in the Ratburi Group (P) is distributed throughout the study area. Quaternary sediments are deposited along the beach (Q_b and Q_{bo}), lagoonal deposits (Q_{lg}) and tidal flat deposits (Q_{mp}) in the eastern part, rarely basal conglomerate (TR).

2.2 Structural Geology

Evidences of geological structures in the western coastal plain of the Gulf of Thailand, especially the major faults and folding are mostly found in highland mountainous, the western and southern parts of the area. Mostly, faults and fractures are in NE-SW and NW-SE directions (Figure 2.1). The low-lying plain was rarely recognized in the past because high weathering conditions. In particular, the central part of the study area, outcrops are not well-exposed and rarely persisted.

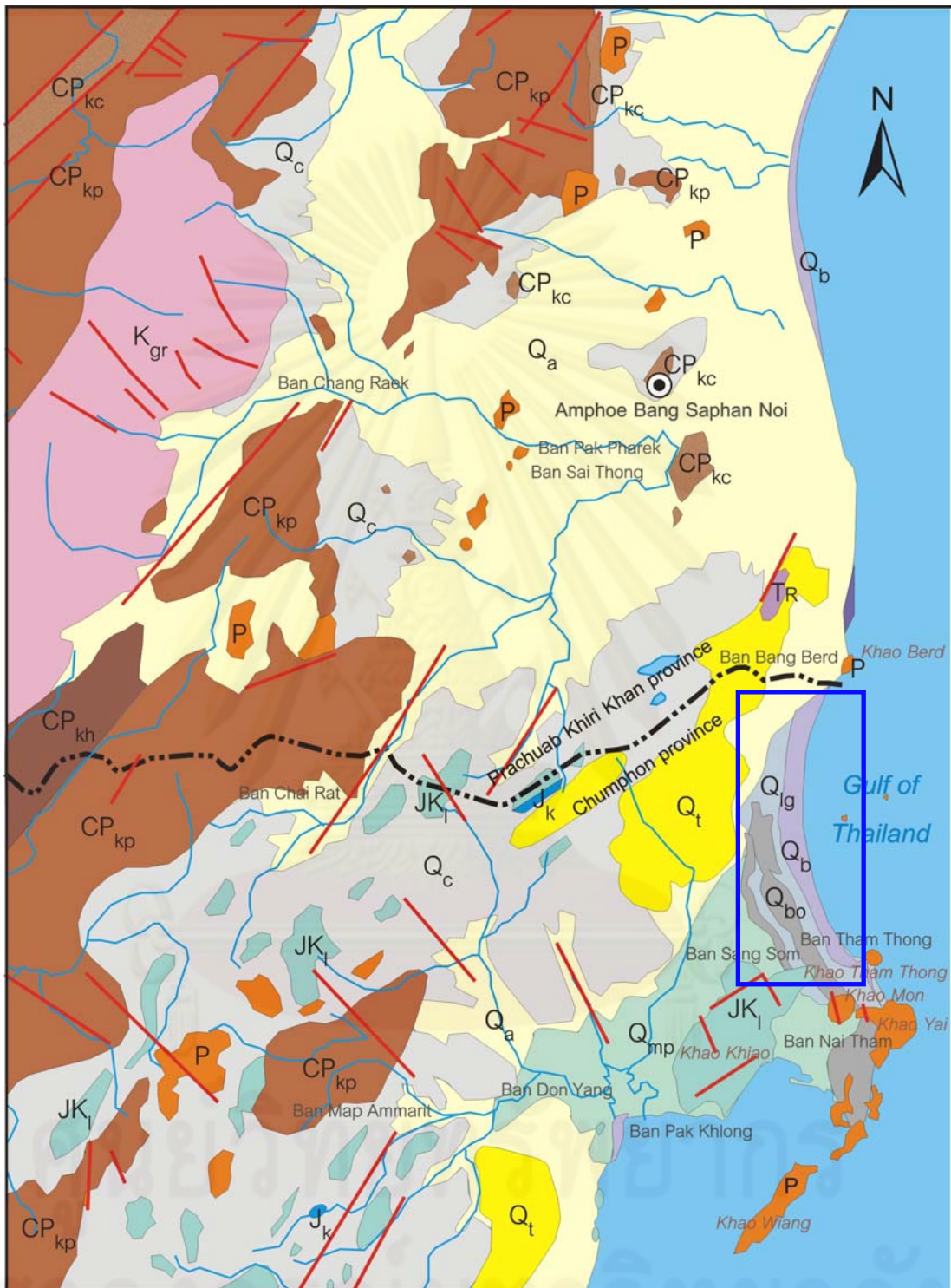


Figure 2.1. Geological map at the western coastal plain of the Gulf of Thailand (modified after Suphawadee Vimuktanandana, Assanee Meesook and Suvapak Imsamut., 2007) (see explanation on the next page). The study area, Bang Berd sand dune is located in blue inset.

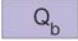
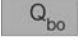
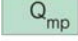
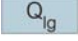
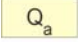
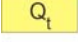
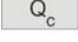






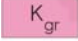

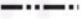



EXPLANATION			
SEDIMENT, SEDIMENTARY AND METAMORPHIC ROCKS			
	Beach deposits: sand, gravel, silt, with mollusc, coral and plant remains.		
	Old beach ridge deposits: sand, medium-course grained, medium sorted, well rounded, with shell fragments.		
	Tidal flat deposits vegetated with mangrove: peat, peaty clay, fine sand and sandy clay.		
	Lagoonal deposits : mud and clay with sand lens, gray to white, medium sorted, subrounded abundant plant remain in upper part.		
	Alluvial deposits: gravel, sand, silt and clay.		
	Terrace deposits: gravel and sand.		
	Colluvial and residual deposits: rock fragments of quartzite, sandstone, siltstone, granite, sand and silt matrixes. Locally is lateritic soil and terrarosa soil.		
	Sandstone, reddish brown, fine-medium grained, angular shaped, good sorting, laminated to thick bedded, interbedded with conglomerate, pebbles of sandstone, quartz and shale, subround to round shaped, sand and silt matrixes.		
	Shale, greenish gray, calcareous, laminated to thick bedded, fossil gastropod, and plantremains; arkosic sandstone at the upper part, white to yellowish brown, fine-to medium-grained, thin to thick bedded, round to angular, good sorting, composed of quartz, feldspar and rock fragments, siliceous and ferrogeneous matrixes.		
	Basal conglomerate, pebbles of limestone, subangular to angular, sandstone and quartz, subround to round, gray lime, red silt and sand matrixes, calcareous cement.		
	Limestone, dolomitic limestone, dolomite, gray to dark gray, massive, locally chert nodules, interbedded with sandstone and shale, with fusulinids, brachiopods, corals, ammonoids and crinoids.		
	Arkosic sandstone, white to light gray, good sorted, medium grained, thin bedded with <i>Posidonomiya</i> sp.		
	Mudstone, greenish gray, gray, well laminated; lenticular fine grained sandstone, intercalated with quartzitic sandstone, fine-to medium-grained, subround, moderately sphericity; and conglomerate lens near the upper part, thin to thick bedded, mudstone showing cleavage fault zone.		
	Pebbly sandstone and pebbly mudstone, greenish gray,gray, fine-to medium-grained, dense and hart, composed of quartz, mudstone, sandstone, limestone and granite, subangular to subrounded, low to moderately sphericity, poor sorted, gravel oriented near fault zone,quartzite, hornfels and meta-sandstone at granite contact.		
IGNEOUS ROCKS			
	Granite fine-to coarse-grained, equigranular and porphyritic texture, stress granite near the fault zone, locally augen shape of feldspar		
SYMBOLS			
	Contact		Approximate internal administrative boundary
	Fault		Amphoe
			River

Figure 2.1. (cont.)

2.3 Geomorphology of the study area

Geomorphological feature of the Bang Berd sand dune can be divided into 3 types (Figure 2.2) based on the principle classifications from aerial photography, i.e., the difference in elevation and vegetation.

2.3.1 Highland area

This landform displays extensively in the southern part of the area. The trend of the mountain range is in the NE-SW direction. The elevation varies approximately from 100 m to 300 m above the mean sea level.

2.3.2 Undulating area

The elevation of this area ranges from 20-80 m from the present mean sea level. This landform covers almost of the entire western part of the study area, consisting of natural levee, swamp and sand dune.

2.3.3 Beach sand

Beach sand displays as flat plain and small undulating terrains close to shore. Inner beach sand ridges are located about 2 km away from the present shoreline. Elevation of this beach ridge and dune is in average 10 m from the present mean sea level.

2.4 Stratigraphy

The sedimentary, sedimentary and metamorphic rocks within the western coastal plain of the Gulf of Thailand can be described by Montri Silpalit, Assanee Meesook and Somchai Lovacharasupaphon (1975), Denchok Monjai (2005), and Suphawadee Vimuktanandana et al. (2007).

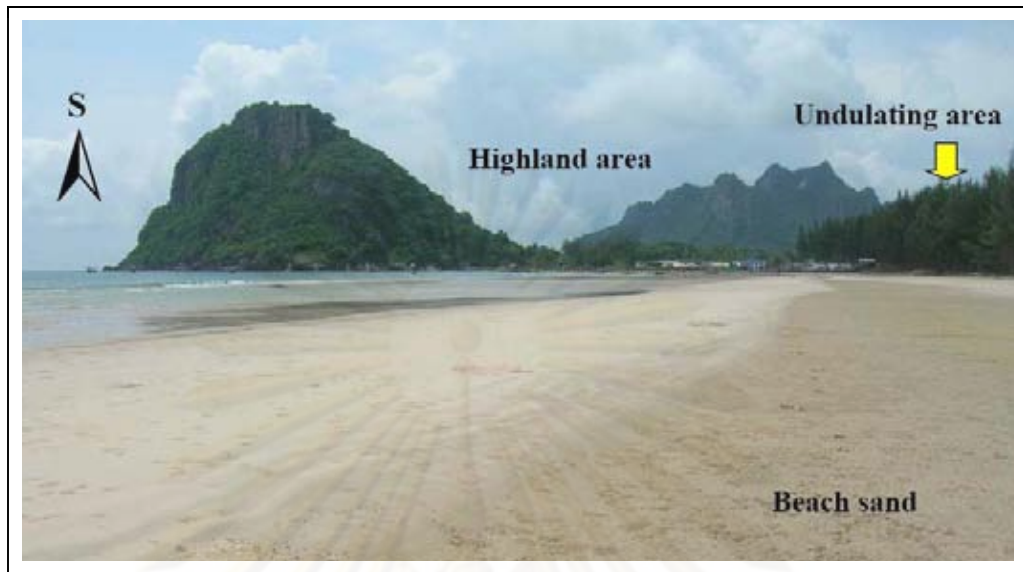


Figure 2.2. Photograph showing highland in the southern part of the study area and beach sand in the eastern part.

2.4.1 Carboniferous-Permian

This unit distributed throughout the western parts of the study area, exposed as highland area, can be divided to 3 formations as follows:

2.4.1.1 Koh He Formation (CP_{kh}): Rocks are pebbly sandstone and pebbly mudstone, greenish gray, gray, fine- to medium-grained, dense and hard, clasts are composed of quartz, mudstone, sandstone, limestone and granite, subangular to subrounded, low to moderately sphericity, poor sorted, gravel oriented near fault zone, quartzite, hornfels and meta-sandstone at granite contact.

2.4.1.2 Khao Phra Formation (CP_{kp}): Rocks are mudstone, greenish gray, gray, well laminated; lenticular fine-grained sandstone, intercalated with quartzitic sandstone, fine- to medium-grained, sub-rounded, moderately sphericity; and conglomerate lens near the upper part, thin- to thick-bedded, mudstone showing cleavages particularly along fault zones.

2.4.1.3 Khao Chao Formation (CP_{kc}): Rocks are arkosic sandstone, white to light gray, good sorted, medium-grained, thin-bedded.

2.4.1 Permian

This unit distributes throughout the study area, exposing as high mountainous area and is composed of limestone, dolomitic limestone, dolomite, gray to dark gray, massive, locally chert nodules (Figure 2.3), interbedded with sandstone and shale. In addition, fossils in limestone such as fusulinids, brachiopods, corals, ammonoids and crinoids were found. This rock unit is recognized as the Ratburi Group.



Figure 2.3. Massive limestone, locally chert nodules at Khao Berd, northern part of the study area.

2.4.2 Triassic

This unit is rarely recognized in the northern part of the study area, exposed as cliffs of red beds near the coast (Figure 2.4). Rocks are composed of basal conglomerate, clasts consist of limestone, subangular to angular, sandstone and quartz, sub-rounded to rounded, gray limestone, red siltstone and sandstone. Matrix and cement are calcareous.



Figure 2.4. The red bed cliff near the coast in the northern part of the study area. Rocks are composed of basal conglomerate, pebbles of limestone, subangular to angular, sandstone and quartz, sub-rounded to rounded with calcareous matrix and cement.

2.4.3 Jurassic

This unit is rarely observed in central low-lying plains and the southern part of the study area. Rocks are composed of shale, greenish gray, calcareous, laminated to thick-bedded, with gastropods and plant remains; arkosic sandstone in the upper part, white to yellowish brown, fine- to medium-grained, thin- to thick-bedded, rounded to angular, good sorting, composed of quartz, feldspar and rock fragments with siliceous and ferrogeneous matrixes.

2.4.4 Jurassic-Cretaceous

This unit is distributed in the southern part of the study area, consisting of sandstone, reddish brown, fine- to medium-grained, angular shape, good sorting, laminated to thick-bedded, interbedded with conglomerate, pebbles of sandstone,

quartz and shale, sub-rounded to rounded, sand and silt matrixes (Figure 2.5). This unit rock is recognized as the Lam Thap Formation (JK_{II}).



Figure 2.5. Reddish brown sandstone interbedded with conglomerate at highway no.3114, northern part of the study area.

2.4.5 Quaternary

This unit is distributed widely throughout the entire study area. It is the youngest unit, which is composed of alluvial deposits, gravel-dominated semi-consolidated sediments with sand silt and clay matrix. This unit can be divided into 7 groups.

2.4.5.1 Colluvial and residual deposit (Q_c) is composed of rock fragments of quartzite, sandstone, siltstone, granite, sand and silt matrixes. In places, lateritic soil and terra rosa soil are found (Figure 2.6).

2.4.5.2 Terrace deposit (Q_t) is composed of gravel and sand.

2.4.5.3 Alluvial deposit (Q_a) is composed of gravel, sand, silt and clay.

2.4.5.4 Tidal flat deposit vegetated with mangrove (Q_{mp}) consists of peat, peat clay, fine sand and sandy clay.

2.4.5.5 Lagoonal deposit (Q_{lg}) comprises mud and clay with sand lens, gray to white, medium sorted, subrounded, abundant plant remains in the upper part.

2.4.5.6 Old beach rich deposit (Q_{bo}) is composed of sand, yellowish brown, medium- to coarse-grained, medium sorted (Figure 2.7), well rounded, with shell fragments.

2.4.5.7 Beach deposit (Q_b) is composed of sand, gravel, and silt (Figure 2.8), with mollusk, coral and plant remains.



Figure 2.6. Rock fragments of quartzite, sandstone, siltstone, granite, sand and silt matrixes of colluvial and residual deposits in the northern part of the study area.



Figure 2.7. Yellowish brown sand of old beach ridge deposit occurs beside beach deposits. Sand's color represents oxidation, distinction with present beach deposits.



Figure 2.8. Beach sediments of sand, gravel and fragment of mollusk are deposited in the northern part of the study area.

CHAPTER III

METHODOLOGY

This chapter describes the methodology (Figure 3.1) used in this work that can generally be divided into 3 periods as follows:

3.1 Office work

3.1.1 To study the relevant literature and previous work.

3.1.2 Collecting the map and aerial photographs.

3.1.3 To interpret the aerial photographs.

3.2 Field investigation

3.2.1 Field reconnaissance

3.2.2 Topographic survey

3.2.3 Ground penetrating radar surveys.

3.2.4 To collect the sample in the field area.

3.3 Laboratory analysis

3.3.1 Interpret the result of Ground penetrating radar surveys.

3.3.2 Particle size analysis. (Malvern, Mastersizer X of The Petroleum and Petrochemical College)

3.3.3 Optically stimulated luminescence (OSL) dating

3.4 Discussion and Conclusion

3.4.1 Interpretation and data correlation

3.4.2 Discussion

3.4.3 Conclusion

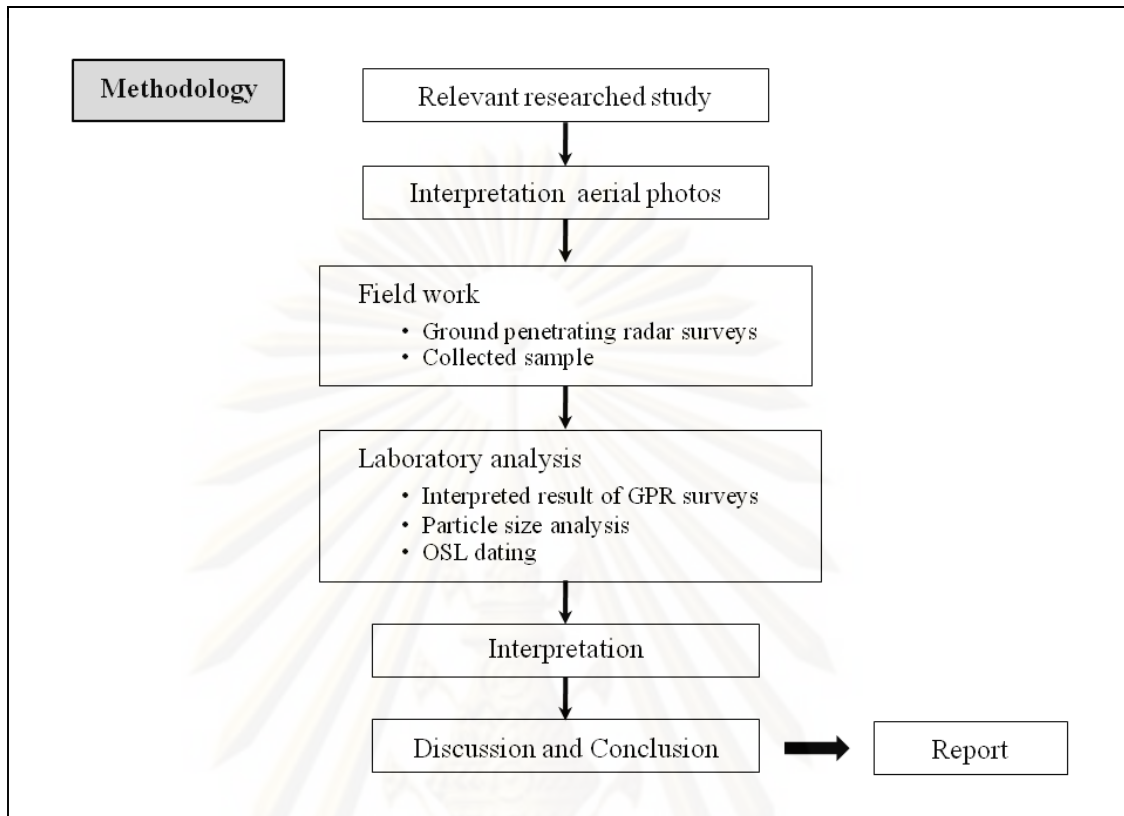


Figure 3.1. Flow chart showing the methodology in this study.

3.1 Office work

Data bases, such as aerial photographs were collected. After data collection process finished, the interpretation of aerial photographs was, then, performed in order to make field work plan, in particular to select the most appropriate areas for detailed study of stratigraphy and shallow seismic survey. All methodology processes are as follows:

3.1.1 Collecting and studying the previous works

Relevant literatures and previous works were compiled and considered in order to understand physical and model of wind blown process, i.e., erosion, elongation and migration of sand dune, types of sand dune. Geological maps covering the study and adjacent areas in different scale were also collected.

3.1.2 Collect the map concerned and aerial photographs.

Data include aerial photographs, with approximate scale of 1:50,000 and topographic map from the Royal Thai Survey Department is used in interpreting the morphological feature. This is the important step to acquire preliminary data in the study area such as present geography, accessibility and so on. The landforms are classified by the aerial photographs. Figure 3.2 shows aerial photographs and the appearance of many landforms.



Figure 3.2. Aerial photograph covering the study area.

3.1.3 Aerial photographs interpretation

The aerial photographic interpretation of sand deposit at Ban Bang Berd is a principal way before moving into field work. The aerial photographic interpretation was based on some photographic features, basically including the changes in colors,

drainage patterns, elevation and vegetations. The identification of surface features or patterns of individual landform is used to locate the interesting area for detailed field mapping. The target areas are expected to visualize the indicator of paleo-environment such as the distribution of dune field where the evidence of wind-blown direction can be inferred. The characteristic of landform from aerial photographic interpretation includes alluvial deposit, beach sand, high land, dune shape and wind direction.

3.2 Field investigation

After the office work was done, field investigation was the next important step. In field investigation, the main aim is to search for good outcrops and check the accuracy of aerial photo interpretation. This section can be divided into 3 steps as follows:

3.2.1 Topographic survey

Topographic survey was carried out prior to ground penetrating radar investigation survey. Main purpose is to make the topographic profile of the study area (Figure 3.3) to see the configuration of beach and topography.



Figure 3.3. Topographic survey for profiling dune morphology along GPR lines.

3.2.2 Ground penetrating radar surveys.

Ground-penetrating radar (GPR) is a geophysical method that basically uses radar pulses to image the subsurface morphology. This non-destructive method uses electromagnetic radiation in the microwave band (UHF/VHF frequencies) of the radio spectrum, and detects the reflected signals from subsurface structures. GPR can be used in a variety of media, including rock, soil, ice, fresh water, pavements and structures. It is capable to detect objects, changes in material, voids and cracks.

GPR uses transmitting and receiving antennas or only containing both functions. The transmitting antenna radiates short pulses of the high-frequency (usually polarized) radio waves into the ground. When the wave hit a buried object or a boundary with different dielectric constants, the receiving antenna records variations in the reflected return signal. The principles involved are similar to reflection seismology, except those of electromagnetic energy is used instead of acoustic energy, and reflections appear at boundaries with different dielectric constants instead of acoustic impedances (Figure 3.4).

The depth range of GPR is limited by the electrical conductivity of the ground, the transmitted center frequency and the radiated power. As conductivity increases, the penetration depth also decreases. This is because the electromagnetic energy is more quickly dissipated into heat, causing a loss in signal strength at depth. Higher frequencies do not penetrate as far as lower frequencies, but give better resolution. Optimal depth penetration is achieved in ice where the depth of penetration can achieve several hundred meters. Good penetration is also achieved in dry sandy soils or massive dry materials such as granite, limestone, and concrete where the depth of penetration could be up to 15 m. In moist and/or clay-laden soils and soils with high electrical conductivity, penetration is sometimes only a few centimeters.

GPR antennas are generally in contact with the ground for the strongest signal strength; however, GPR air launched antennas can be used above the ground.

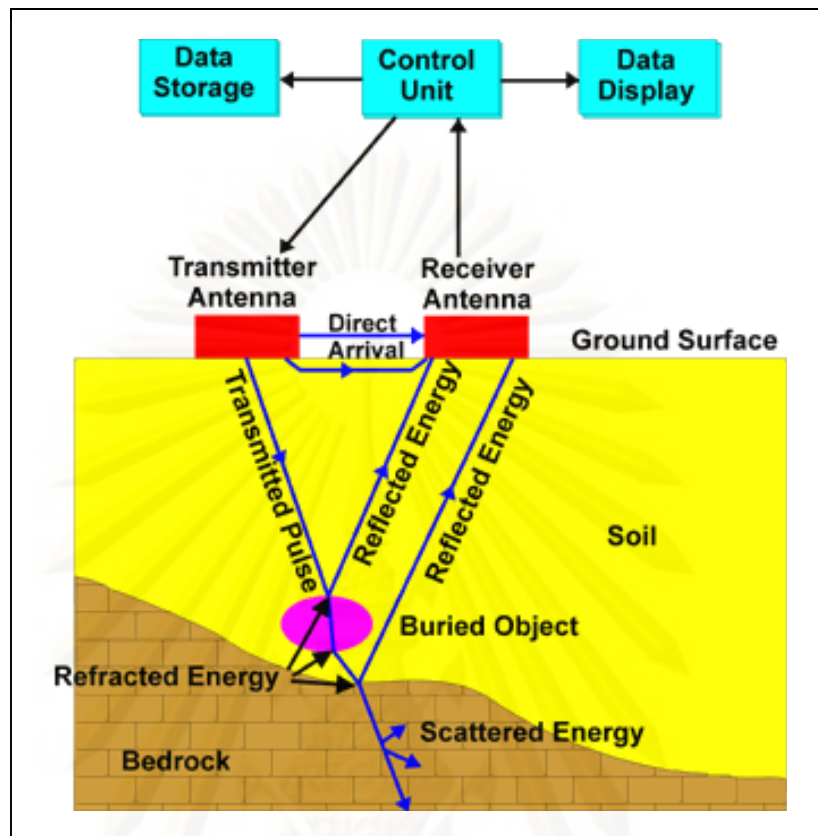


Figure 3.4. Application of ground penetrating radar consists of transmitter antenna and receiver antenna. Where the transmitter antenna generates an EM pulse that travels into the subsurface and then reflect off an interface or scatters off point sources, where it is recorded by receiver antenna (Available from: <http://www.emrl.byu.edu>).

3.2.3 Collecting field samples

This step is the most important to collect sedimentological samples and observe sedimentary structures that were created during the formation of sand dune. Samples were collected for analysis of grain size from dune, beach, and channel; samples were obtained by pitting and augering (Figure 3.6). Systematic collection of samples for OSL dating in laboratory was also carried out (Figure 3.7).

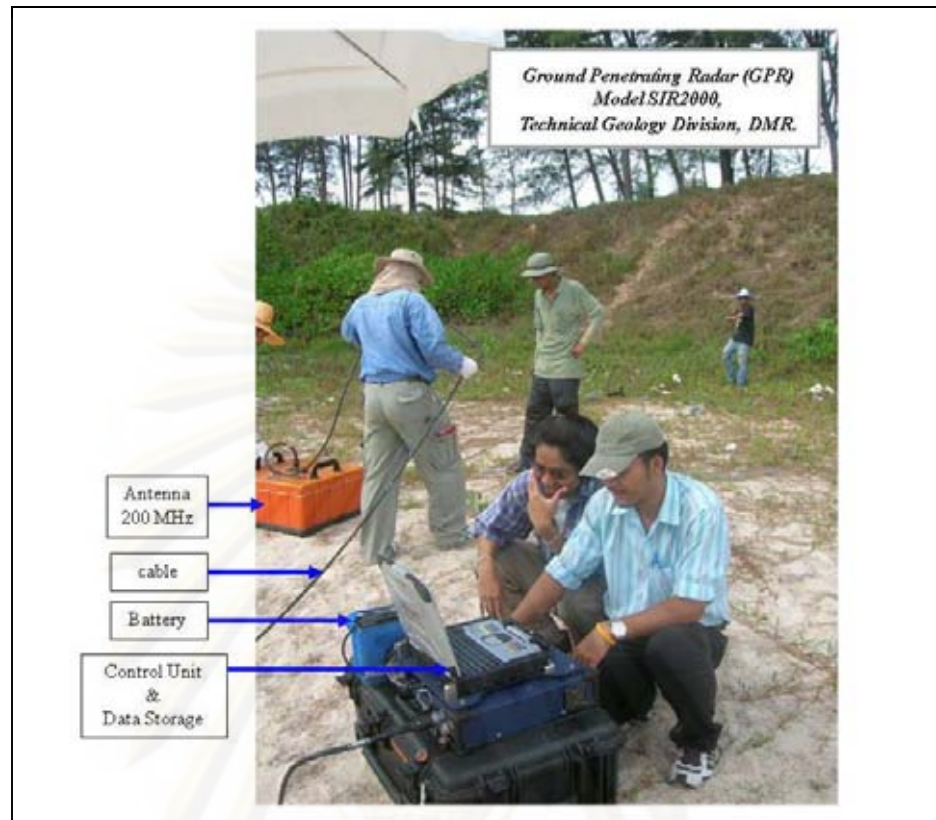


Figure 3.5. GPR model SIR 2000 of DMR used to study subsurface structure of dune with transmitter antenna 200 MHz and depth of penetration is 5 m.

3.3 Laboratory analyses

Grain size analysis

Random 41 samples of sand dune were analyzed the distribution of grain size by Malvern Laser Granulometry at the Petroleum and Petrochemical College, Chulalongkorn University. This later technique is commonly applied to study sedimentary properties of sand and finer grain sizes.

Weighted percent by volume and particle diameter are plotted in form of graphs in order to show distribution of grain size in each sample, then using result of grain size analysis to calculation of statistic parameters to define degree of sorting (Table 3.1-3.3) (Folk, 1968) and plot of standard deviation & skewness to analyze environment deposits (Figure 3.9) (Pettijohn, 1975).



Figure 3.6. Methodology used to collect sample for analysis grain size to define environment deposits, by pitting and auguring.



Figure 3.7. Methodology used to collect sample for define absolute age by optically stimulated luminescence (OSL) dating. Collecting the samples from the top of profile dune is every 0.15 m.

Table 3.1. Calculation of statistic parameters by using result of grain size analysis (after Folk, 1968).

Mean	$(\phi_{16} + \phi_{50} + \phi_{84})/3$
Skewness	$\frac{(\phi_{84} + \phi_{16}) - 2\phi_{50}}{2(\phi_{84} - \phi_{16})} + \frac{(\phi_{95} + \phi_{5}) - 2\phi_{50}}{2(\phi_{95} - \phi_{5})}$
Standard deviation	$((\phi_{84} - \phi_{16})/4) + ((\phi_{95} - \phi_{5})/6.6)$

Table 3.2. Range of standard deviation, using to indicated degree of sorting (after Folk, 1968).

Standard deviation	degree of sorting
under 0.35	very well sorted
0.35-0.50	well sorted
0.51-0.71	moderated well sorted
0.71-1.0	moderated sorted
1.0-2.0	poorly sorted
2.0-4.0	very poorly sorted
over 4.0	extremely sorted

Table 3.3 Classification of skewness (after Folk, 1968).

Skewness	degree of skewness
+1.00 to +0.30	strongly fine skewed
+0.30 to +0.10	fine - skewed
+0.10 to -0.10	near - symmetrical
-0.10 to -0.30	coarse - skewed
-0.30 to -1.00	Strong coarse - skewed

Eolian environment

Sand dune

Sorting good, skewness mostly < 1 coarse-grained tail generally absent.

Loess sediments

Poorly sorted, skewness mostly < 1 much fine grained fraction.

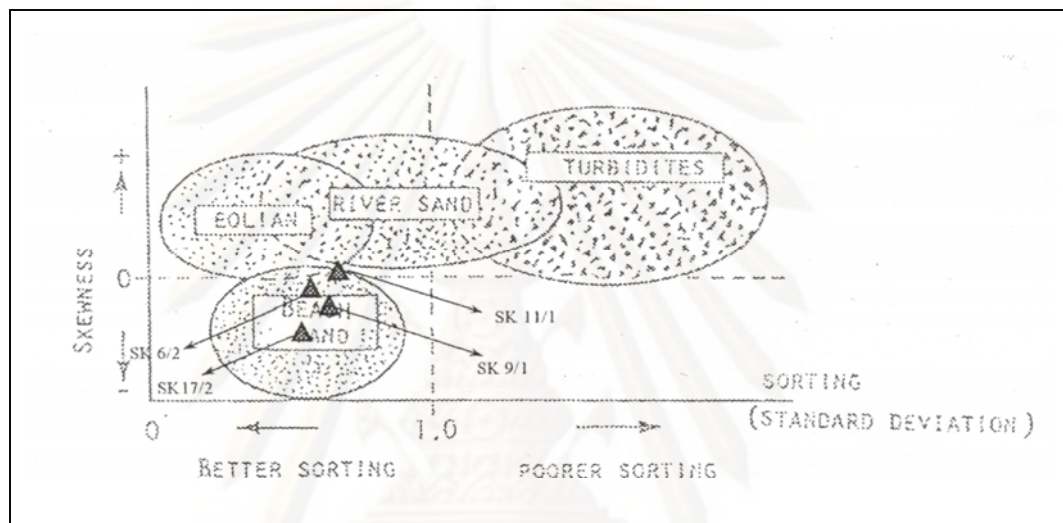


Figure 3.9. Graphs show plot of standard deviation & skewness of grain size distribution to analyzed environment deposition (after Pettijohn, 1975).

3.3.2 Optically stimulated luminescence dating

Optically stimulated luminescence is a method in determining the age of burial of quartz or feldspar bearing sediments based upon principles of radiation and excitation within crystal lattices, and stems from the fact that imperfections in a crystal lattice have the ability to store ionizing energy (Aitken, 1998; Botter-Jensen et al., 2003; Lian, 2007). Radiation within sediments comes from alpha, beta, and gamma radiations emitted during the decay of ^{235}U , ^{238}U , ^{232}Th , ^{40}K , and ^{87}Rb , and their daughter products, both within the mineral grains and in their surroundings (Lian, 2007), and from cosmic rays (Figure 3.10).

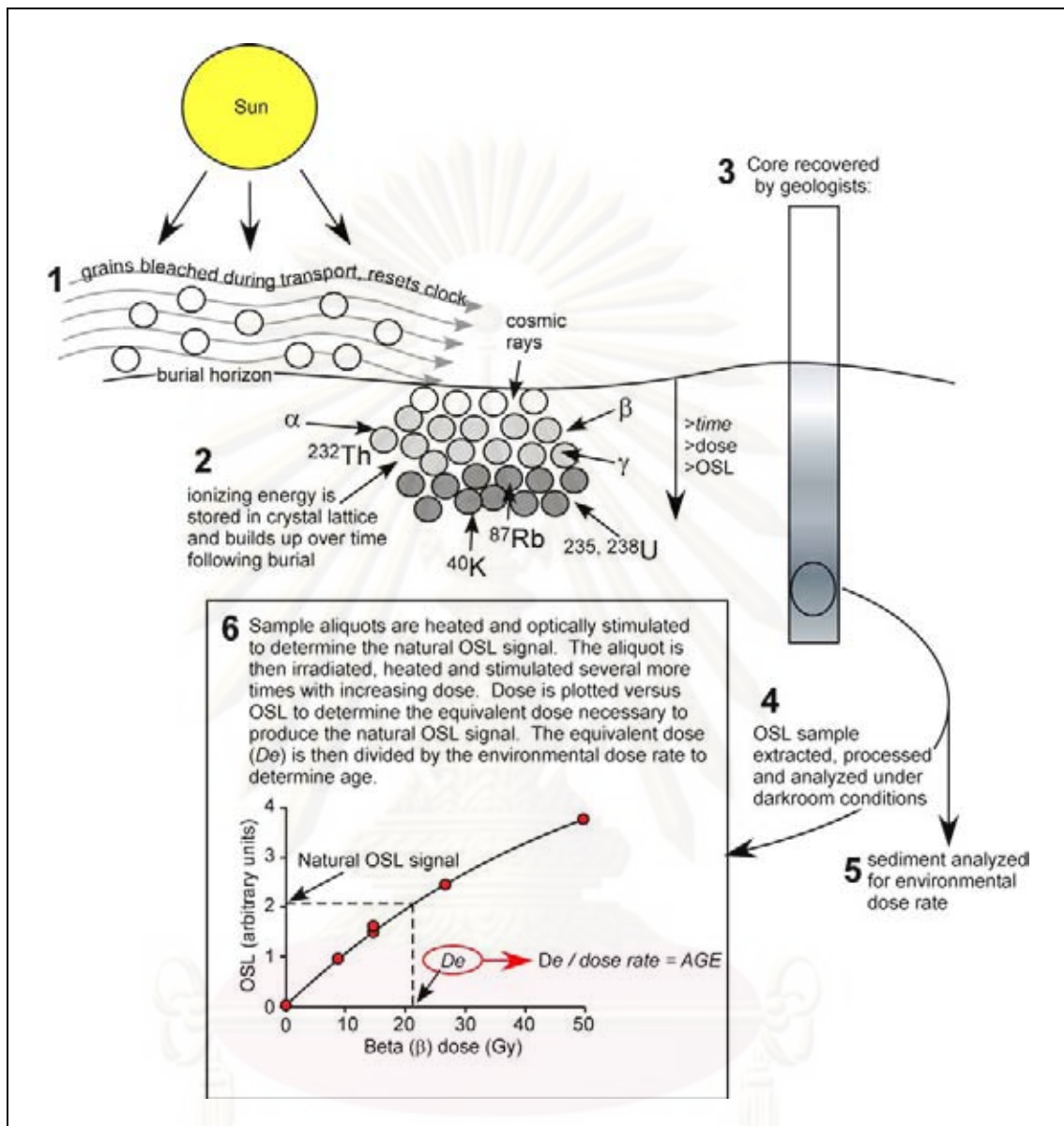


Figure 3.10. Generalized processes that produce the luminescence signal (steps 1 and 2), and the sampling and analytical procedure to determine the age of deposition (steps 3 through 6) (Available from: <http://core.ecu.edu>).

Radiation is absorbed by the crystal lattice upon sediment burial, and over time, excites electrons causing them to migrate within the crystal and become stored in “traps” resulting from crystal lattice defects. This energy is then released as photons in visible wavelengths (luminescence) upon photon irradiation either by exposure to sunlight or artificial light, or by heating ($\sim 500^{\circ}\text{C}$) thus resetting the clock. Under

controlled laboratory conditions, assuming the sample was collected under light-restricted conditions, controlled exposure of the sample to photons yields a luminescence response (the equivalent dose, D_e), the intensity of which is a function of the dose rate within the sediment, and the length of time the sample was exposed to the background radiation. In order to measure the age, two factors must be known; 1) the environmental dose rate and 2) the laboratory dose of radiation that produces the same intensity of luminescence as did the environmental radiation dose (the equivalent dose). Dividing the equivalent dose by the dose rate yields time. Although the fundamental concept is straight-forward, there are many caveats that must be accounted for stemming from partial bleaching of grains during burial, mixing of grains by bioturbation, and pedogenic (soil formation) processes that alter the dose rate over time (Bateman et al., 2003; 2007).

Samples for OSL analysis are typically collected from opaque core tubes (aluminum or black pvc tubes) that are pushed into the sediment using coring equipment (vibracore, geoprobe, etc.), or by manual insertion into sediment exposures along natural bluffs or man-made pits. Samples are then extracted for processing under dark-room conditions. Typical processing of a sample for OSL analysis includes treatment with HCl and H_2O_2 to remove carbonate and organics. This is followed by sieving, heavy liquid (Li- or Na-polytungstate) separation, and (sometimes) magnetic separation to concentrate quartz sands of the appropriate size. Finally, etching with HF is performed to remove the outermost “rind” of the quartz grain. All of the processing must be done under dark-room conditions.

The main component of an OSL laboratory is the “Reader” (Figure 3.11). This device facilitates the determination of D_e , and the creation of a luminescence “growth” curve, which plots luminescence intensity versus laboratory dose rates (beta dose), for a particular sample aliquot (one sample containing ~100 grains). The single aliquot regeneration (SAR) protocol (Murray and Wintle, 2000) is the technique of choice for a variety of applications, and was used for analyses associated with this USGS

investigation. This is done by first exposing the sample aliquot to a known quantity of photons (blue wavelength) and determining the luminescence that occurs in response. The sample is then irradiated with increasing radiation levels (beta), and re-exposed to determine the luminescence that occurs at each irradiation level. The equivalent dose is then determined by applying a regression to the data, and determining the radiation dose that corresponds to the initial luminescence signal. Determining the age is then a simple function of dividing the paleodose by the dose rate that is measured on the surrounding sediments.

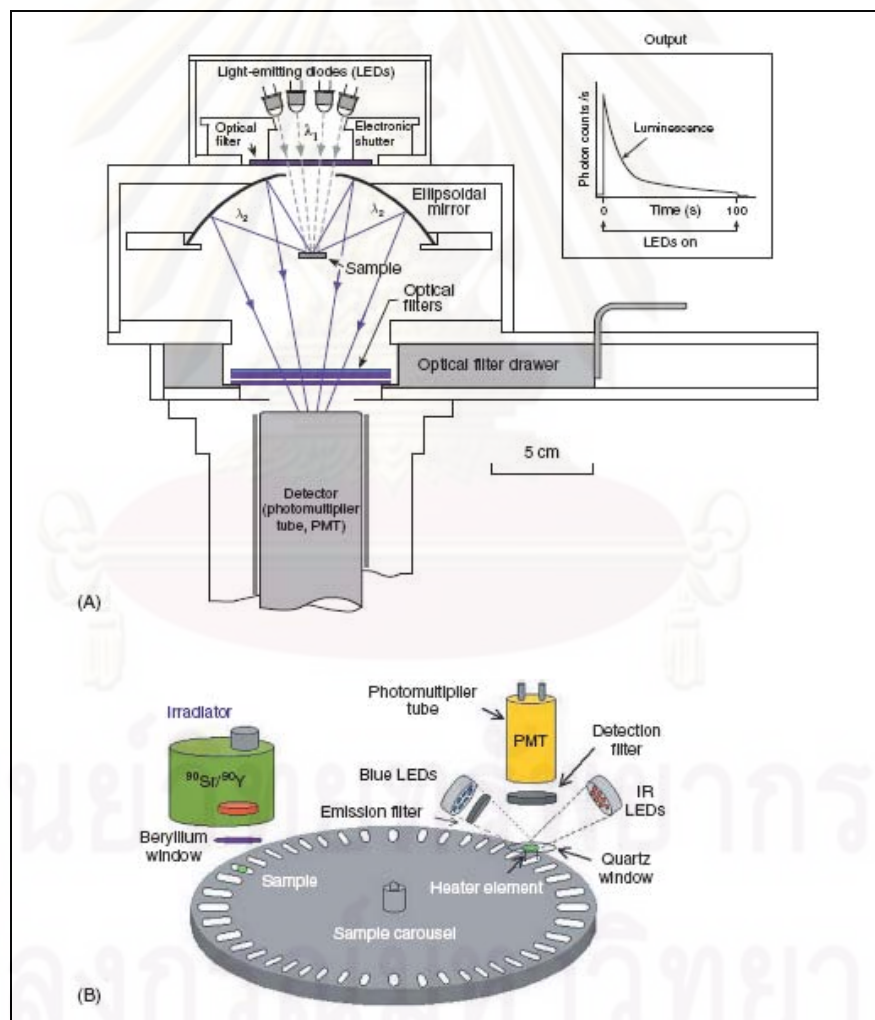


Figure 3.11. Equipment that comprises the “reader”, which is necessary for measuring the paleodose, irradiating the sample, heating the sample, and deriving a “growth” curve (from Lian, 2007) (Available from: <http://core.ecu.edu>).

OSL is used in at least two different applications: optical dating of ancient materials (mainly geological sediments, but also sometimes fired pottery, bricks etc., although in the latter case thermoluminescence is used more often), and as a method of radiation dosimetry which is the measurement of accumulated radiation dose in the tissues of health care, nuclear, research and other workers, as well as in building materials in regions of nuclear disaster.

The difference between radiocarbon dating and luminescence dating is that the former is used to date organic materials and luminescence dating to date minerals, like quartz and feldspars. Events that can be dated using OSL dating are for the deposition of geological sediments after being transported by air (eolian sediments) or rivers (fluvial sediments).

Materials and the time span covered by OSL dating

Luminescence dating is applicable to a wide range of sediments. Most commonly, quartz or feldspar grains, ubiquitous in any sediment are used for D_e determination. Best suited are aeolian sediments such as dune sands or loess. Waterlain sediments such as fluvial, glaciofluvial or littoral deposits can be problematic with respect to OSL dating, due to partial resetting of the luminescence signal during transport and deposition. However, recent methodological approaches, in particular, dating of individual grains of quartz, are able to deal with incomplete bleaching.

3.4 Discussion and Conclusion

Interpretation and data correlation

This step is interpreted signal of GPR and data correlation based on all data from aerial photography, sand sampling, grain size analysis, GPR signals and absolute age from OSL dating. This correlation was used for constructing models to explain the formation of sand dune in the study area.

The feature of internal structure within the dune is possible to classify into GPR units using the principles of radar stratigraphy, which relies on the identification of systematic terminations or boundaries, to qualitatively classify different reflection patterns from the profiles. This classify is the first used of GPR facies in this area and can be served as a basis for comparisons with other studies parabolic dune and may also serve as a reference for comparing with other dune morphologies.

Interpret transect 2D GPR data, the characteristic reflection patterns of radar signal related to environment deposits in this thesis is mainly followed the terminology proposed by Neal (2004) and Hogenholz et al. (2007). In order to identify and describe environment deposits followed Overmeeren (1998) and Hogenholz et al. (2007), correlated with DMR logs (2006), dune morphology and hand augers drilling in field work.



ศูนย์วิทยทรัพยากร
จุฬาลงกรณ์มหาวิทยาลัย

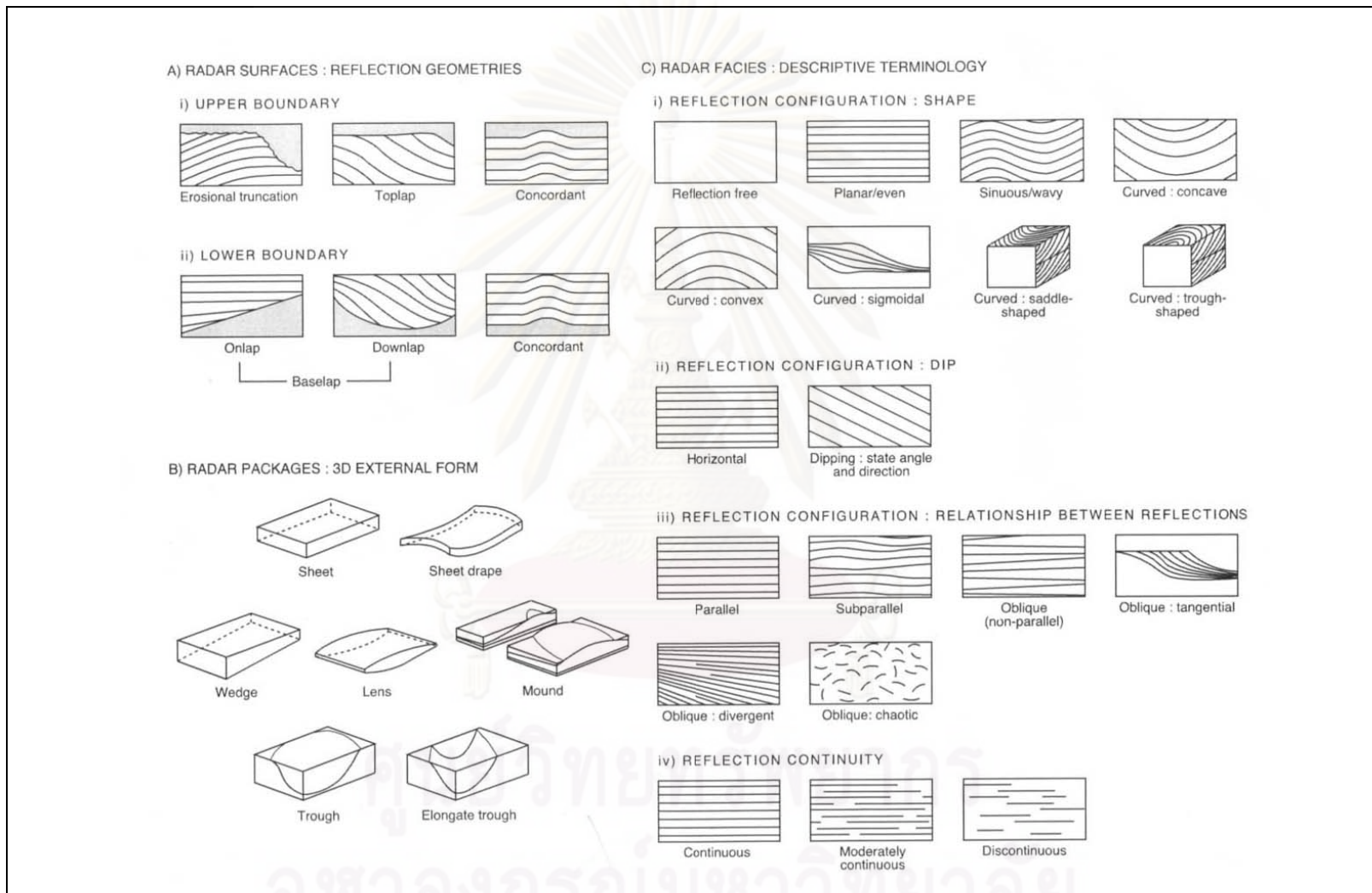


Figure 3.12. Terminology to define and describe radar surfaces, radar packages and radar facies (Neal, 2004).

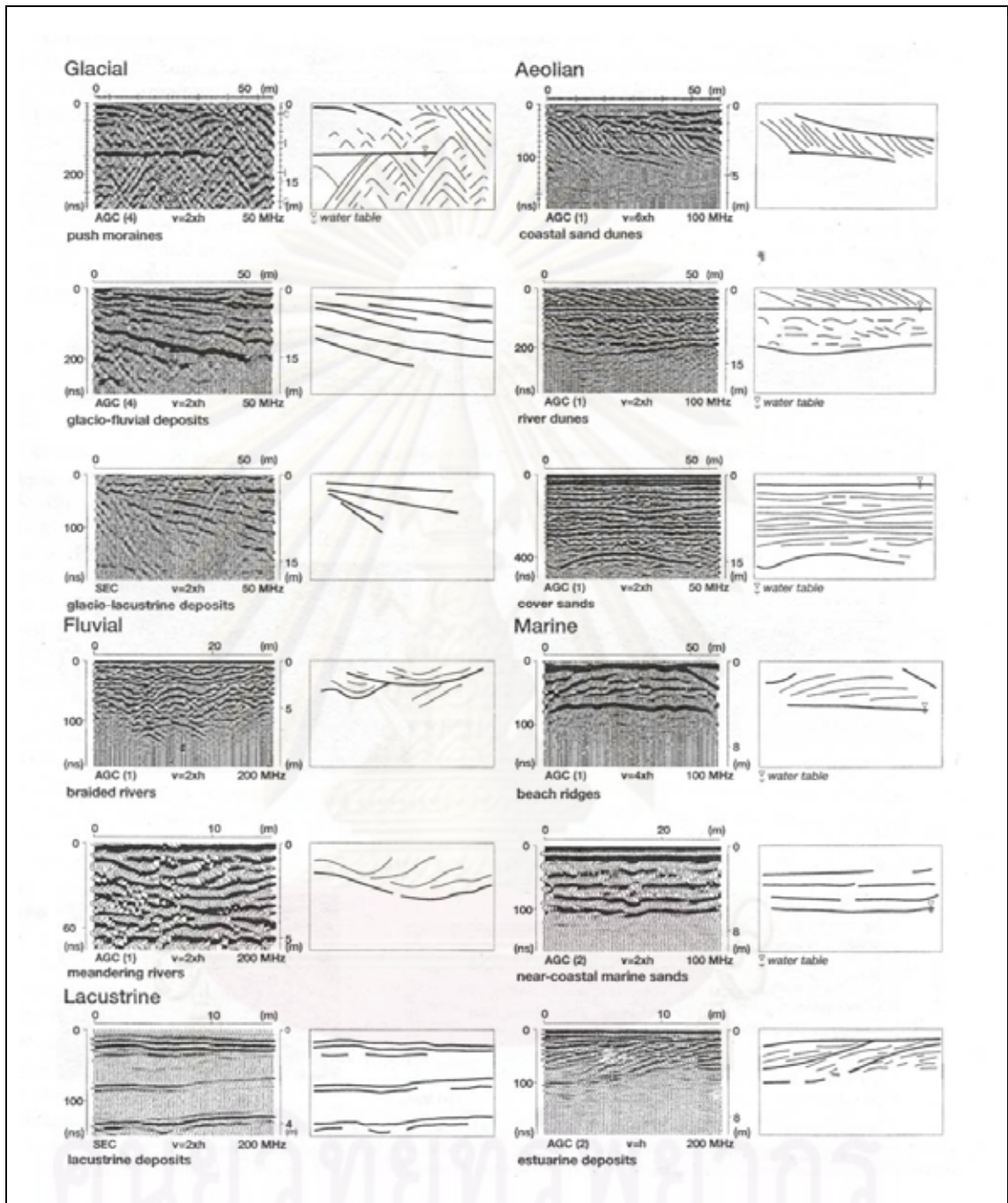


Figure 3.13 Radar facies chart of characteristic reflection patterns from various sedimentary environments (Overmeeren, 1998).

Table 3.4. Radar facies element of different sedimentary depositional environment (Overmeeren, 1998).

environment	reflection amplitude	continuity reflections	Reflection configuration	External form (geometry) of facies unit
GLACIAL				
push moraine	low	non or low	chaotic with diffractions	sometimes glacio-tectonic structures
glacio-fluvial	high	high	parallel stratified sequences	sheet or fan
glacio-lacustrine	medium	high	parallel to divergent	sheet or wedge (wedge shape at edges)
AEOLIAN				
coastal sand dune:	low	limited	cross-bedding	cross-bedding and boundary
sand peat	high	high	undulating	planes
river dune:	low	limited	cross-bedding	cross-bedding units underlain
sands loam base	high	high	horizontal	by flat base layer
cover sands	medium	high	coherent parallel, occasionally cross-bedding	sheet
FLUVIAL				
braided rivers	low	low	wavy, discontinuous; prograded of trough-shaped; diffraction	channel fill or troughs
Meandering rivers	low	low	sigmoid	point bars
LACUSTRINE				
fen pools	high	high	sigmoid	sheet or wedge
MARINE				
beach ridge	low	limited	oblique (low angle slope)	mound; high-amplitude peat reflections at edges
estuarine deposits	medium	limited	oblique set	longitudinal cross-bedding in tidal channel fill
Littoral deposits	low	large	parallel stratified	sheet

CHAPTER IV

RESULT OF STUDY

This chapter shows all results of this work, which can be described in ascending order.

4.1 Aerial photo interpretation

4.1.1 Sedimentary units

Geology and geomorphology of the study area are interpreted from aerial photographs and, then, complied with all previous works that can be divided into 9 geomorphological units (Figure 4.1) as follows:

4.1.1.1 Limestone (Ls): this unit appears in the northern, western and southern parts of the study area. These landforms show in the aerial photographs as karst topography and dark gray tone.

4.1.1.2 Sandstone interbedded with conglomeratic sandstone (Sst): this unit dominates in the southern part of the study area. The landforms shown in the aerial photographs are gray tone color. The light gray tone in the aerial photographs represents sedimentary rocks in comparison with the previous geological mapping by DMR (2006). These landforms are commonly displayed in the aerial photographs as small mesa morphology.

4.1.1.3 Colluvial deposits (Q_c): this unit appears in the western part of the study area and contains gentle angle of slope along the plain from the west to the east.

4.1.1.4 Terrace deposits (Q_t): this unit is located in the western part of the study area formed by former meandering channels.

4.1.1.5 Alluvial deposits (Q_a): this unit dominates in the western part of the study area prior from the relict terraces of small channels.

4.1.1.6 Lagoonal deposits (Q_{lg}): this unit is a part of coastal plain and located in the central part of the study area. The landform was clearly identified from the aerial photographs as gray tone color. The gray tone in the aerial photographs also represents sediments deposited within swale between dune ridges covering with dense vegetation.

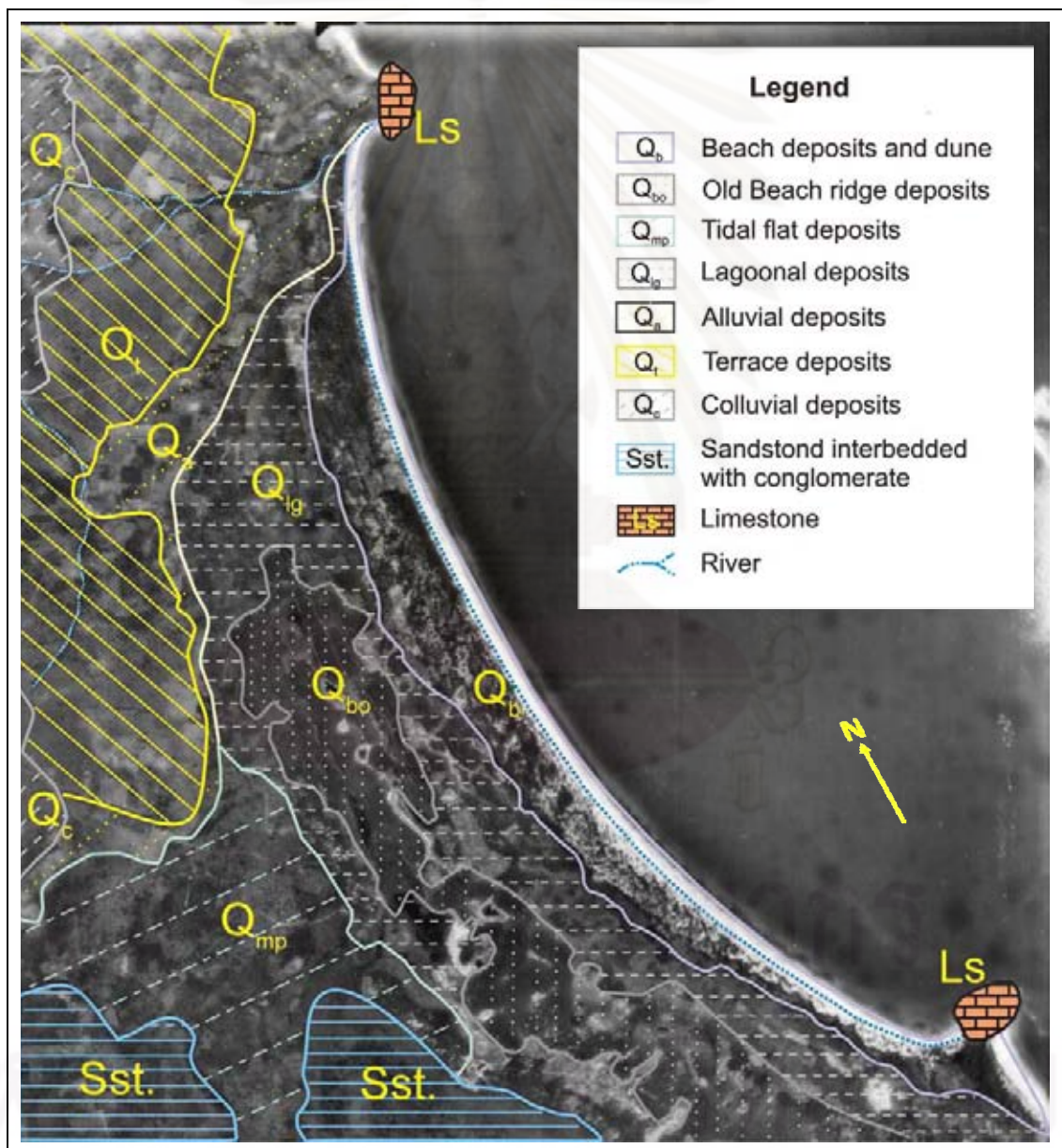


Figure 4.1. Geomorphological units in this area overlain on aerial photograph (details in text).

4.1.1.7 Tidal flat deposits (Q_{mp}): this unit can be seen clearly in the southern part of the study area. The landforms seen in the aerial photographs were represented by gray tone color to which they can be inferred as the mangrove area.

4.1.1.8 Old beach ridge deposits (Q_{bo}): this unit covers almost half of the eastern part of the study area. Series of beach ridges show clearly in the aerial photographs as light gray tone color with irregular topography of ridges and swales.

4.1.1.9 Beach deposits and dune (Q_b): this unit dominates in the eastern part of the study area where the elevation of dune is higher than beach ridge plain nearby. These landforms are the main target for this thesis. They show in the aerial photographs as dark gray tone and white tone color. The dark gray tone in the aerial photographs represents sand sediments and plants growing on the sand dune, and white tone in the aerial photographs represents beach.

4.1.2 Distribution of sand dune and dune morphology

Bang Berd sand dune is distributed between the northern part of Changwat Chumphon and adjacent areas in the southern part of Changwat Prachuap Khiri Khan. Recently, this area is commonly hit by many wind directions (Appendix E), wherever winds periodically reverse direction. Thus, the present area has characteristic of compound dune (smaller dunes of similar type and slip face orientation are superimposed). Star dune in the southern part of the area represents a wind regime that has changed the intensity or direction after the formation of the dune.

As a result from aerial photograph interpretation, dune field distributes along the coastal plain mostly parallel to the present shoreline. In general, dune field can be subdivided into two zones; the coastal dune close to shore and the former dune close to the swampy area in the west (Figure 4.1).

Coastal dune lies parallel to the shoreline in almost north-south trending with dimension of the dune body as wider as 500-600 m in the north and subsequently

narrower to the south. Dune in the northern part of the area owns very low elevation with small irregular topography in comparison with the southern part. However, the widest dune field is recognized in the middle part of the area where the highest elevation reached about 20 m above the present mean sea level. Dune in the southern part becomes narrow but the elevation is somewhat equivalent to dune in the middle part of the area. Old sand dune is interpreted to overly on top of the former beach deposits with its wider distribution than those younger dunes.

Dune morphology shows the majority of parabolic and transverse patterns, star shapes were rarely and locally recognized (Figure 4.2). Parabolic shape dominates in the outer part of dune field close to shore; transverse morphology is localized in the western end of dune field; star pattern is locally recognized in the southern portion. Most of dune shapes indicate the major direction of wind blown from the east to the west.

4.2 Topographic survey

The elevation of dune field varies from 10 m in average to 25 m above the underlying beach ridge plain. Topography of dune fields in this area changes from the highest dune in the southern part of the study area, slightly low to the north. A detailed topographic survey along shore normal transects perpendicular to the shoreline is shown in Figure 4.3 (Appendix A). Most of dune topography display as parabolic and transverse morphologies of dune crest and swale within dune field itself (Figure 4.4).

4.3 Ground penetrating radar (GPR)

The aim of this result section is to show the interpretation from GPR images aiming to document and enhance the internal dune structures within the dune. GPR was undertaken at Bang Berd sand dune during October 2008. A survey shore-normal and shore-parallel transects were laid out and a total of 5 transects, with a total length of 1,510 m (Figure 4.5) were also assigned to characterize the continuity of deposit, boundary between beach and dune and thickness of dune. In this study, GPR surveys were done in the outer part of dune field (parabolic dune) close to shore at different

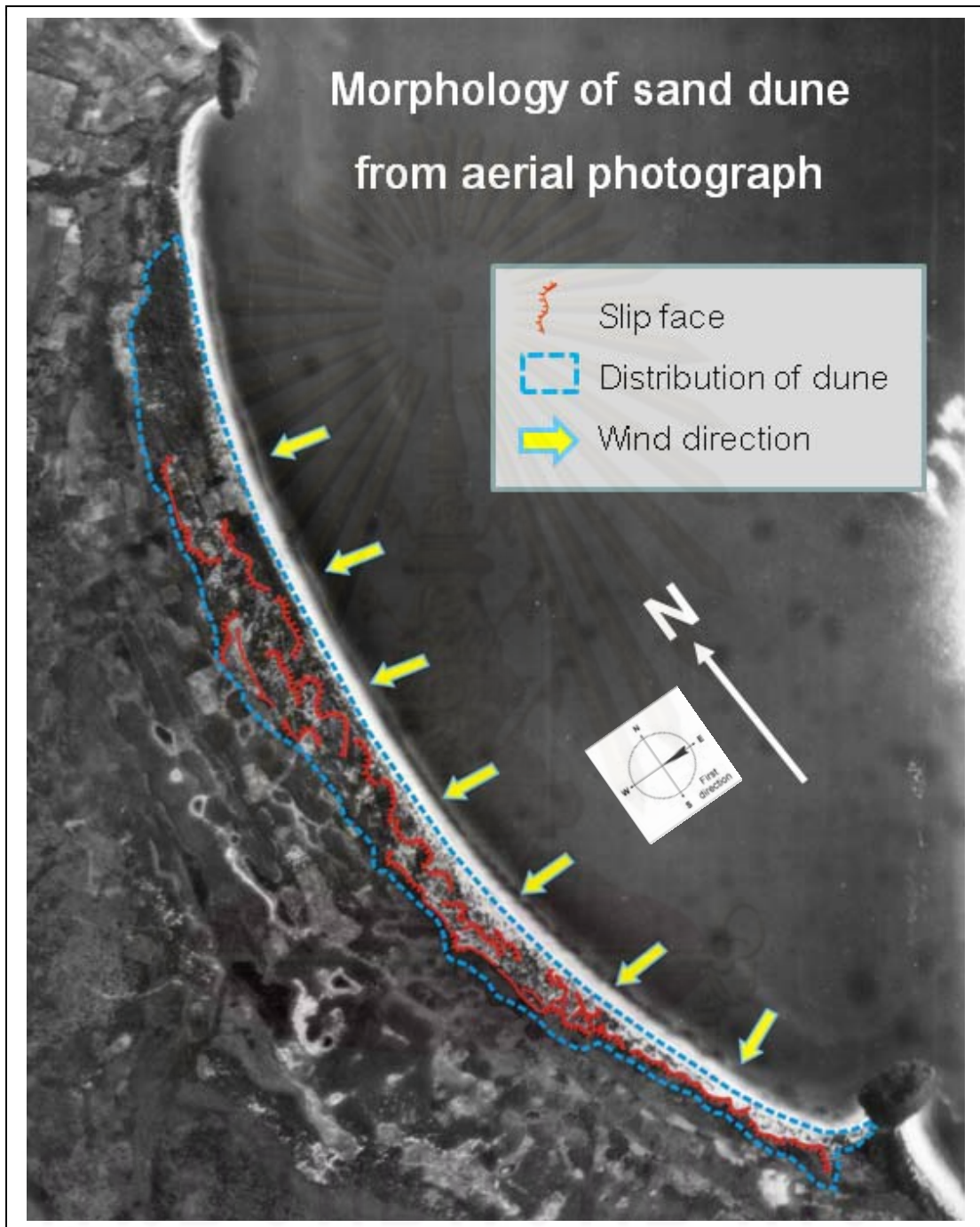


Figure 4.2. Patterns of sand dune with their distributions, parabolic shape dominates in the outer part of dune field close to shore; star pattern is locally recognized in the southern portion and transverse morphology is localized in the western end of dune field. The major direction of wind blown was from the east to the west.

portions, plus 200 MHz GPR was used. The radar frequency and the properties of sand dunes limited the penetration of the radar signal to the uppermost 5 m. The reflections are recorded in real time and displayed on a monitor in the field to provide real-time data quality. During the survey, traces were collected every 0.50 m. Topography was also measured at 0.50 m spacing along the same GPR profiles using high accuracy survey camera.

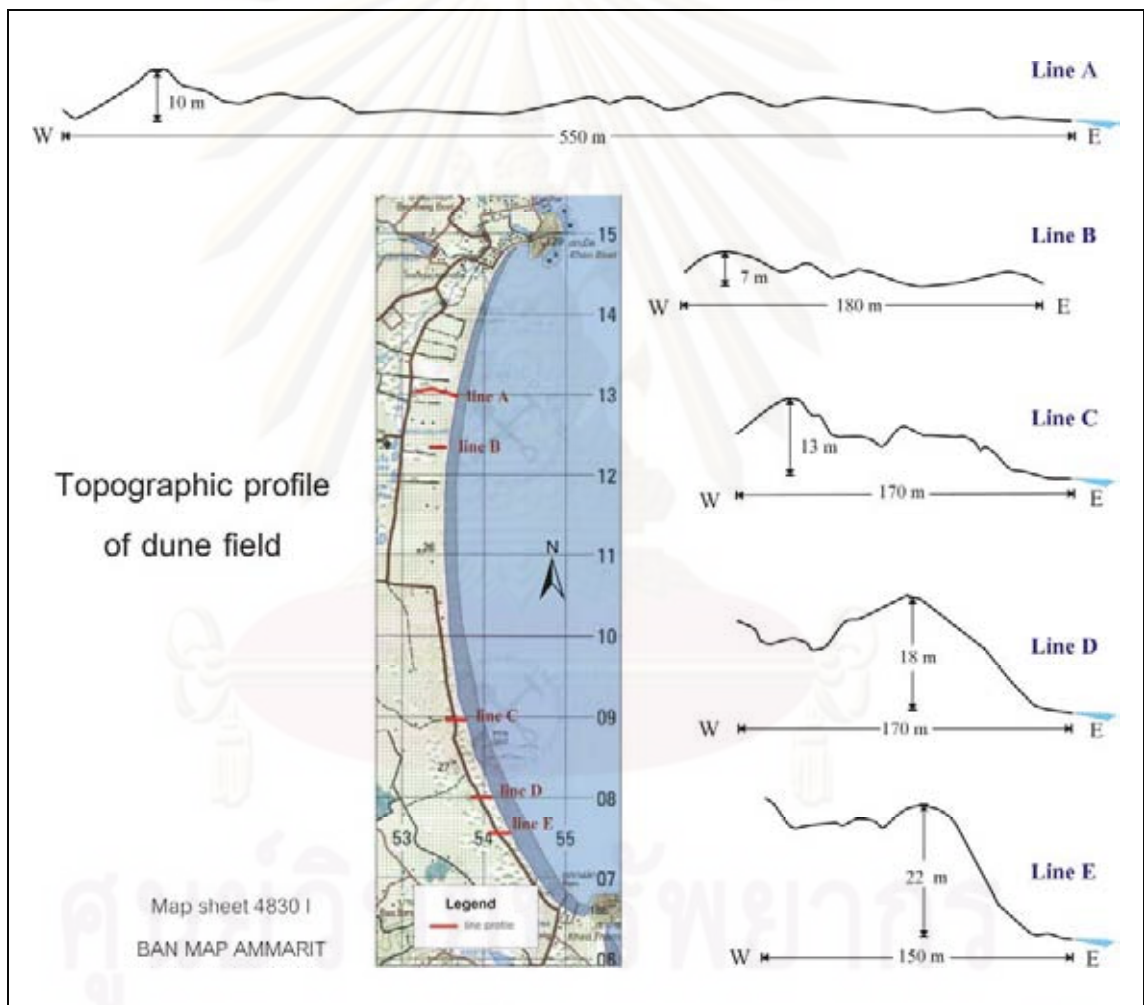


Figure 4.3. Topographic profiles of dune field in the outer part of dune field close to shore at different portions. The highest elevation of dune crest is recognized at line E with about 25 m above the present mean sea level, southern part of dune field.

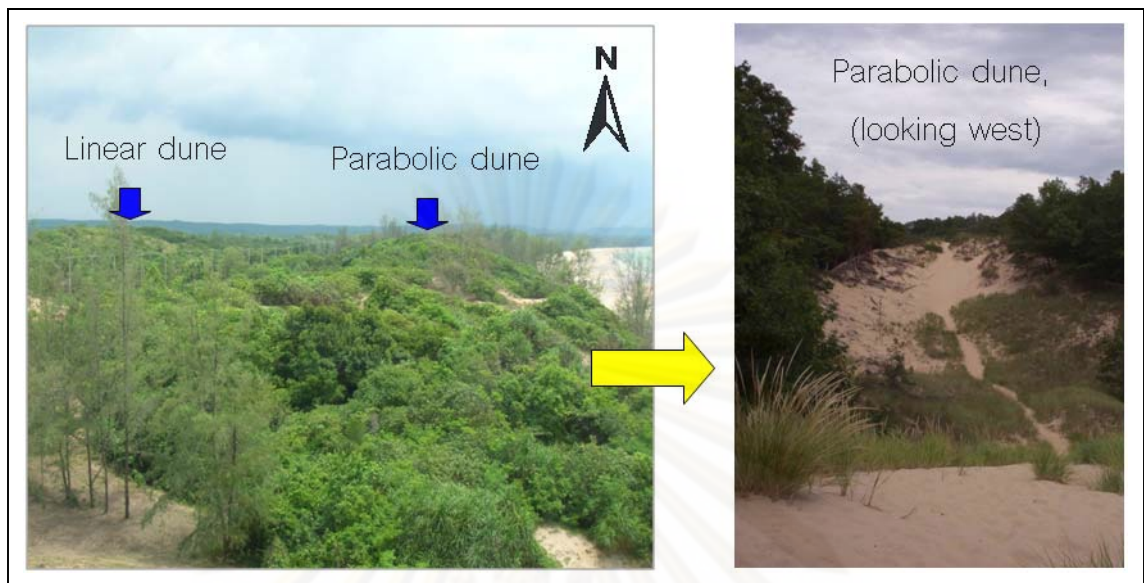


Figure 4.4. Parabolic shape dominates in the outer part of dune field close to shore, transverse morphology is localized in the western end of dune field; star pattern is locally recognized in the southern portion.

Basically, GPR lines were conducted along – transects oriented parallel and perpendicular to the dune's downwind axis (Appendix A). Transects parallel to the prevailing wind are labeled as GPR 4, GPR 5, GPR 7, GPR 9, GPR 10, GPR 11, and GPR 12. Transects perpendicular to the prevailing wind, on the top of dune are labeled GPR 3, GPR 6, GPR 8, GPR 13, and GPR 14. Consequently, the profiles were not extended onto the slip face.

Transect 2D GPR data

GPR transects of the actively migrating of dune; their locations are shown in Figure 4.5 (inset, red line). Figures 4.5 to 4.11 show the interpretation of the main features in the radargram. The characteristic reflection patterns of radar signal related to environment deposits in this thesis is mainly followed by Overmeeren (1998) and Hogenholz et al. (2007) and correlate with DMR logs (2006), and hand augers drilling.

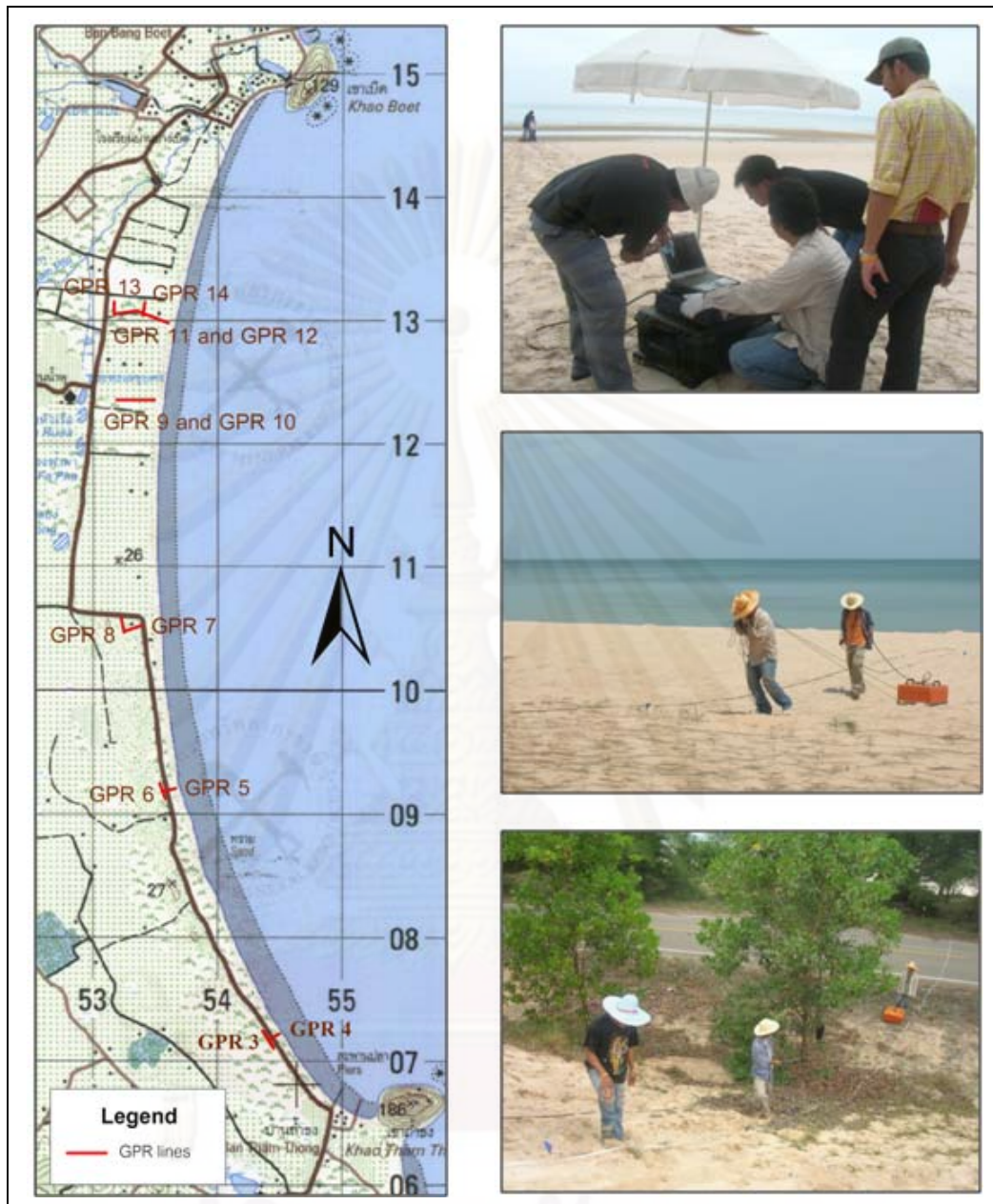


Figure 4.5. GPR lines survey was conducted along – transects oriented parallel to the prevailing wind are labeled as GPR 4, GPR 5, GPR 7, GPR 9, GPR 10, GPR 11, and GPR 12 perpendicular to the prevailing wind, on the top of dune are labeled GPR 3, GPR 6, GPR 8, GPR 13, and GPR.

GPR profiles oriented parallel to the prevailing wind

The resolution in the radargrams was sufficient enough to view in detail of the macro-scale internal sedimentary structures. They can be divided in terms of the environment of deposition into 3 types. They are marine environment, eolian environment and channel filled deposits (Havholm et al., 2003) (Figure 4.6). All profiles show the clear contact between marine sediments on bottom and eolian sediment on top. The radar profile indicates that small channel filled deposits occur only underlying beach ridge at GPR 11.

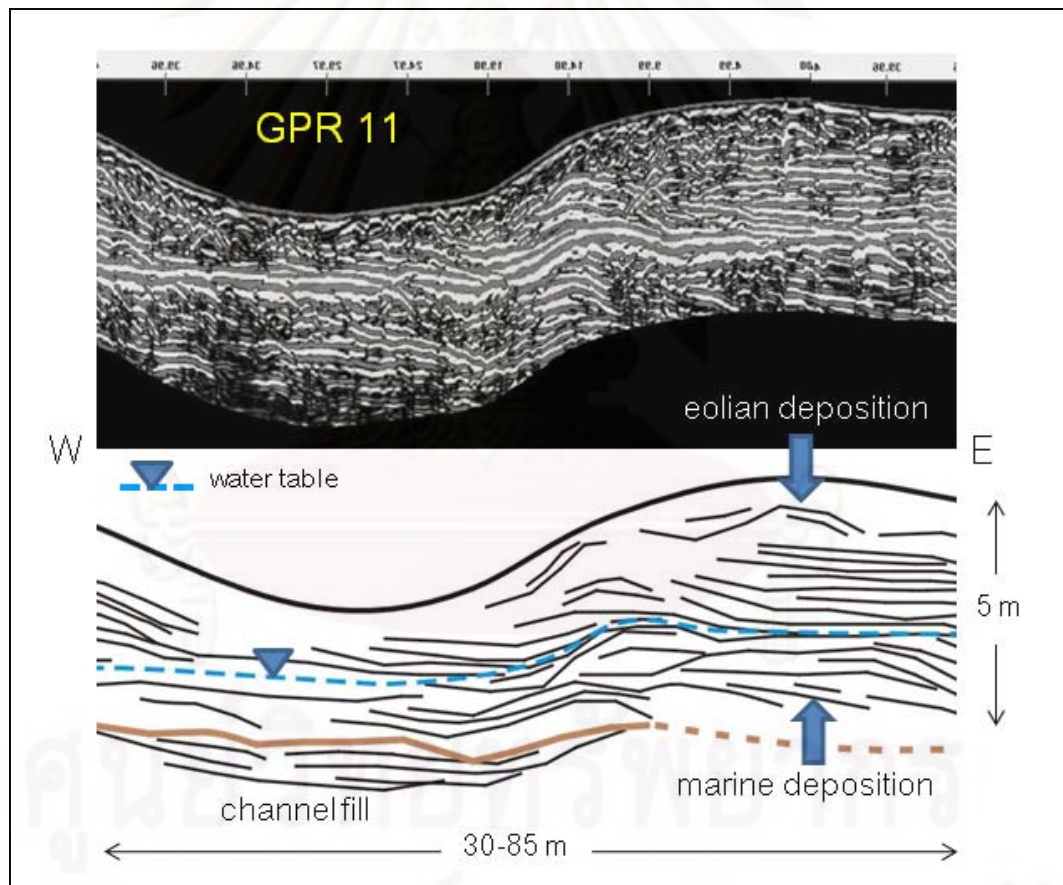


Figure 4.6. Processed GPR profile in E-W direction, the characteristic reflection patterns of radar signal related to eolian deposits on top (reflection continuous and horizontal or slightly undulating), marine deposits on bottom (reflection oblique dipping seaward of beach ridge), and channel fill is overlain by beach ridge (reflection trough).

The sandy composition of the eolian environments offers good conditions for GPR surveying. The characteristics of eolian deposits can be divided to 2 units, including coastal sand dune (unit D1) with cross-bedding in foresets and bounding planes; and covered sand (unit D2) with parallel continuous reflections (Galgaro et al., 2000) (Figure 4.7). The typical feature of eolian structure is cross bedding and the erosional surface.

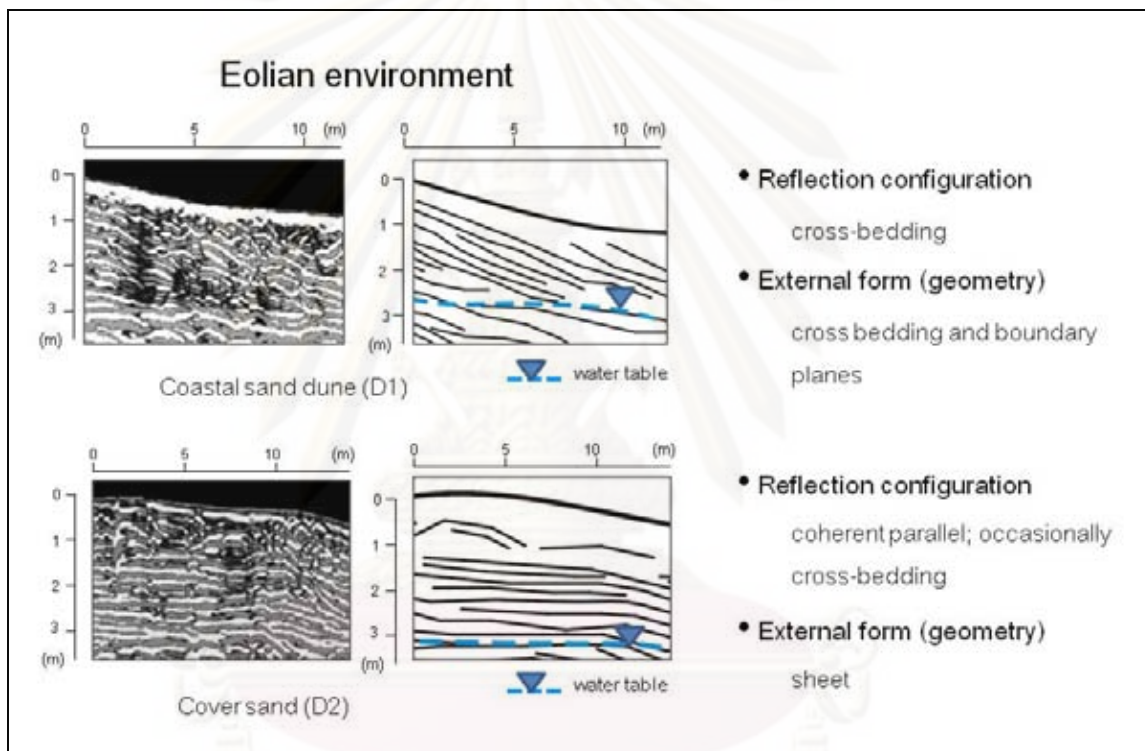


Figure 4.7. Characteristic reflection patterns of eolian environment can be divided into 2 units as the coastal sand dune (D1) with cross bedding in foresets and bounding planes, and covered sand (D2) with parallel, continuous reflections overlying.

The 200 MHz radar section in Figure 4.7 is an example of a radar image of coastal sand dune, which is imaged almost entirely below the water table. Sets of short foresets dipping rather steeply to the east are bounded by more horizontal erosional surface, representing coastal sand dune. Covered sand deposits by wind are in large

parts of the Bang Berd sand dune. The reflections of covered sands deposits are continuous and horizontal or slightly undulating. The shallowest high-amplitude reflection represents the water table.

Radar profile of GPR 9 and GPR 10 shows contact between three different dune generations to which they represented at least 3 depositional events. They can be divided a phase of dune depositions into 3 subunits (subunits d1, d2 and d3 in Figure 4.8) by third order bounding surface (mark 1, 2 and 3 in Figure 4.8) and the difference of angle foresets. Eolian subunit d1 represents the depositional history that appears to be more complexity, judging by variation of the foresets dips, inside d1. Units d2 and d3 show interface separating different dune generations and dip angles about 30° in W-E direction. Therefore, judging by the similarities of the foresets dips inside D1, D2 and D3, the prevailing past wind was probably from the east to the west. All subunits represent the coastal sand dune with cross-bedding in foresets and bounding planes. Sets of foreset dip are rather steeply to the east.

GPR profile shows major slip faces at the western part of dune (Figure 4.9), representing the probable major direction of wind blown. In the first state of its formation, the wind was expected to blow from the east to the west. Although, radar signal at the top most of the dune in some place was chaotic, but it represented the direction of wind change seasonally.

The characteristics of marine deposits can be divided into 2 units. The first is beach ridge (unit B1) generally dipping seaward and the second is littoral deposit (unit B2) (Figure 4.10). Beach ridge with systematic stratification dipping a few degrees towards the sea is one of characteristic features (Jol et al., 2002; Neal et al., 2003; Bennet et al., 2009).

The 200 MHz radar section in Figure 4.10 is an example of a radar image of a beach ridge. The deeper horizontal, continuous high-amplitude reflection inside the beach ridge structure has negative polarity and represents the regional water table.

Littoral marine deposits are horizontally continuous over large distance. They consist of parallel, horizontal and well-stratified sands. The sands were deposited in a near coastal (littoral) environment.

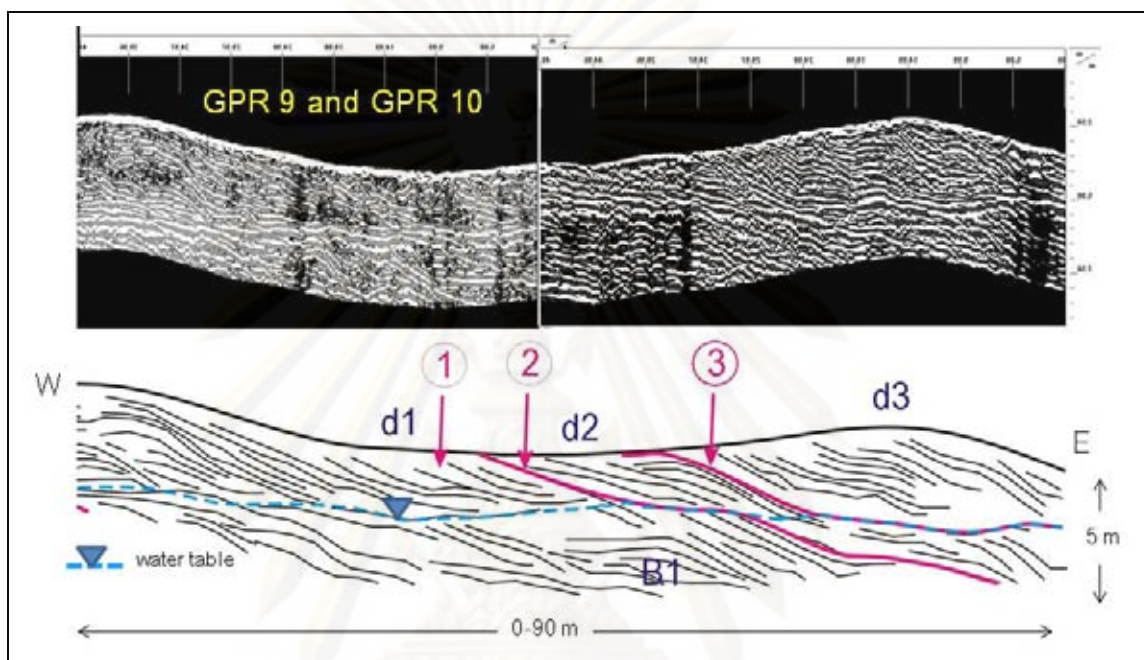


Figure 4.8. Event depositions of dune can be divided into 3 events (subunits d1, d2 and d3) by third order bounding surface (mark 1, 2 and 3): mark 1-individual forest, mark 2-interface separating different dune generations or second bounding surface, and mark 3-third order bounding surface. The water table represents a surface of beach ridge deposit (B1), underneath dune deposits.

The regional water table can be related with continuous high-amplitude reflection inside the beach ridge structure. The water table was also detected and its depth was checked by measuring the depth from hand auger drilling and DMR logs.

Channel filled deposit (unit C) underneath beach ridges is represented by trough- or channel-shaped reflections configuration (Ekes and Hickin, 2001; Bowling et al., 2007) (Figure 4.11). The boundary between beach ridge and channel filled is characterized by gravel bed found in hand auger drilling.

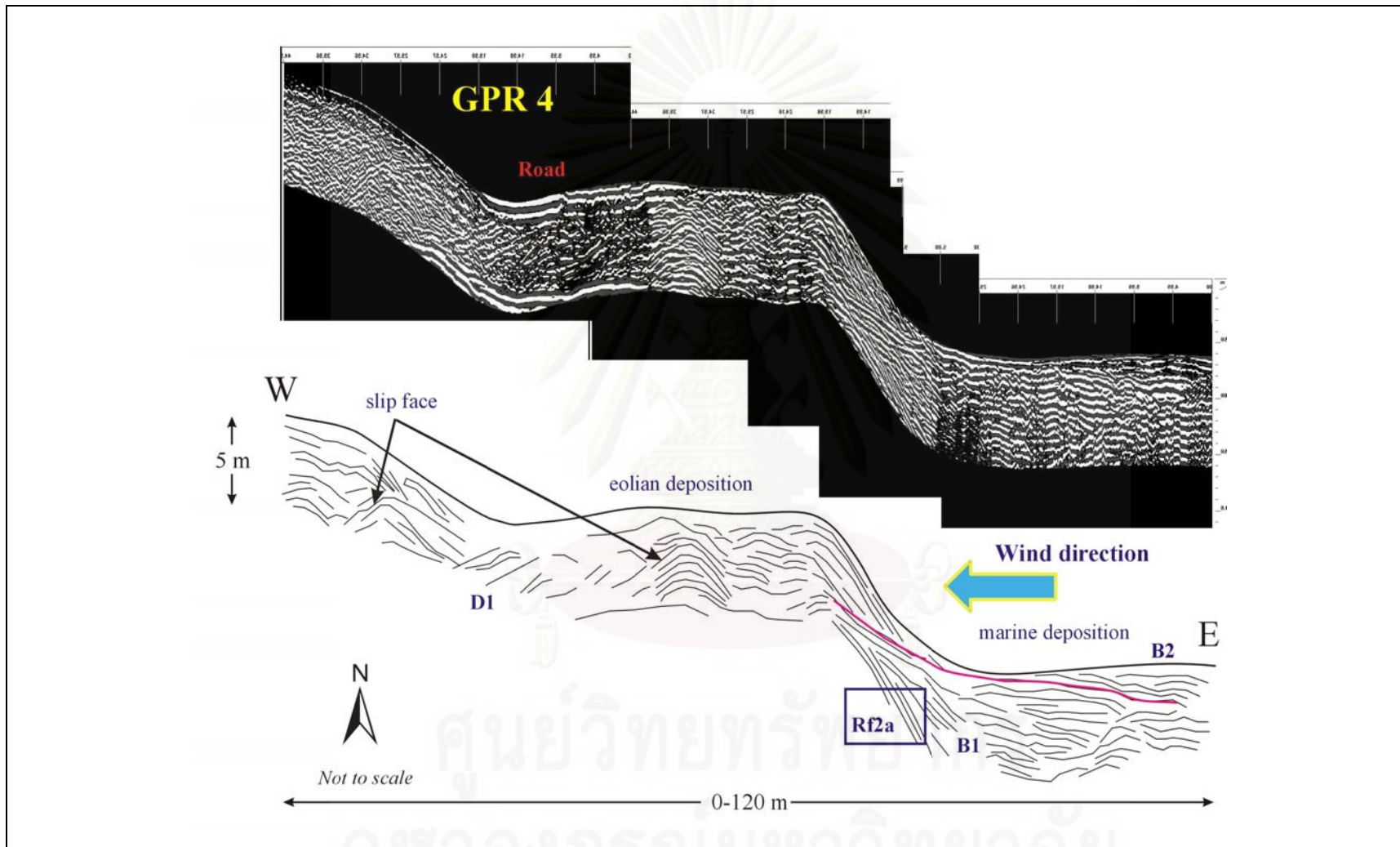


Figure 4.9. GPR profile oriented parallel to the dune's downwind axis show the slip face at the western part of dune.

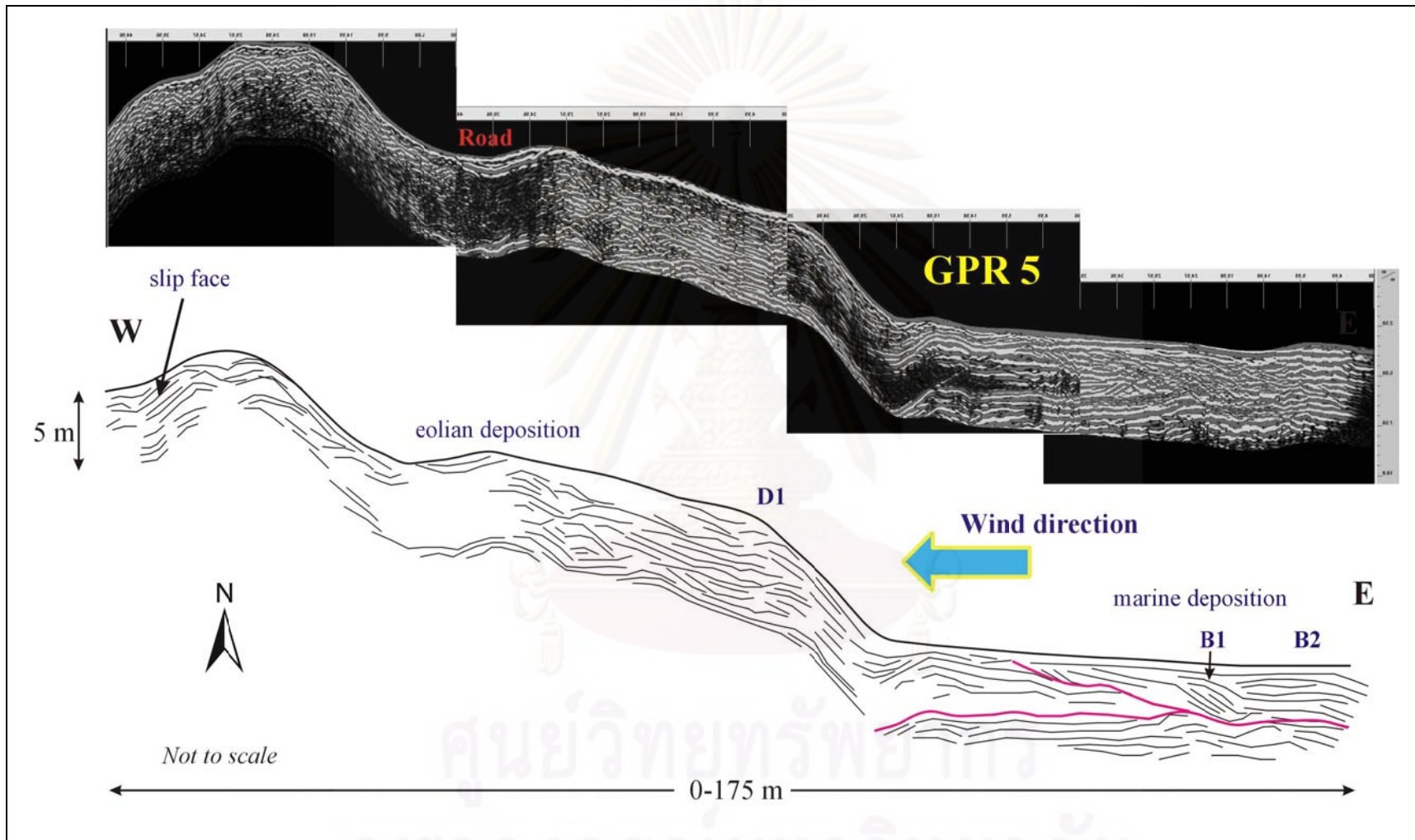


Figure 4.9. (cont.)

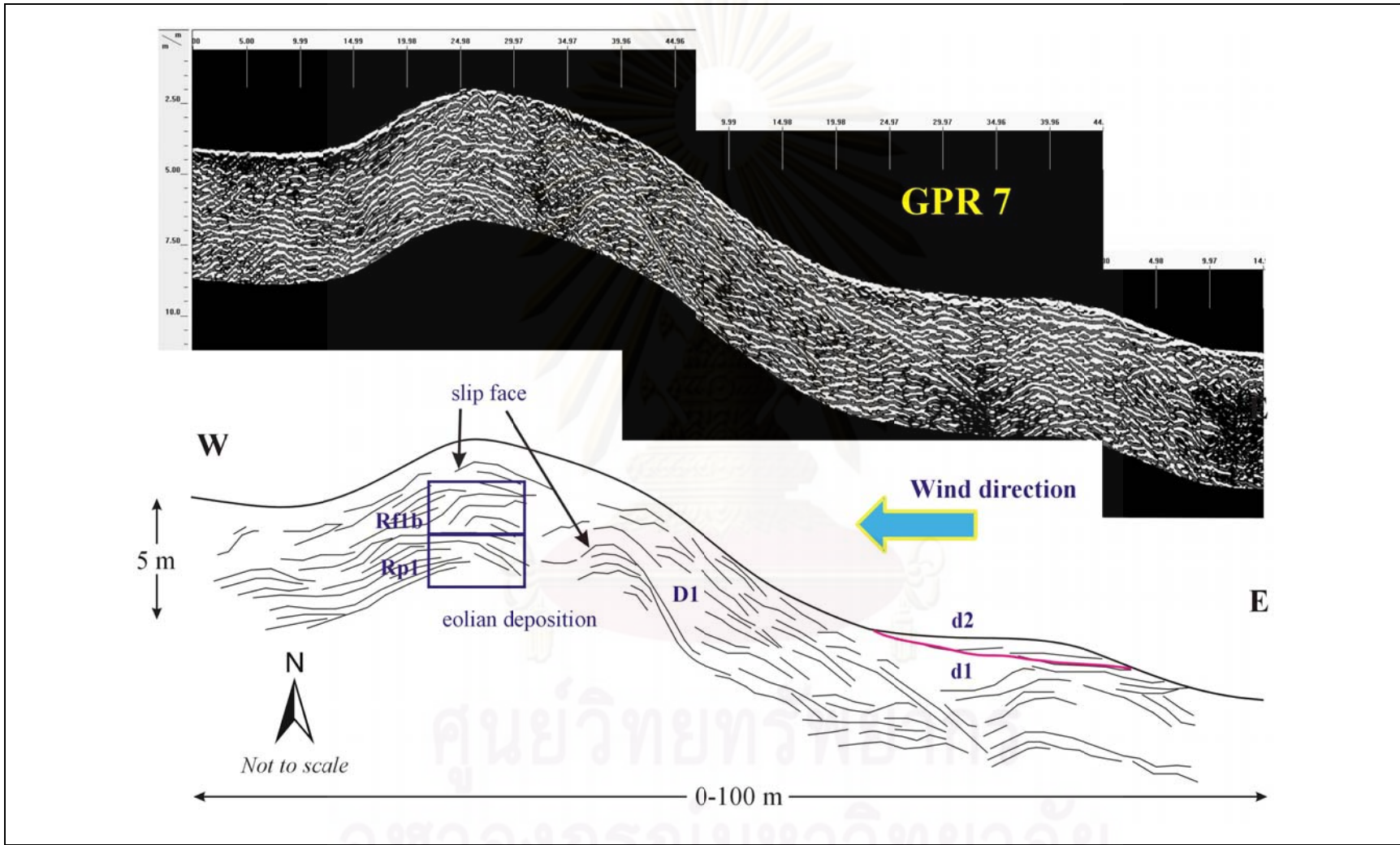


Figure 4.9. (cont.)

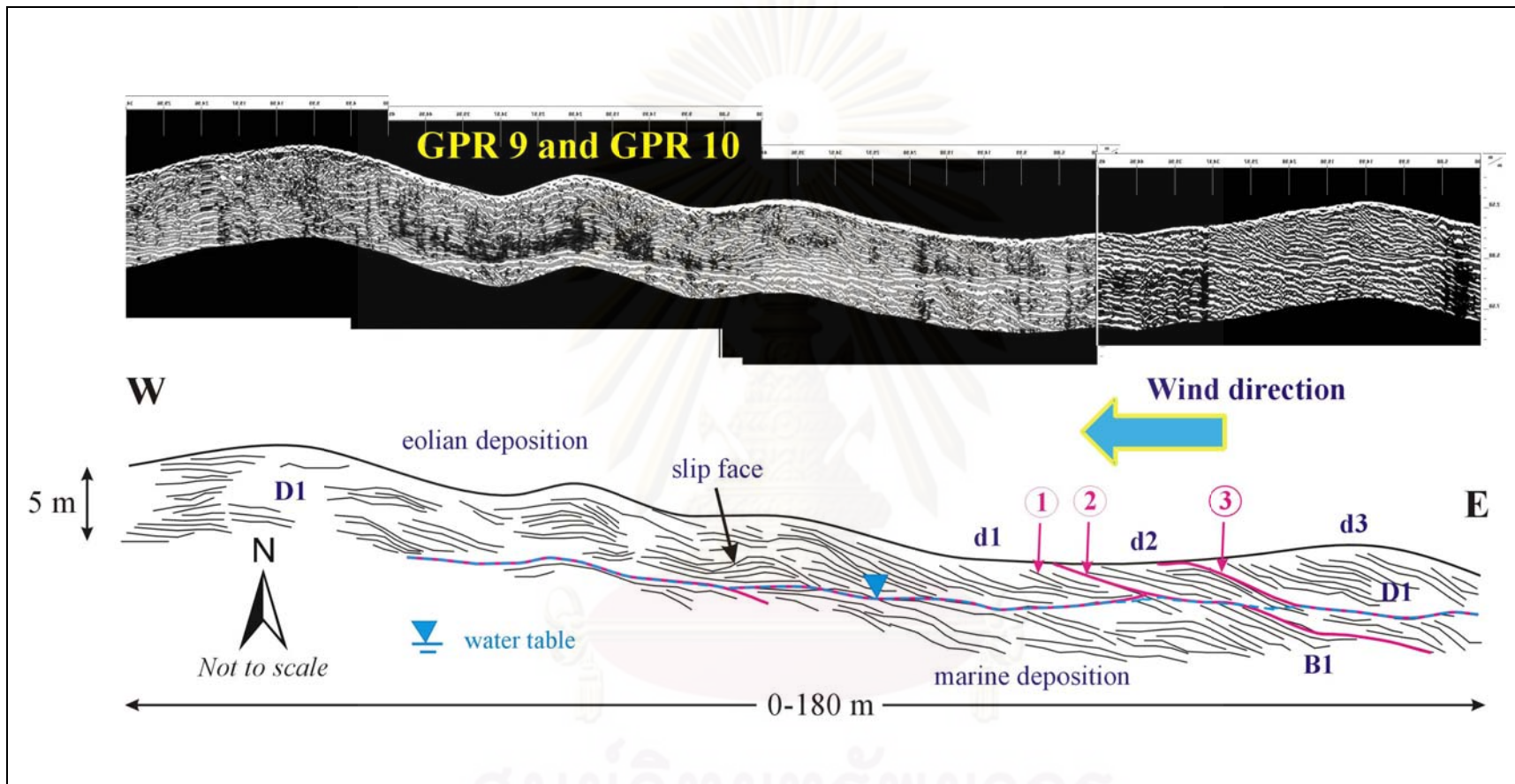


Figure 4.9. (cont.)

ศูนย์วิทยทรัพยากร
จุฬาลงกรณ์มหาวิทยาลัย

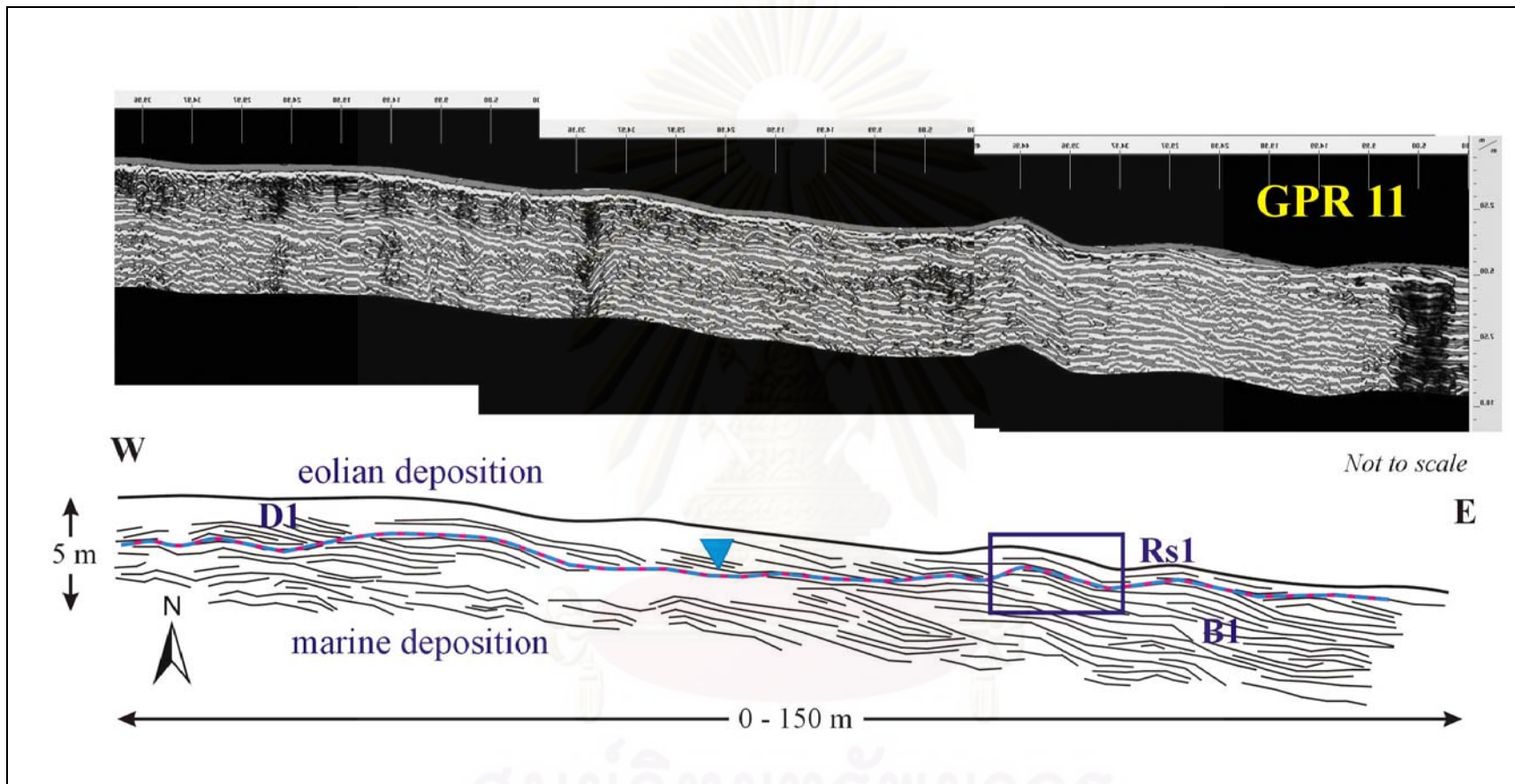


Figure 4.9. (cont.)

ศูนย์วิทยทรัพยากร
จุฬาลงกรณ์มหาวิทยาลัย

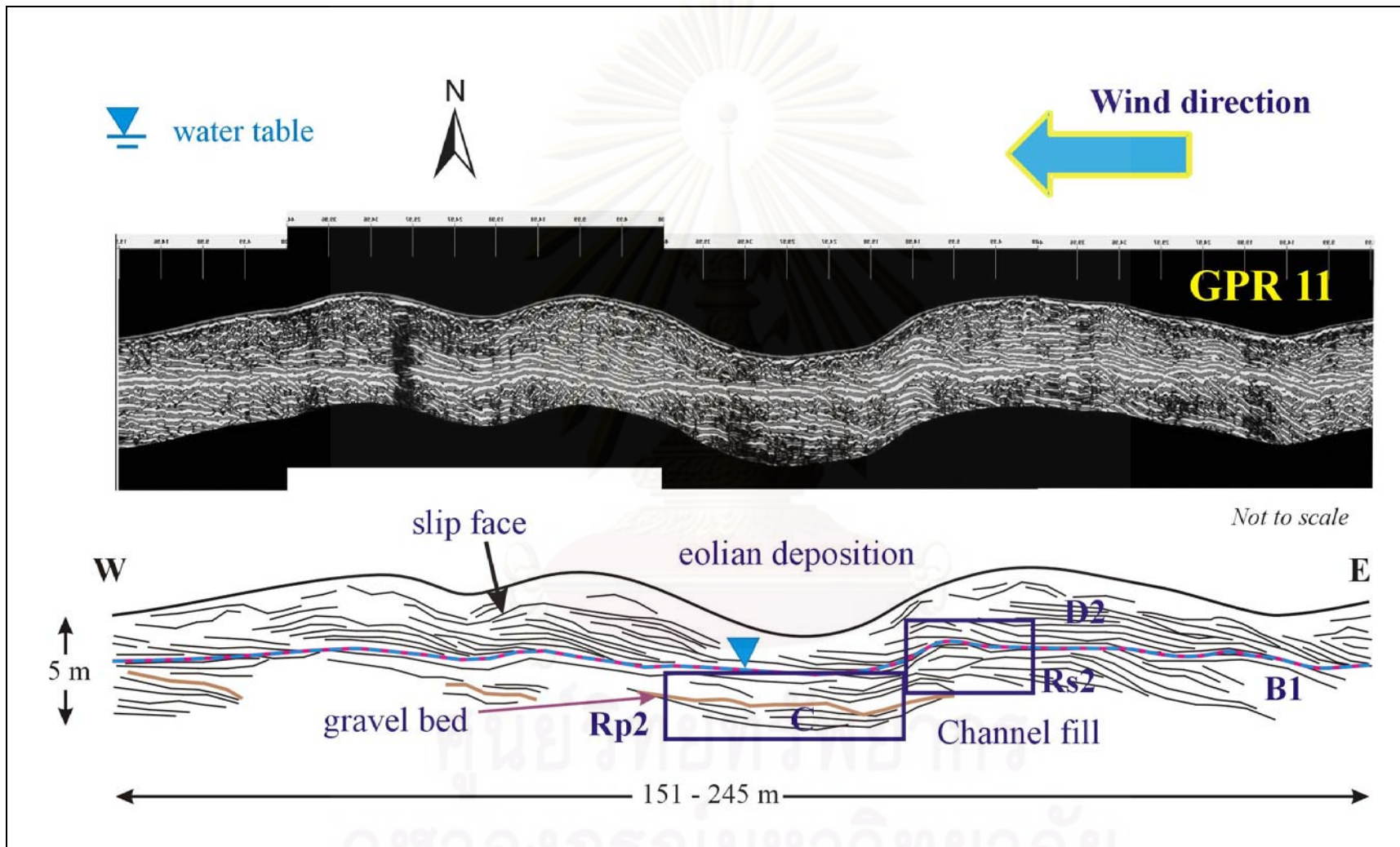


Figure 4.9. (cont.)

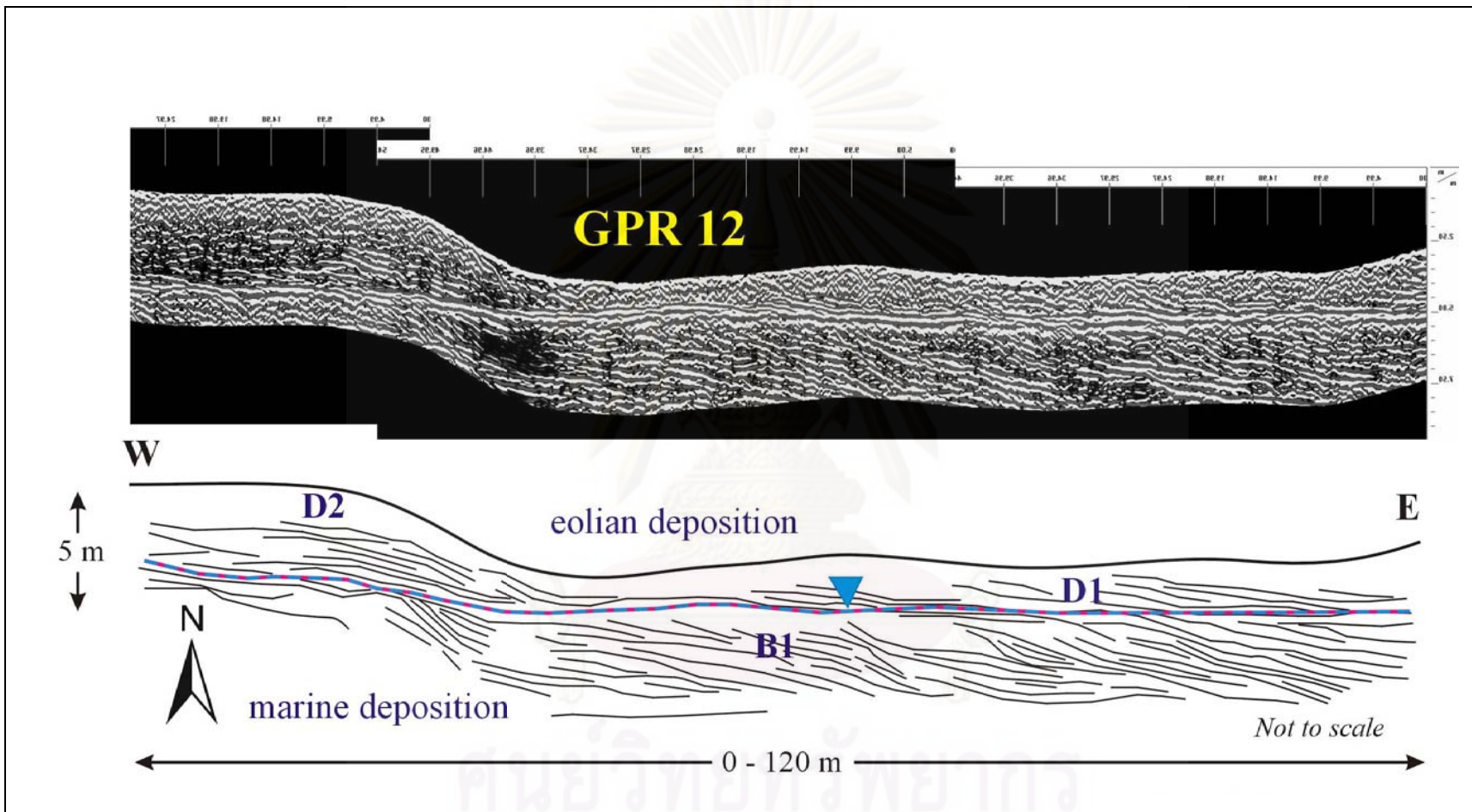


Figure 4.9. (cont.)

ศูนย์วิจัยทรัพยากร
จุฬาลงกรณ์มหาวิทยาลัย

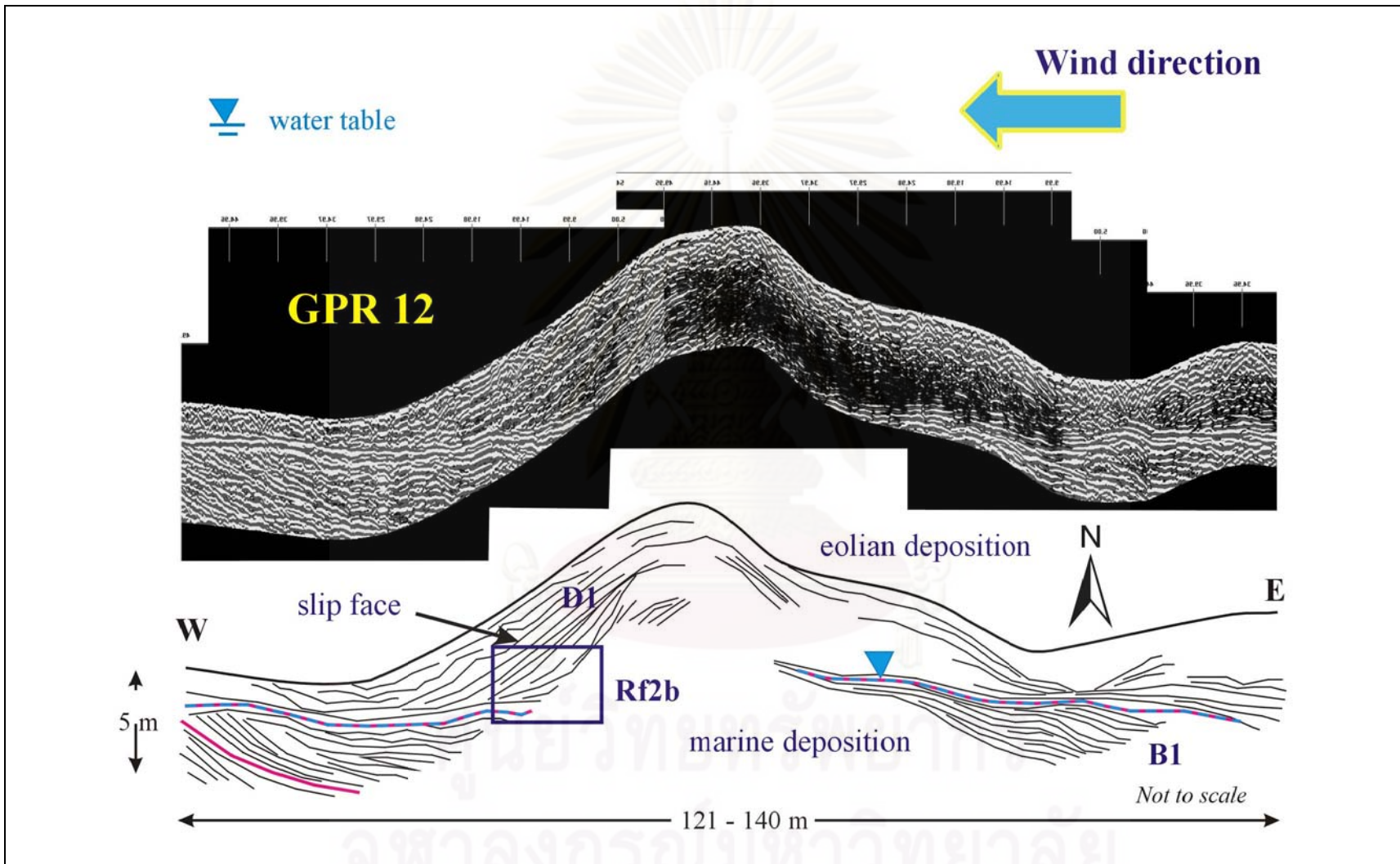


Figure 4.9. (cont.)

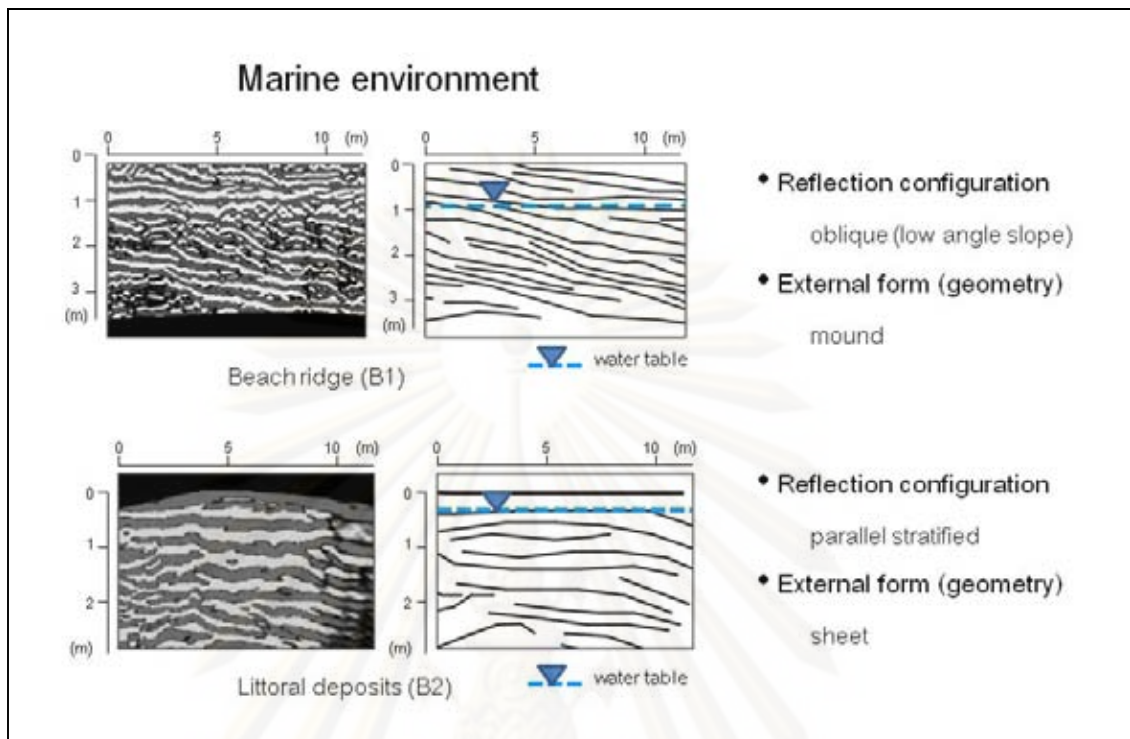


Figure 4.10. Characteristic reflection patterns of marine environment can be divided into 2 units, including beach ridge (B1) with oblique (low angle slope) reflection configuration, and littoral deposits (B2) with parallel stratified reflection configuration.

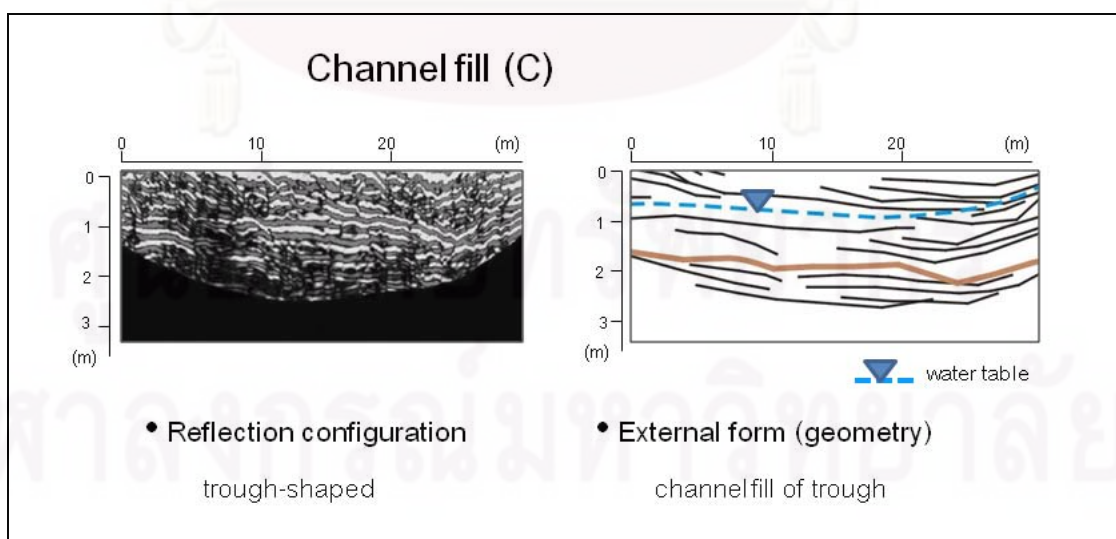


Figure 4.11. Characteristic reflection patterns of channel filled (C) with trough- or channel- shaped reflections.

GPR profiles oriented perpendicular to the prevailing wind.

According to GPR transects of the actively migrating on the crest of dune, the reflection configuration shows characteristic of coastal sand dune (D1) with cross-bedding in foresets and bounding planes, covered sand (D2) with coherent parallel or cross-bedding, beach ridge (B1) with parallel stratification and the contact between marine sediments underneath eolian sediment (Figure 4.12). The regional water table can be related with continuous high-amplitude reflection inside the beach ridge structure. Radar signal of beach ridges are sub-parallel and continuous.

Radar surfaces, Packages, and Facies

Radar lines along the windward slope and the crest of dune reveals downwind dipping foreset bedding planes characteristic to which this structure is commonly recognized in the parabolic dunes, as well as other features visible within and below the dunes.

From the foregoing description of the radar profiles, those features of internal structure within the dune is possible to classify into GPR units using the principles of radar stratigraphy, which relies on the identification of systematic terminations or boundaries, to qualitatively classify different reflection patterns from the profiles. This classification is the first used of GPR facies in this area and can be served as a basis for comparison with the other studied parabolic dune and may also serve as a reference for comparing with other dune morphologies.

The main features from the radar profiles can be classified into 2 radar surfaces, 2 radar packages and 5 radar facies (Figure 4.13). A qualitative scene was used to describe the relative dip of reflections because, however, it is not known whether or not the migration produced accurate dip angles (i.e., high-, moderate-, and low- angle). It is important to recognize that the discrimination of sedimentary surfaces, packages, and facies is highly subjective and dependent on the term of reference. Therefore, the classification of radar surface in this thesis is mainly followed the terminology proposed

by Neal (2004) and Hogenholz et al. (2007) as previously stated in chapter 3. Identification and description of the environment deposits are based on Overmeeren (1998) and Hogenholz et al. (2007), correlation with DMR logs (2006) and hand augers drilling in field work.

Radar surfaces are termed as the bounding surfaces and represent depositional breaks or unconformities in the sedimentary sequence. Radar packages are depositional units consisting of genetically related strata that are bounded top and bottom by radar surfaces or bounding surfaces. Radar facies are composed of sets or reflections with distinctive shapes, dip, and continuity that represent the bedding and internal structure of a sedimentary facies (Cagnoli and Ulrych, 2001).

In this survey, 2 radar facies are concordant (Rs1) and erosional truncation (Rs2) were identified, 2 radar packages are spur (Rp1) and trough (Rp2) and the other 5 radar facies include planar (Rf1a) and wavy (Rf1b) which represent the reflection configuration of shape. High angle planar (Rf2b), and high-oblique angle tangential (Rf3b) represent the reflection configuration of dip.

Result from GPR showed some obvious macro-scale sedimentary patterns, especially the lateral and vertical extensions of the older dune superimposed by the younger one. Clear boundary of dune and the underlying prograded beach ridge plain is also detected from GPR. Based on macro-scale sedimentary patterns, lee and stoss angles of some burial dunes ascribed mainly two directions of wind. First was formed by wind blown from the north to the south and second was in almost northwest to southeast direction. This result in analyzing wind direction based on GPR signals is corresponded well with dune morphology interpreted from aerial photographs and the modern record of wind blown direction.

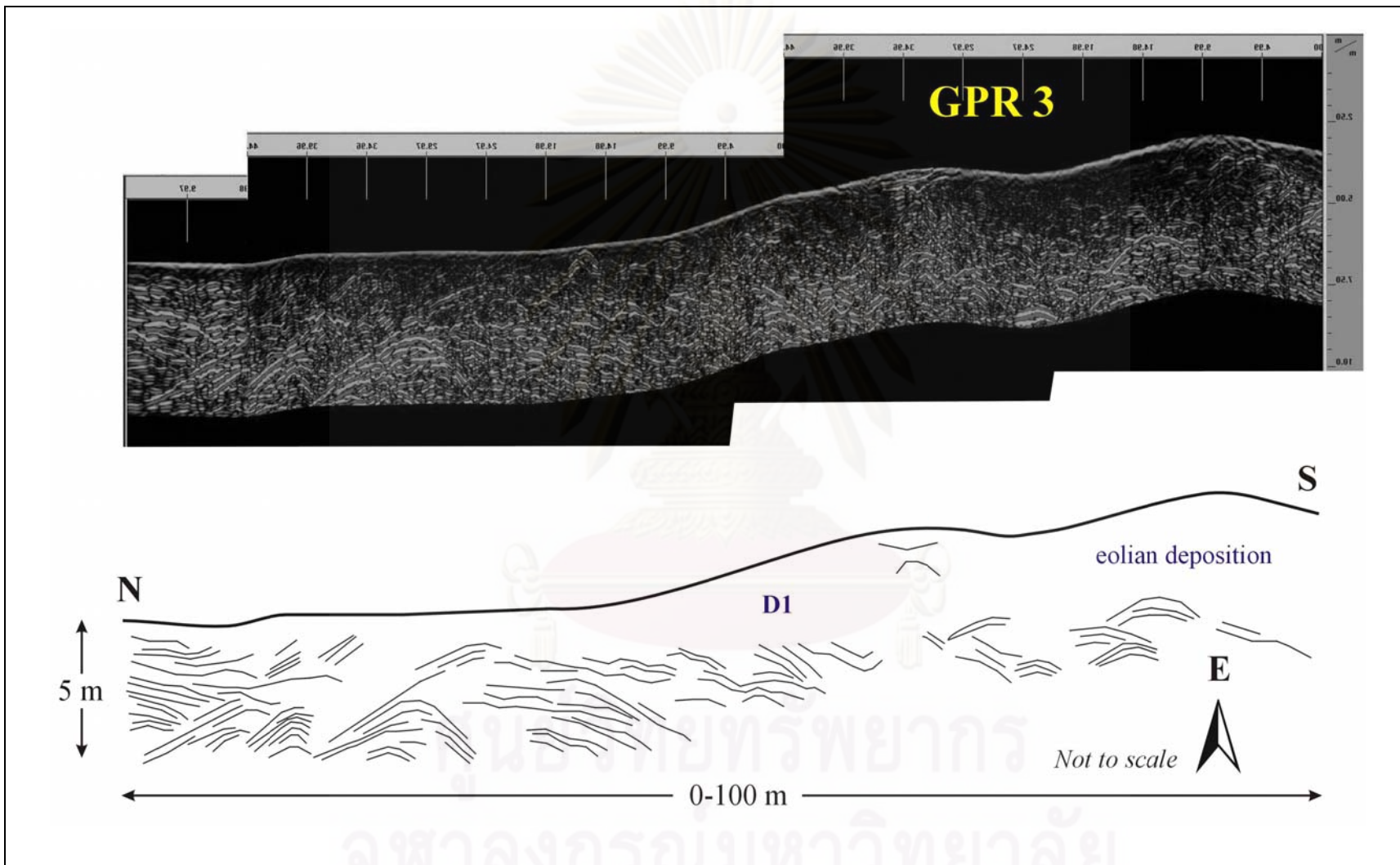


Figure 4.12. GPR profile oriented perpendicular to the dune's downwind axis.

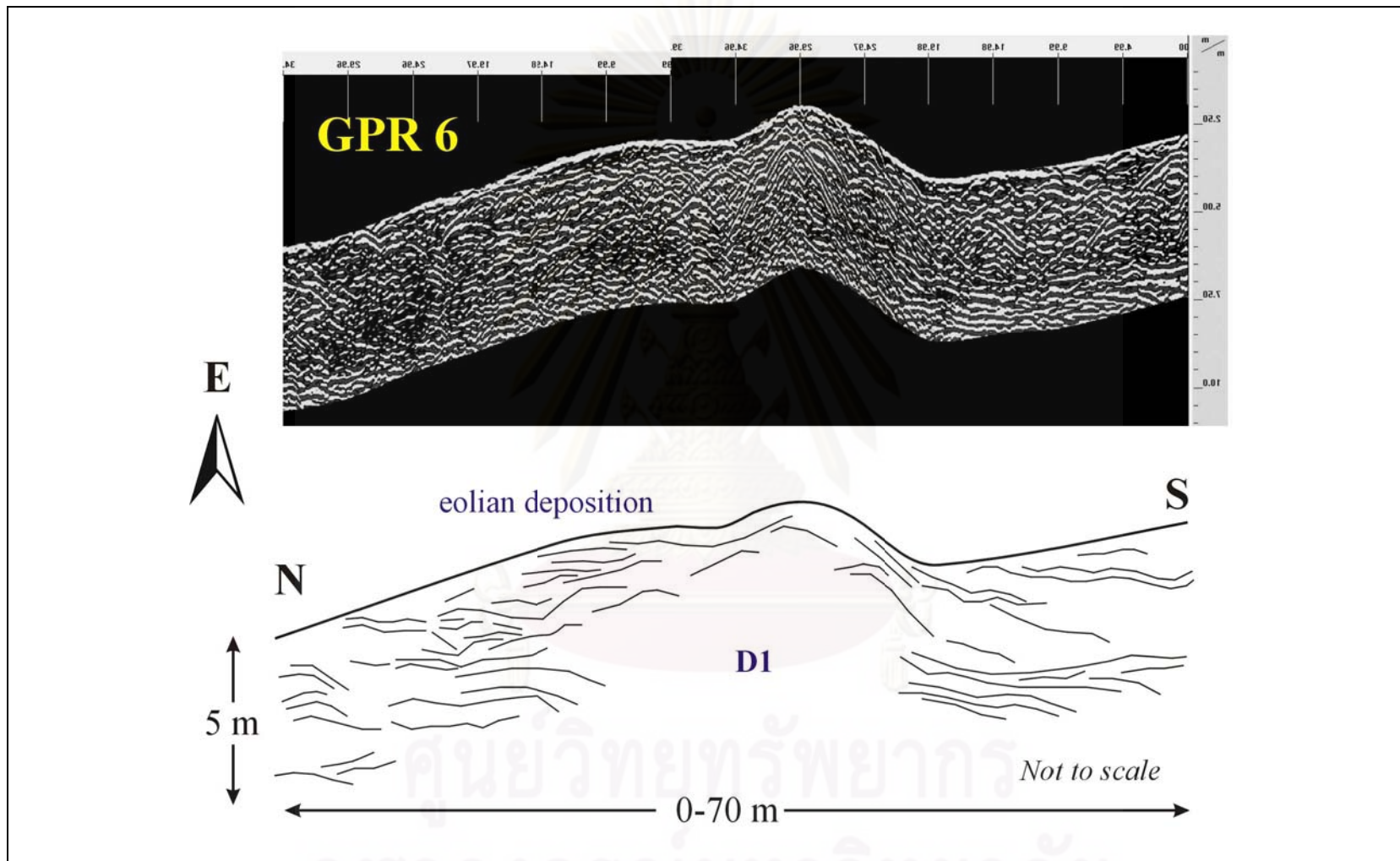


Figure 4.12. (cont.)

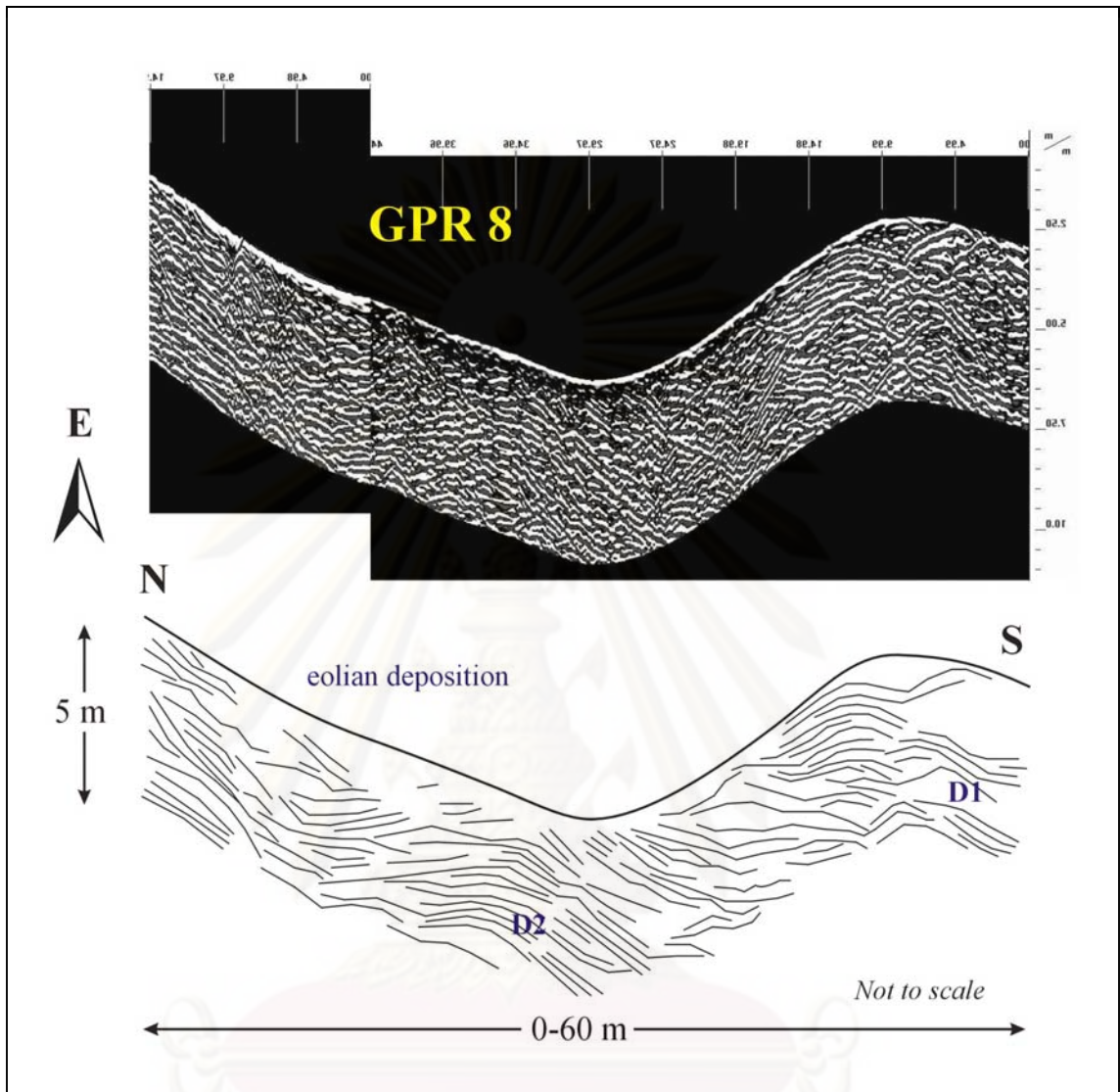


Figure 4.12. (cont.)

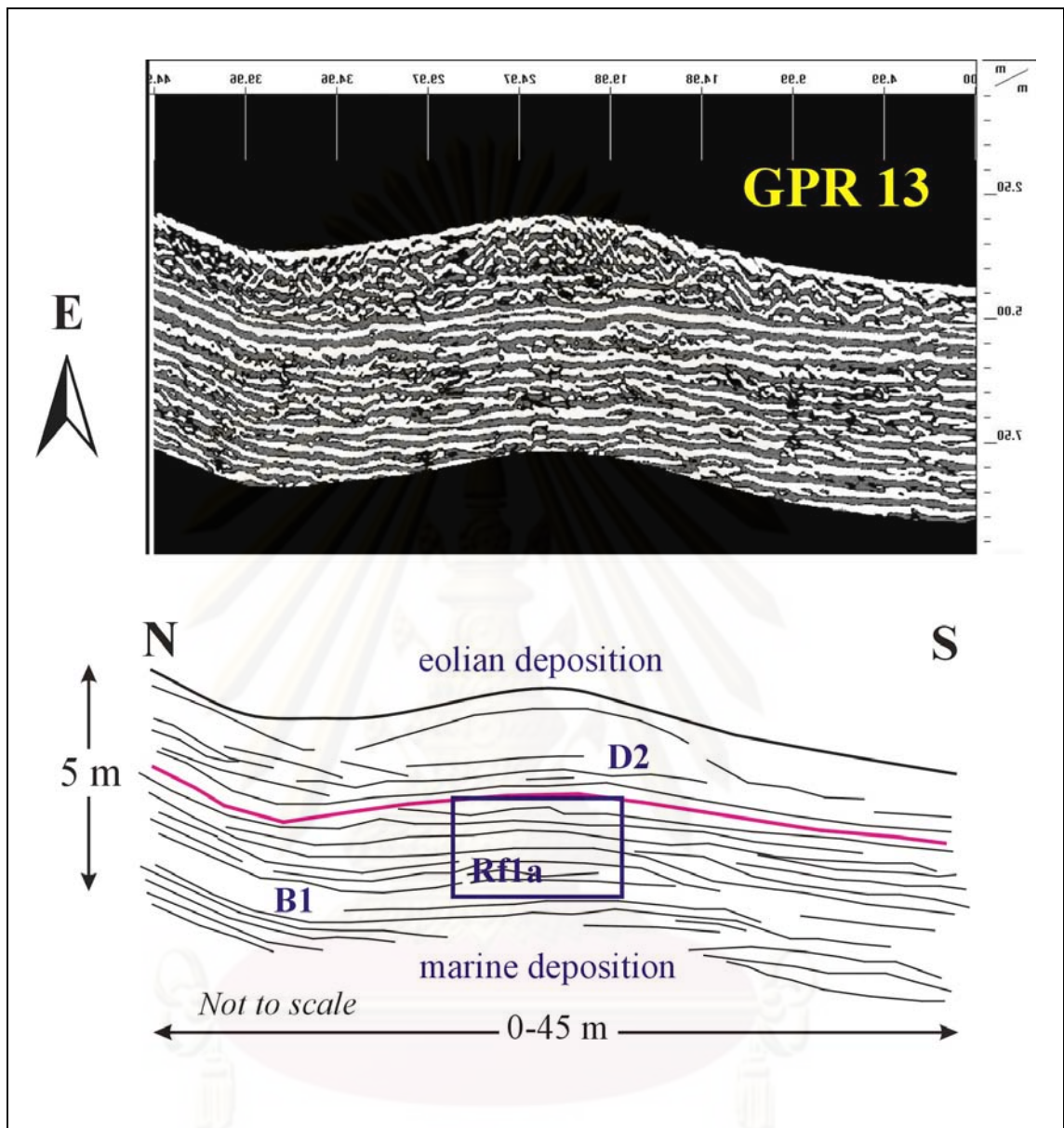


Figure 4.12. (cont.)

ศูนย์วิทยทรัพยากร
จุฬาลงกรณ์มหาวิทยาลัย

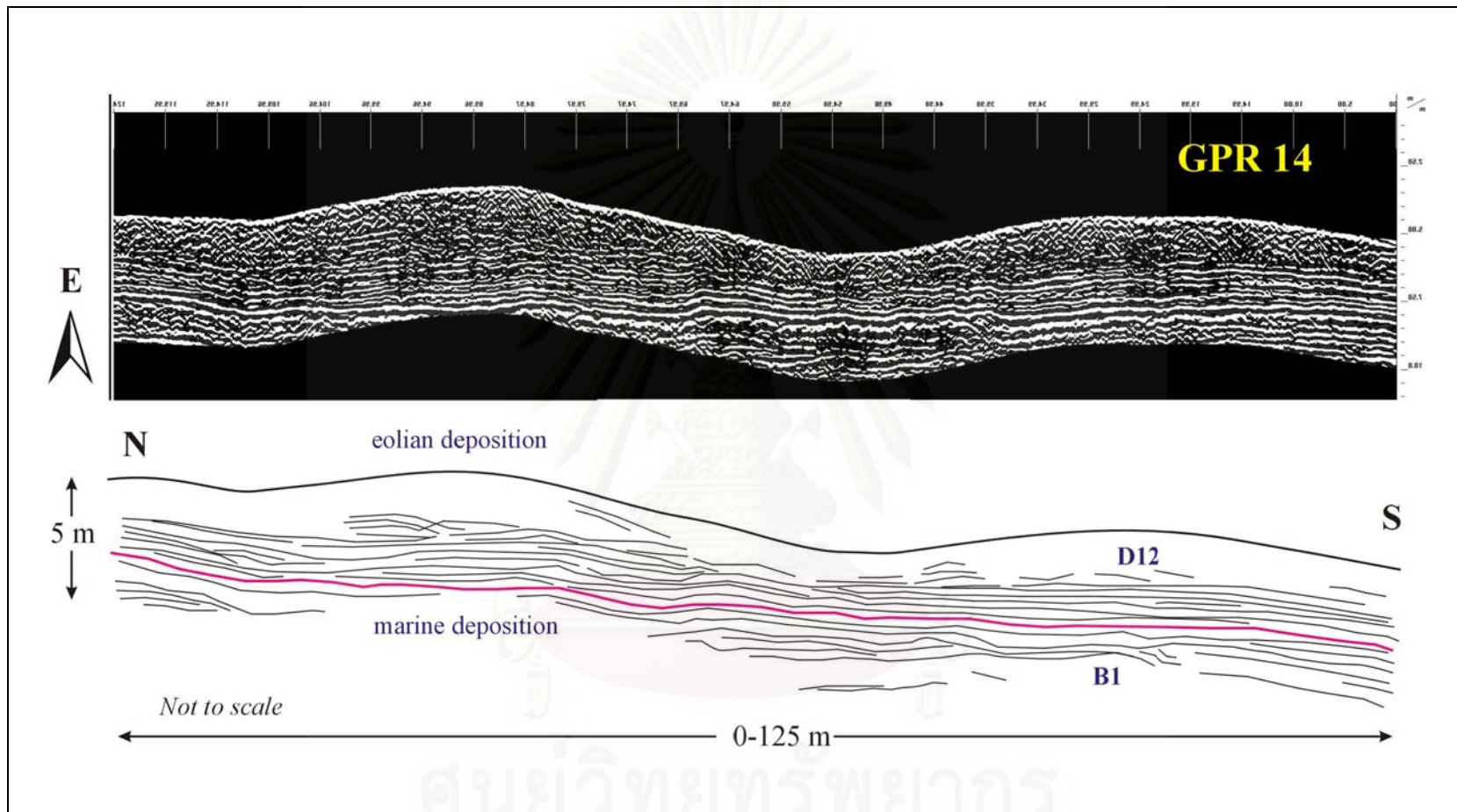


Figure 4.12. (cont.)

ศูนย์วิทยทรัพยากร
จุฬาลงกรณ์มหาวิทยาลัย

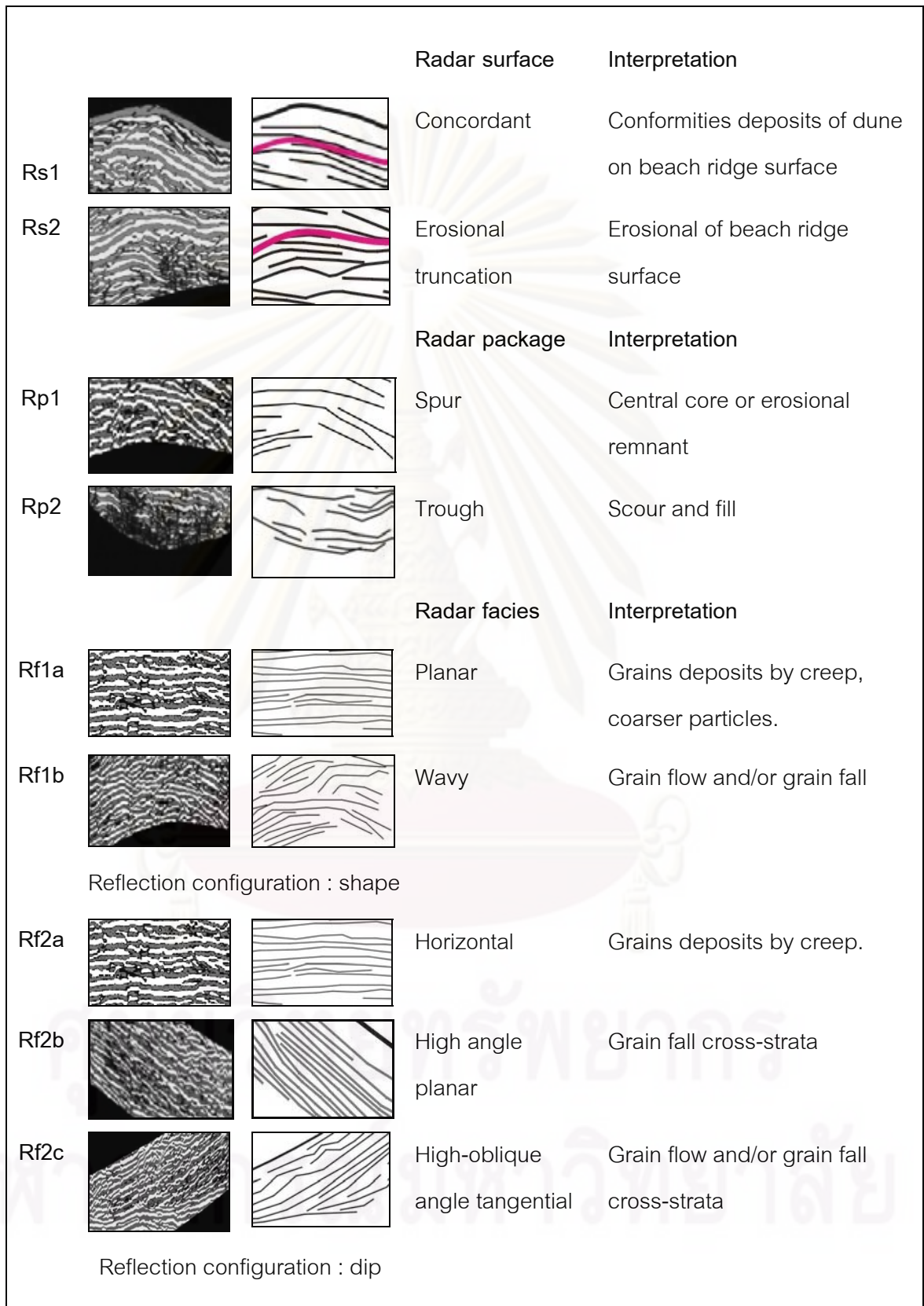


Figure 4.13. Characteristics of radar signals recognized in GPR profile.

Interpretation result of GPR surveys

The stratigraphic units from the radargrams show eolian deposit, marine deposit and channel filled (Figure 4.6). Eolian deposits have signal representing grain movement to form dune, and comprised sets of reflection with distinctive shape, dip and continuity that represent the bedding and internal structure of a sedimentary facies. The eolian deposition can be divided into 2 units that are coastal sand dune (D1) and cover sand (D2). Events deposition of dune identified by third order bounding surface can be divided into three sub-units. They are d1, d2, d3, representing to three events deposition at least.

The parallel stratified reflection configuration of littoral deposit from GPR signal can correlate with the profile of sand sheet at the coastal, northern part of the study area (Figure 4.14). The characteristic of seaward prograded can be defined as beach ridge. In field work, the sediments between dune and beach ridges are classified by their roundness and color (Figure 4.15). A trough-shaped reflection underneath beach ridges layer defines the channel filled. The radar surface between the dune deposit, beach ridge and channel fill, represents to the different depositional sequences.

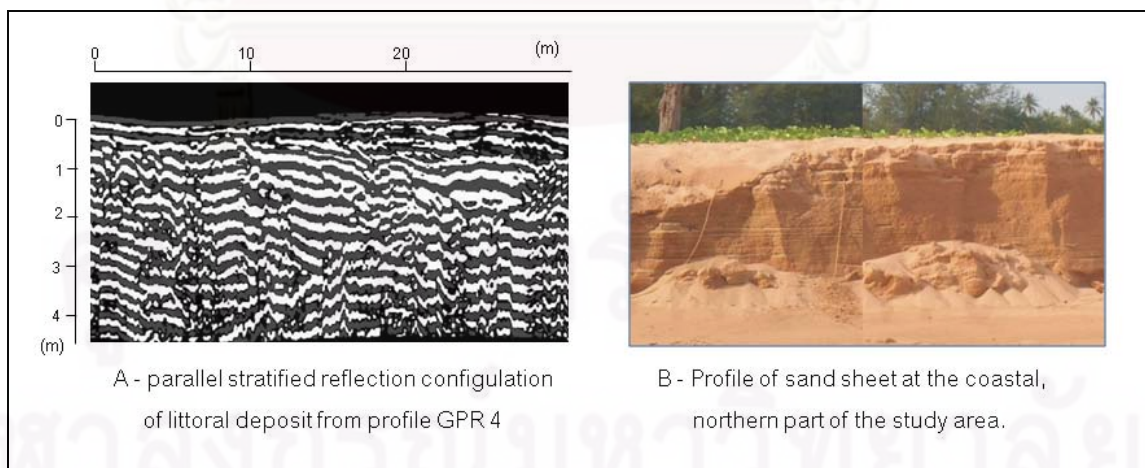
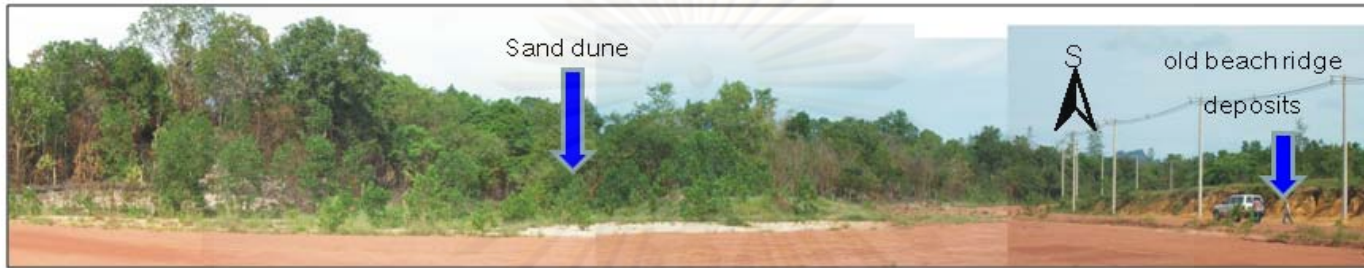


Figure 4.14 The reflection parallel stratified of littoral deposit from GPR signal correlate with the profile of sand sheet at the coastal, northern part of the study area.



A-The morphology of dune field and old beach ridge at the southern part of study area



B-Sediment of dune deposits is light brown color, fine-medium grained, subrounded.



C-Sediment of old beach ridge deposits is yellowish brown colors, medium-coarse grained, subangular.

Figure 4.15. The difference between sediments of dune deposits and old beach ridge deposits.

4.4 Internal structures in dune

In this study, some exposures of dune field show macro-scale internal structures that may correspond well with the GPR signals. Location in Figure 4.16 (0554025E 1207820N) is one example of boundary units that can be inferred the break of dune deposition to which dunes formed at least 3 depositional events (Figure 4.16). The event boundary features are characterized by dense rootlets and high organic, very fine sand layer.

However, the micro-scale internal structure within dune is rarely recognized. This is probably because dune texture itself contains very homogenous of fine- to very fine-grained sand mainly and strongly deformed by modern bioturbation (Figure 4.17). Only small inclined and parallel laminations are localized.

4.5 Grain size analysis

Grain size analysis shows the distribution of grain size of sand and can be applied for calculating statistic parameters. The result from statistic parameters calculation can be helped as support data in explaining the depositional environments (Friedman, 1961) in the study area.

Sediment samples were obtained from dune itself, the old beach ridge, beach, river, and terrace (Figure 4.18) to analyze the distribution of grain size by Malvern, Mastersizer laser granulometry (Appendix B). A total of 41 samples were undertaken (Figure 4.19).

Particle size showed the variety in result of grain size distribution among samples, which varies from fine to very fine sand and very well sorted. These values were computed in descriptive term formulas of Folk (1968) (Appendix A). The range of mean diameter is between 404 - 286 μm . The range of standard deviation is between 0.098-0.080, and the range of skewness is between -0.047-0.163. Plot of standard deviation and skewness represents group of environment of deposition. The range of value falls into eolian environment (Figure 4.20).

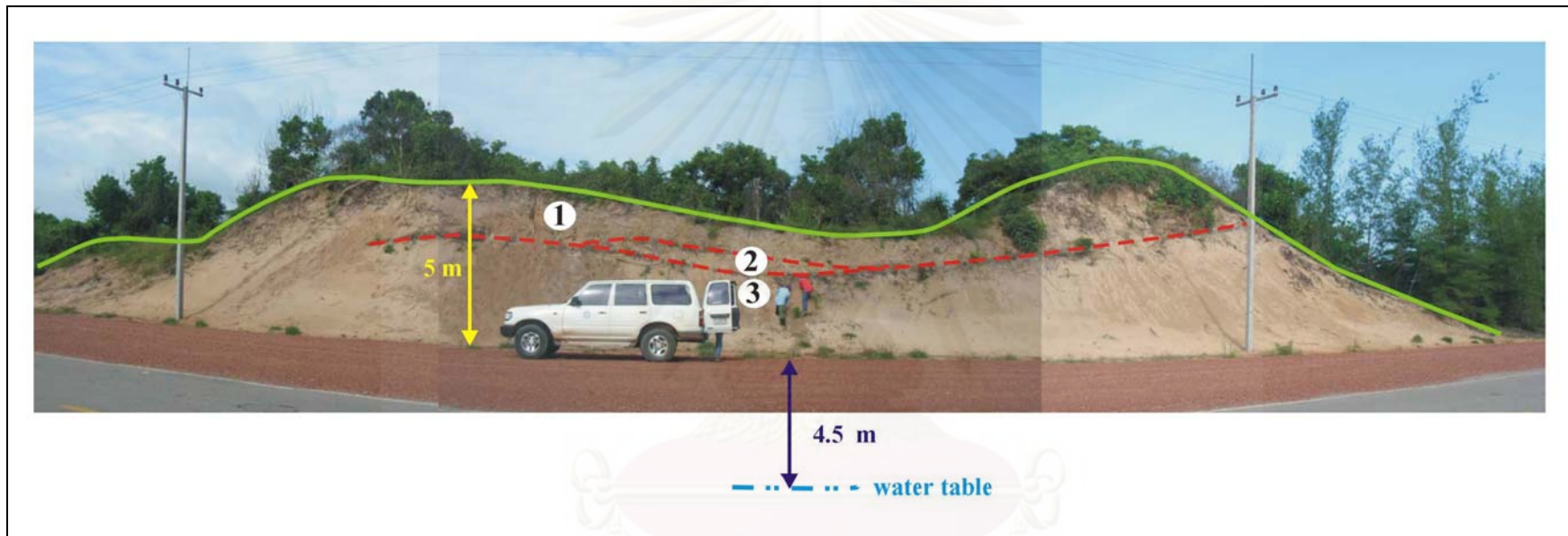


Figure 4.16. Event boundaries of dune deposition are clearly seen from outcrop, southern part of dune field. Within 5 m thick of dune, at least 3 depositional events were identified.

ศูนย์วิทยทรัพยากร
จุฬาลงกรณ์มหาวิทยาลัย

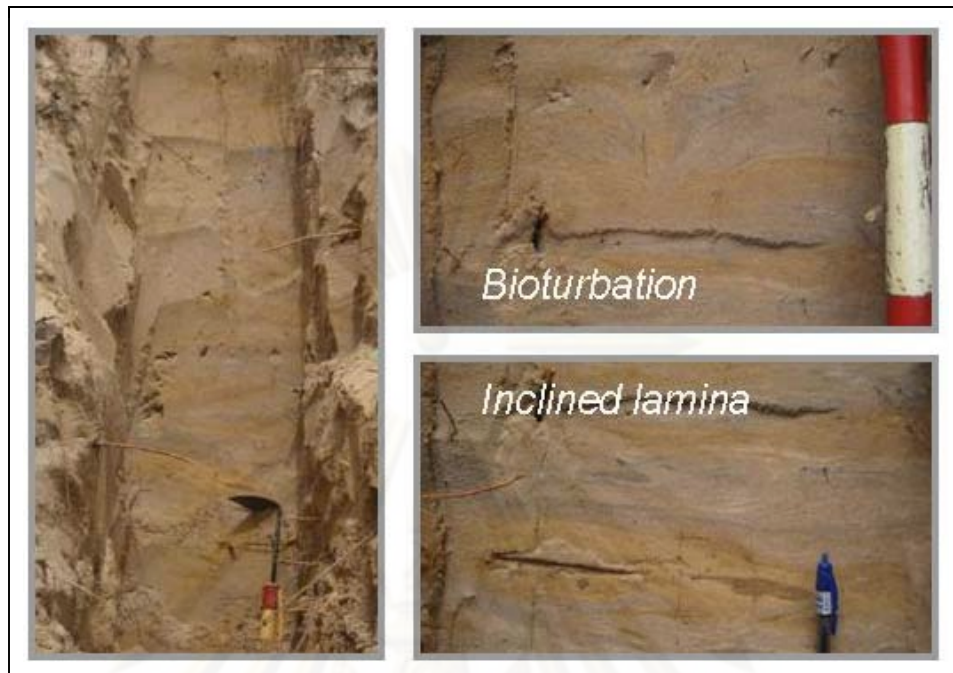


Figure 4.17. Rare micro-scale sedimentary structures of parallel and inclined lamination persisted in dune. Some rootlets as one bioturbation are also preserved.

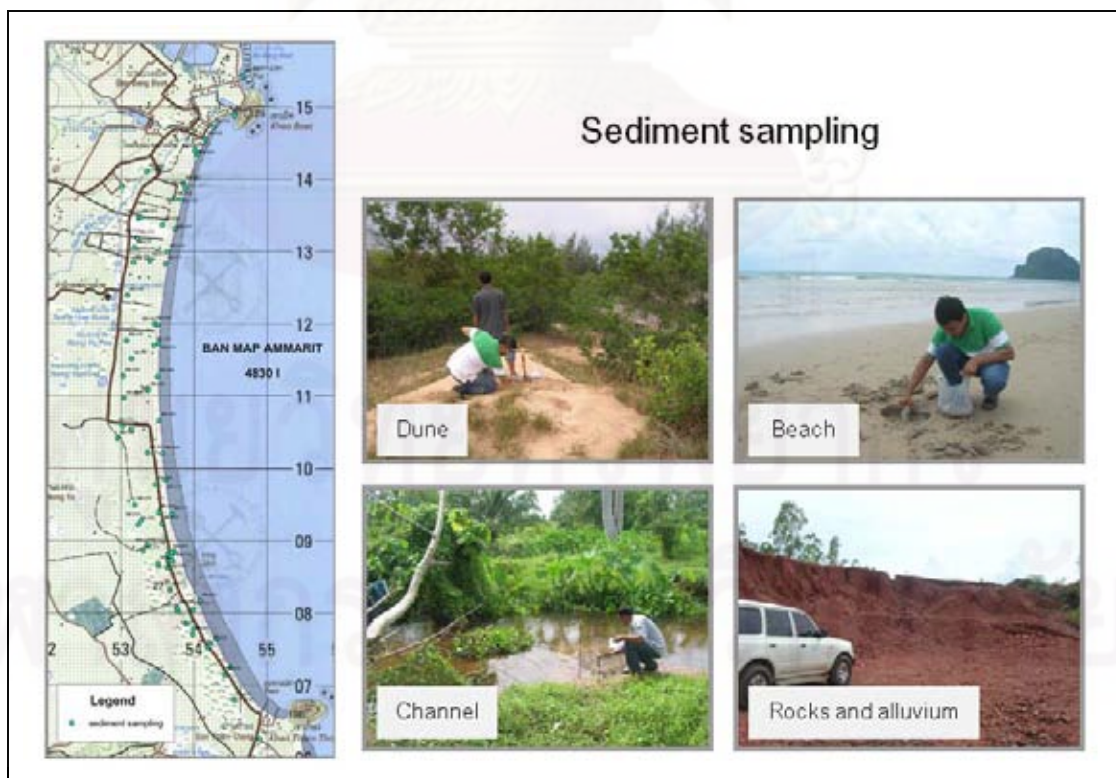


Figure 4.18. Map showing locations of sediment samples for grain size analysis.

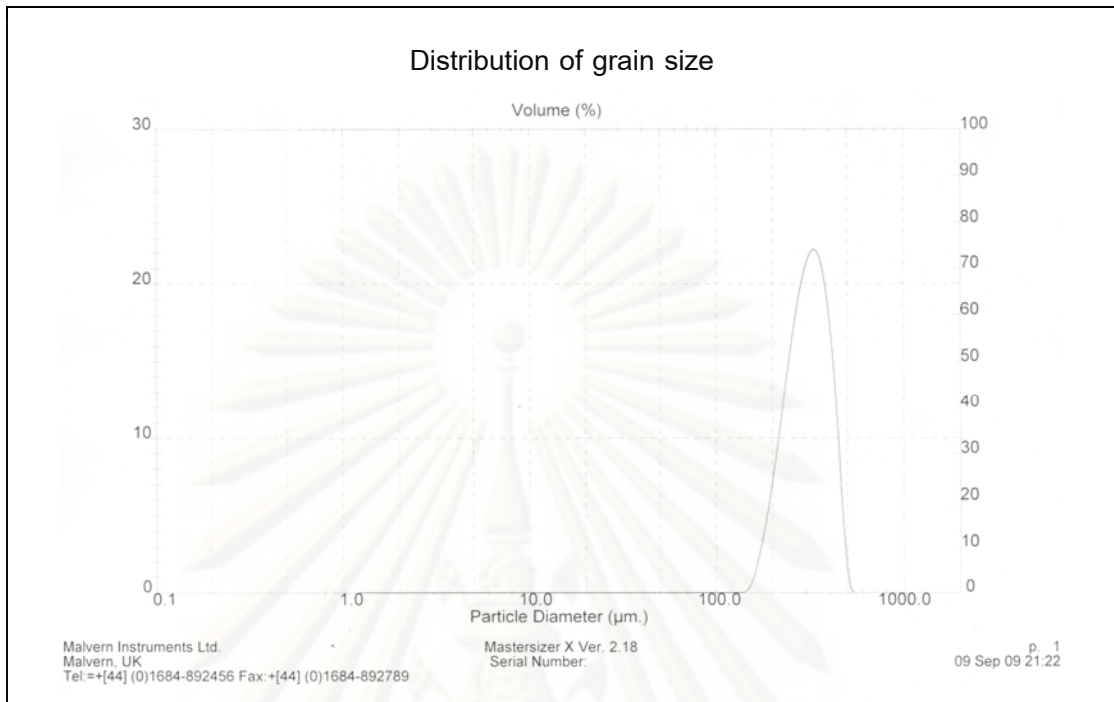


Figure 4.19. Graphs showing distribution of grain size analyzed by Malvern, Mastersizer laser granulometry.

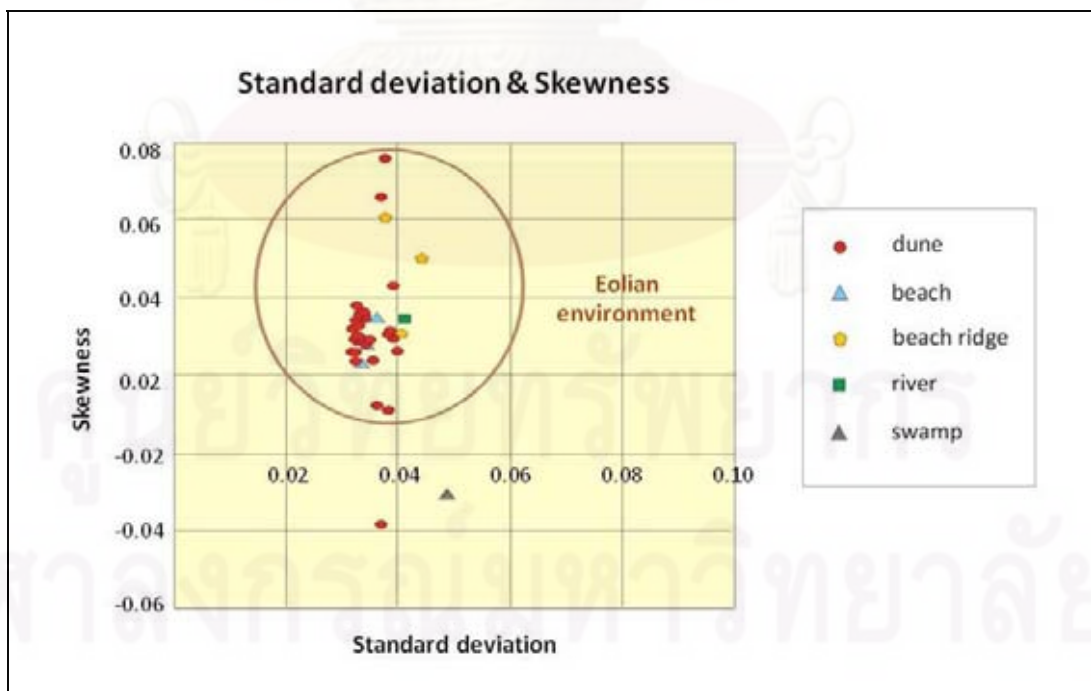


Figure 4.20. Histogram plot showing distribution of statistic parameters and their assemblages in interpreting depositional environment.

4.6 Optically stimulated luminescence (OSL) dating

Samples for OSL dating were taken (see Figure 4.16), with the spacing of samples is 0.15 m from topmost layer of dune profile. Result of OSL dating of sand grains indicates the age of sediment deposit at 2,220 - 2,960 years ago (Table 4.1).

Table 4.1. Result of OSL dating sand dune sediments.

Sample No.	U (ppm)	U (Error)	Th (ppm)	Th (Error)	K (%)	K (Error)	W (%)	AD (Gy/ka)	AD (Error)	ED (Gy)	ED (Error)	Age (Yr)	Error (Yr)
BB-2	1.28	0.04	5.6	0.27	0.24	0.02	1.56	1.15	0.10	2.60	0.0020	2250	180
BB-3	1.13	0.04	4.66	0.27	0.35	0.02	1.49	1.16	0.08	2.88	0.0035	2470	170
BB-4	1.13	0.04	4.56	0.22	0.19	0.02	0.75	0.99	0.07	2.93	0.0020	2960	200
BB-5	1.09	0.04	5.21	0.25	0.13	0.02	0.70	0.97	0.08	2.49	0.0030	2570	220
BB-6	1.27	0.04	4.19	0.29	0.13	0.02	0.68	0.94	0.08	2.48	0.0019	2650	220

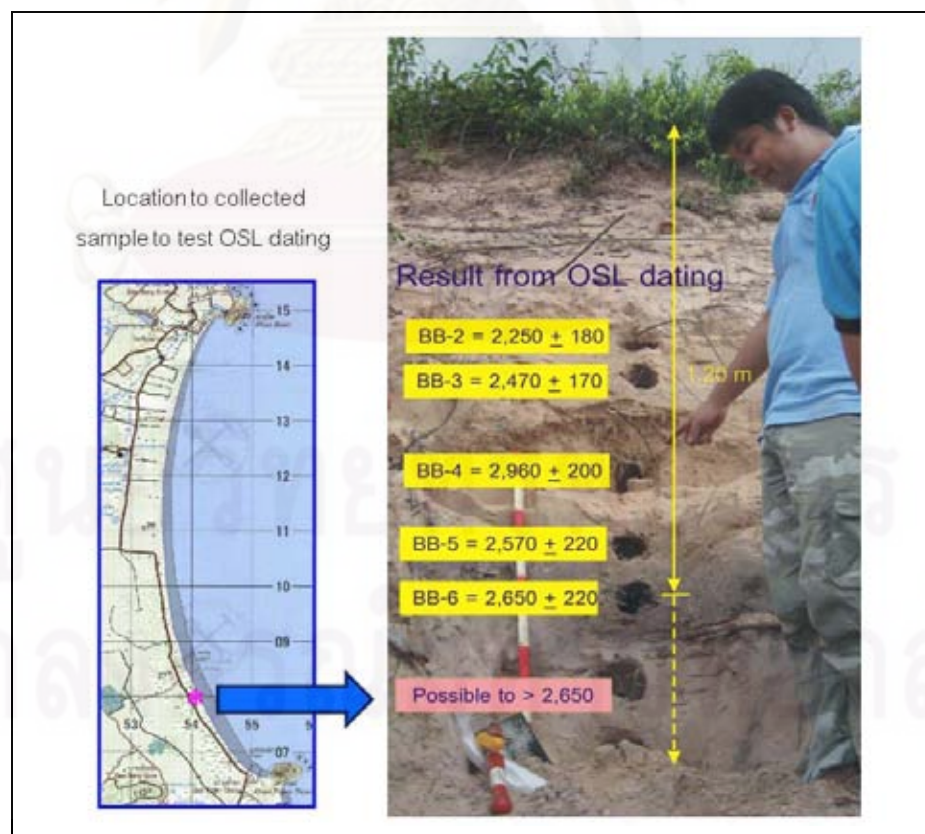


Figure 4.21. OSL dating defined age on top of dune deposition.

CHAPTER 5

DISCUSSION AND CONCLUSION

5.1 Discussion

5.1.1 Wind-blown directions from dune morphology

This discussion section will be based on the result from previous chapters. According to the result from aerial photograph interpretation, topographic survey, GPR survey, the observation of sedimentary structures recognized in the outcrops, the formation of sand dune may reflect its formation by both eolian environment and by the influence of coastal wind and wave (Jacobberger, 1989).

Dune field distributes along the coastal plain mostly parallel to the present shoreline. In general, dune field can be sub-divided into two zones; the coastal dune close to shore and the former dune close to the swampy area in the west

Different units of rocks and sedimentary deposits can be divided by aerial photograph interpretation into 9 units that are composed of limestone (Ls), sandstone interbedded with conglomeratic sandstone (Sst), colluvial deposits (Q_c), terrace deposits (Q_t), alluvial deposits (Q_a), lagoonal deposits (Q_{lg}), tidal flat deposits (Q_{mp}), old beach ridge deposits (Q_{bo}) and beach deposits and dune.

Dune morphology from aerial photograph shows a majority of parabolic and transverse pattern; star shapes were rarely and locally recognized. Parabolic shape dominates in the outer part of dune field close to shore, transverse morphology is localized in the western end of dune field; star pattern is locally recognized in the southern portion. They formed as the wind is able to carry sediments from the beach in a landward direction and they were deposited wherever the obstruction hinders further transportation (Moody and Graham, 1995; Sanjeevi, 1996; Livingstone et al., 2007). Source of sediment supply to form the dune is likely the key limiting factor in dune

development of this area. Most of dune shapes indicated the major directions of wind blown oriented from the east to the west.

Bang Berd sand dune is recognized between the northern part of Changwat Chumphon and adjacent areas in the southern part of Changwat Prachuap Khiri Khan. Recently, this area is commonly hit by many wind directions (Appendix E), wherever winds periodically reverse direction. Thus, this area owns the characteristic of compound dune (smaller dunes of similar type and slip face orientation are superimposed) and star dune at southern part of the area, representing to a wind regime that has changed the intensity or direction after the formation of the dune.

It is interesting that dunes in this area formed where constructive waves encourage the accumulation of sand, and where prevailing onshore winds possibly blow this sand inland. There need to be obstacles e.g. vegetation, pebbles etc. to trap the moving sand grains. As the sand grains were trapped they started to accumulate, initiating dune formation. The wind then started to affect the mound of sand by eroding sand particles from the windward side and subsequently deposited them on the leeward side. Gradually, this action caused the dune to migrate in land, as it does so it accumulated more and more sand.

5.1.2 Wind blown direction from GPR

Although the limitation of penetration by GPR (5 m depth) precluded a complete assessment of the dune's internal structure, the exceptionally good resolution of the data enabled discrimination of primary sedimentary structures such as sets of cross-strata, troughs, spurs, and bounding surfaces. The distribution of these features helps elucidate the recent depositional history of the dune and provides an important contribution for understanding the morpho-dynamics of parabolic dunes.

A ground penetrating radar survey over the surface of an active parabolic sand dune in the outer part of dune field close to shore provides excellent details of the internal structure. Despite only 5 m limited depth of GPR penetration, the radar signal

was able to resolve a variety of high-angle, low angle, and curved reflections that are interpreted as primary sedimentary structure. Radar profiles parallel to the direction of migration revealed a complex arrangement of cross-strata that reflects different phases in the development of dune. The first and earliest phase is characterized by low-angle reflections that represent pre-existing aeolian strata, either sand sheet or dune marginal deposits. The second phase is characterized by high-angle reflections that represent downwind migration dominated by grain flow strata. The third phase is characterized by a variety of high-, moderate-, and low- angle reflections that represent a more complex pattern of migration involving grain flow, grain fall, and ripple deposition.

GPR profile showed the major slip faces at the western part of dune, representing the probable major direction of wind blown that was expected from the east to the west. Although, radar signal at the top most of the dune in some places was chaotic, but it represents that winds have changed the direction seasonally after dune formation.

The collection of radar profiles obtained in this study can be summarized into 2 radar surfaces, 2 radar packages and 5 radar facies. This detailed imaging of the internal structure provides new details on the formation and morpho-dynamic process of active parabolic dunes in the coast of Gulf of Thailand.

5.1.3 Dune formation

The environmental history of coastal dune systems in Bang Berd sand dune, Changwat Chumphon has been examined by using geomorphological, GPR, and sedimentological techniques and results of dating from optically stimulated luminescence (OSL). The stratigraphy and depositional environment were determined from GPR surveys 12 lines, and correlated with DMR logs (2006).

Result from GPR surveys can be able to divide the depositional environment into 3 types. They are dune deposition, marine deposition and channel filled. Mostly, GPR reflection shows the contact between the eolian deposits on top and beach ridge on

bottom, corresponding to the characteristic of morphology (Figure 5.1) and unit of sediment from DMR logs (2006) (Figure 5.2).

In location where the dune superimposed on beach ridge (BB 1 of DMR, 2006) correlated with GPR profile of GPR 9 and GPR 10 (same as location), the depositional events of dune can be divided into at least 3 events. The event break in GPR is represented by a third order bounding surface and the difference in the angle forests, corresponding to dune sediment interbedded with organic sand three layers (Figure 5.3). Beside, the event depositional break from GPR 5 corresponds to the dune stratigraphy of BB 5 (DMR logs, 2006), same as the location shown in Figure 5.4, and the macro sedimentary structure represents the event break in dune profile in the southern part of the area.

Landward inclined foreset angle of slip faces indicates the paleo-wind directions from the east to the west. Difference in foreset dipping angles and size reflected the magnitude of wind blown in different period of times.

All data from GPR, geomorphology and core logs led to build the idealized cross section of Bang Berd sand dune shown in Figure 5.5.

The goal of this thesis is to characterize sedimentology and morphology of sand dune in the study area for evaluating the possible sources of dune and build up model dune formation of the study area as shown in Figure 5.6.

The sequence of event outlined in the model above reflects the interaction of several major controls on the development of coastal dunes (Davis, 1985), including: the volume of sediment supply to the beach; the role of foredune growth and stabilization by plants; and the effects of transgression or regression on dune development and stability. These are discussed in the context of the proposed model and their implications for dune development elsewhere.

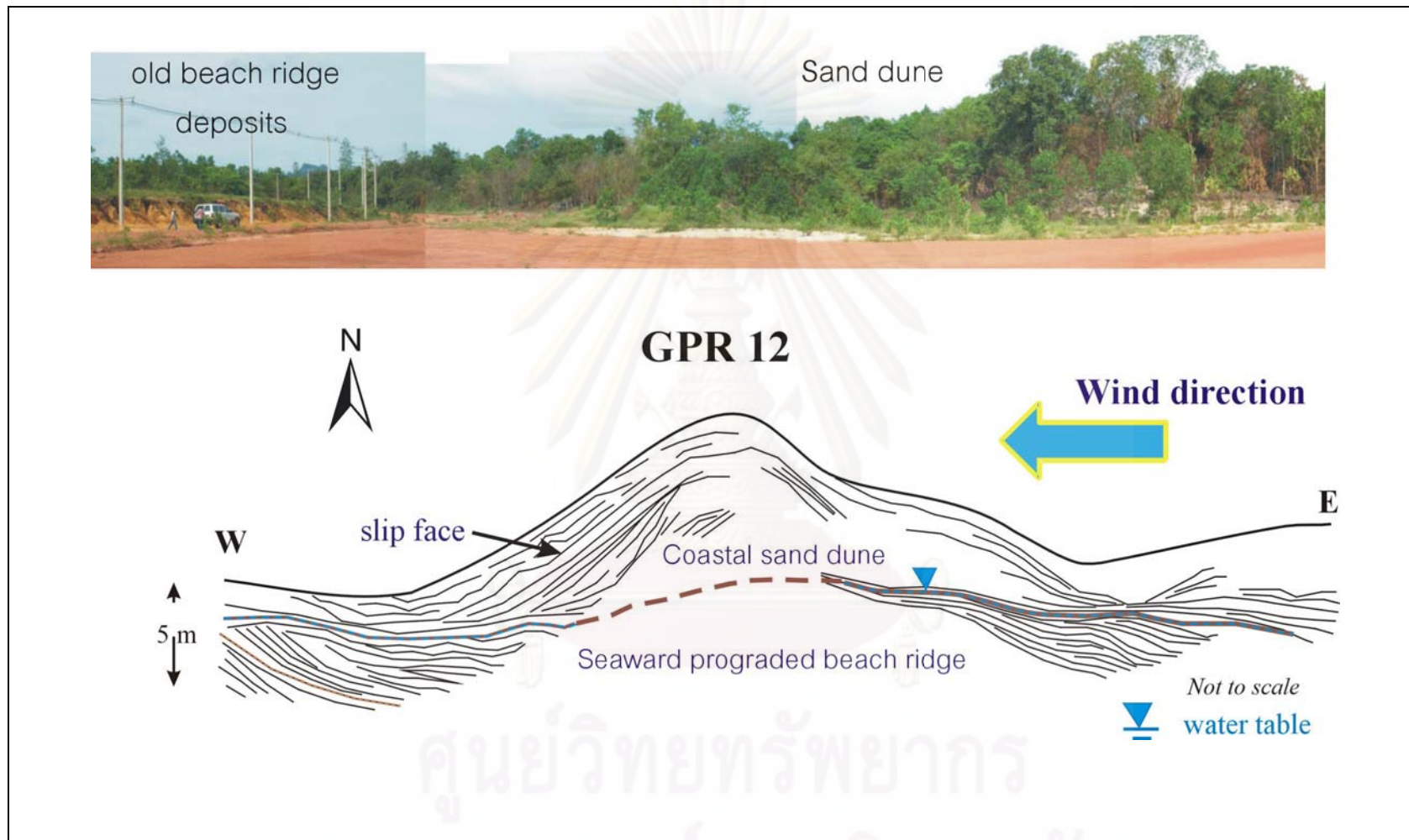


Figure 5.1. Dune morphology correlated with GPR signal can separated dune deposits with seaward prograded beach ridge by characteristic of clearly reflection configuration to represent environment deposition.

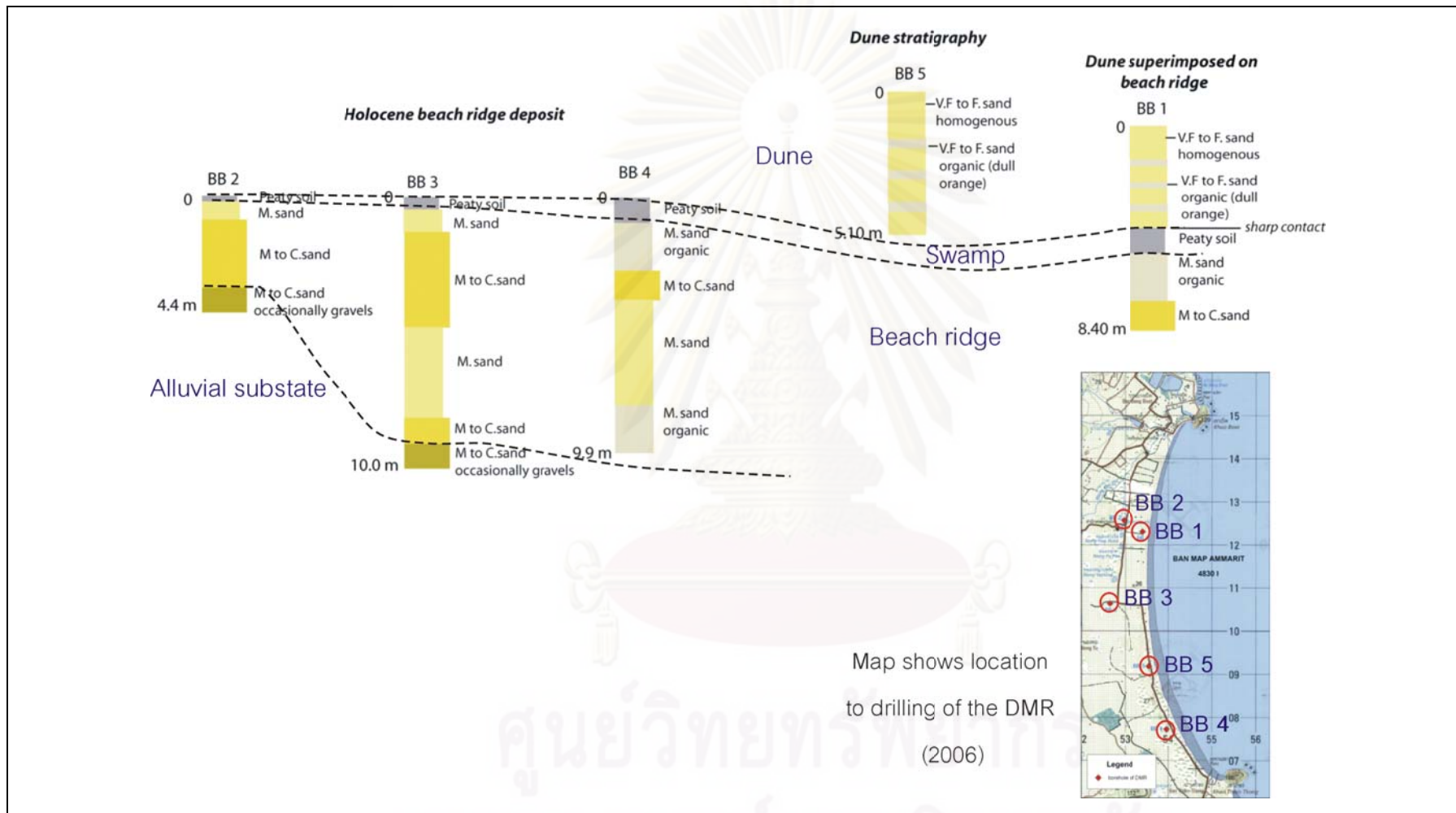


Figure 5.2. The Stratigraphical profile along west-east transects (Data modified from DMR logs, 2006) divided the stratigraphy to 4 units; as dune deposits, swamp deposits, beach ridge and alluvial deposits.

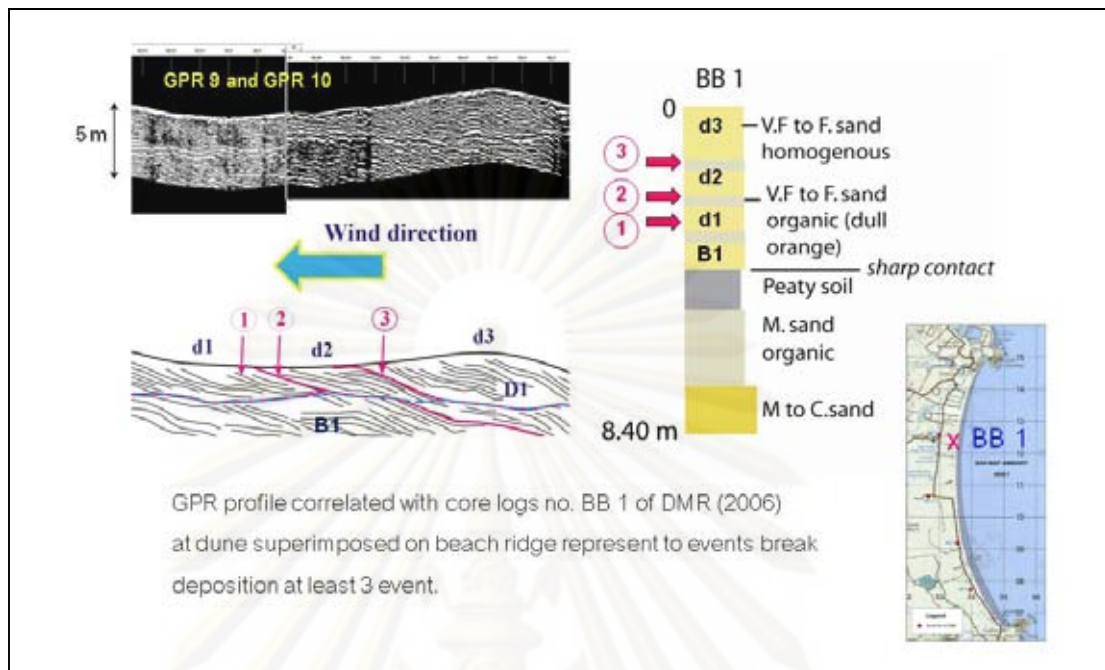


Figure 5.3. The events separated from depositional break of dune in GPR profile and core logs no. BB 5 (DMR, 2006). Dune stratigraphy represents at least 3 events.

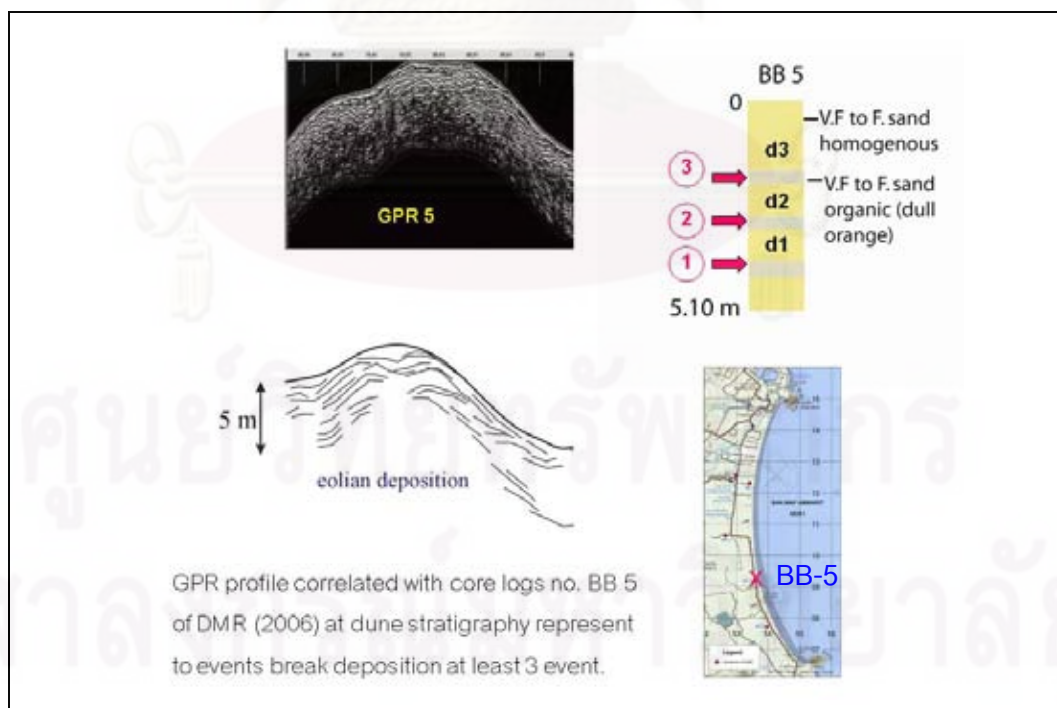


Figure 5.4. The events break deposition of dune in GPR profile and core logs no. BB 5 (DMR, 2006) at dune stratigraphy, represents at least 3 events deposition.

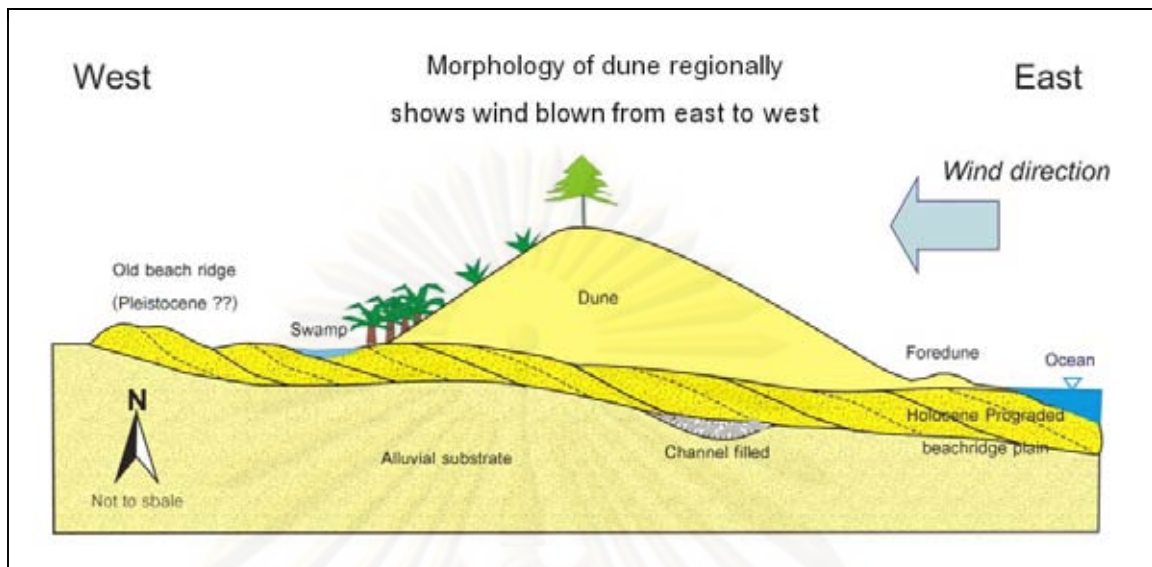


Figure 5.5. Idealized cross section of Bang Berd sand dune. Morphology of dune regionally shows wind blown from the east to the west.

The geologic map (DMR, 2007) shows the highland area of sedimentary rock and igneous rock at the western part of the southern. The slope of morphology is decreased from the highland at the western part to the undulating area and beach in the eastern part. Coastal dune formation was formed as it needed the sand supply, strong of wind and area which sand can be accumulated.

Based on dune sedimentology, GPR and aerial photographs, the major sources of fine to medium-grained sand to form a majority of parabolic and transverse dunes here are possibly from the dry Quaternary sediments (Pell and Chivas, 1995; Newsome and Ladd, 1999) locating in the western parts of the bay.

The result of petrography of sample sedimentary rock and igneous rock surrounding the study area (Appendix C) is thought to be the possible and suitable sources to supply large amount of sand in to this dune field. Their basements are composed of arkosic sandstone of the Khao Chao Formation (CP_{kc}), the Lam Thap formation (JK_l) in the western part of the study area, mostly are fine- to medium-grained (0.125-0.25 mm) mainly composed of quartz (40-50%), feldspar and rock fragments, subangular-subrounded, moderate-good sorting. Petrology of rock basements is

corresponded well with the morphological configuration of the study area that there decreases in topographical slope from the west to the east, so that it was suitable to transport along slope and then deposit in the low lying area in the eastern part of the area.

Thus, possible sources of sand supply to from the Bang Berd sand dune are thought to come from the sedimentary rock of the highland area locating in the western part of the area. Most of weathered sedimentary rocks were then possibly eroded and transported to deposit as a low lying plain in the central and the eastern parts of the area.

Consequently, the formation of dune, at onshore sand supply was caused by marine and aeolian agents; this supply provided the basis for subsequent dune formation, corresponded well with the reflection configuration of GPR and dune morphology from the aerial photograph.

Figure 5.6 shows the model of dune formation in the study area that can be explained as follows.

Stage I: Formation of alluvial substrate (Carignano, 1999; Muhs and Holliday, 2001) (Figure 5.6 a), during Holocene sea level rise (SLR). Hard rocks in the highland area (the western part of area), especially sedimentary rock is easy to weather and erode. Slope declines from the west to the east, possible to the more rapid supply of large amount of sand accommodation space exceeded the fluvial sedimentary flux and sands began to accrete over the previous low stand fluvial deposits (stage I in Figure 5.6). The flooding surface is characterized by a system channel filled between beach ridge and dune deposits in GPR signal. Corresponding to the reflection profiling in this area is channel cut and filled of DMR (1990). The presence of Holocene freshwater marsh sediments on the beach near Ban Bang Berd also suggests that a channel extended further seaward than the present shoreline.

The volume of sediment from the alluvium substrate would have been quite large initially. However, the supply of sediment from offshore would have decreased as sediment stored in shallow water was exhausted and an equilibrium profile established.

Stage II: Transgression (Figure 5.6 b), before the mid-Holocene highstand. During sea level transgression overtop the bedrock, influx of the sea covered areas of previously exposed land and sediment was swept onshore through channels. Wave energy at the shoreline increases, leading to the formation of a continuous sandy beach overlies the alluvial substrate.

Stage III: Regression (Figure 5.6 c). The reverse processes of transgression, submerged seafloor are exposed above sea level. The seaward prograding beach ridge deposits underlie the dune field are likely formed during the early to middle Holocene; where some are currently exposed to the surface. Some of these older sands may represent the dry environment during the mid-Holocene where the river distributaries are rejuvenated leading to an increase in the supply of sand and silt. Meanwhile, beaches are widened and beach ridge dunes may possibly be able to form.

Stage IV: Early dune formation (Figure 5.6 d) at the end of the transgression and regression. Most dune building occurred probably in association with specific climatic and morpho-sedimentary conditions, principally periods of easterly circulation, a greater frequency of severe Gulf of Thailand storms, RSL fall, and sediment and accommodation space availability.

Series of prograded beach ridges underneath sand dune indicated seaward deposition. This seaward progradation of beach ridges are inferred its formation after the mid-Holocene highstand. Thus, the formation of dune may have occurred during a dry condition probably during and after the mid-Holocene regression (Spensor et al., 1998; Xianwan et al., 1999; Thomas and Shaw, 2002; Nichol et al., 2003; Wang et al., 2003; Sudan et al., 2004; Tomazelli and Dillenburg, 2007; Fitzsimmons and Relfer, 2008).

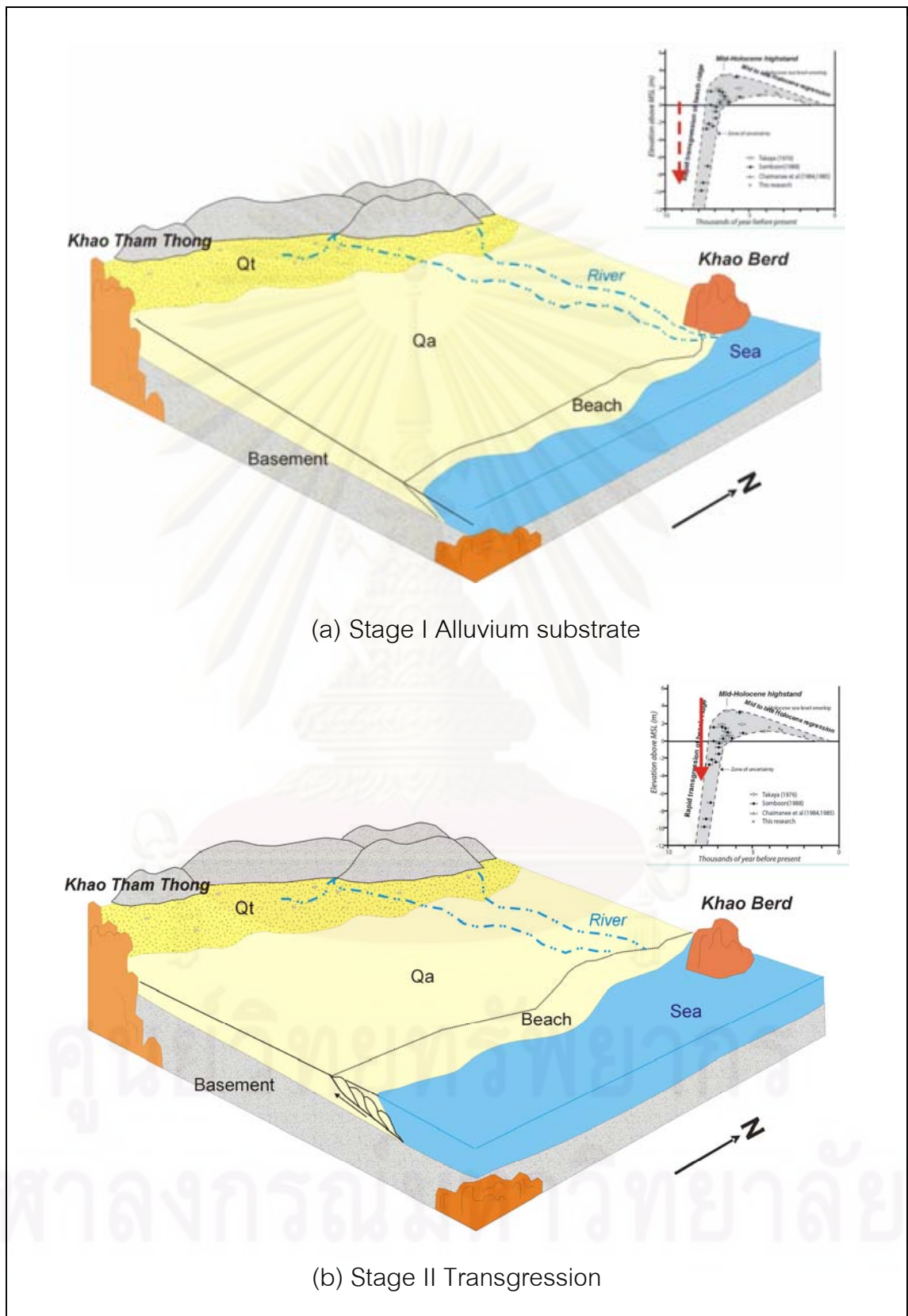


Figure 5.6. The schematic model for the formation stage of Bang Berd sand dune.

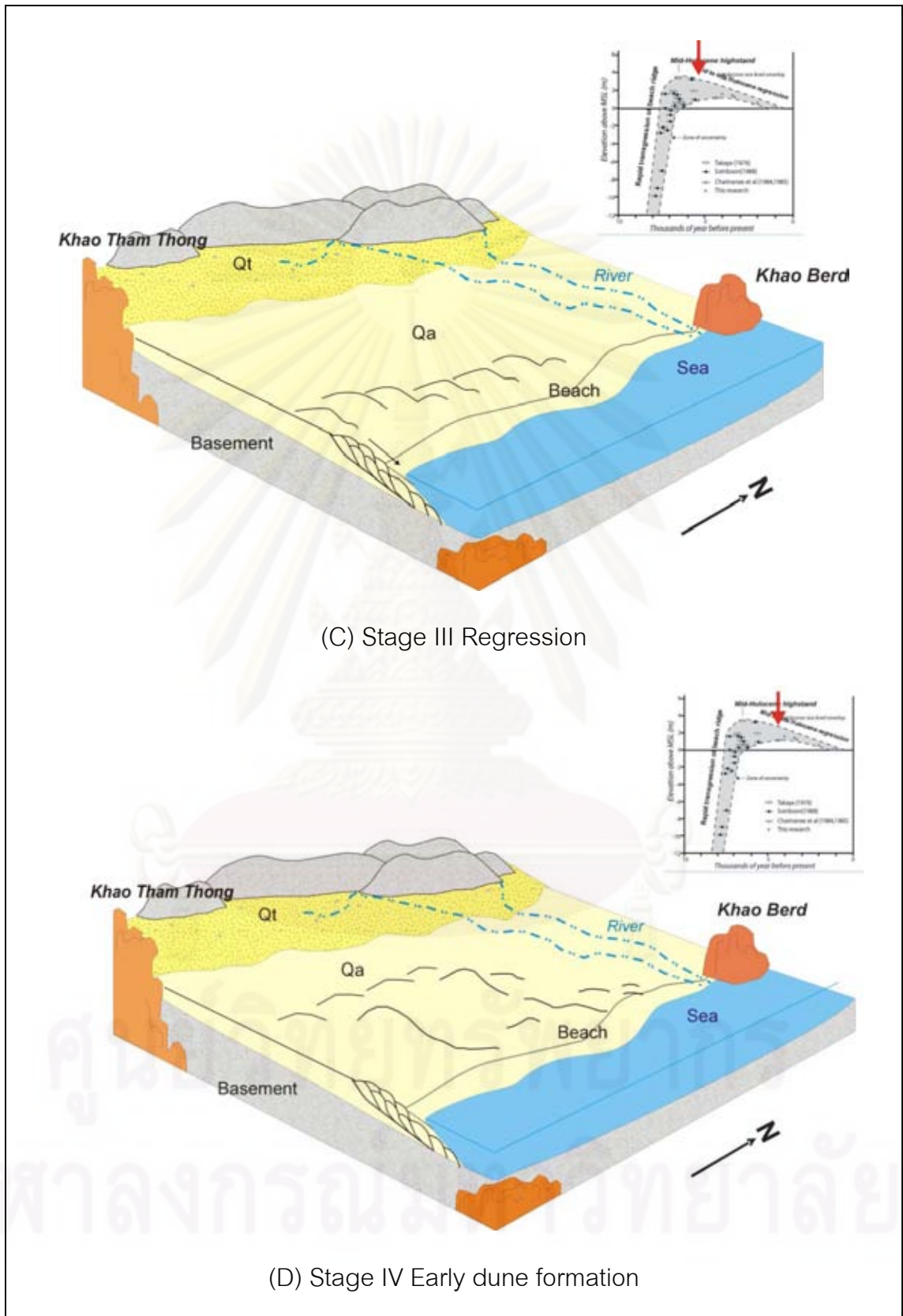


Figure 5.6. (cont.)

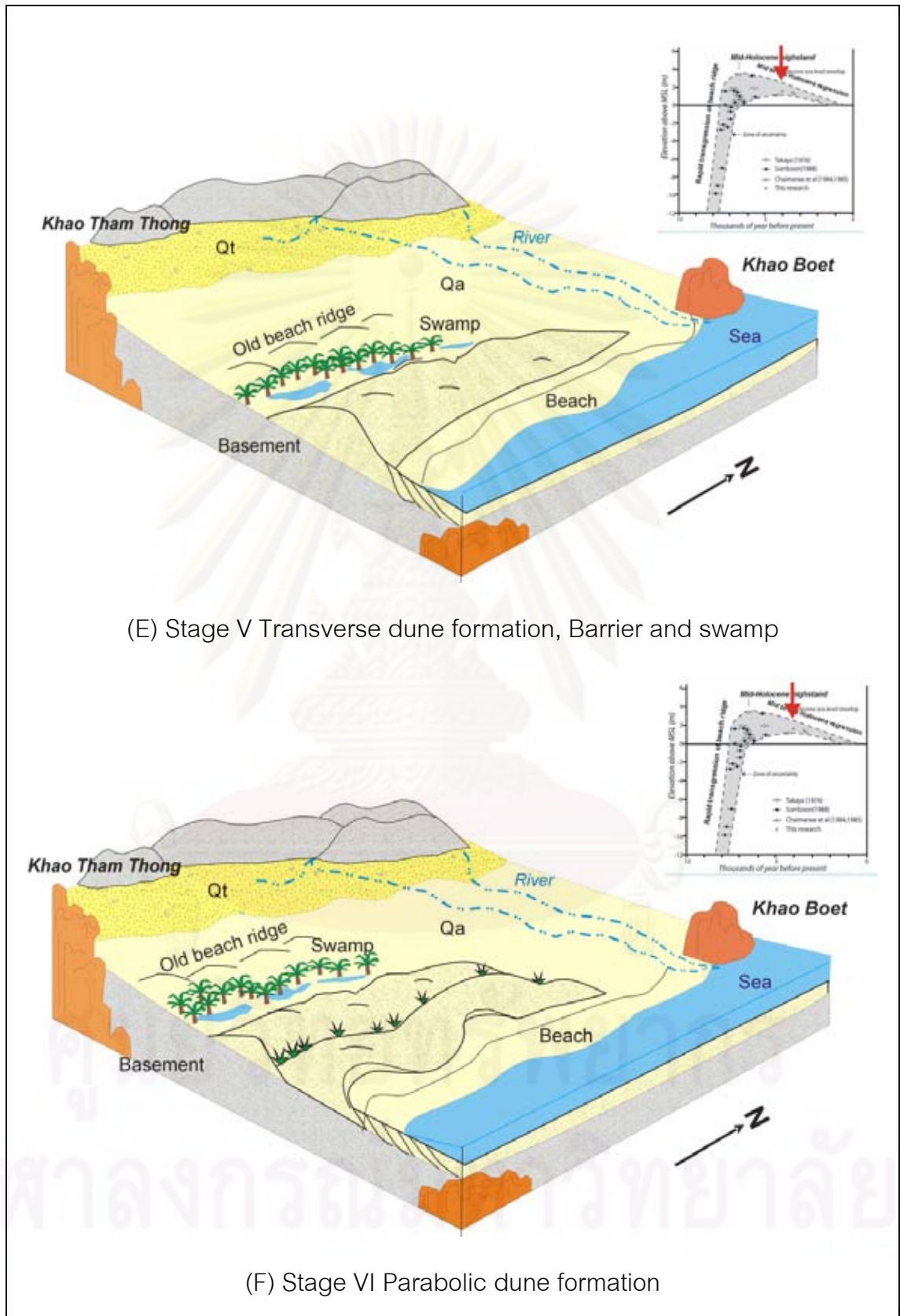


Figure 5.6. (cont.)

Almost all dune systems are associated with regressive shorelines consequently upon a fall in relative sea level (RSL) from its Holocene highstand peak, and indicate RSL functioned as a macro-scale control on dune development (Qui et al., 2004; Reesink and Bridge, 2007; Hearty and O'Leary, 2008). Where dunes are anchored on terrestrial sediment, dune expansion may have been either transgressive or regressive in nature. Where near-shore marine sediments form the dune substrate, a regressive (prograding) dune model seems most likely (Dougherty et al., 2004).

Stage V: Transverse dune, barrier and swamp formation (Figure 5.6 e), a transverse dune ridge is established landward of the beach and grows rapidly because of the abundant sediment supply during RSL is fall after mid-Holocene. The presence of trees ahead of the dune promotes the precipitation of sand at the top of the lee slope, encouraging vertical growth and restricting landward migration (Khadkikar, 2003; Hoekstra et al., 2004).

At the end of this stage, the transverse dune is stable; barrier and swamp are developed and vegetative responded to protecting dune from further instability and cutting off sediment supply (Pontee et al., 1998; Oliveira, et al., 2008). Orientations of the transverse dunes also indicate a paleo-wind blown from the east to the west.

Stage VI: Parabolic dune formation. As water levels receded, a series of transverse dunes was formed on the emerging plain. The alongshore continuity of the transverse dune ridges decreased as the shoreline become compartmentalized, and dune height is restricted by the overall decrease in sediment supply from offshore and alongshore, and the reduced beach width resulting from the sheltering effect of the emerging offshore islands

Interval of 2,220-2,960 years ago confirmed its formation in the late Holocene to which an earlier dry phase is expected to cause the extensive eolian sands. Orientations of the parabolic dunes indicate a paleo-wind blown from the east to the west.

Possible inferred time of dune formation correlated with the sea-level envelop for Thailand during Holocene (Montri Choowong et al., 2004) and OSL dating is shown in Figure 5.7.

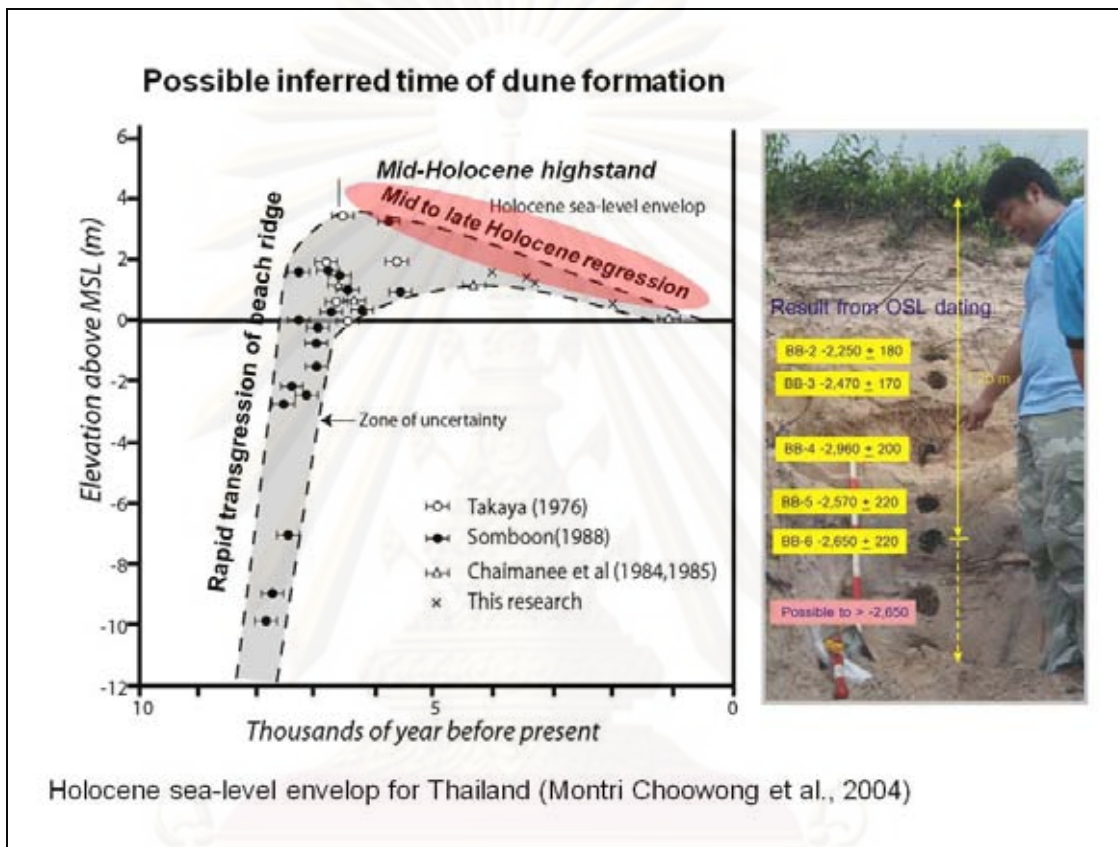


Figure 5.7. Possible time of dune formation correlated with the sea-level envelop for Thailand during Holocene (Montri Choowong et al., 2004) and OSL dating in the top-half of parabolic dune profile reveal that the formation of formation of sand dune Bang Berd may have occurred during a dry condition probably during and after the mid-Holocene regression.

Dune instability has continued intermittently until the present, although on a smaller scale, and consequently most of the present dune forms are relatively recent. The beach face and dune landforms were affected by wave attack, storm, cyclone, and wind erosion are influenced to the presence of erosion in dune (Little et al, 1978; Busby and Merritt, 1999; Andrew et al., 2002; Liu et al., 2007); the scarp dune is, then,

occurred in the southern part of the area (Figure 5.8). Recently, sediment supplied to form dune was decreased because of the construction of the highway crossing the shoreface and dune field. This recent construction denies wind to transport the sand to form dune.

5.2 Conclusion

Results of study can be concluded as follows:

- Dune in this area shows a majority of parabolic and transverse pattern; where as star shapes are localized.
- Dune texture is characterized by very homogenous fine- to medium-grained sand mainly. Very rare micro-scale sedimentary structures were observed.
- Major direction of wind blown was expected from the east to the west direction.
- OSL dating in the top-half of parabolic dune profile reveal that the formation of parabolic dune section was at around 2,220-2,960 years ago.
- Possible sources of sand to form Bang Berd sand dune are thought to come from the sedimentary rocks locating in the western part of the bay are eroding and transported to deposit at alluvium substrate in the eastern part of the area , then transported to deposit by wind to form dune. The minor part on top of dune profile shows some clues of its formation during storms.
- Formation of dune may have occurred during a dry condition probably during and after the mid-Holocene regression.

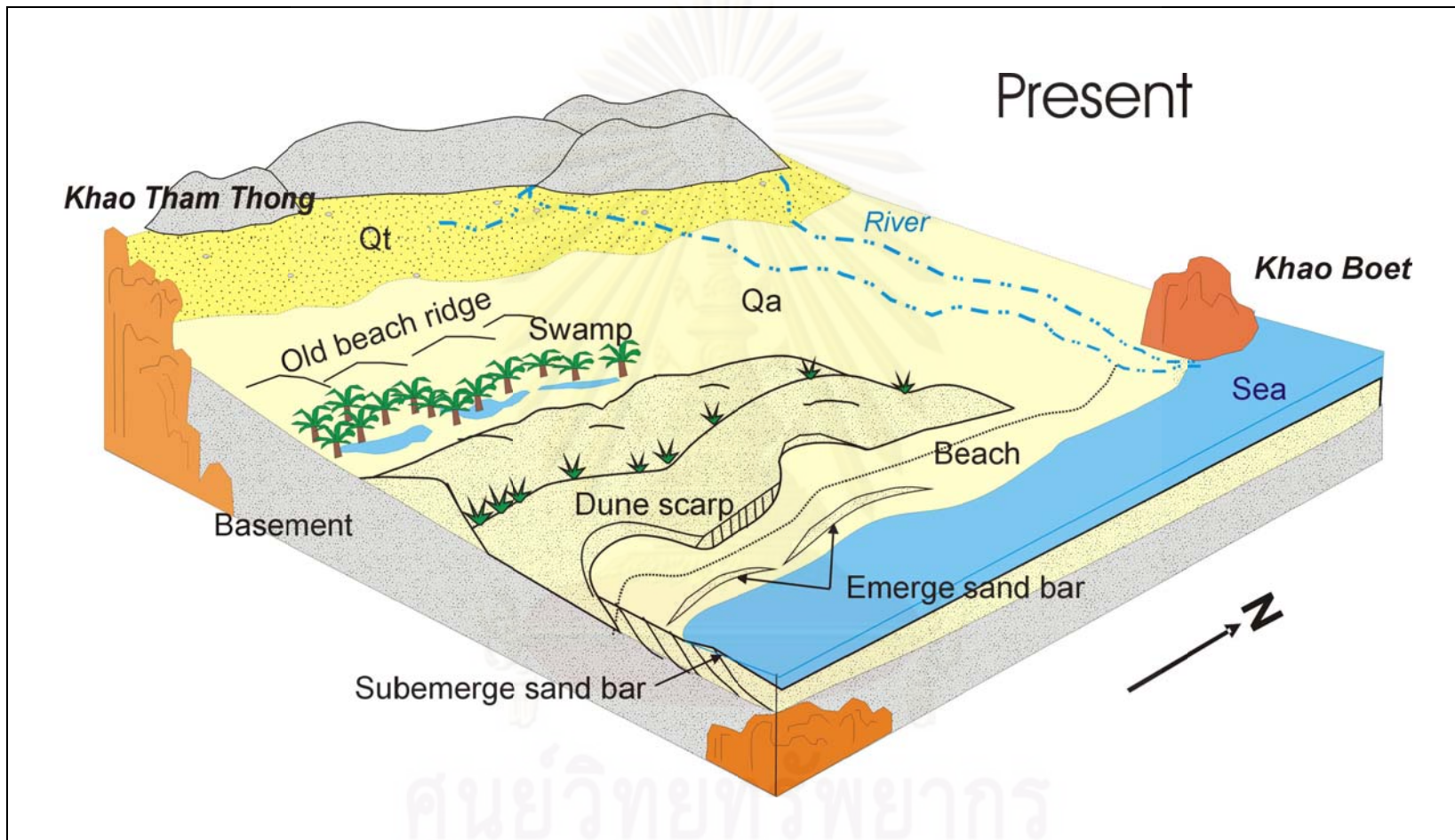


Figure 5.8. The present morphological features of Bang Berd sand dune.

REFERENCES

- Aagaard, T., Orford, J. and Murray, A. 2007. Environmental controls on coastal dune formation; Skallingen Spit, Denmark. *Geomorphology* 83: 29-47.
- Aitken, M.J. 1998. An Introduction to Optical Dating. *Oxford Science Publications*, Oxford, UK. 267 p.
- Andrew, B. A., Gares, P. A. and Colby, J. D. 2002. Techniques for GIS modeling of coastal dunes. *Geomorphology* 48: 289-308.
- Baddock, M. C., Livingstone, I. and Wiggs, G. F. 2006. The geomorphological significance of airflow patterns in transverse dune interdune. *Geomorphology* 87: 322-336.
- Bagnold, R. A. 1941. The Physics of blown sand and desert dune. *Progress in Physical Geography* 18: 91-96. London: Methuen.
- Bateman, M., Frederick, C., Jaiswal, M., Singhvi, A. 2003. Investigations of the effects of pedoturbation on luminescence dating. *QSR* 22: 1169-1176.
- Bateman, M. D., Boulter, C. H., Carr, A. S., Frederick, C. D., Peter, D., and Wilder, M. 2007. Preserving the palaeoenvironmental record in Drylands: Bioturbation and its significance for luminescence-derived chronologies. *Sedimentary Geology* 195: 5-19.
- Bennet, M. R., Cassidy, N. I. and Pile, I. 2009. Internal structure of a barrier beach as revealed by ground penetrating radar (GPR): Chesil beach, UK. *Geomorphology* 104: 218-229.
- Botter-Jensen, L., McKeever, S., Wintle, A. 2003. Optically Stimulated Luminescence Dosimetry. *Elsevier*, Amsterdam. 355 p.
- Bowling, J. C., Harry, D.L., Rodriguez, A. B. and Zheng, C. 2007. Integrated geophysical and geological investigation of a heterogeneous fluvial aquifer in Columbus Mississippi. *Journal of Applied Geophysics* 62: 58-73.

- Buynevich, I. V., FitzGerald, D. M. and Heteren, S. V. 2004. Sedimentary records of intense storms in Holocene barrier sequences, Maine, USA. *Marine Geology* 210: 135-148.
- Busby, J. P. and Merritt, J. W. 1999. Quaternary deformation mapping with ground penetrating radar. *Journal of Applied Geophysics* 41: 75-91.
- Carignano, C. A. 1999. Late Pleistocene to recent climate change in Cordoba Province, Argentina: Geomorphological evidence. *Quaternary International* 57/58: 117-134.
- Cagnoli, B. and Ulrych, T.J. 2001. Singular value decomposition and wavy reflections in ground-penetrating radar images of base surge deposits. *Journal of Applied Geophysics* 48: 175-182.
- Clemmensen, L. B., Andreasen, A., Nielsen, S. T. and Sten, E. 1996. The late, Holocene coastal dunefield at Vejers, Denmark: characteristics, sand budget and depositional dynamics. *Geomorphology* 17: 79-98.
- Clemmensen, L. B., Murray, A., Heinemeier, J. and Jong, R. D. 2009. The evolution of Holocene coastal dunefields, Jutland, Denmark: A record of climate change over the past 5000 years. *Geomorphology* 105: 303-313.
- Davis, R. A. Jr. 1985. *Coastal Sedimentary Environments; Beach and nearshore zone*. Springer-Verlag: Newyork Heidelberg Berlin. 420 p.
- Dawson, S., Smith, D. E., Jordan, J. and Dawson, G. 2004. Late Holocene coastal sand movements in the Outer Hebrides, N.W. Scotland. *Marine Geology* 210: 281-306.
- Denchok Monjai. 2005. *Geologic map of Ban Map Ammarit (Map sheet 4830 I) scale 1: 50,000*. Department of Mineral Resources.
- Department of Mineral Resources, Economic Geology Division. 1990. Geological survey the mineral resources of offshore, area Prachuap Khiri Khan province. *Economic geology report 7*: 130 p.
- Department of Mineral Resources, Environmental Geology Division. 2006. *Bang Berd Sand dune: Geological preservation site*. 53 p.

- Dougherty, A. J., FitzGerald, D. M. and Buynevich. 2004. Evidence for storm-dominated early progradation of Castle Neck barrier, Massachusetts, USA. *Marine geology* 210: 123-134.
- Eisma, D. 1965. Eolian sorting and roundness of beach and dune sand. *Netherlands Journal of Sea Research* 4: 541-555.
- Ekes, C. and Hickin, E. J. 2001. Ground Penetrating radar facies of the paraglacial Cheekye Fan, southwestern British Columbia, Canada. *Sedimentology Geology* 143: 199-217.
- Fitzsimmons, K. E. and Relfer, M. W. 2008. Sedimentary history and the interpretation of Late Quaternary dune records: Examples from the Tirari desertm Australia and the Kalahari South Africa. *Chungara Revista de Antropologia Chilena* 40: 295-308.
- Friedman, G. M. 1961. Distinction between dune, beach, and river sands from their textural characteristics. *Journal of Sedimentary Research* 31(4): 514-529.
- Folk, R. L. 1968. *Petrology of sedimentary rock*. Austin, Texas: phill's: 85 p.
- Friedman, G. M. 1961. Distinction between dune, beach, and river sands from their textural characteristics. *Journal of Sedimentary Research* 31: 514-529.
- Galgaro, A., Finzi, E., Tosi and Luigi. 2000. An experiment on a sand-dune environment in Southern Venetian coast based on GPR, VES and documentary evidence. *Annali Di Geofisca* 43 (2): 289-295.
- Giannini, P. C. F., Sawakuchi, A. O., Martinho, C. T. and Tatumi, S. H. 2007. Eolian depositional episodes controlled by Late Quaternary relative sea level changes on the Imbituba–Laguna coast (southern Brazil). *Marine Geology* 237: 143-168.
- Girardi, J. and Davis, D. M. 2010. Parabolic dune reactivation and migration at Napeague, NY, USA: Insights from aerial and GPR imagery. *Geomorphology* 114: 530-541.

- Havholm, K. G., Bergstrom, N. D., Jol, H. M. and Running G. L. 2003. GPR survey of a Holocene aeolian/fluvial/lacustrine succession, Lauder Sandhills, Manitoba, Canada. *The Geological Society of London*: 47-54.
- Hearty, P. J. and O'Leary, M. J. 2008. Carbonate eolianites, quartz sands, and Quaternary sea-level cycles, Western Australia: A chronostratigraphic approach. *Quaternary Geochronology* 3: 26-55.
- Hoekstra, P., Bell, P., Santen, P. M., Roode, N., Levoy, F. and Whitehouse, R. 2004. Bedform migration and bedload transport on an intertidal shoal. *Continental Shelf research* 24: 1249-1269.
- Hugenholtz, C. H. and Moorman. 2007. Ground penetrating radar (GPR) imaging of the internal structure of an active parabolic sand dune. *The Geological Society of America: Special paper* 432: 35-45.
- Isla, F. I. and Espinosa, M. A. 1995. Coastal environment changes associated with Holocene sea level fluctuation: Southeastern Buenos Aires, Argentina. *Quaternary International* 26: 55-60.
- Jacobberger, P. A. 1989. Reflectance Characteristics and Surface Processes in Stabilized Dune Environments. *Remote Sensing Environment* 28: 287-295.
- Jol, M. H., Lawton, D. C. and Smith, D. G. 2002. Ground penetrating radar: 2-D and 3-D subsurface imaging of a coastal barrier spit, Long Beach, WA, USA. *Geomorphology* 53: 165-181.
- Khadkikar, A. S. 2003. Bedform migration and bar evolution in a late Quaternary monsoon-influenced river, Gujarat, western India. *Sedimentology Geology* 157: 277-289.
- Lian, O.B., 2007. Luminescence Dating, in: Encyclopedia of Quaternary Science. Elsevier. 3,576 p.
- Little, I. P., Armitage, T. M. and Gilkes, R. J. 1978. Weathering of quartz in dune sands under subtropical conditions in eastern Australia. *Geoderma* 20: 225-237.

- Liu, Z., Yan, Q., Liu, B., Ma, J. and Luo, Y. 2007. Persistent soil seed bank in *Agriophyllum squarrosum* (Chenopodiaceae) in a deep sand profile: Variation along a transect of an active sand dune. *Journal of Arid Environments* 71: 236-242.
- Livingstone, I., Wiggs, G. F. S. and Weaver, C. M. 2007. Geomorphology of desert sand dunes: A review of recent progress. *Earth-Science Reviews* 80: 239-257.
- Meteorological station at Changwat Chumphon. 2009. *Frequency distribution of the wind direction at Changwat Chumphon between 1981-2009*.
- Meteorological station at Changwat Prachuap Khiri Khan. 2009. *Frequency distribution of the wind direction at Changwat Prachuap Khiri Khan between 1981-2009*.
- Montri Choowong, Ugai, H., Titima Charoentitirat, Punya Charusiri, Veerote daorerk, Rattakorn Songmuang and Rottana Ladachart. 2004. Holocene Biostratigraphical Records in Coastal Deposits from Sam Roi Yod National Park, Prachuap Khiri Khan, Western Thailand. *The Natural History Journal of Chulalongkorn University* 4(2): 1-18.
- Montri Silpalit, Assanee Meesook and Somchai Lovacharasupaphon. 1975. *Geologic map of Changwat Prachuap Khiri Khan (NC 47-3) scale 1: 250,000*. Department of Mineral Resources.
- Moody, L. E. and Graham, R. C. 1995. Geomorphic and pedogenic evolution in coastal sediments, central California. *Geoderma* 67: 181-201.
- Moura, D., Pires, C. V., Albardeiro, L., Boski, T., Rodrigues, A.L. and Tareco, H. 2007. Holocene sea level fluctuations and coastal evolution in the central Algarve (southern Portugal). *Marine Geology* 237: 127-142.
- Muhs, D. R. and Holliday, V. T. 2001. Origin of late Quaternary dune fields on the Southern High Plains of Texas and New Mexico. *Geological Society of America*: 75-87.

- Murray, A.S. And Wintle, A.G. (2000) Luminescence dating of quartz using an improved single-aliquot regenerative-dose protocol. *Radiation Measurements* 32: 57-73.
- Nattawut Prachantasen, Montri Choowong, Santi Pailoplee, and Sumet Phunthuwongraj. 2008. Sedimentary characteristics of sand dune from Bang Berd, Chumphon Province, Western Thailand. *Bulletin Earth Science Thailand (BEST)* 1 (1&2): Department of Geology, Faculty of Science, Chulalongkorn University: 28-34.
- Neal, A., Richards, J. and Pye, K. 2003. Sedimentology of coarse-clastic beach-ridge deposits, Essex, southeast England. *Sedimentology Geology* 162: 167-198.
- Neal, A. 2004. Ground-penetrating radar and its used in sedimentology: principles, problems and progress. *Earth-Science Review* 66: 261-330.
- Newsome, D. and Ladd, P. 1999. The use of quartz grain microtextures in the study of the origin of sand terrains in Western Australia. *Catena* 35: 1-17.
- Nichol, S. L., Lian, O. B. and Carter, C. H. 2003. Sheet-gravel evidence for a late Holocene tsunami run-up on beach dunes, Great Barrier Island, New Zealand. *Sedimentology Geology* 155: 129-145.
- O'Neal, M. L. and McGeary, S. 2002. Late Quaternary stratigraphy and sea-level history of the northern Delaware Bay margin, southern New Jersey, USA: a ground penetrating radar analysis of composite Quaternary coastal terraces. *Quaternary sciences review* 21: 929-946.
- Oliveira, J. G. Jr., Medeiros, W. E., Tabosa, W. F. and Vital, H. 2008. From Barchan to Domic shape: Evaluation of a coastal sand dune in northeastern Brazil based on GPR Survey. *Revista Brasileira de Geofisica* 26(1): 5-20.
- Orford, J. D., Murdy, J. M. and Wintle, A. G. 2003. Prograded Holocene beach ridges with superimposed dunes in north-east Ireland: mechanisms and timescales of fine and coarse beach sediment decoupling and deposition. *Marine Geology* 194: 47-64.

- Overmeeren, R. A. 1998. Radar facies of unconsolidated sediments in The Netherlands: A radar stratigraphy interpretation method for hydrogeology. *Journal of applied geophysics* 40: 1-18.
- Pederson, K. and Clemmensen, L. B. 2005. Unveiling past aeolian landscapes: A ground-penetrating radar survey of a Holocene coastal dunefield system, Thy, Denmark. *Sedimentology Geology* 177: 57-86.
- Pell, S. D. and Chivas, A. R. 1995. Surface features of sand grains from the Australian Continental Dunefield. *Paleography, Paleoclimatology, Paleoecology* 113: 119-132.
- Pettijohn, F. J. 1975. *Sedimentary rock*. New York: Harper & Row. 628 p.
- Pontee, N. I., Jean-Pierre Tastet, J. P. and Masse, L. 1998. Morpho-sedimentary evidence of Holocene coastal changes near the mouth of the Gironde and on the Medoc Peninsula, SW France. *Oceanologica Acta* 21: 243-261.
- Qui, G. Y., Lee, I. N., Shimizu, H., Gao, Y. and Ding, G. 2004. Principles of sand dune fixation with straw checkerboard technology and its effects on the environment. *Journal of arid Environments* 56: 449-464.
- Reesink, A. J. H. and Bridge, J. S. 2007. Influence of superimposed bedforms and flow unsteadiness on formation of cross strata in dunes and unit bars. *Sedimentology Geology* 202: 281-296.
- Royal Thai Survey Department. 2000. *Topographic map of Map sheet scale 1:50,000 of Ban Map Ammarit (4830 I) L 7018 (1)*.
- Sanjeevi, S. 1996. Morphology of dunes of the Coromandel coast of Tamil Nadu: A satellite data based approach for coastal landuse planning. *Landscape and Urban Planning* 34: 189-195.
- Santalla, I. R., García, M. J. S., Montes, I. M., Ortiz, D. G., Crespo, T. M. and Raventos, J. S. 2009. Internal structure of the aeolian sand dunes of El Fangar spit, Ebro Delta (Tarragona, Spain). *Geomorphology* 104: 238-252.

- Saye, S. E., Wal, V. D., Pye, K. and Blott, S. J. 2005. Beach–dune morphological relationships and erosion/accretion: An investigation at five sites in England and Wales using LIDAR data. *Geomorphology* 72: 128-155.
- Smith, B. J. and Whalley, W. B. 1981. Late Quaternary drift deposits of north Central Nigeria examined by scanning electron microscopy. *Catena* 8: 345-367.
- Sponsor, C. D., Plater, A. J. and Long, A. J. 1998. Rapid coastal change during the mid- to late Holocene: the record of barrier estuary sedimentation in the Romney March region, southeast England. *The Holocene* 8: 143-163.
- Sudan, P., Whitmore, G. and Uken, R. 2004. Quaternary evolution of the coastal dunes between Lake Hlabane and cape St Lucia, KwaZulu-Natal. *South African Journal of Geology* 107: 355-376.
- Suphawadee Vimuktanandana, Assanee Meesook and Suvapak Imsamut. 2007. *Geologic map of changwat Chumphon*. Department of Mineral Resources.
- Switzer, A. D., Bristow, C. S. and Jones, B. G. 2005. Investigation of large-scale washover of a small barrier system on the southeast Australian coast using ground penetrating radar. *Sedimentary Geology* 183: 145-156.
- Tamura, T., Murakami, F., Nanayama, F., Watanabe, K. and Saito, Y. 2008. Ground-penetrating radar profiles of Holocene raised-beach deposits in the Kujukuri strand plain, Pacific coast of eastern Japan. *Marine Geology* 248: 11-27.
- Thomas, D. S. G. and Shaw, P. A. 2002. Late Quaternary environmental change in central southern Africa: new data, synthesis, issues and prospects. *Quaternary Science reviews* 21: 783-797.
- Tomazelli, L. and Dillenburger, S. R. 2007. Sedimentary facies and stratigraphy of a last interglacial coastal barrier in south Brazil. *Marine geology* 244: 33-45.
- Wang, X., Dong, Z., Qu, J., Zhang, J. and Zhao, A. 2003. Dynamic processes of a simple linear dune—a study in the Taklimakan Sand Sea, China. *Geomorphology* 52: 233-241.

Xianwan, L., Sen, L. and Jianyou, S. 1999. Wind tunnel simulation experiment of mountain dunes. *Journal of Arid Environments* 42: 49-59.

Available from : <http://www.cartage.org>

Available from : <http://www.emrl.byu.edu>

Available from : <http://www.indiana.edu>

Available from : <http://www.guaddunes.com>

Available from : <http://digital-desert.com>

Available from : <http://pirun.ku.ac.th>

Available from : <http://core.ecu.edu>



ศูนย์วิทยทรัพยากร
จุฬาลงกรณ์มหาวิทยาลัย



APPENDICES

ศูนย์วิทยทรัพยากร
จุฬาลงกรณ์มหาวิทยาลัย

APPENDIX A

LOCATION OF GROUND PENETRATING RADAR SURVEY

Table A-1. Location of GPR survey.

Station (m)	Location		
	X	Y	Z
GPR 3			
L3-0	554415.56	1207153.53	11.83
L3-5	554412.71	1207157.57	12.48
L3-10	554409.51	1207161.44	12.36
L3-15	554406.11	1207164.99	11.96
L3-20	554403.27	1207169.13	11.42
L3-25	554400.13	1207173.00	11.19
L3-30	554396.82	1207176.74	11.32
L3-35	554393.62	1207180.50	11.24
L3-40	554390.51	1207184.44	10.85
L3-45	554387.42	1207188.31	10.48
L3-50	554384.25	1207192.02	9.79
L3-55	554380.63	1207195.70	9.25
L3-60	554377.27	1207199.10	9.03
L3-65	554373.64	1207202.56	8.79
L3-70	554370.01	1207206.03	8.77
L3-75	554366.41	1207209.47	8.77
L3-80	554362.73	1207212.93	8.70
L3-85	554359.06	1207216.34	8.67
L3-90	554355.69	1207219.85	8.36
L3-95	554352.12	1207223.29	8.73
L3-100	554348.66	1207226.91	8.74
GPR 4			
L4-0	554509.28	1207222.34	0.20
L4-5	554504.89	1207219.89	0.37
L4-10	554500.49	1207217.44	0.30

Table A-1. (cont.)

Station (m)	Location		
	X	Y	Z
L4-15	554496.10	1207214.99	0.26
L4-20	554491.70	1207212.54	0.15
L4-25	554487.30	1207210.08	0.13
L4-30	554482.88	1207207.75	0.31
L4-35	554478.53	1207205.37	0.43
L4-40	554474.56	1207203.21	2.16
L4-45	554470.95	1207201.10	4.84
L4-50	554462.28	1207197.03	7.30
L4-55	554457.93	1207194.64	7.32
L4-60	554453.52	1207192.27	7.63
L4-65	554449.19	1207189.85	7.67
L4-70	554444.79	1207187.40	7.93
L4-75	554440.48	1207184.87	7.89
L4-80	554436.19	1207182.37	7.53
L4-85	554431.72	1207180.02	7.40
L4-90	554427.36	1207177.71	7.04
L4-95	554423.19	1207175.29	7.54
L4-100	554418.94	1207172.77	8.84
L4-105	554414.74	1207170.39	10.04
L4-110	554410.48	1207167.98	11.14
L4-115	554406.24	1207165.48	11.78
L4-120	554402.26	1207162.61	12.34
GPR 5			
L5-0	553691.44	1209241.87	0.33
L5-5	553686.09	1209242.80	0.71
L5-10	553681.19	1209243.57	0.61
L5-15	553676.23	1209244.17	0.23
L5-20	553671.43	1209245.03	0.32
L5-25	553666.51	1209245.76	0.60

Table A-1. (cont.)

Station (m)	Location		
	X	Y	Z
L5-30	553661.52	1209246.42	0.73
L5-35	553656.59	1209247.00	0.87
L5-40	553651.58	1209247.70	1.06
L5-45	553646.66	1209248.31	1.25
L5-50	553641.63	1209248.94	1.35
L5-55	553636.63	1209249.54	1.45
L5-60	553631.74	1209250.56	1.93
L5-65	553626.89	1209251.48	1.92
L5-70	553622.43	1209252.53	3.56
L5-75	553618.12	1209253.40	5.96
L5-80	553613.42	1209254.59	7.03
L5-85	553608.58	1209255.39	7.62
L5-90	553603.58	1209256.03	8.09
L5-95	553598.71	1209256.43	8.85
L5-100	553593.82	1209257.13	9.15
L5-105	553588.88	1209257.87	9.56
L5-110	553584.05	1209258.35	10.32
L5-115	553578.85	1209259.27	10.38
L5-120	553574.24	1209259.90	9.87
L5-125	553569.46	1209260.59	10.02
L5-130	553564.74	1209261.26	11.97
L5-135	553560.64	1209261.69	14.18
L5-140	553556.20	1209263.09	15.51
L5-145	553551.44	1209264.41	15.56
L5-150	553546.46	1209265.53	15.59
L5-155	553542.03	1209267.96	14.13
L5-160	553537.92	1209270.46	13.68
L5-165	553533.57	1209272.64	12.40
L5-170	553529.74	1209274.92	10.10

Table A-1. (cont.)

Station (m)	Location		
	X	Y	Z
GPR 6			
L6-0	553509.00	1209205.00	16.52
L6-5	553510.28	1209209.48	15.84
L6-10	553511.56	1209213.96	15.62
L6-15	553512.84	1209218.44	15.45
L6-20	553514.12	1209222.92	15.30
L6-25	553515.40	1209227.40	16.52
L6-30	553516.68	1209231.88	17.39
L6-35	553517.96	1209236.36	16.41
L6-40	553519.24	1209240.84	16.39
L6-45	553520.52	1209245.32	16.21
L6-50	553521.80	1209249.80	15.68
L6-55	553523.08	1209254.28	15.02
L6-60	553524.36	1209258.76	14.44
L6-65	553525.64	1209263.24	13.68
L6-70	553526.92	1209267.72	13.33
GPR 7			
L7-0	553240.00	1210455.00	20.74
L7-5	553243.32	1210457.29	20.81
L7-10	553246.64	1210459.57	20.61
L7-15	553249.95	1210461.86	20.97
L7-20	553253.27	1210464.14	22.10
L7-25	553256.59	1210466.43	22.80
L7-30	553259.91	1210468.71	22.62
L7-35	553263.23	1210471.00	22.10
L7-40	553266.54	1210473.28	21.27
L7-45	553269.86	1210475.57	20.17
L7-50	553273.18	1210477.85	18.71
L7-55	553276.50	1210480.14	17.51

Table A-1. (cont.)

Station (m)	Location		
	X	Y	Z
GPR 8			
L7-60	553279.82	1210482.42	16.25
L7-65	553283.13	1210484.71	15.26
L7-70	553286.45	1210486.99	14.80
L7-75	553289.77	1210489.28	14.55
L7-80	553293.09	1210491.56	14.35
L7-85	553296.41	1210493.85	14.36
L7-90	553299.72	1210496.13	14.00
L7-95	553303.04	1210498.42	12.99
L7-100	553306.36	1210500.70	12.86
L8-0	553264.00	1210462.00	20.72
L8-5	553262.72	1210466.15	21.82
L8-10	553261.44	1210470.30	21.42
L8-15	553260.16	1210474.45	20.41
L8-20	553258.88	1210478.60	18.98
L8-25	553257.60	1210482.75	17.81
L8-30	553256.32	1210486.90	17.37
L8-35	553255.04	1210491.05	17.43
L8-40	553253.76	1210495.20	18.03
L8-45	553252.48	1210499.35	18.65
L8-50	553251.20	1210503.50	19.41
L8-55	553249.92	1210507.65	20.27
L8-60	553248.64	1210511.80	21.59
L8-65	553247.36	1210515.95	22.27
GPR 9			
L9-0	553465.51	1212306.59	8.87
L9-5	553460.34	1212306.97	8.87
L9-10	553455.47	1212307.74	9.77
L9-15	553450.59	1212308.19	10.05

Table A-1. (cont.)

Station (m)	Location		
	X	Y	Z
L9-20	553445.68	1212309.21	9.82
L9-25	553440.80	1212309.93	9.57
L9-30	553435.80	1212310.58	9.16
GPR 10			
L10-0	553417.01	1212316.63	9.95
L10-5	553411.87	1212317.42	9.62
L10-10	553406.89	1212318.06	9.63
L10-15	553401.93	1212318.74	9.78
L10-20	553397.05	1212319.04	9.92
L10-25	553392.20	1212319.73	10.38
L10-30	553387.17	1212320.33	10.65
L10-35	553382.31	1212320.96	11.23
L10-40	553377.33	1212321.90	11.64
L10-45	553372.40	1212322.54	11.61
L10-50	553367.38	1212323.21	11.52
L10-55	553361.47	1212323.59	11.32
L10-60	553357.45	1212323.97	11.97
L10-65	553352.63	1212324.51	12.60
L10-70	553347.63	1212325.42	12.91
L10-75	553342.80	1212326.21	12.37
L10-80	553337.81	1212326.32	11.85
L10-85	553332.74	1212326.75	12.30
L10-90	553327.93	1212328.07	12.80
L10-95	553323.09	1212328.75	13.54
L10-100	553318.19	1212329.64	14.03
L10-105	553313.27	1212329.86	14.41
L10-110	553308.33	1212330.52	14.30
L10-115	553303.49	1212330.95	14.01
L10-120	553298.57	1212331.16	13.82

Table A-1. (cont.)

Station (m)	Location		
	X	Y	Z
L10-125	553293.64	1212332.05	13.28
L10-130	553288.62	1212332.76	12.83
GPR 11			
L11-0	553626.00	1212974.00	-1.66
L11-5	553621.20	1212975.75	-1.38
L11-10	553616.40	1212977.50	-1.46
L11-15	553611.60	1212979.25	-1.67
L11-20	553606.80	1212981.00	-1.35
L11-25	553602.00	1212982.75	-0.93
L11-30	553597.20	1212984.50	-0.71
L11-35	553592.40	1212986.25	-0.81
L11-40	553587.60	1212988.00	-0.72
L11-45	553582.80	1212989.75	0.31
L11-50	553578.00	1212991.50	-0.10
L11-55	553573.20	1212993.25	0.31
L11-60	553568.40	1212995.00	0.54
L11-65	553563.60	1212996.75	0.86
L11-70	553558.80	1212998.50	0.98
L11-75	553554.00	1213000.25	1.42
L11-80	553549.20	1213002.00	1.72
L11-85	553544.40	1213003.75	1.74
L11-90	553539.60	1213005.50	1.72
L11-95	553534.80	1213007.25	1.60
L11-100	553530.00	1213009.00	1.72
L11-105	553525.20	1213010.75	2.13
L11-110	553520.40	1213012.50	2.44
L11-115	553515.60	1213014.25	2.52
L11-120	553510.80	1213016.00	2.54
L11-125	553506.00	1213017.75	2.54

Table A-1. (cont.)

Station (m)	Location		
	X	Y	Z
L11-130	553501.20	1213019.50	2.56
L11-135	553496.40	1213021.25	2.79
L11-140	553491.60	1213023.00	2.84
L11-145	553486.80	1213024.75	3.00
L11-150	553482.00	1213026.50	2.33
L11-155	553477.20	1213028.25	1.91
L11-160	553472.40	1213030.00	2.20
L11-165	553467.60	1213031.75	2.62
L11-170	553462.80	1213033.50	2.85
L11-175	553458.00	1213035.25	3.32
L11-180	553453.20	1213037.00	3.43
L11-185	553448.40	1213038.75	3.62
L11-190	553443.60	1213040.50	3.57
L11-195	553438.80	1213042.25	3.29
L11-200	553434.00	1213044.00	2.70
L11-205	553429.20	1213045.75	1.49
L11-210	553424.40	1213047.50	1.18
L11-215	553419.60	1213049.25	0.97
L11-220	553414.80	1213051.00	1.24
L11-225	553410.00	1213052.75	1.96
L11-230	553405.20	1213054.50	2.95
L11-235	553400.40	1213056.25	3.67
L11-240	553395.60	1213058.00	3.70
L11-245	553390.80	1213059.75	3.37
L11-250	553386.00	1213061.50	2.79
L11-255	553381.20	1213063.25	2.93
L11-260	553376.40	1213065.00	3.49
L11-265	553371.60	1213066.75	3.79
L11-270	553366.80	1213068.50	3.65

Table A-1. (cont.)

Station (m)	Location		
	X	Y	Z
L11-275	553362.00	1213070.25	3.10
L11-280	553357.20	1213072.00	2.96
L11-285	553352.40	1213073.75	2.51
L11-290	553347.60	1213075.50	2.07
L11-295	553342.80	1213077.25	1.77
GPR 12			
L12-0	553361.00	1213063.00	2.57
L12-5	553355.96	1213063.29	2.03
L12-10	553350.92	1213063.58	1.66
L12-15	553345.88	1213063.87	1.75
L12-20	553340.84	1213064.16	1.77
L12-25	553335.80	1213064.45	1.69
L12-30	553330.76	1213064.74	1.60
L12-35	553325.72	1213065.03	1.50
L12-40	553320.68	1213065.32	1.59
L12-45	553315.64	1213065.61	1.66
L12-50	553310.60	1213065.90	1.91
L12-55	553305.56	1213066.19	1.98
L12-60	553300.52	1213066.48	1.84
L12-65	553295.48	1213066.77	1.62
L12-70	553290.44	1213067.06	1.54
L12-75	553285.40	1213067.35	1.34
L12-80	553280.36	1213067.64	1.44
L12-85	553275.32	1213067.93	1.67
L12-90	553270.28	1213068.22	2.49
L12-95	553265.24	1213068.51	3.64
L12-100	553260.20	1213068.80	4.14
L12-105	553255.16	1213069.09	4.35
L12-110	553250.12	1213069.38	4.37

Table A-1. (cont.)

Station (m)	Location		
	X	Y	Z
L12-115	553245.08	1213069.67	4.33
L12-120	553240.04	1213069.96	4.38
L12-125	553235.00	1213070.25	4.60
L12-130	553229.96	1213070.54	4.79
L12-135	553224.92	1213070.83	4.24
L12-140	553219.88	1213071.12	3.39
L12-145	553214.84	1213071.41	3.07
L12-150	553209.80	1213071.70	3.70
L12-155	553204.76	1213071.99	4.94
L12-160	553199.72	1213072.28	5.64
L12-165	553194.68	1213072.57	6.09
L12-170	553189.64	1213072.86	6.52
L12-175	553184.60	1213073.15	7.48
L12-180	553179.56	1213073.44	9.23
L12-185	553174.52	1213073.73	9.20
L12-190	553169.48	1213074.02	8.78
L12-195	553164.44	1213074.31	7.25
L12-200	553159.40	1213074.60	5.97
L12-205	553154.36	1213074.89	4.62
L12-210	553149.32	1213075.18	3.54
L12-215	553144.28	1213075.47	2.54
L12-220	553139.24	1213075.76	1.90
L12-225	553134.20	1213076.05	1.78
L12-230	553129.16	1213076.34	2.00
L12-235	553124.12	1213076.63	2.25
L12-240	553119.08	1213076.92	2.43
GPR 13			
L13-0	553123.00	1213066.00	1.82
L13-5	553126.80	1213070.00	2.02

Table A-1. (cont.)

Station (m)	Location		
	X	Y	Z
L13-10	553130.60	1213074.00	2.24
L13-15	553134.40	1213078.00	2.69
L13-20	553138.20	1213082.00	3.19
L13-25	553142.00	1213086.00	3.26
L13-30	553145.80	1213090.00	2.88
L13-35	553149.60	1213094.00	2.66
L13-40	553153.40	1213098.00	2.59
L13-45	553157.20	1213102.00	3.35
L13-50	553161.00	1213106.00	3.19
L13-0	553123.00	1213066.00	1.82
L13-5	553126.80	1213070.00	2.02
L13-10	553130.60	1213074.00	2.24
L13-15	553134.40	1213078.00	2.69
L13-20	553138.20	1213082.00	3.19
GPR 14			
L14-0	553379.00	1213051.00	2.97
L14-5	553380.08	1213055.56	3.24
L14-10	553381.16	1213060.12	3.57
L14-15	553382.24	1213064.68	3.83
L14-20	553383.32	1213069.24	3.90
L14-25	553384.40	1213073.80	3.85
L14-30	553385.48	1213078.36	3.88
L14-35	553386.56	1213082.92	3.70
L14-40	553387.64	1213087.48	3.29
L14-45	553388.72	1213092.04	2.88
L14-50	553389.80	1213096.60	2.59
L14-55	553390.88	1213101.16	2.53
L14-60	553391.96	1213105.72	2.78
L14-65	553393.04	1213110.28	3.31

Table A-1. (cont.)

Station (m)	Location		
	X	Y	Z
L14-70	553394.12	1213114.84	3.65
L14-75	553395.20	1213119.40	4.11
L14-80	553396.28	1213123.96	4.40
L14-85	553397.36	1213128.52	4.94
L14-90	553398.44	1213133.08	4.95
L14-95	553399.52	1213137.64	4.85
L14-100	553400.60	1213142.20	4.51
L14-105	553401.68	1213146.76	4.20
L14-110	553402.76	1213151.32	3.76
L14-115	553403.84	1213155.88	3.81
L14-120	553404.92	1213160.44	3.86
L14-125	553406.00	1213165.00	3.93

ศูนย์วิทยทรัพยากร
จุฬาลงกรณ์มหาวิทยาลัย

APPENDIX B

GRAIN SIZE ANALYSIS

Table B-1. Location of collected sample and statistic parameter.

No.	Sample name	Location		Standard deviation	Skewness	Kurtosis
		E	N			
1	BB 1-1	0553064	1205902	0.082	0.082	0.926
2	BB 1-2	0553064	1205902	0.092	0.031	0.940
3	BB 1-3	0553064	1205902	0.084	0.088	0.915
4	BB-001	554497	1207275	0.085	0.086	0.920
5	BB-002	554414	1207173	0.082	0.095	0.949
6	BB-003	554078	1208190	0.083	0.088	0.950
7	BB-004	553977	1208063	0.091	0.059	0.933
8	BB-006	553668	1208344	0.088	0.073	0.922
9	BB-011	553694	1209384	0.086	0.07	1.158
10	BB-012	554546	1206825	0.081	0.06	0.905
11	BB-013	554901	1206283	0.096	0.191	0.894
12	BB-015	553173	1213064	0.093	0.163	0.937
13	BB-019	553730	1208863	0.082	0.065	1.119
14	BB-020	553660	1208739	0.11	0.126	0.952
15	BB-021	553695	1208745	0.097	0.105	0.972
16	BB-022	553633	1208816	0.101	0.077	0.946
17	BB-023	553641	1208641	0.083	0.076	0.947
18	BB-025	554373	1218043	0.08	0.081	0.957
19	BB-026	553344	1214114	0.094	-0.047	0.840
20	BB-034	552946	1210433	0.098	0.108	0.942
21	BB-034-2	552946	1210433	0.098	0.065	0.950
22	BB-034-3	552946	1210433	0.082	0.082	0.926
23	BB-036	553358	1208949	0.092	0.031	0.940
24	BB-040	553508	1211748	0.084	0.088	0.915

Table B-1. (cont.)

No.	Sample name	Location		Standard deviation	Skewness	Kurtosis
		E	N			
25	BB-043	553512	1210676	0.085	0.086	0.920
26	BB-049	553064	1211785	0.082	0.095	0.949
27	BB-052	553230	1213467	0.083	0.088	0.950
28	BB-053	553254	1213480	0.091	0.059	0.933
29	BB-056	553229	1209241	0.080	0.066	1.001
30	BB-057	553991	1207805	0.082	0.085	1.318
31	BB-058	553773	1208045	0.085	0.088	0.935
32	BB-062	554174	1207545	0.082	0.073	0.916
33	BB-064	554224	1207598	0.097	0.079	0.916
34	BB-065	553556	1209256	0.098	0.074	0.915
35	BB-068	553077	1212408	0.096	0.077	0.939
36	BB-069	553160	1212857	0.096	0.028	0.938
37	BB-070	553384	1212886	0.083	0.077	1.200
38	BB-074-1	553208	1213204	0.084	0.089	0.870
39	BBTL-1	0553214	1213195	0.081	0.072	0.916
40	BBTL-2	0553214	1213195	0.08	0.066	0.915
41	BBTL-3	0553214	1213195	0.082	0.085	0.927

(Test by The Petroleum and Petrochemical College, Chulalongkorn University)

ศูนย์วิทยทรัพยากร
จุฬาลงกรณ์มหาวิทยาลัย

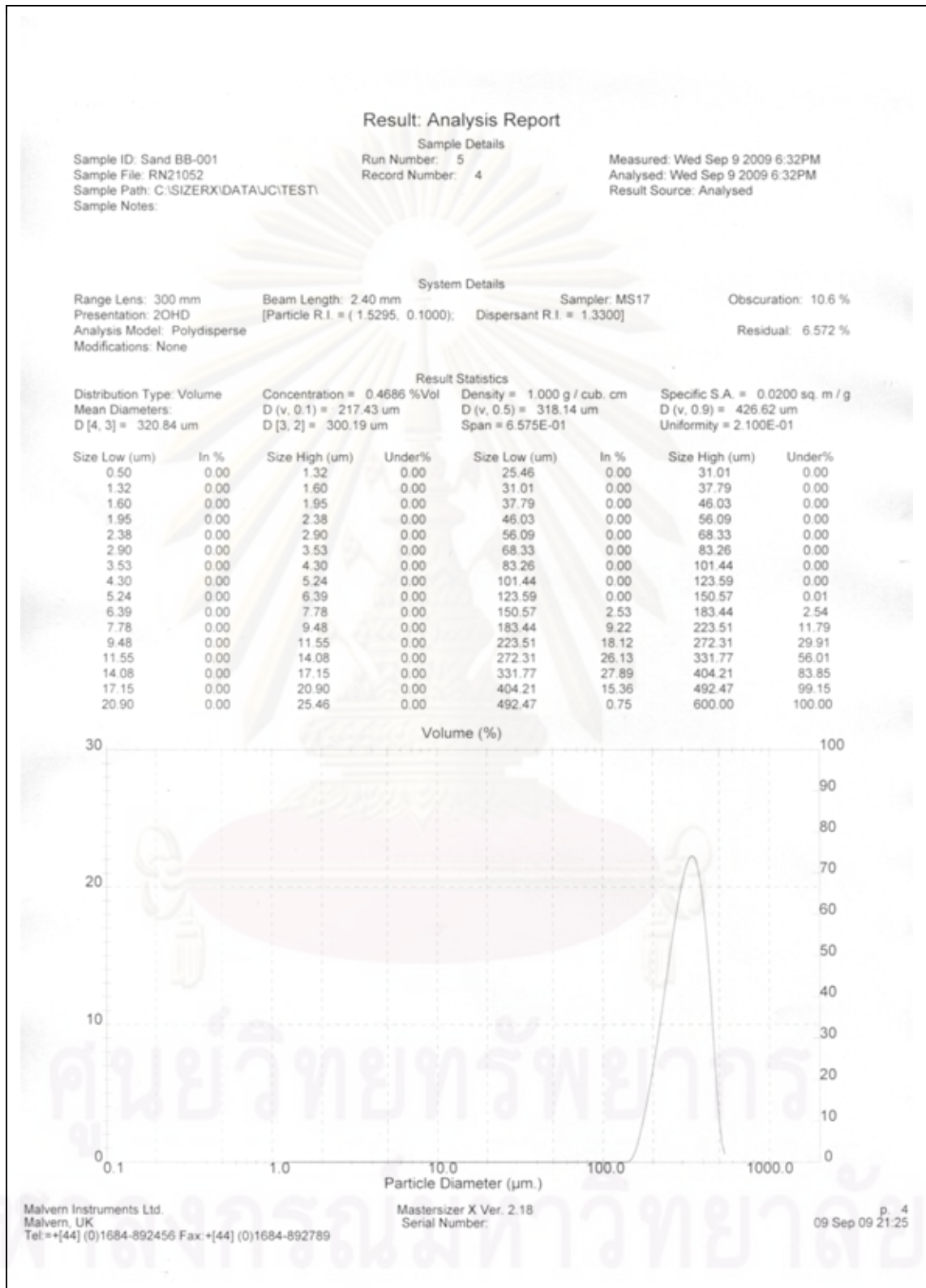


Figure B-1. Result of grain size analysis no.BB-001.

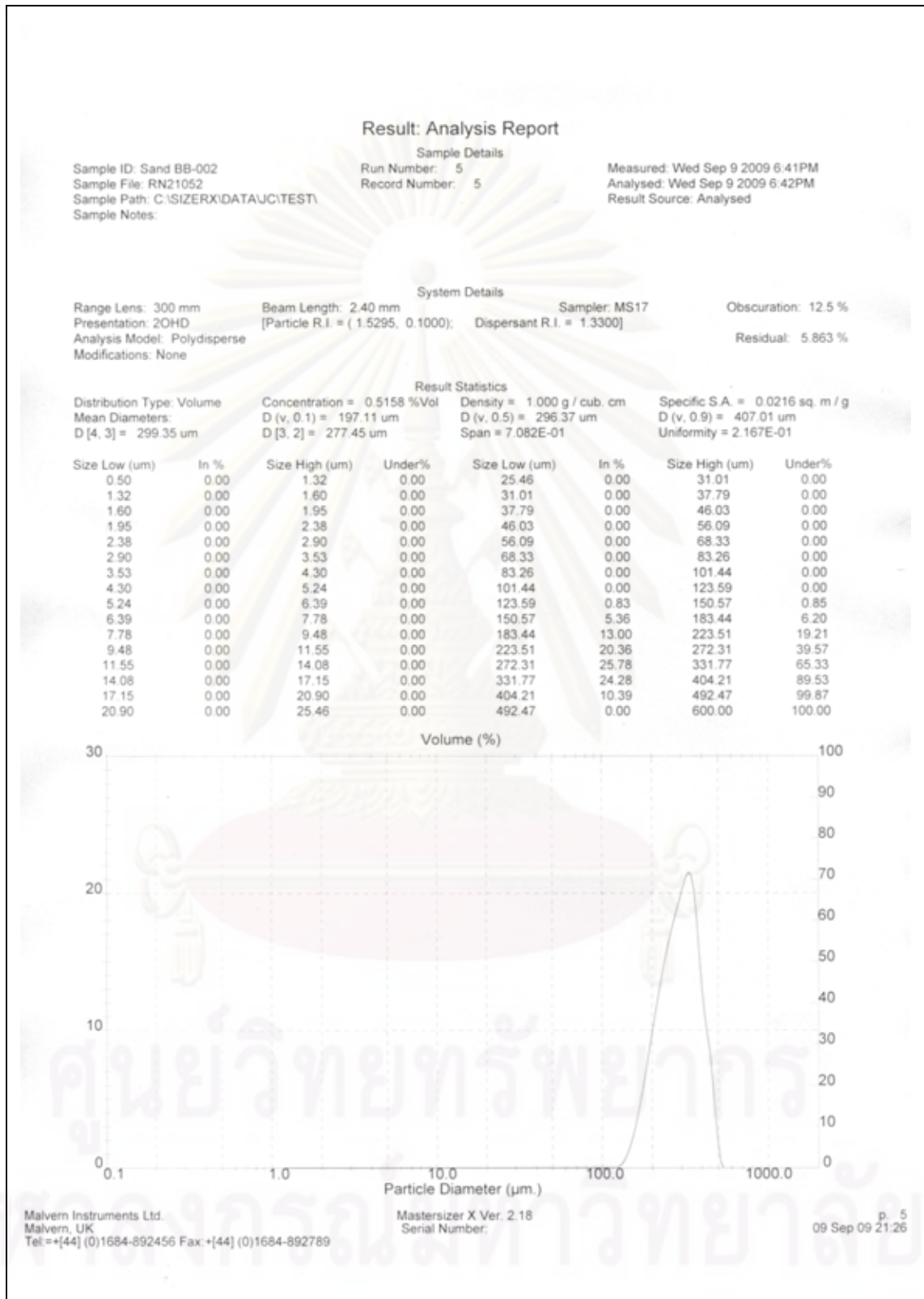


Figure B-2. Result of grain size analysis no.BB-002.

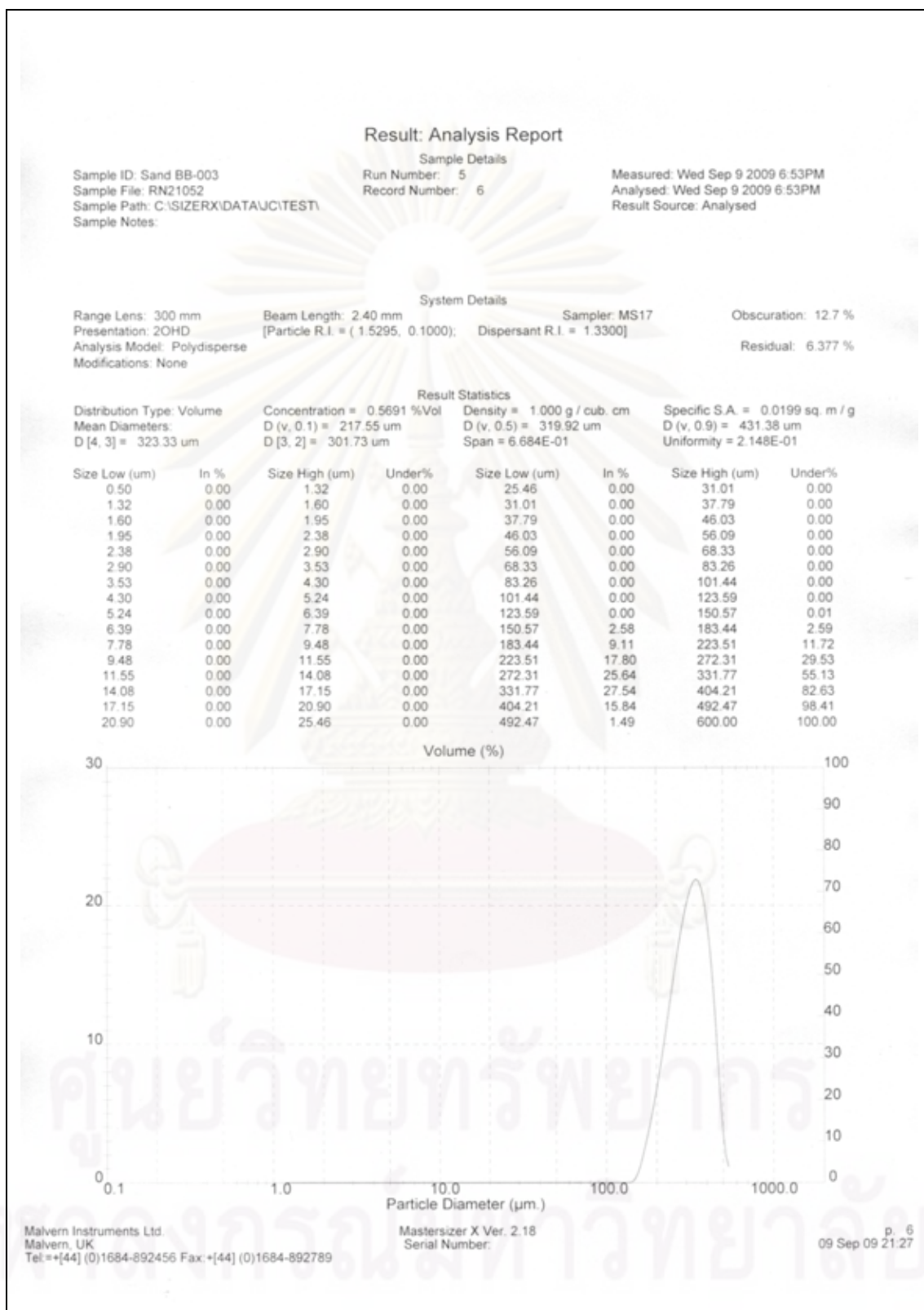


Figure B-3. Result of grain size analysis no.BB-003.

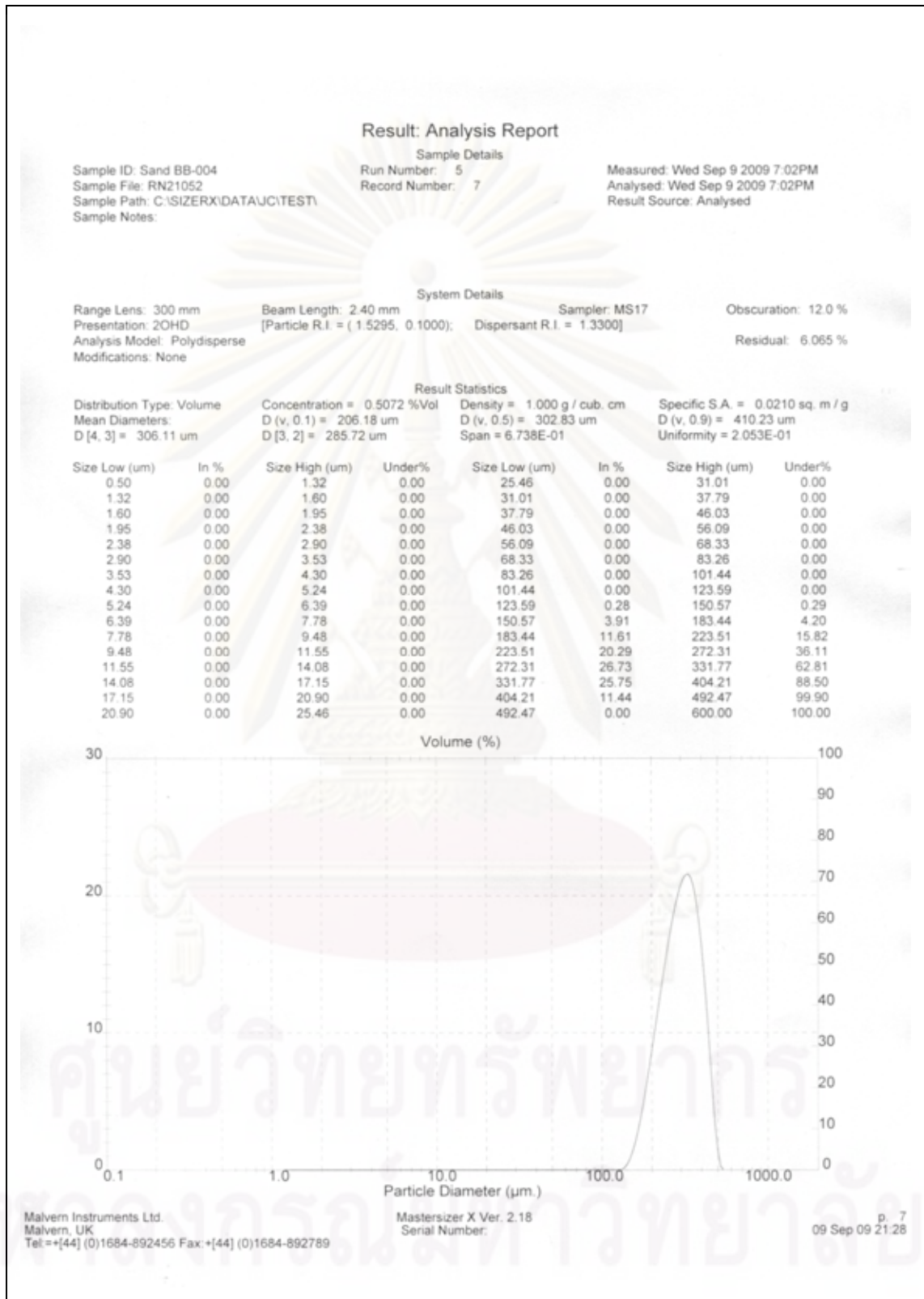


Figure B-4. Result of grain size analysis no.BB-004.

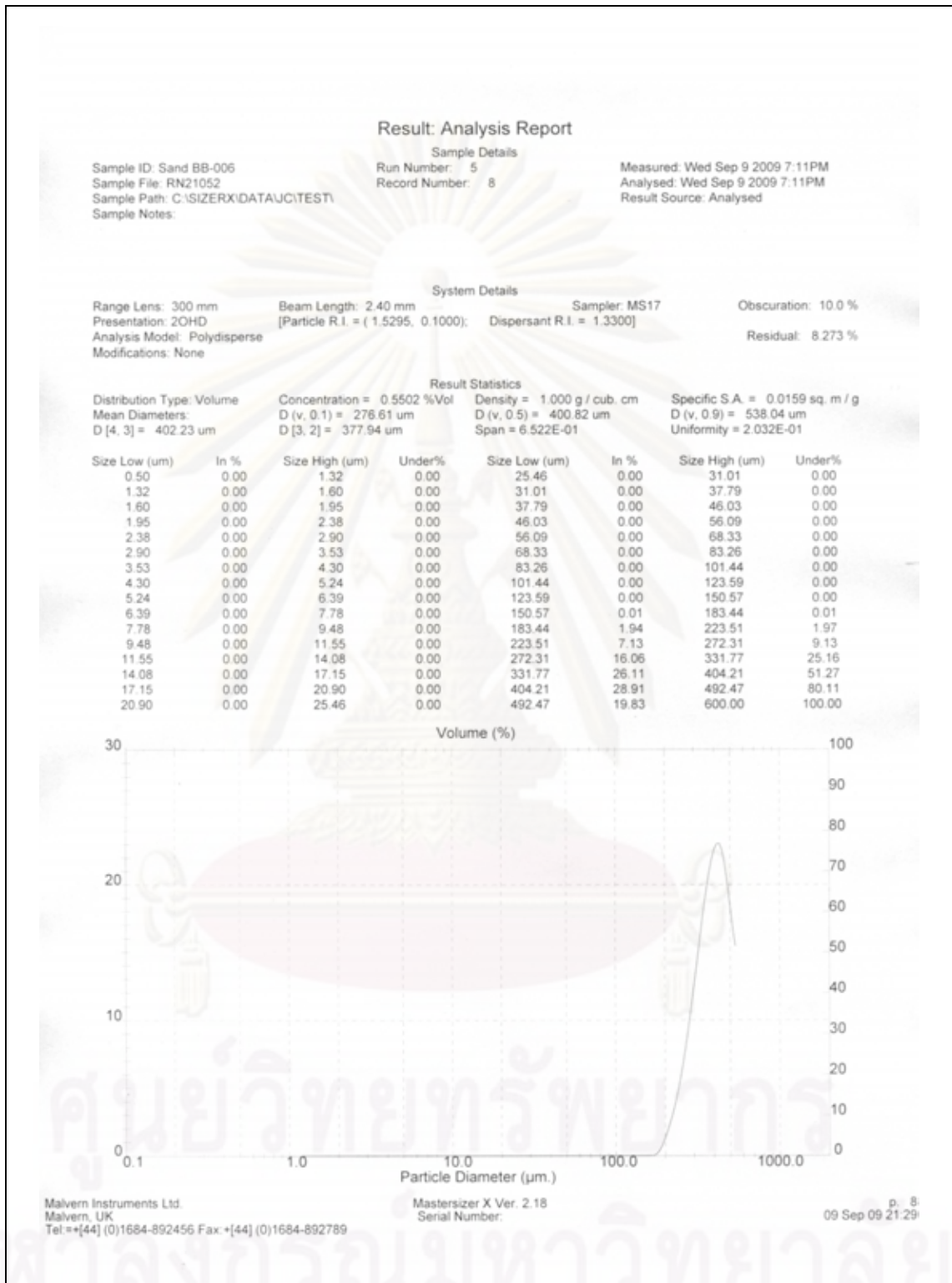


Figure B-5. Result of grain size analysis no.BB-006.

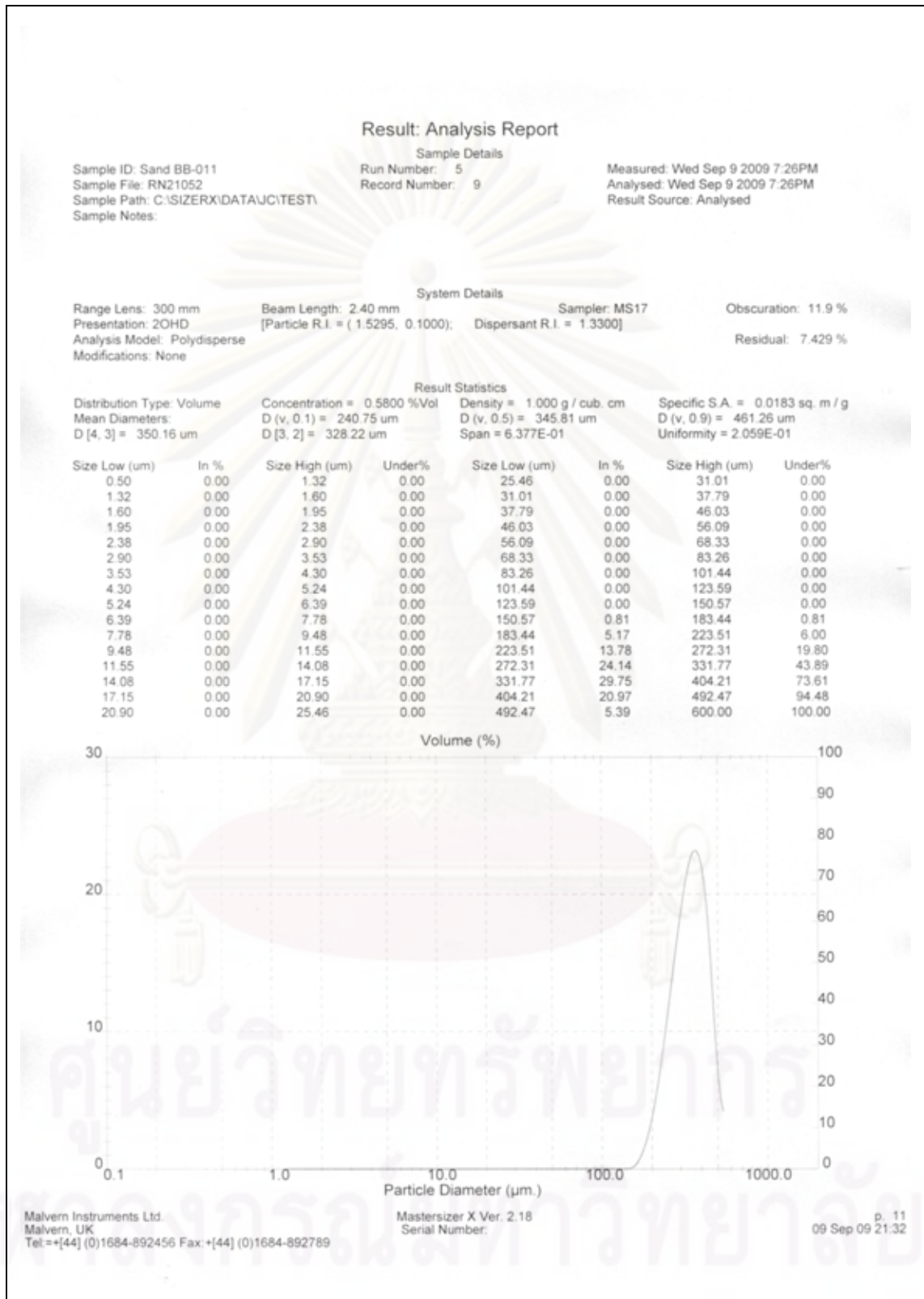


Figure B-6. Result of grain size analysis no.BB-011.

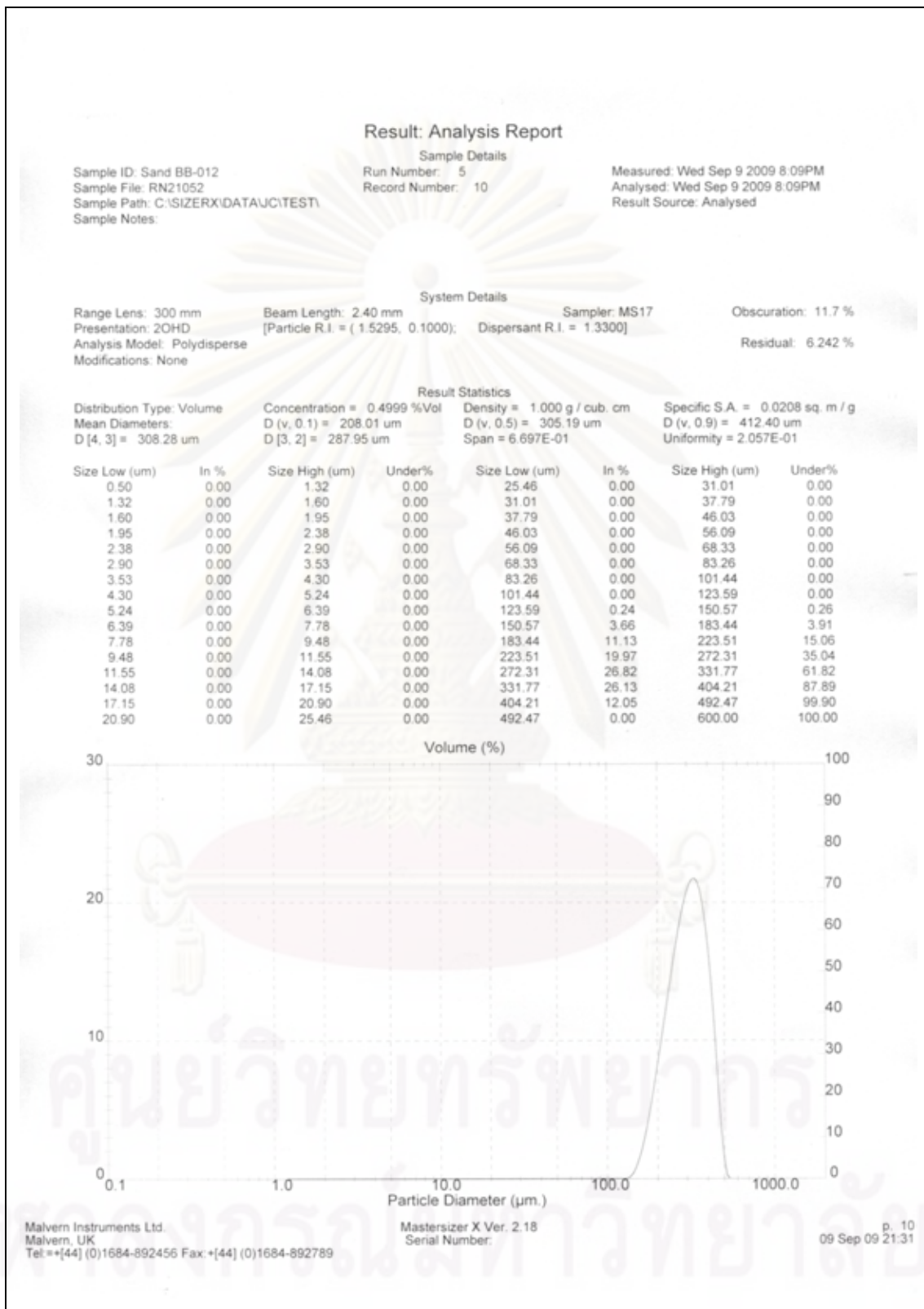


Figure B-7. Result of grain size analysis no.BB-012.

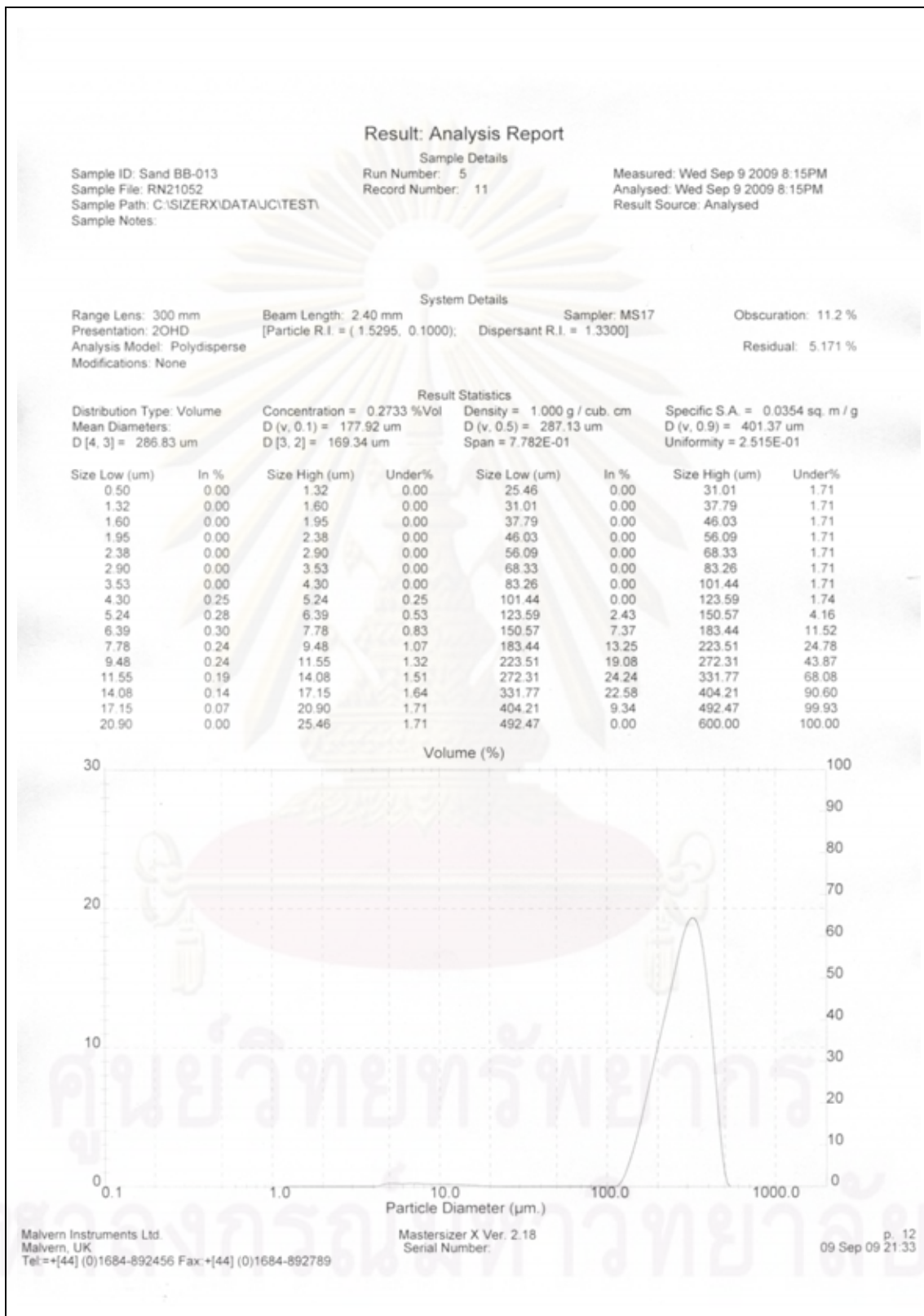


Figure B-8. Result of grain size analysis no.BB-013.

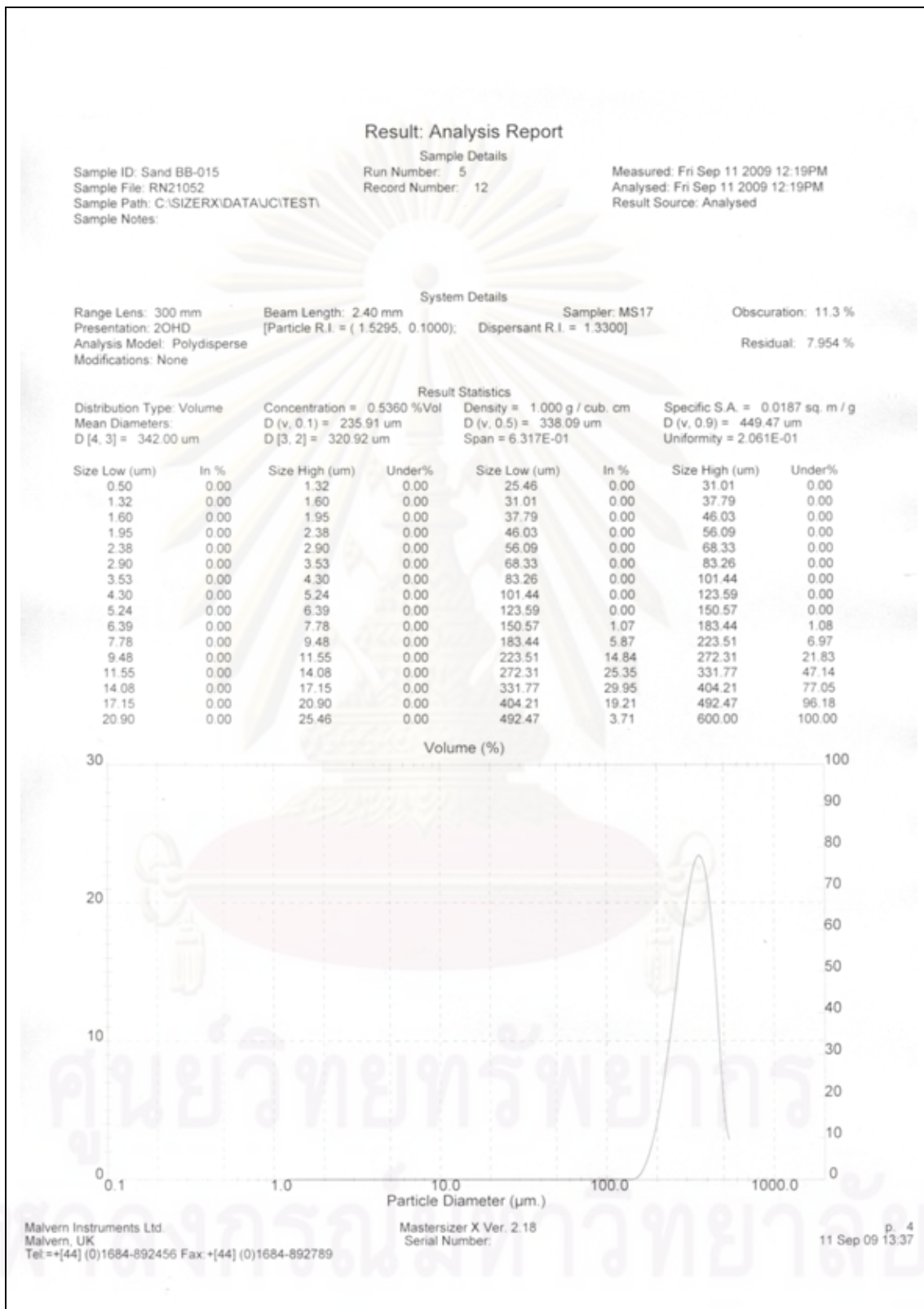


Figure B-9. Result of grain size analysis no.BB-015.

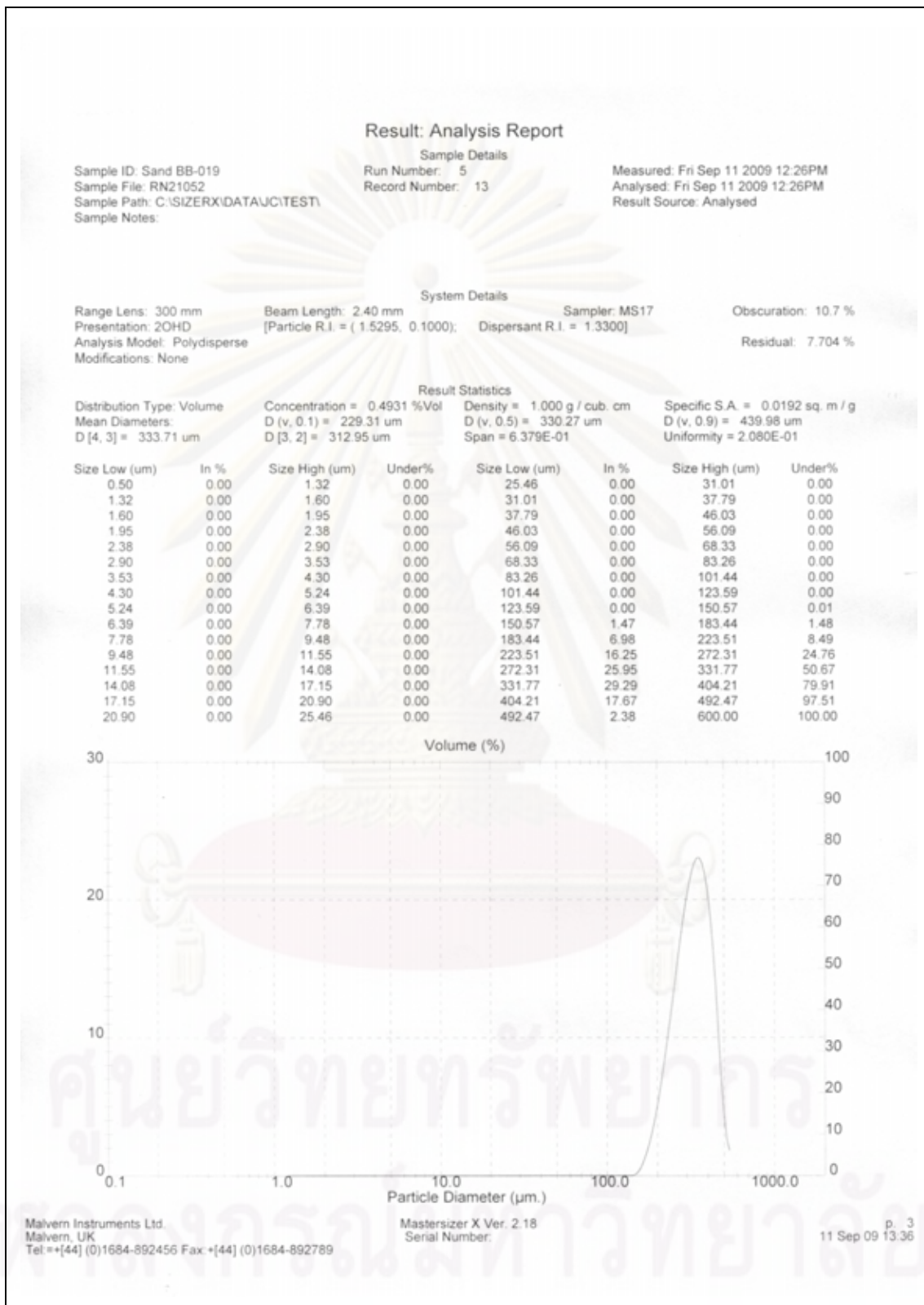


Figure B-10. Result of grain size analysis no.BB-019.

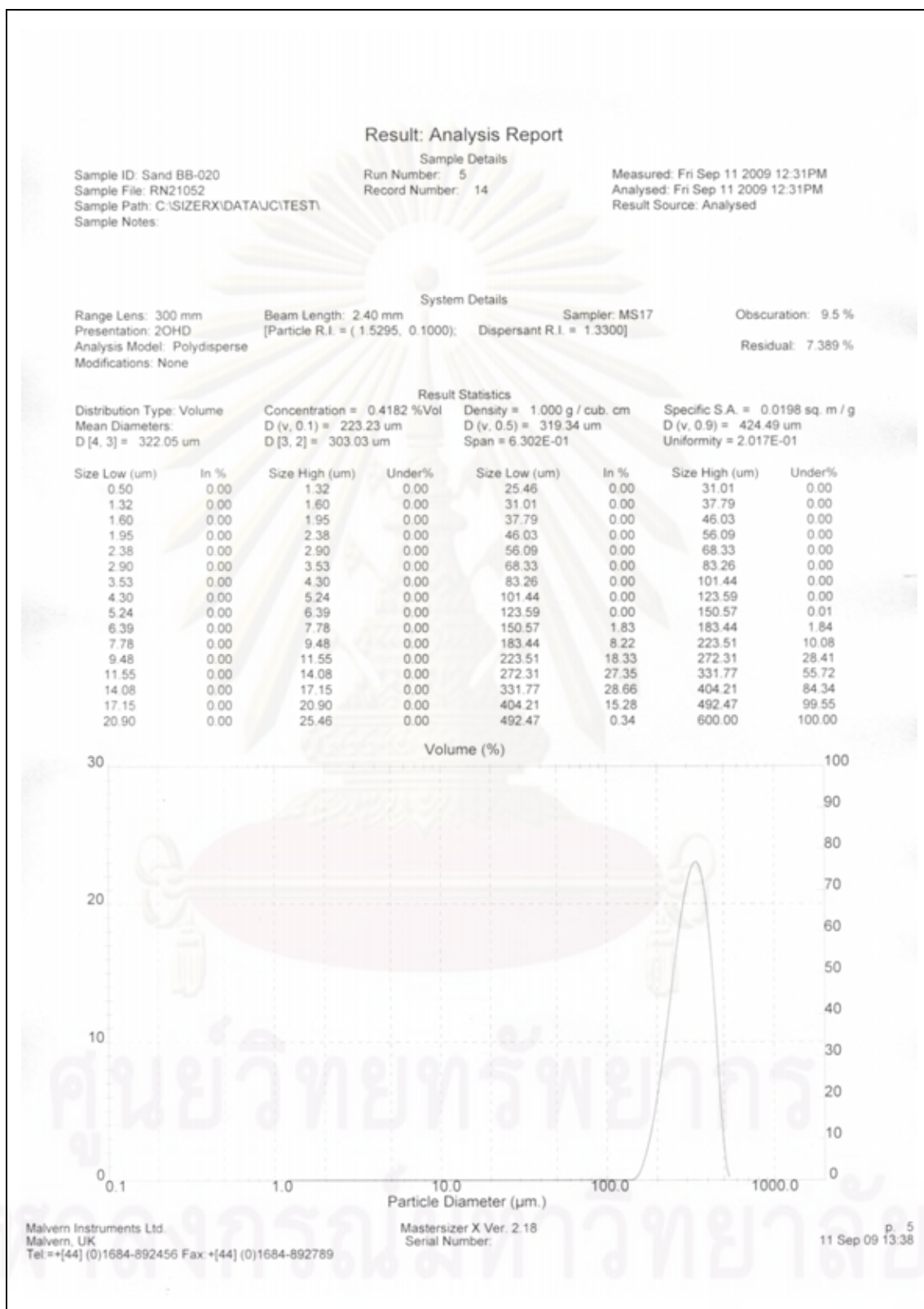


Figure B-11. Result of grain size analysis no.BB-020.

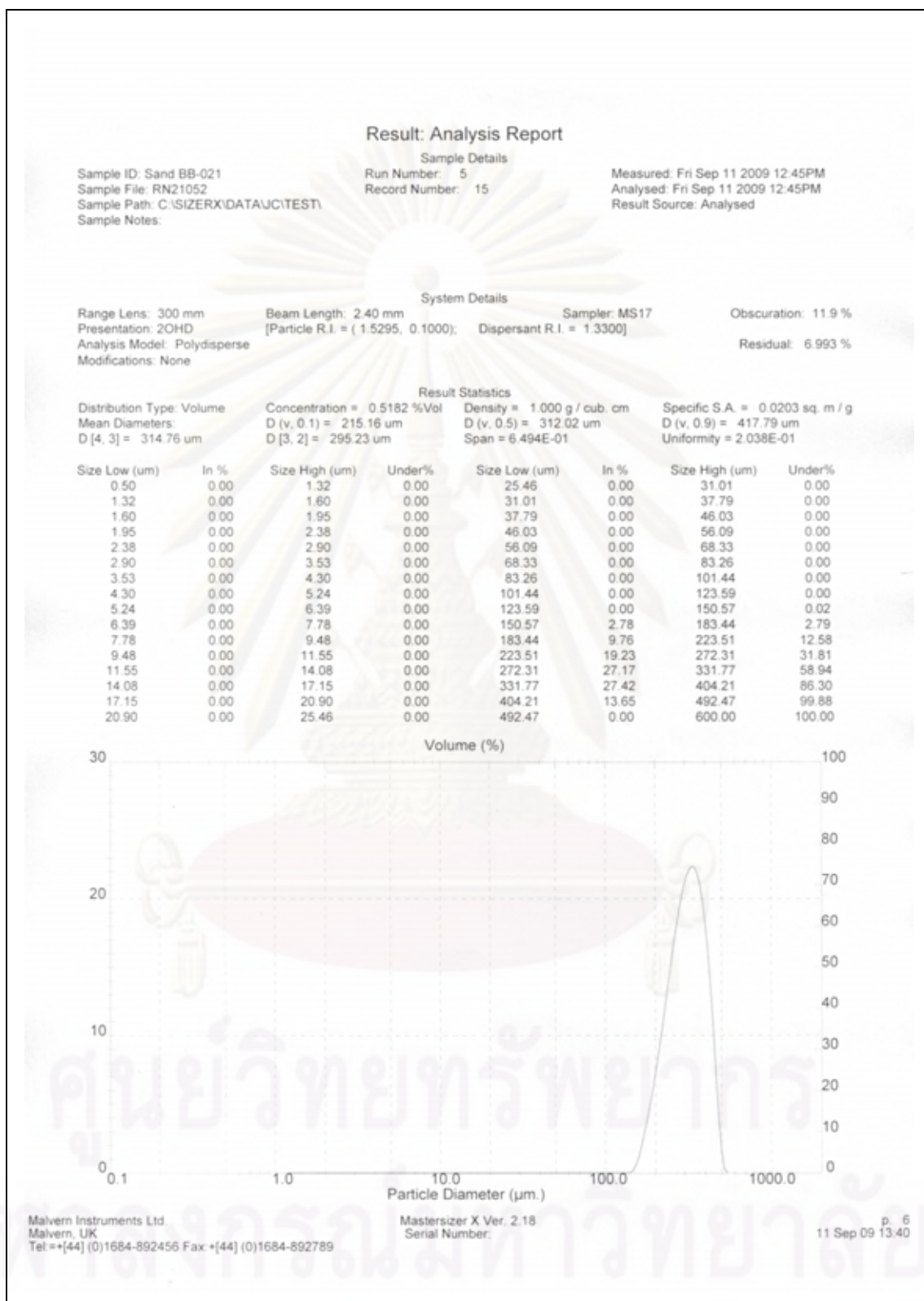


Figure B-12. Result of grain size analysis no.BB-021.

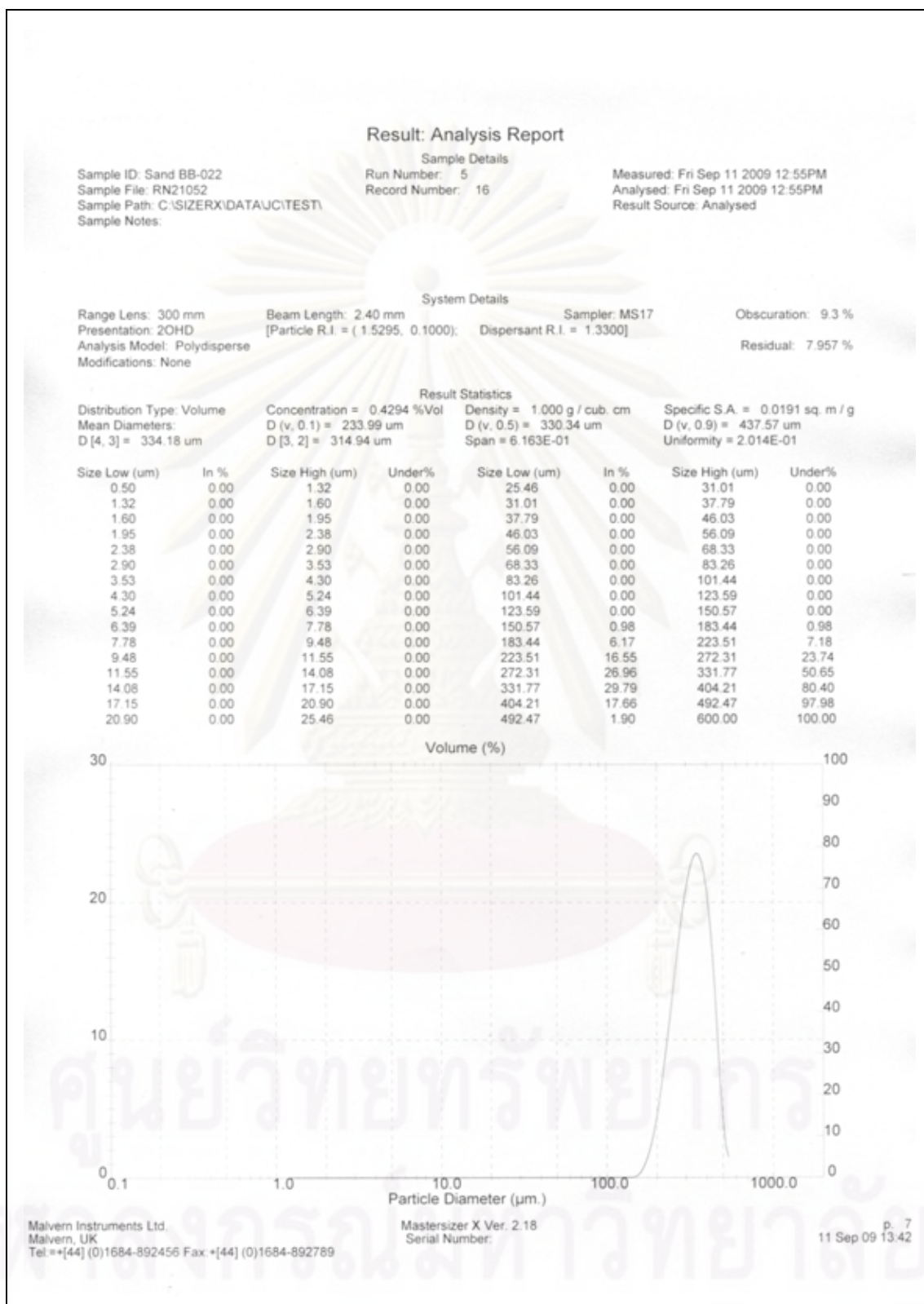


Figure B-13. Result of grain size analysis no.BB-022.

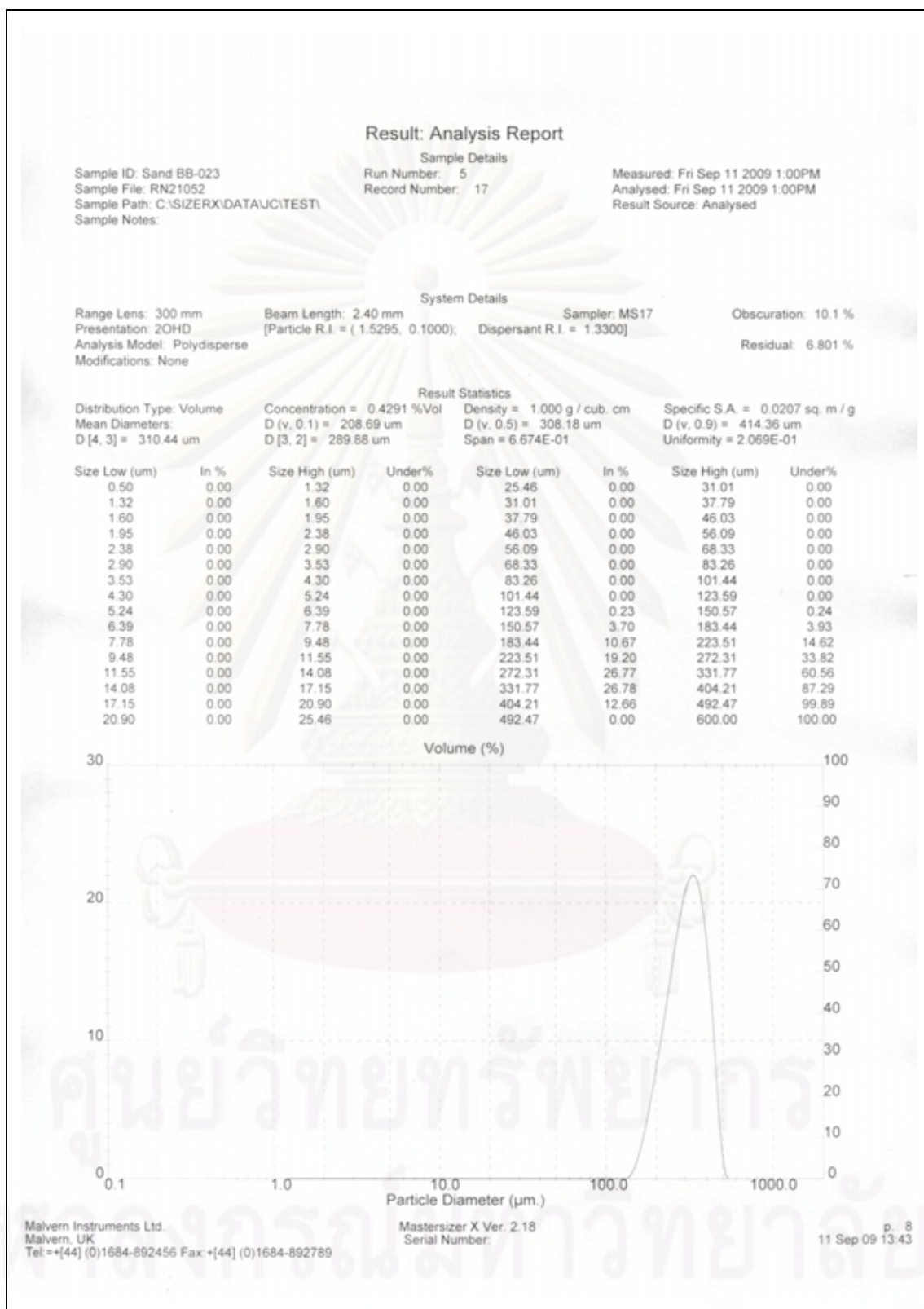


Figure B-14. Result of grain size analysis no.BB-023.

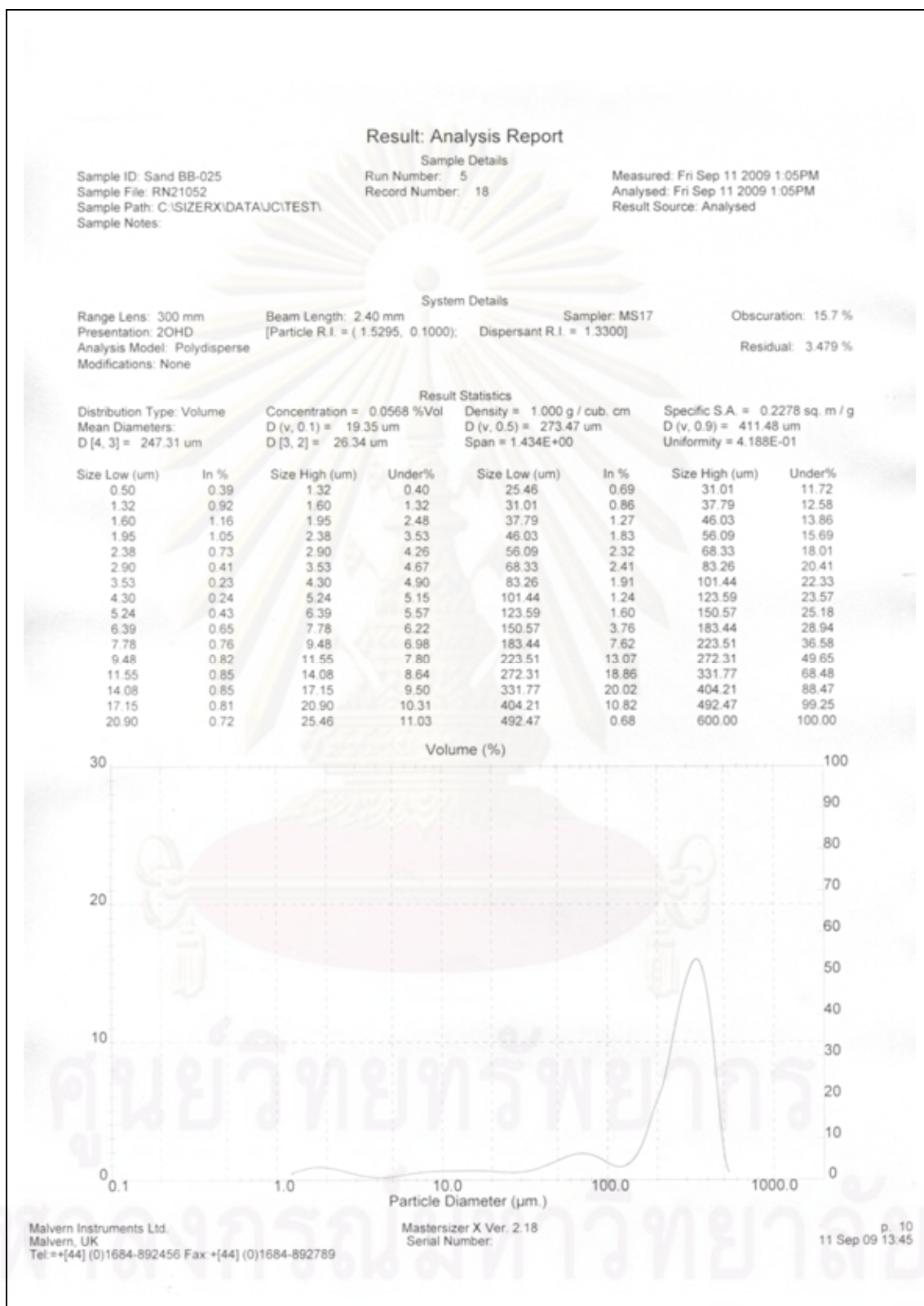


Figure B-15. Result of grain size analysis no.BB-025.

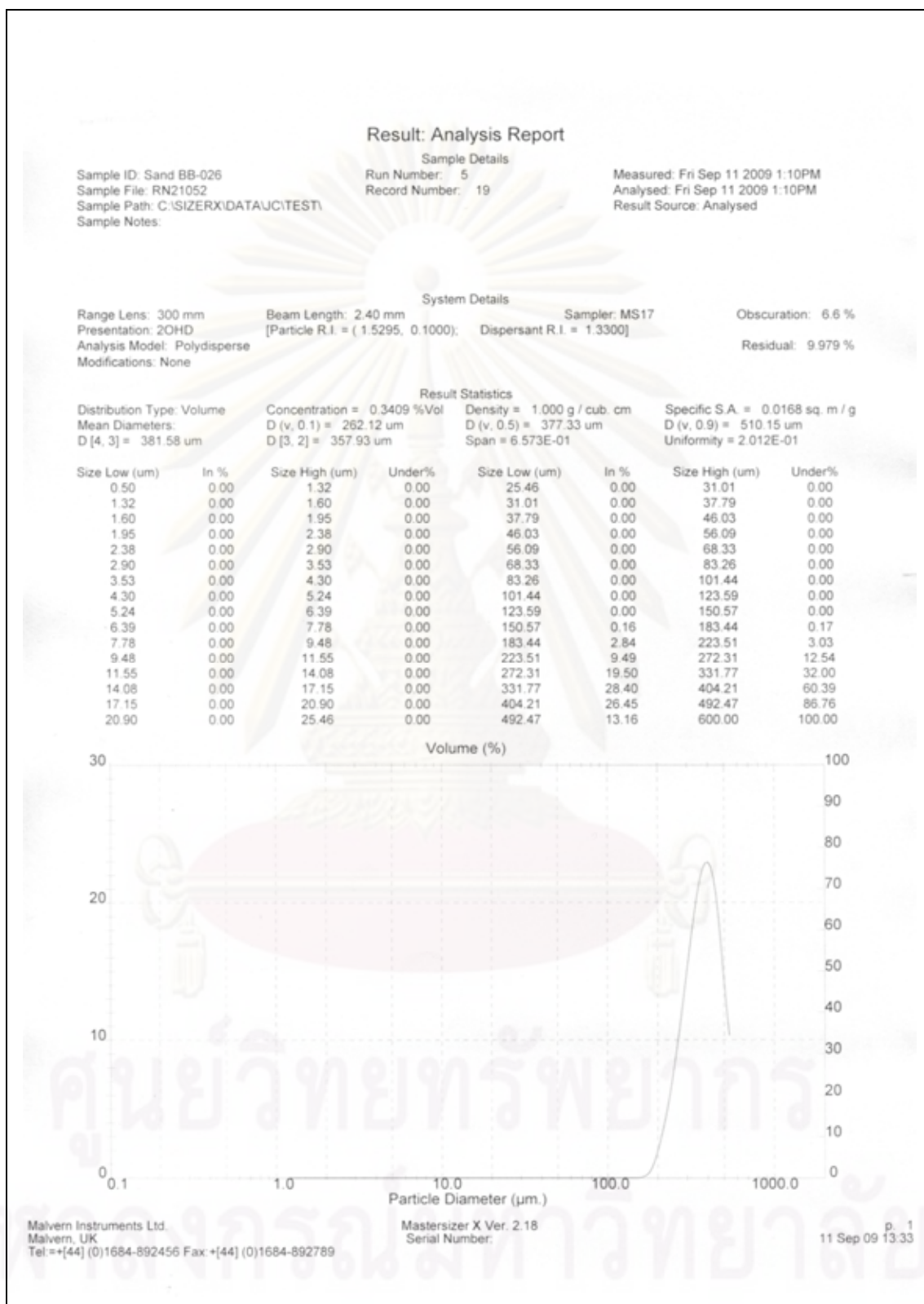


Figure B-16. Result of grain size analysis no.BB-026.

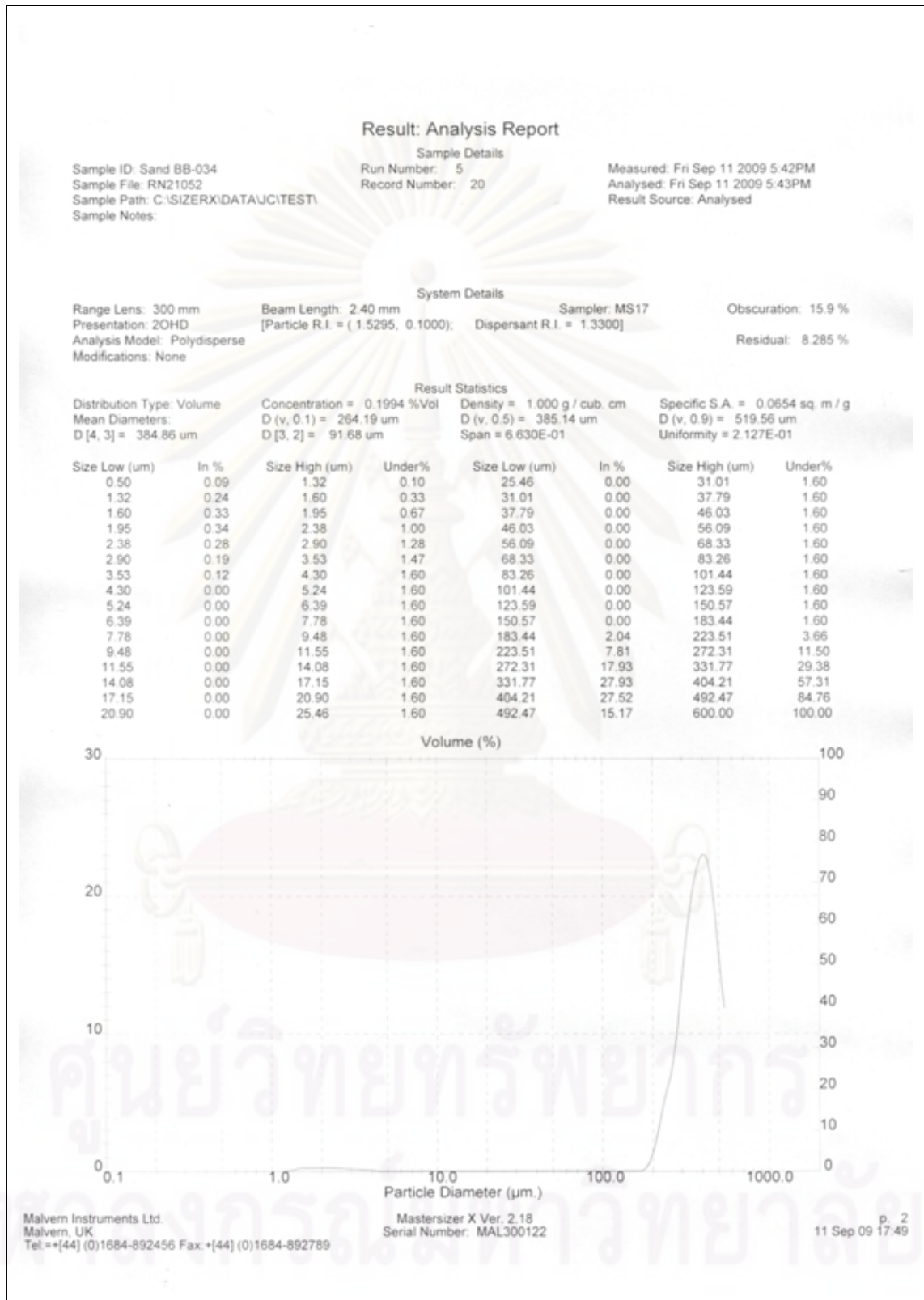


Figure B-17. Result of grain size analysis no.BB-034.

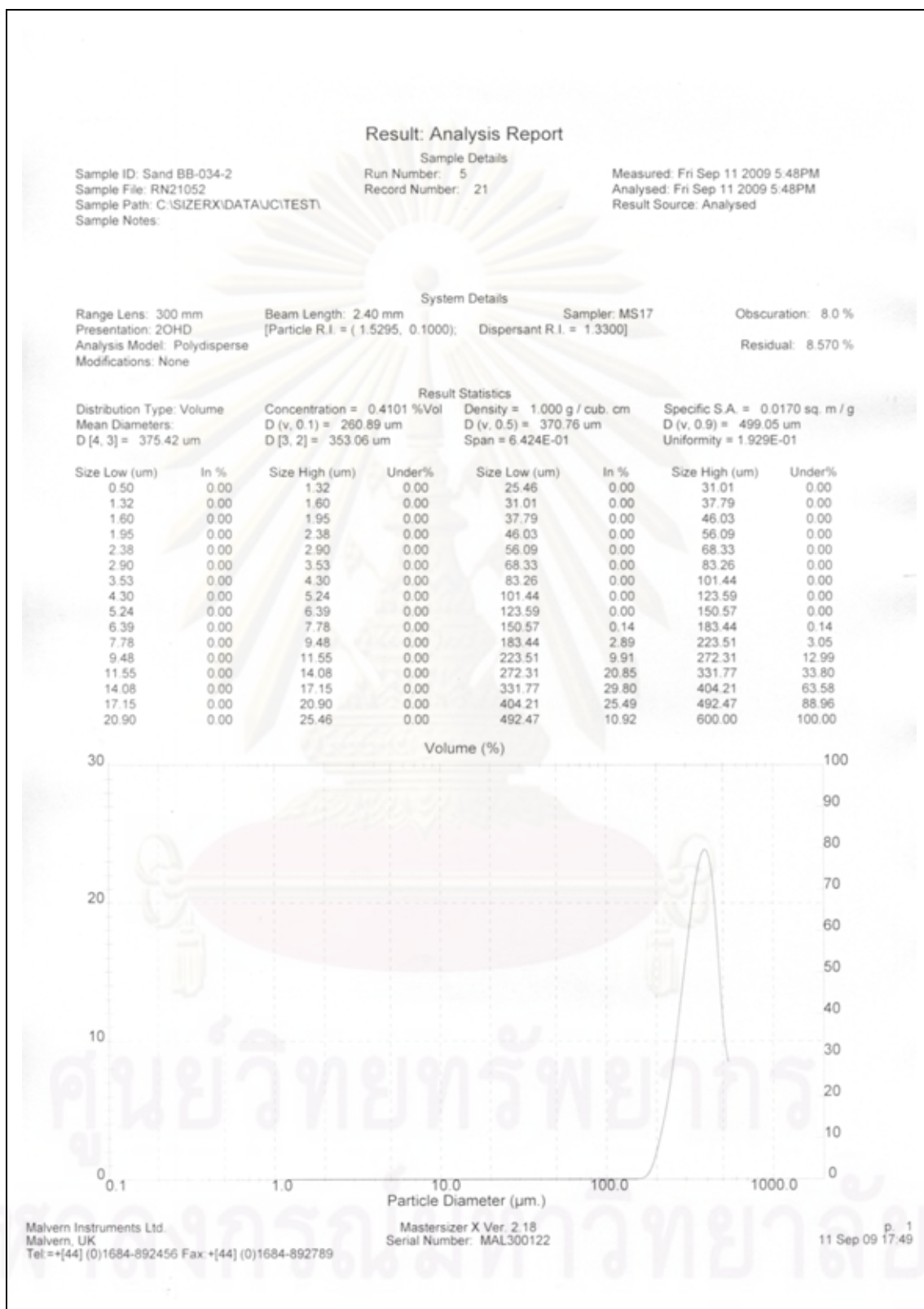


Figure B-18. Result of grain size analysis no.BB-034-2.

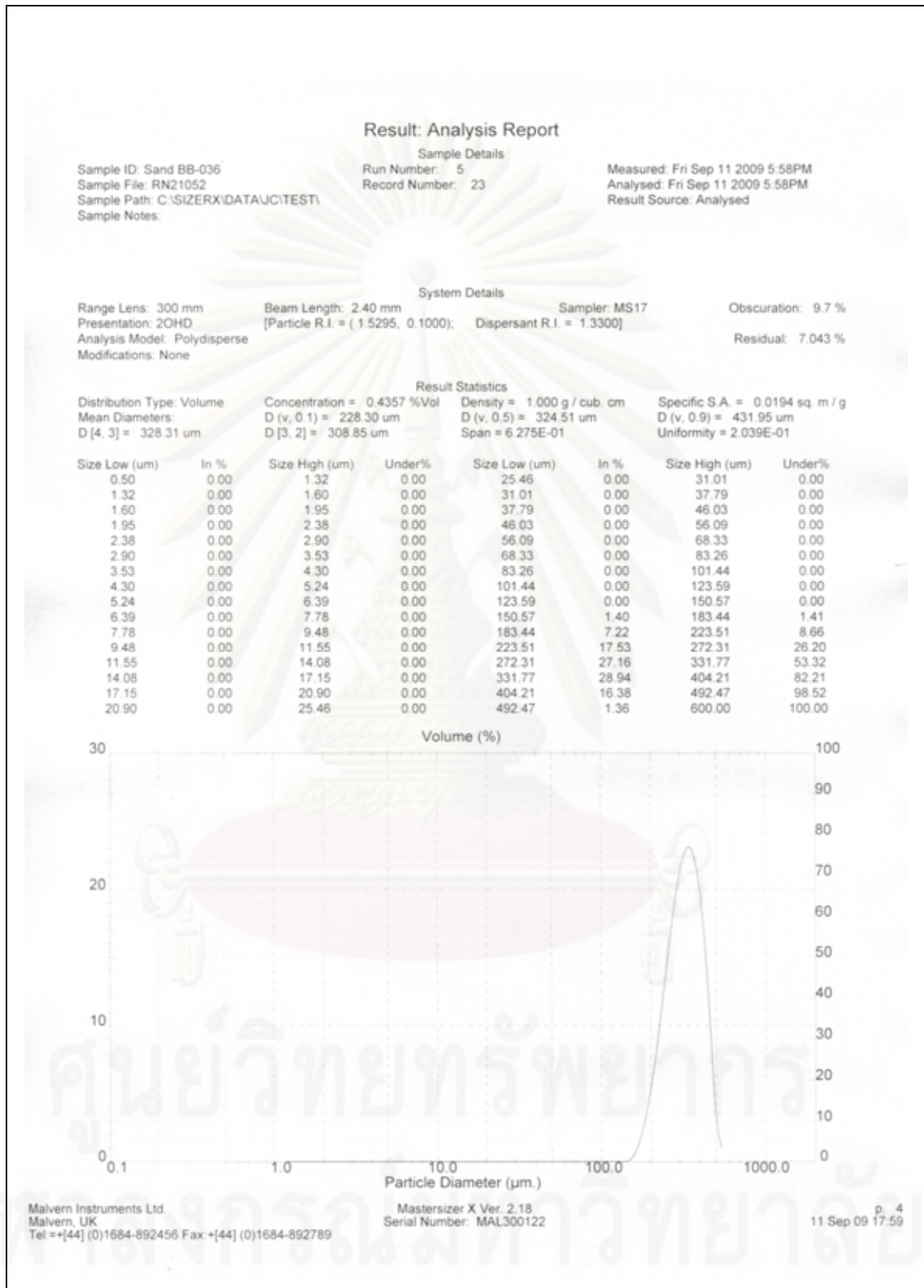


Figure B-19. Result of grain size analysis no.BB-036.

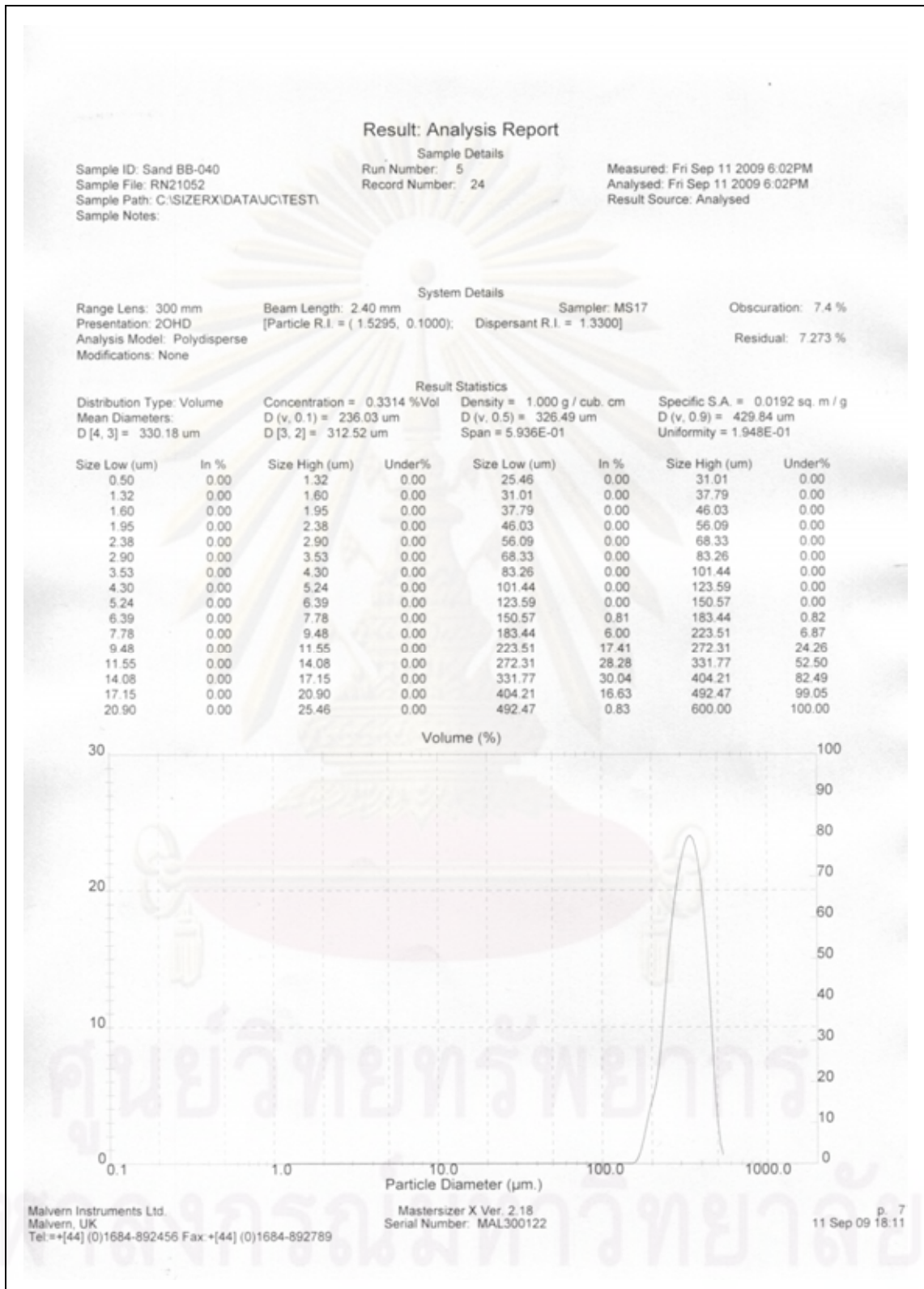


Figure B-20. Result of grain size analysis no.BB-040.

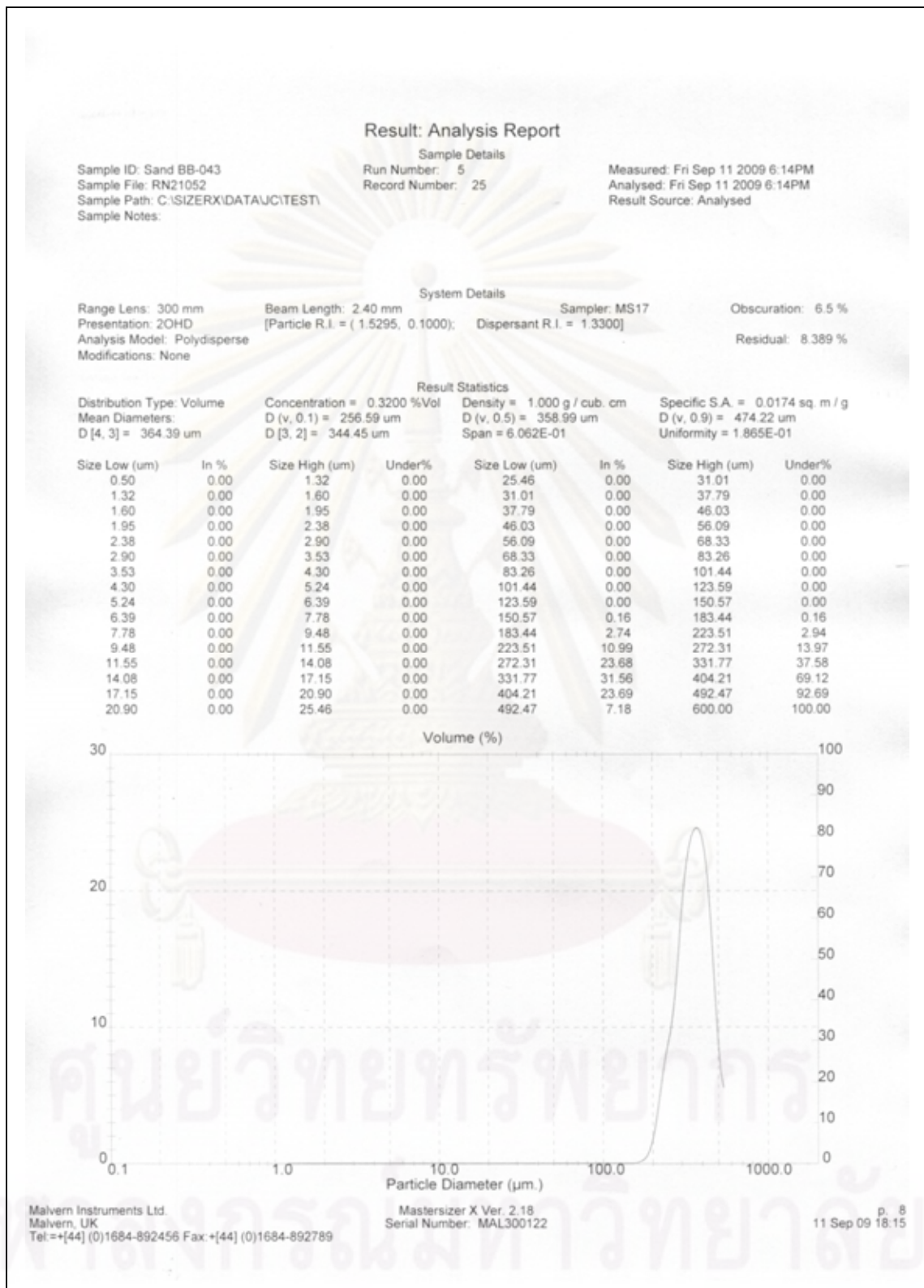


Figure B-21. Result of grain size analysis no.BB-043.

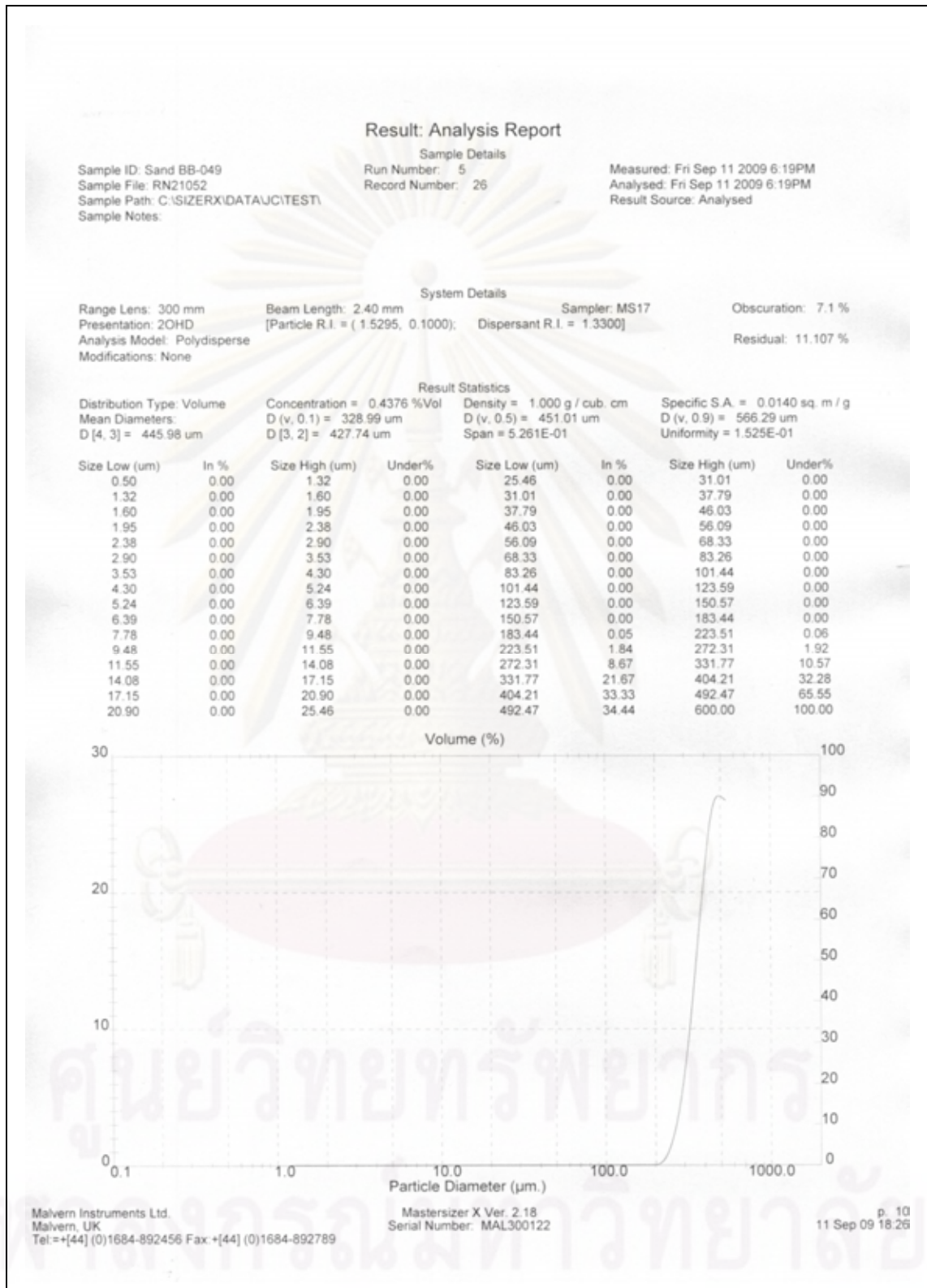


Figure B-22. Result of grain size analysis no.BB-049.

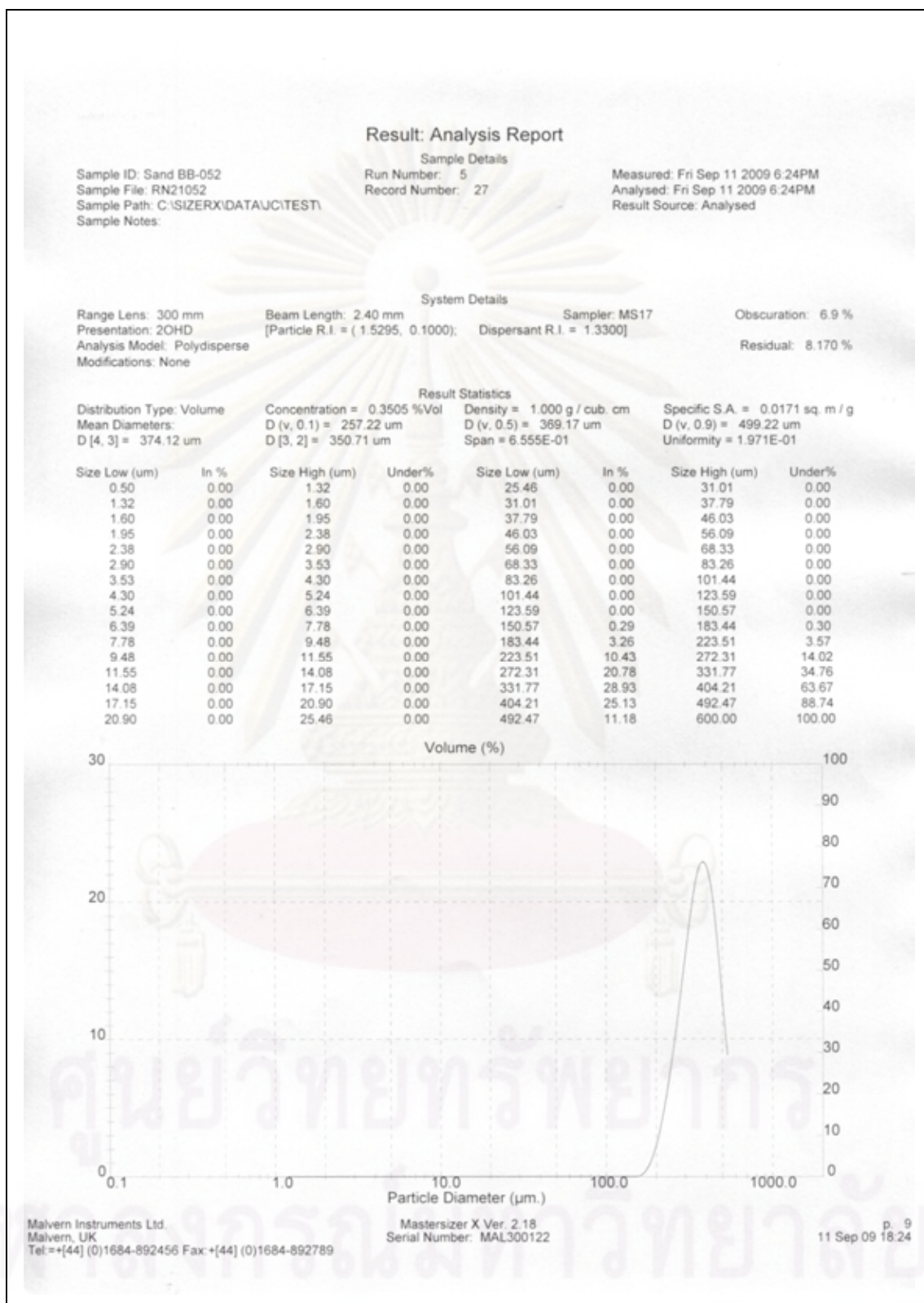


Figure B-23. Result of grain size analysis no.BB-052.

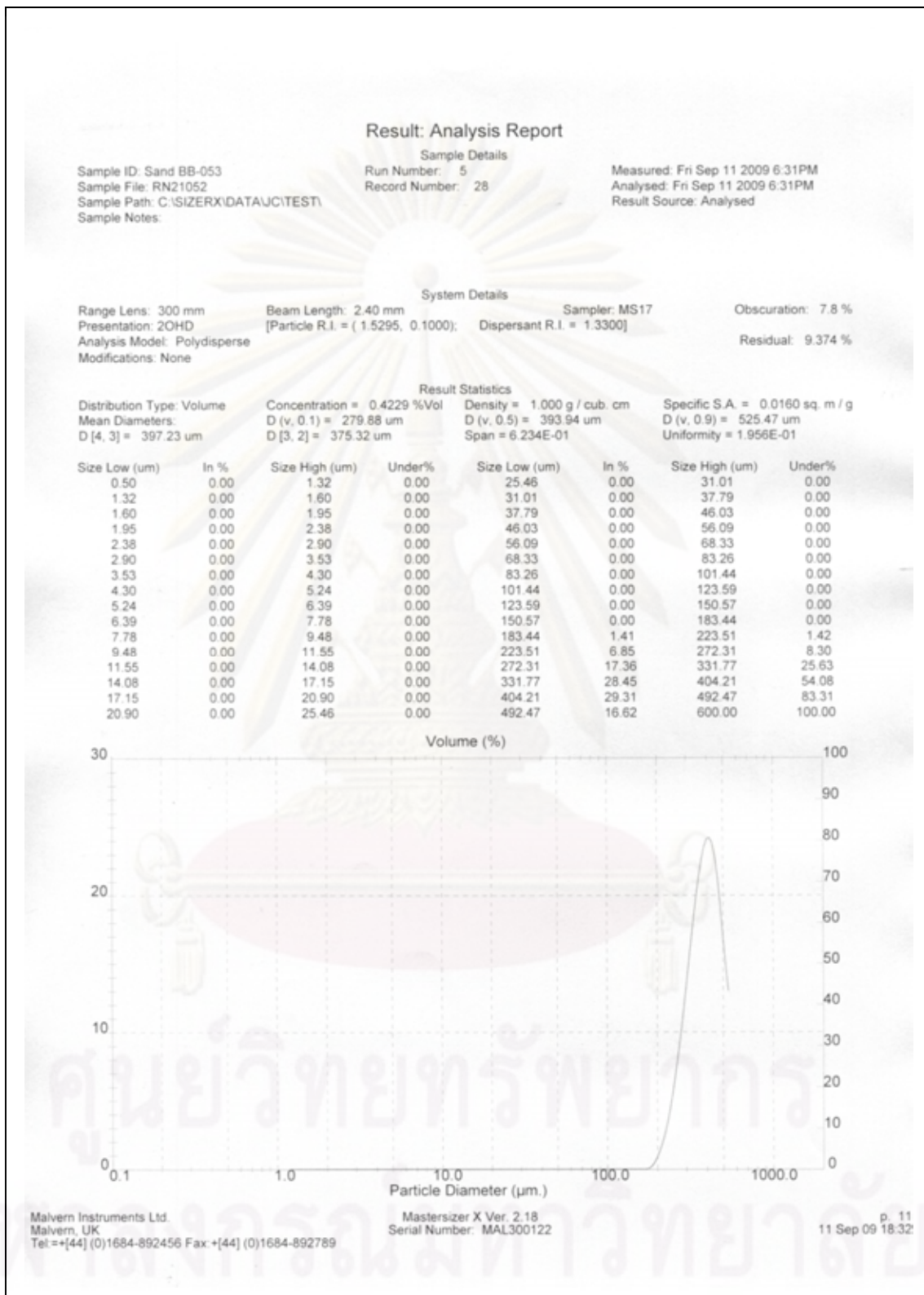


Figure B-24. Result of grain size analysis no.BB-053.

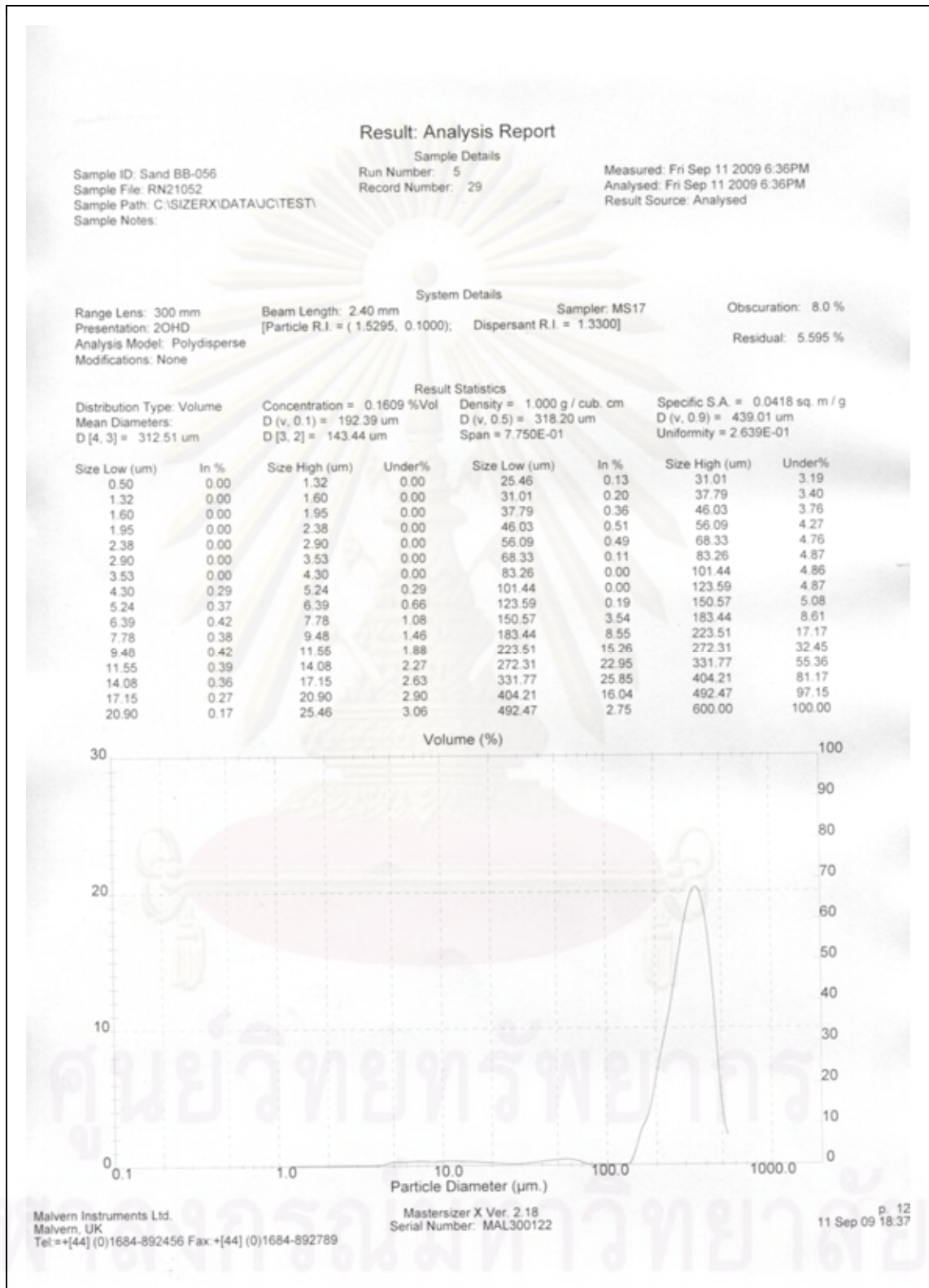


Figure B-25. Result of grain size analysis no.BB-056.

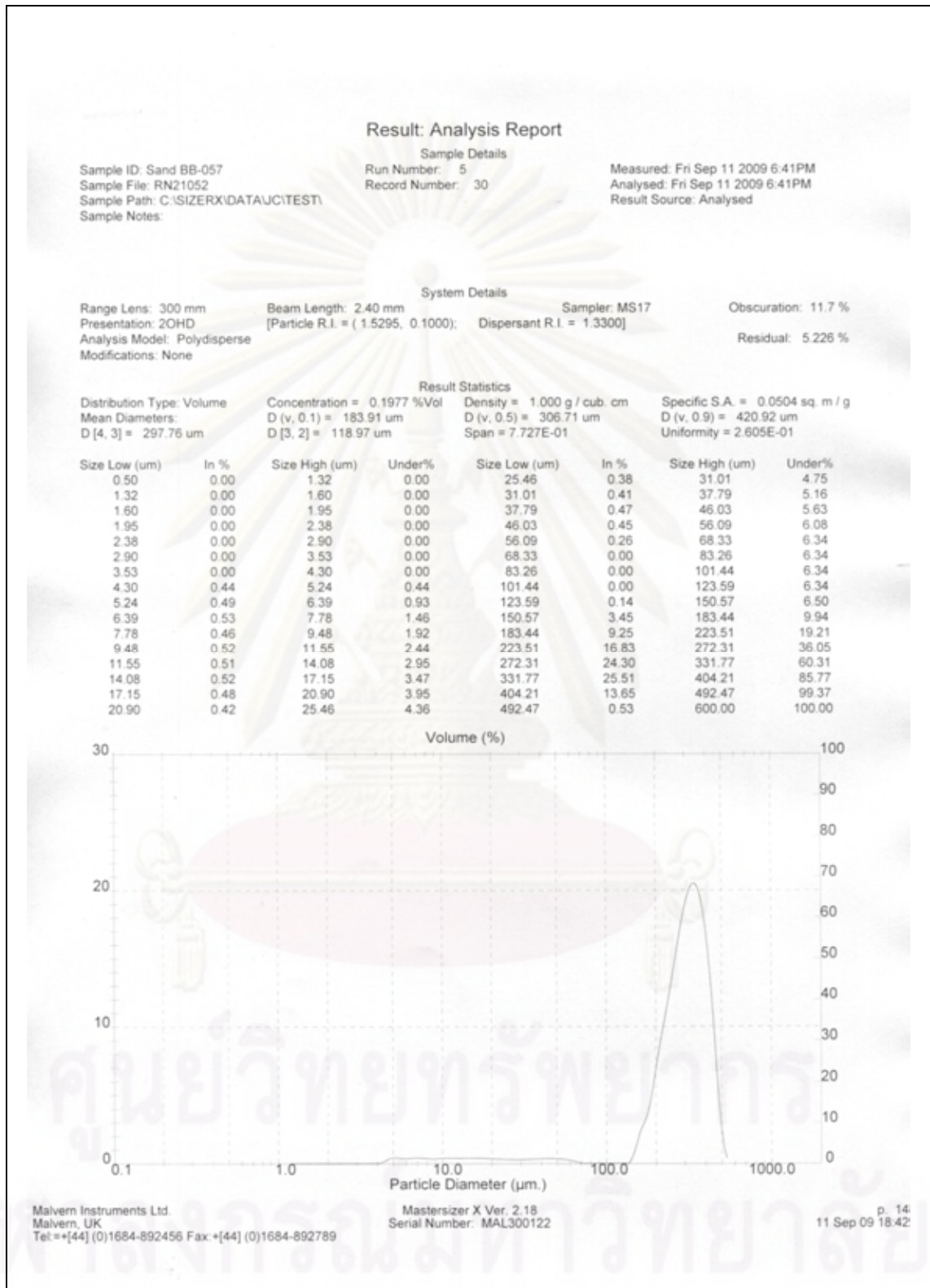


Figure B-26. Result of grain size analysis no.BB-057.

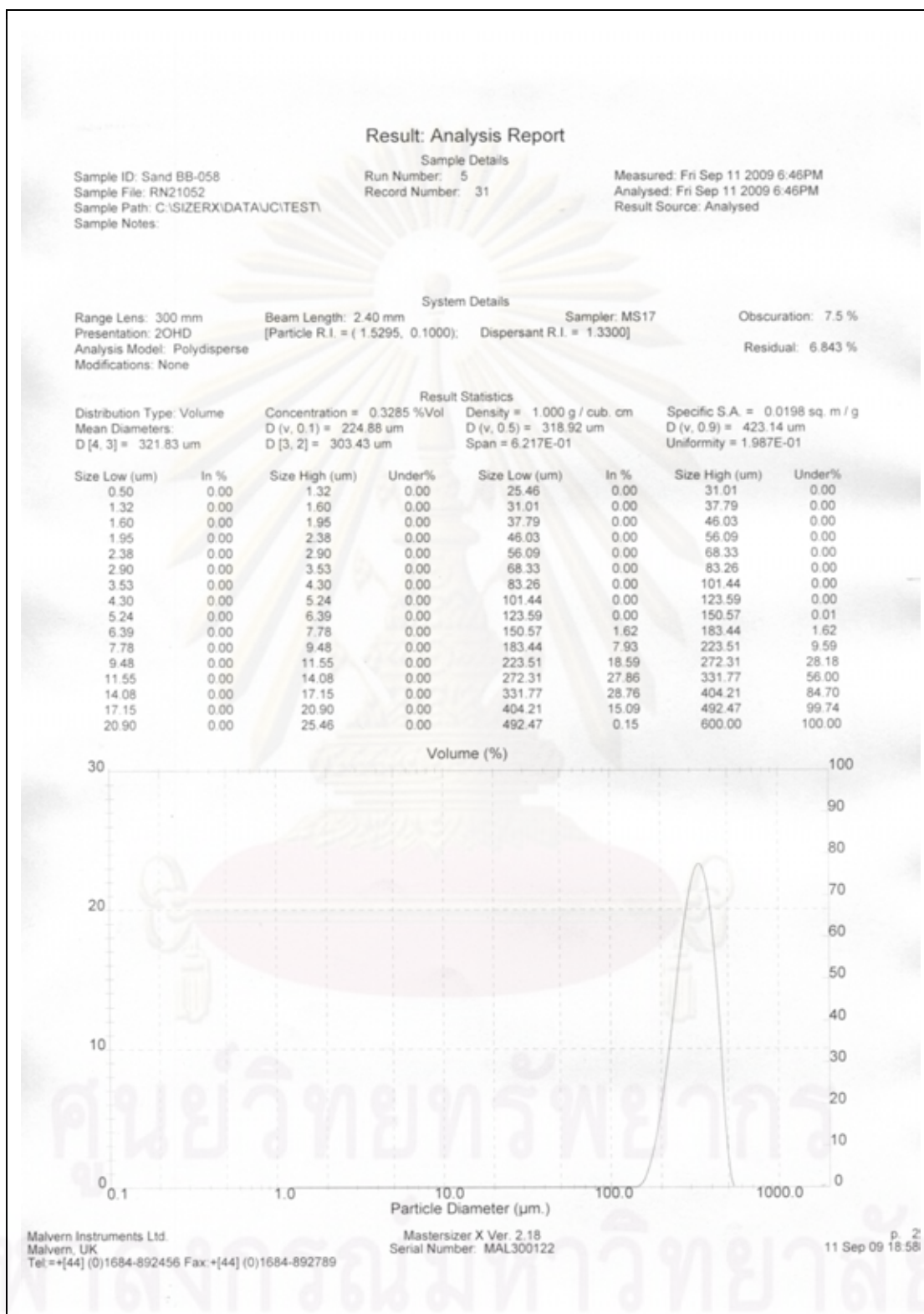


Figure B-27. Result of grain size analysis no.BB-058.

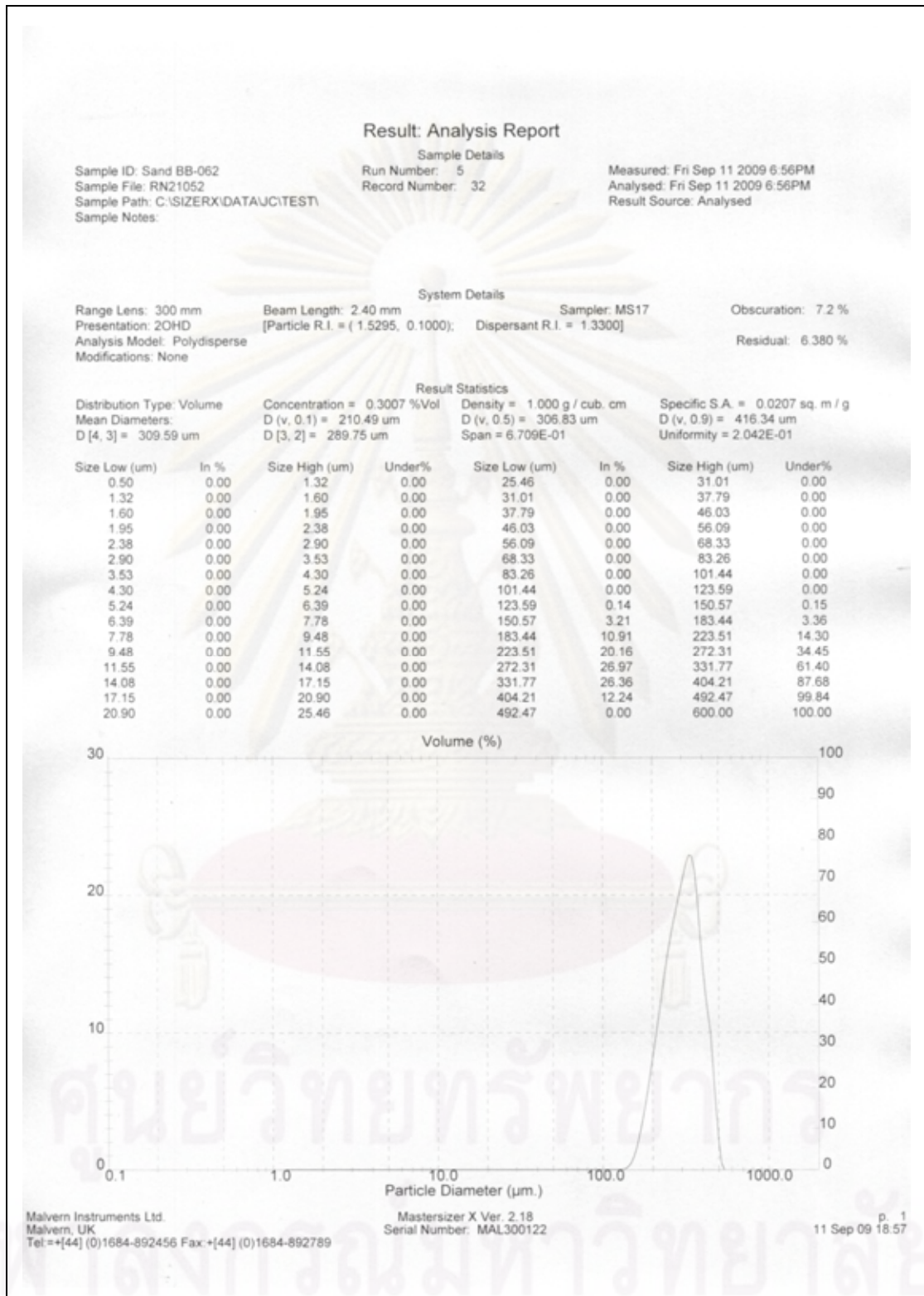


Figure B-28. Result of grain size analysis no.BB-062.

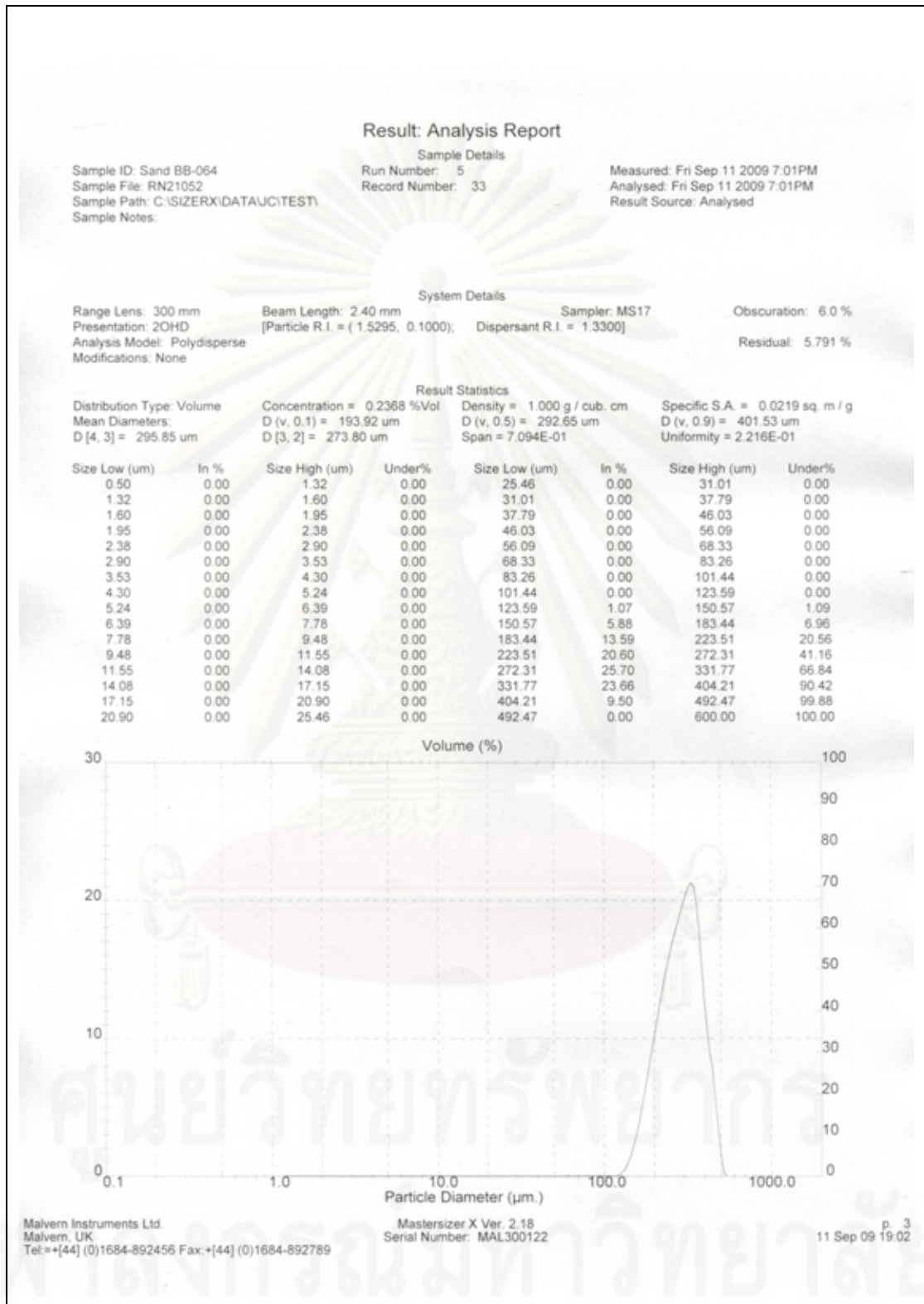


Figure B-29. Result of grain size analysis no.BB-064.

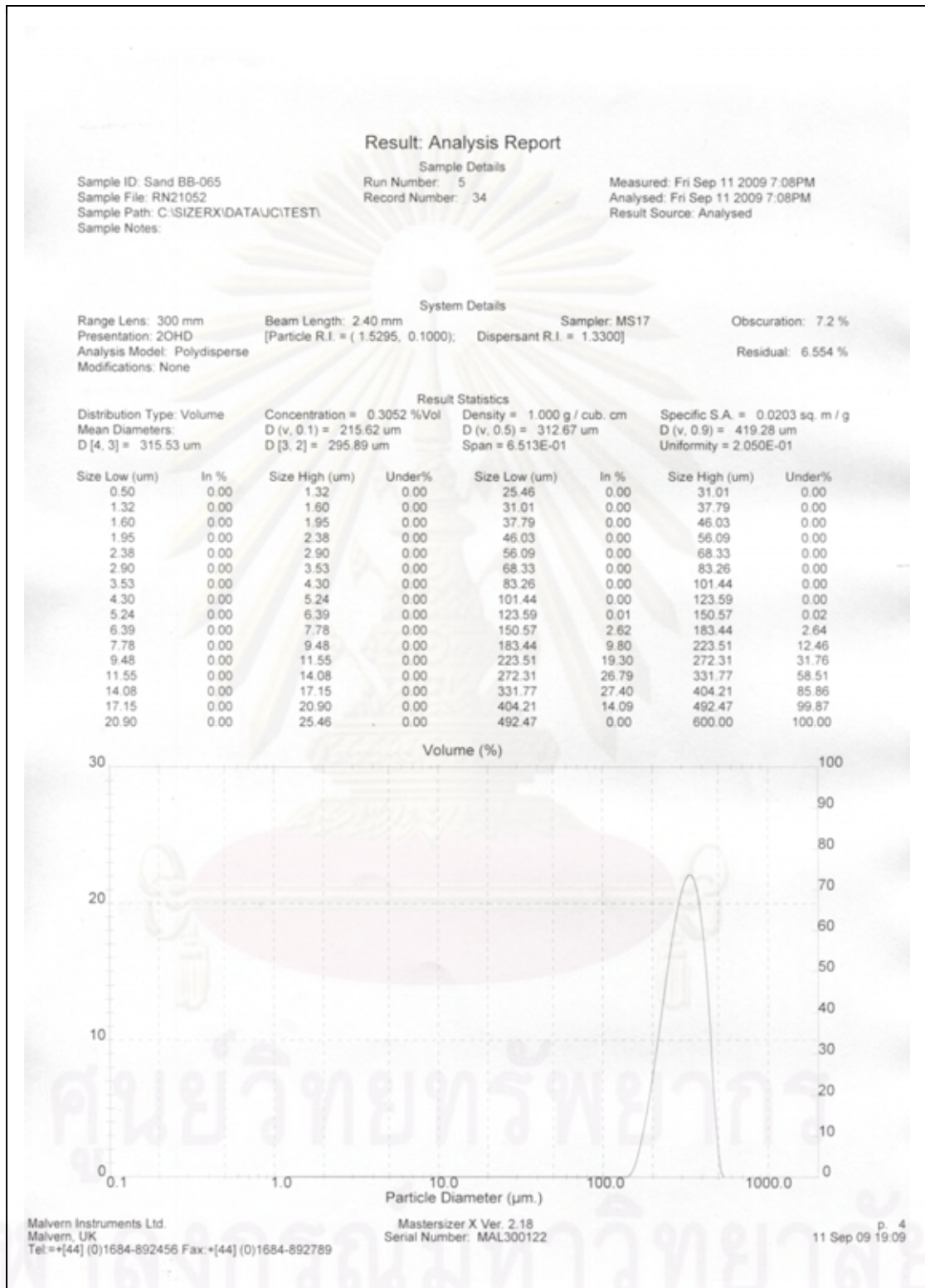


Figure B-30. Result of grain size analysis no.BB-065.

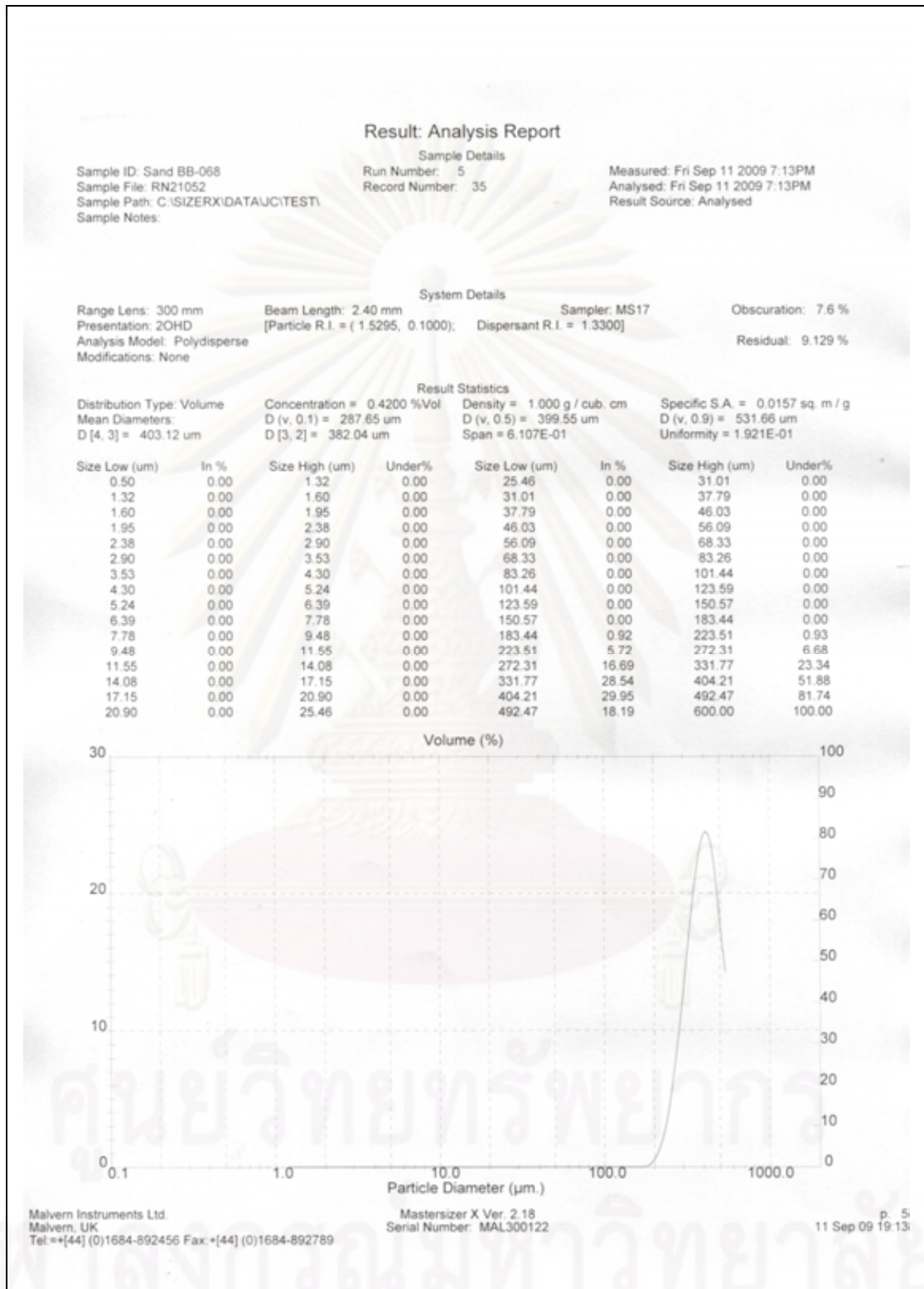


Figure B-31. Result of grain size analysis no.BB-068.

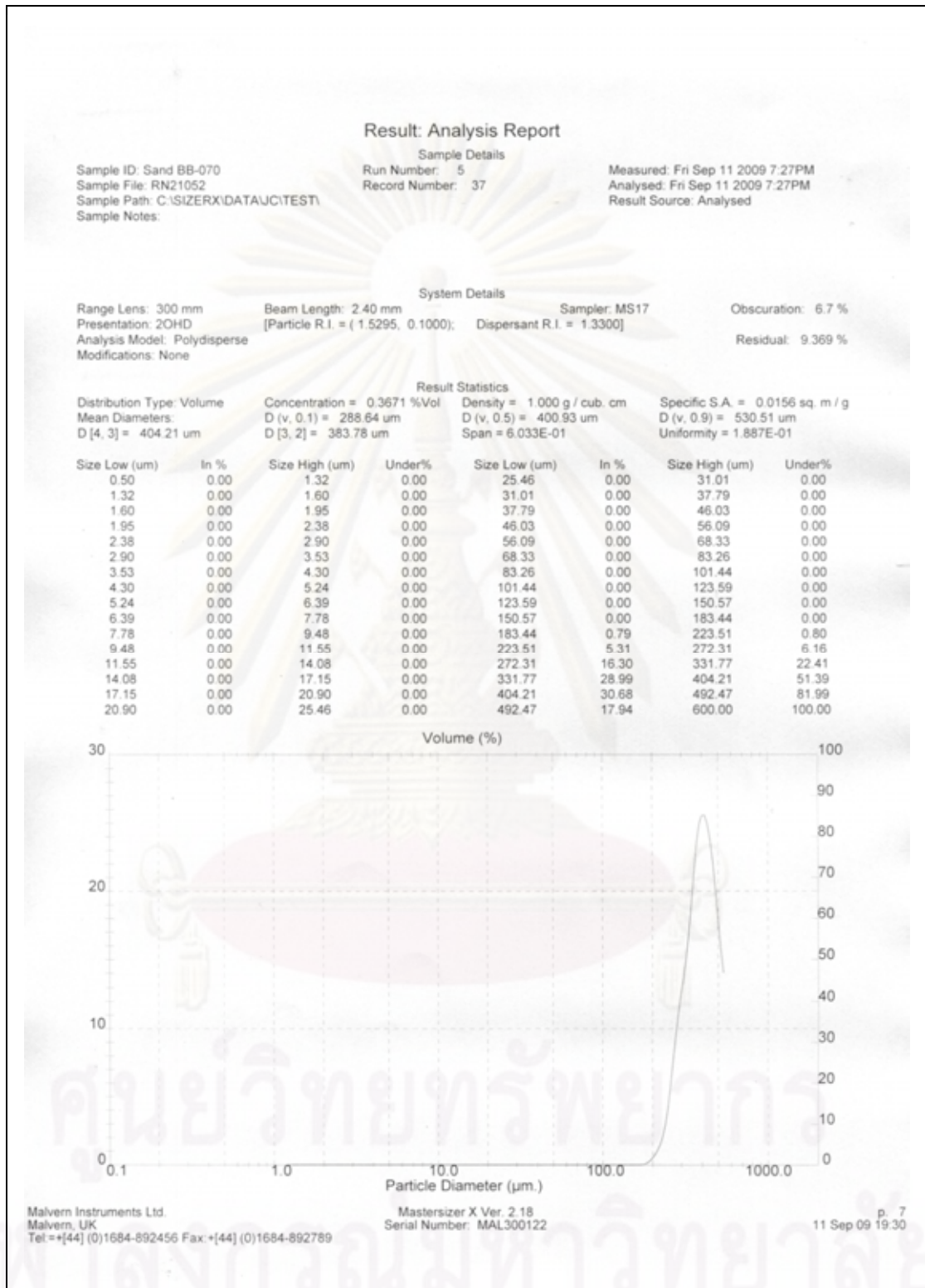


Figure B-32. Result of grain size analysis no.BB-069.

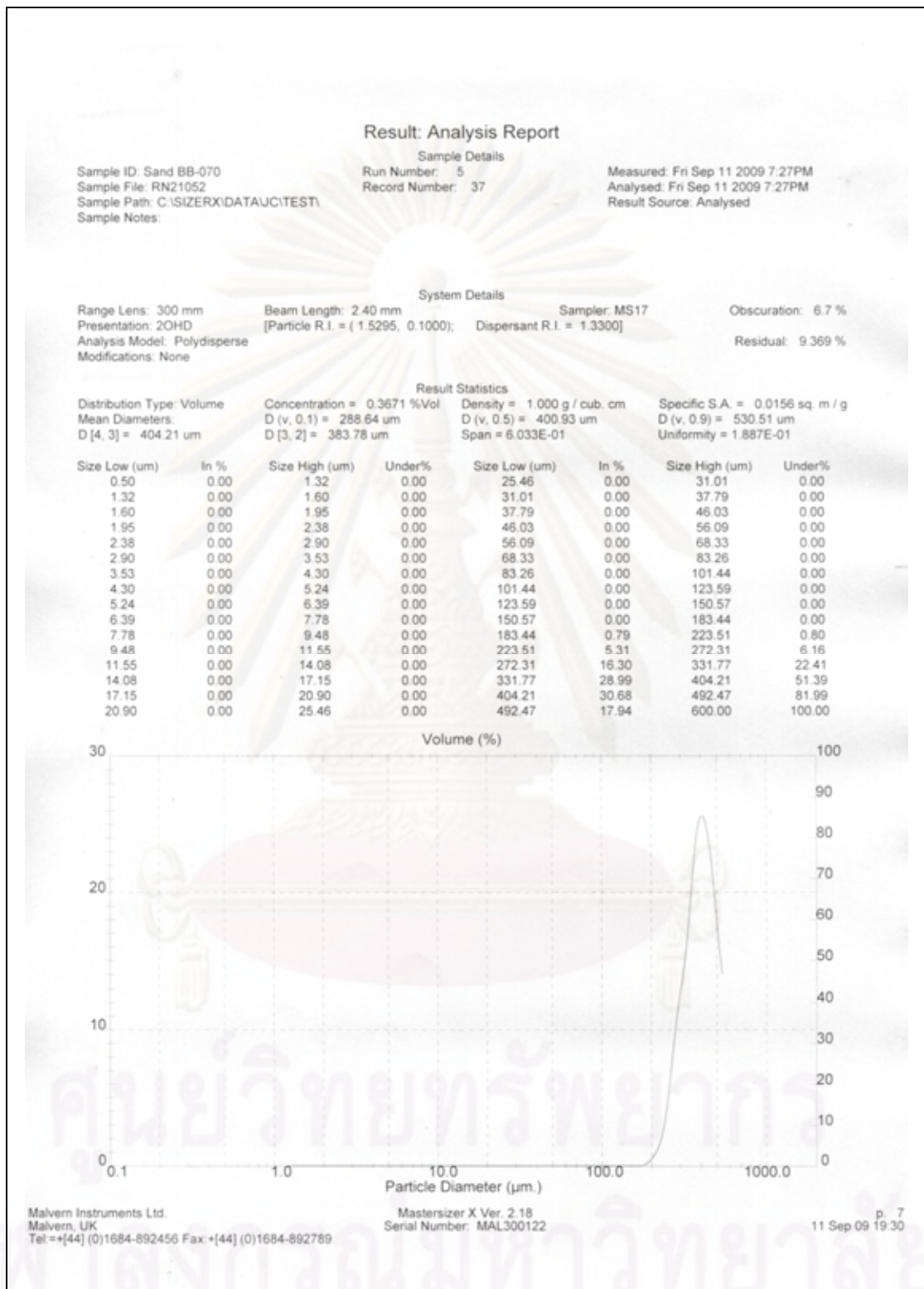


Figure B-33. Result of grain size analysis no.BB-069.

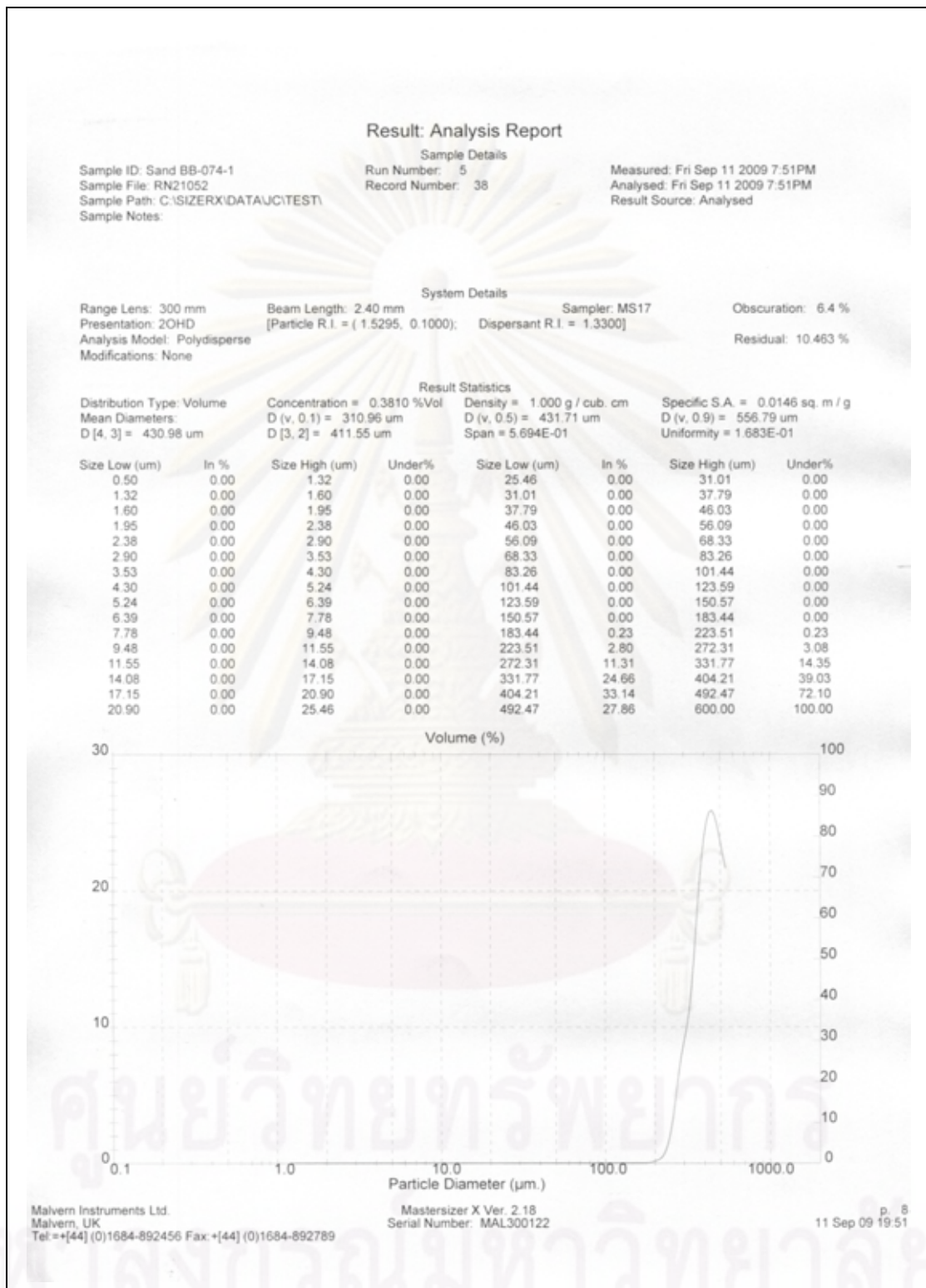


Figure B-34. Result of grain size analysis no.BB-074-1.

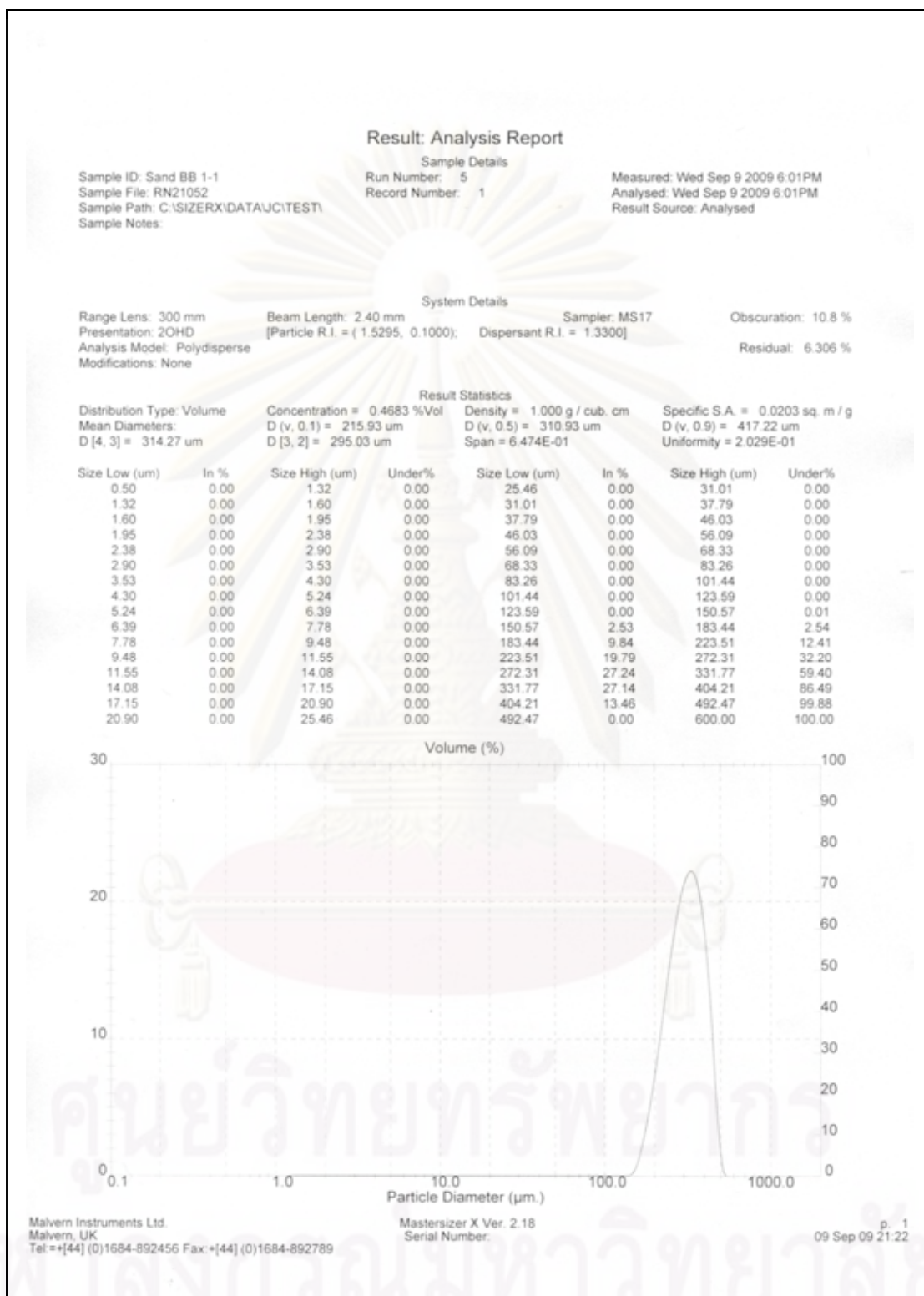


Figure B-35. Result of grain size analysis no.BB-074-1.

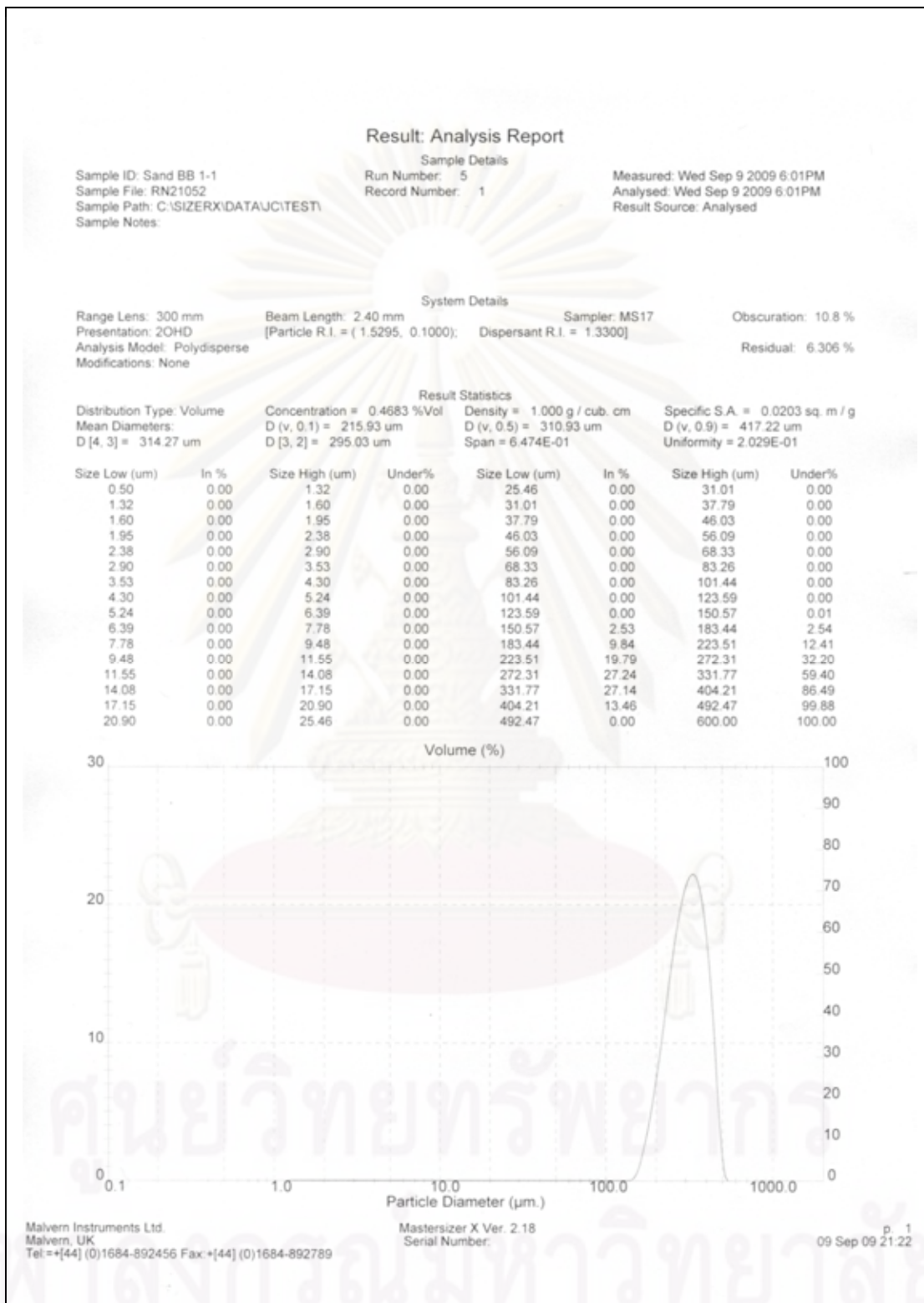


Figure B-36. Result of grain size analysis no.BB 1-1.

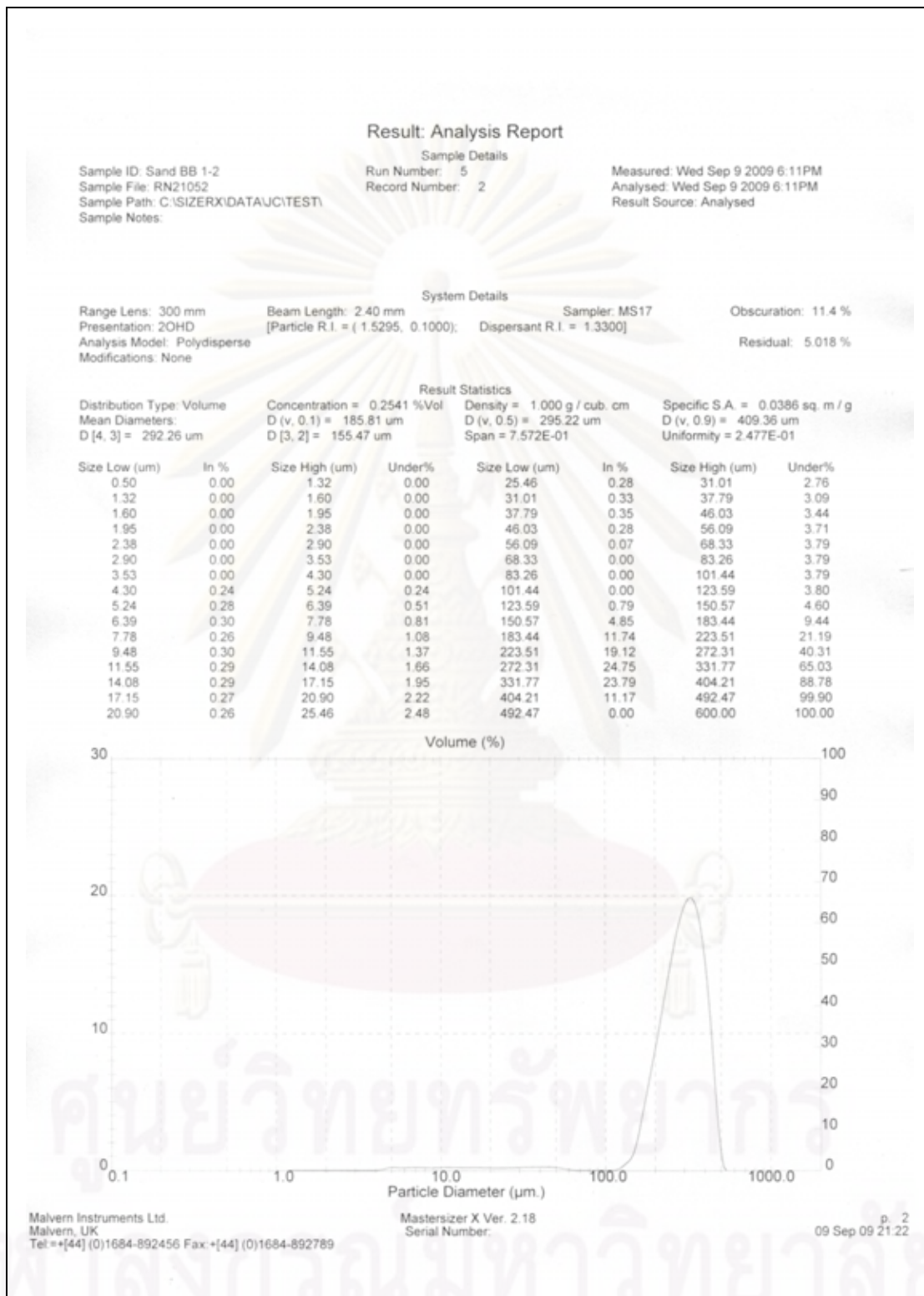


Figure B-37. Result of grain size analysis no.BB 1-2.

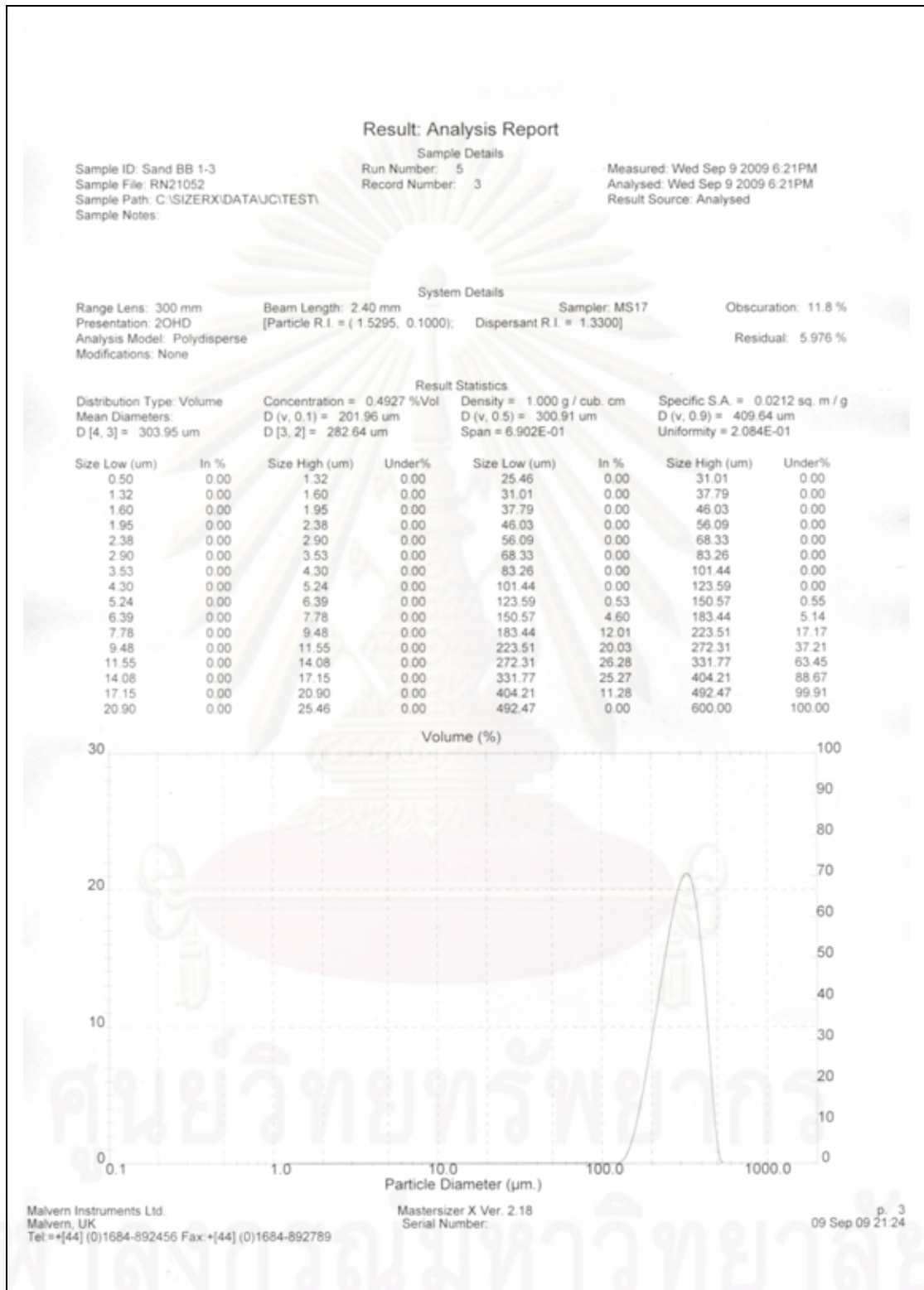


Figure B-38. Result of grain size analysis no.BB 1-3.

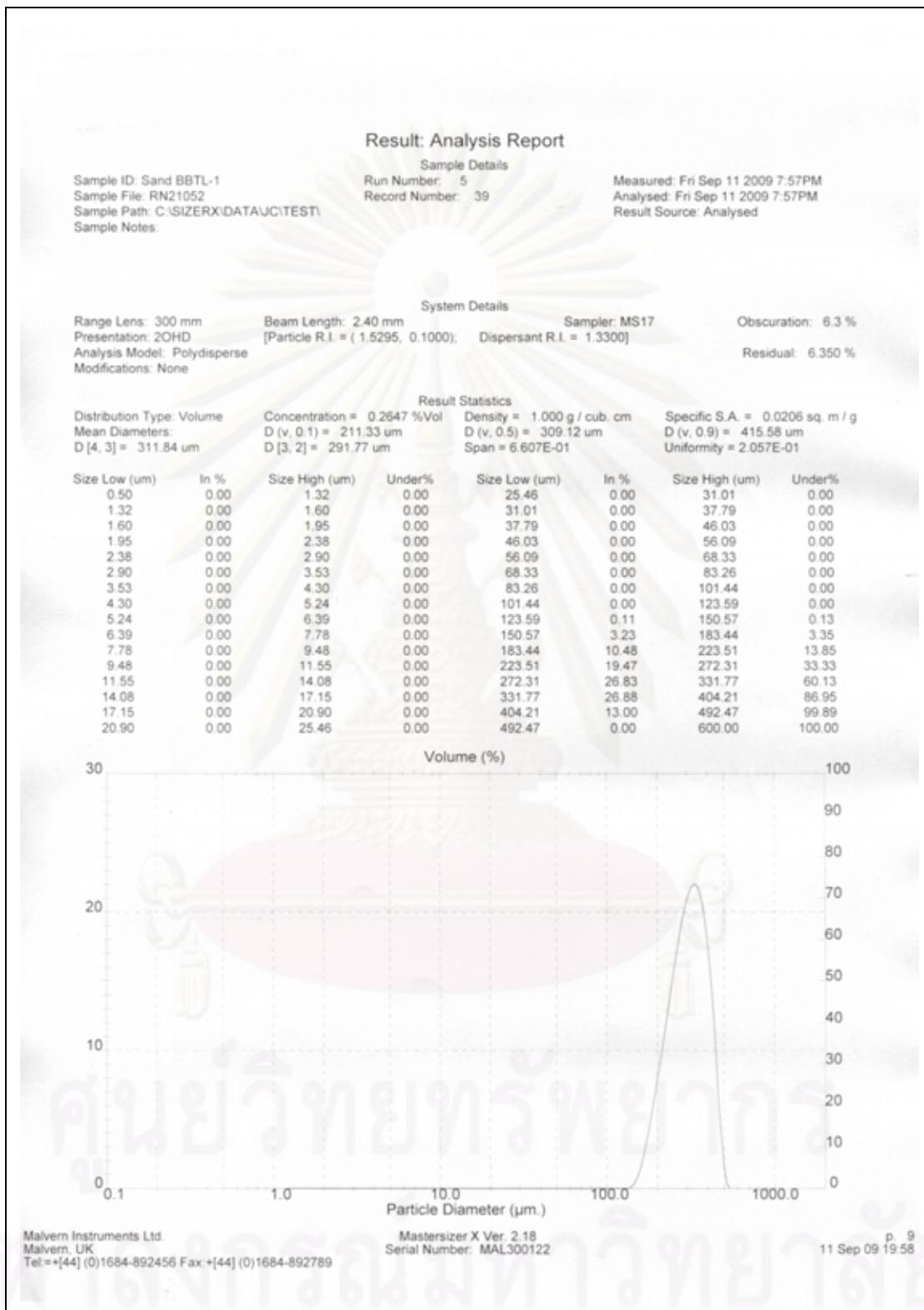


Figure B-39. Result of grain size analysis no.BBTL-1.

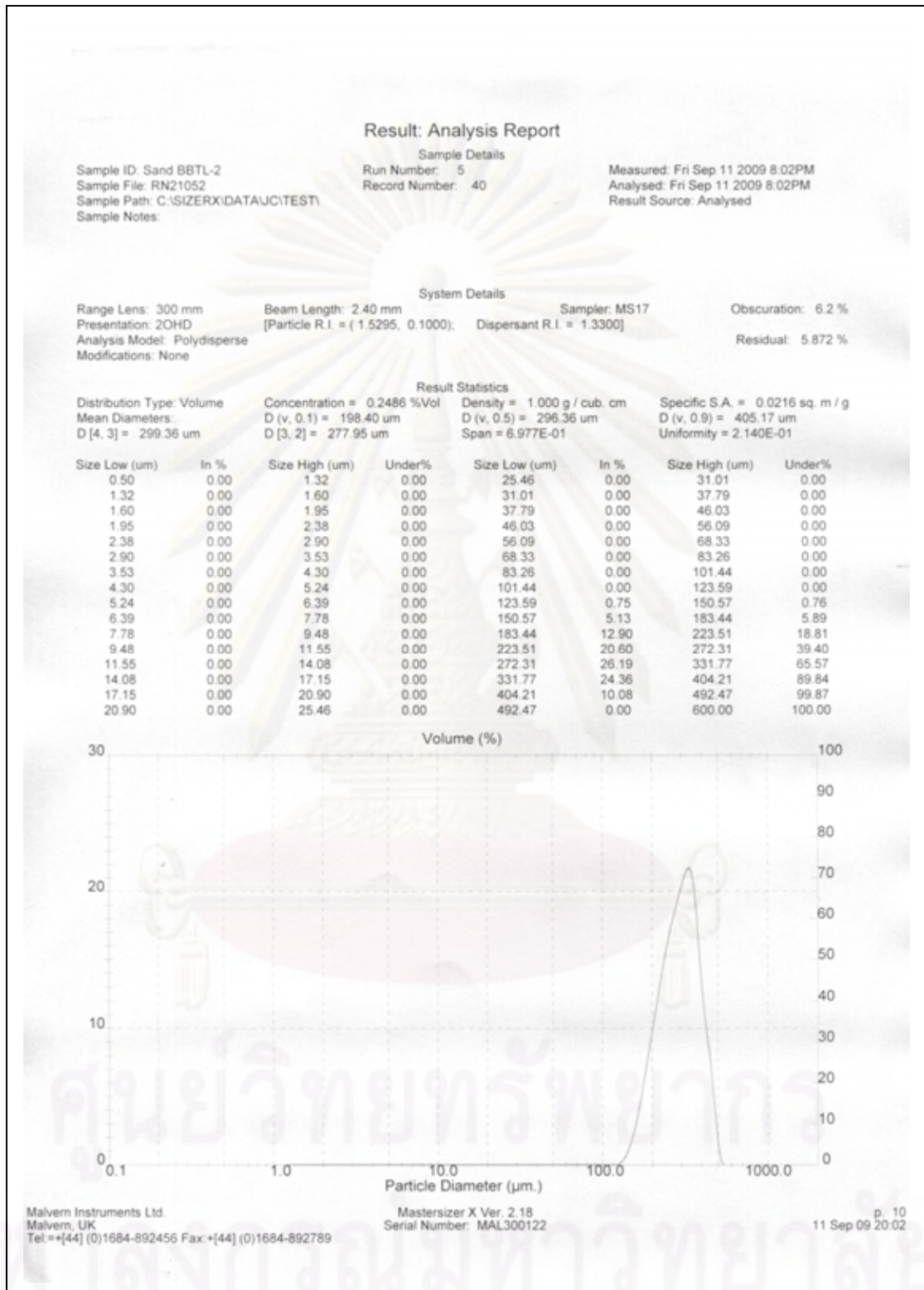


Figure B-40. Result of grain size analysis no.BBTL-2.

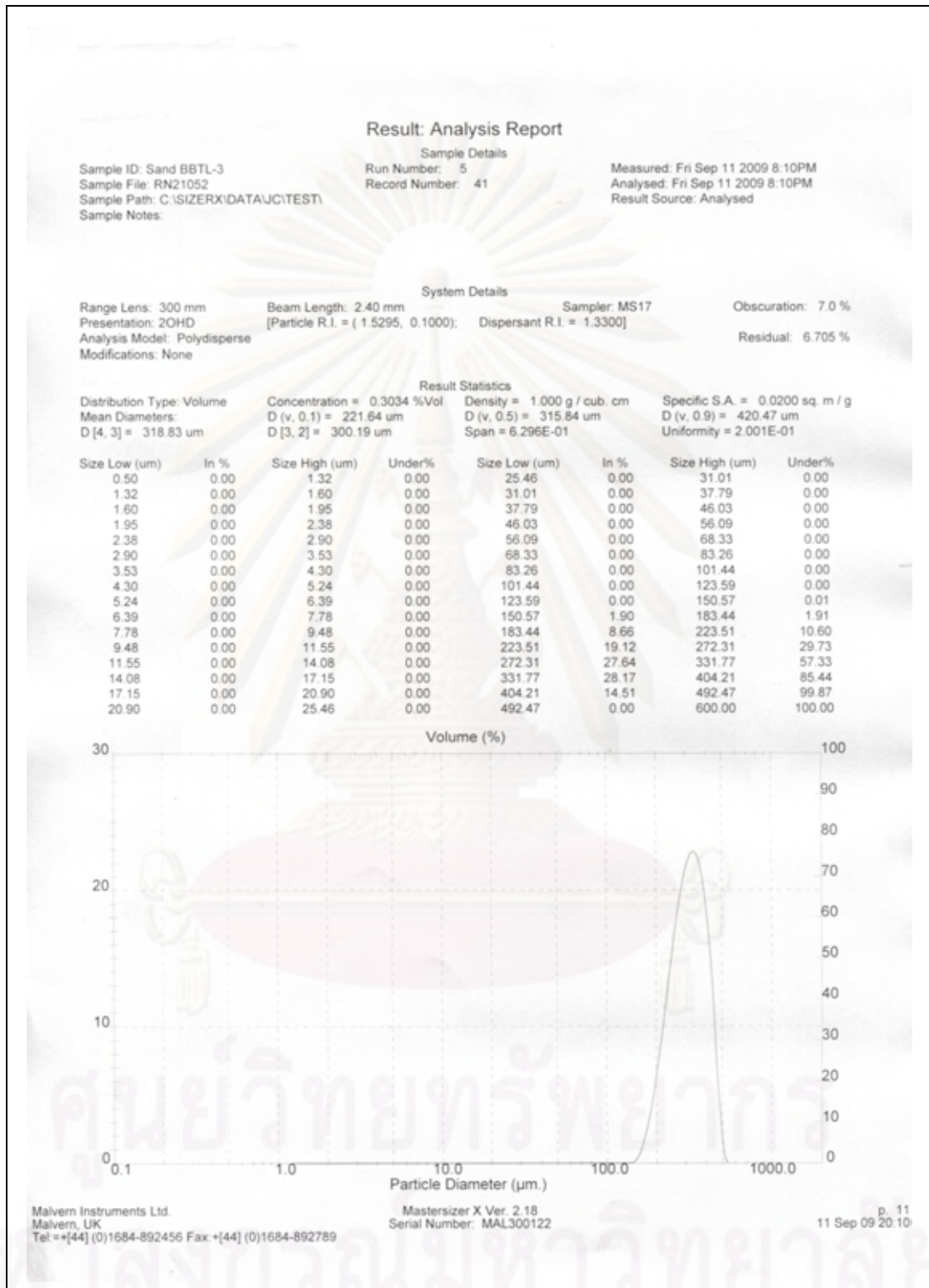


Figure B-41. Result of grain size analysis no.BBTL-3.

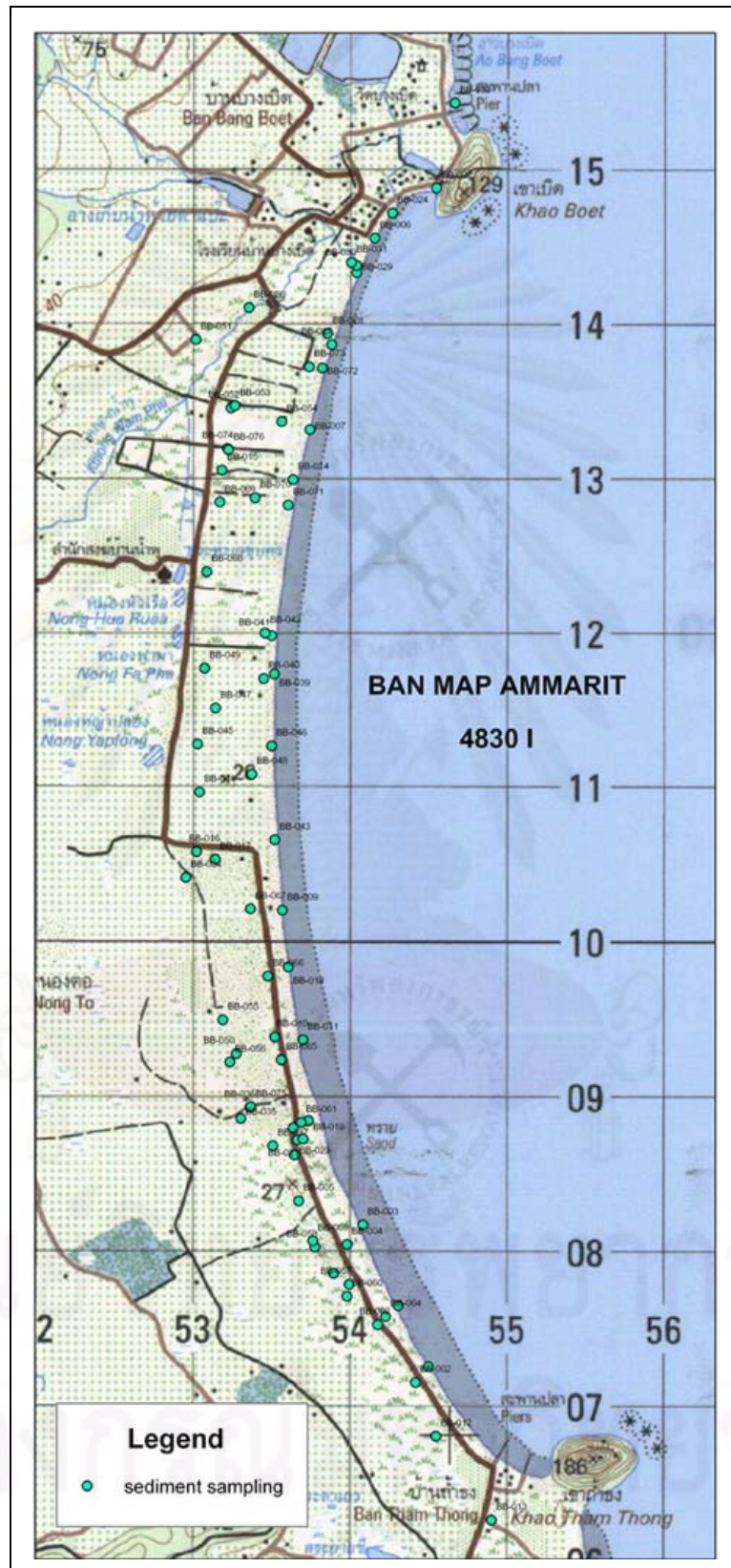


Figure B-42. Location to collected the sample for analysis by distribution of grain size.

APPENDIX C

PETROLOGY

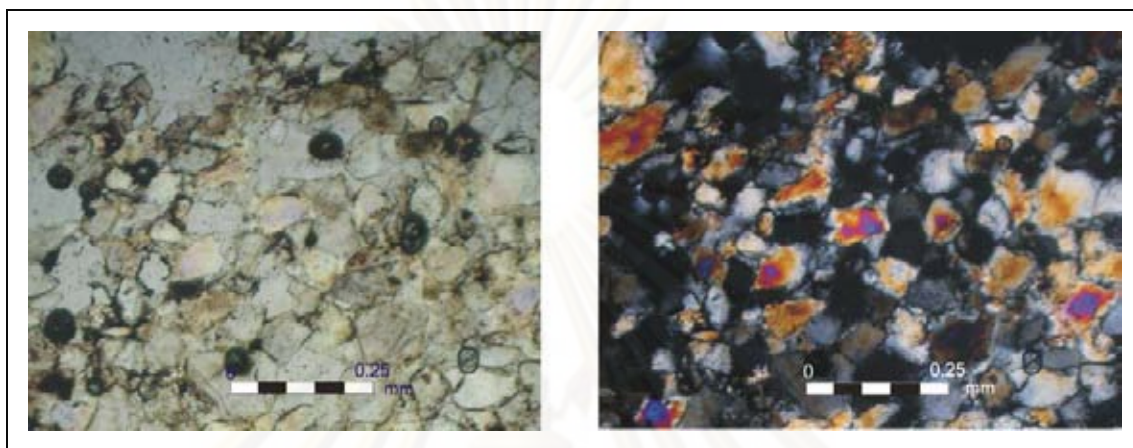


Figure C-1. Petrology characteristic of sample no.BB-01 (sandstone (JK₁) at 0553000 E 1205896 N, Ban Sang Som)) is fine-grained (0.125-0.250 mm), mainly composed of quartz (40-50%), feldspar and rock fragments of chert; rarely of mica and opaque mineral, the cementing is iron oxide, subangular-subrounded, moderate sorting.

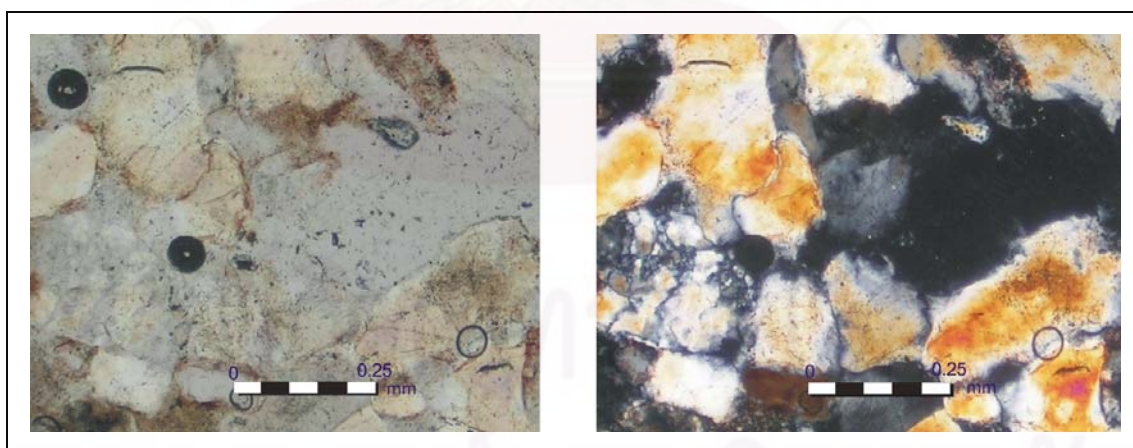


Figure C-2. Petrology characteristic of sample no.BB-01 (sandstone (TR_m) at 0550576 E 1215708 N) is fine-medium grained (0.125-0.500 mm), mainly composed of quartz (40-50%), feldspar and rock fragments of chert and quartzite; rarely of mica and opaque mineral, the cementing is iron oxide, subangular-subrounded, poor sorting.

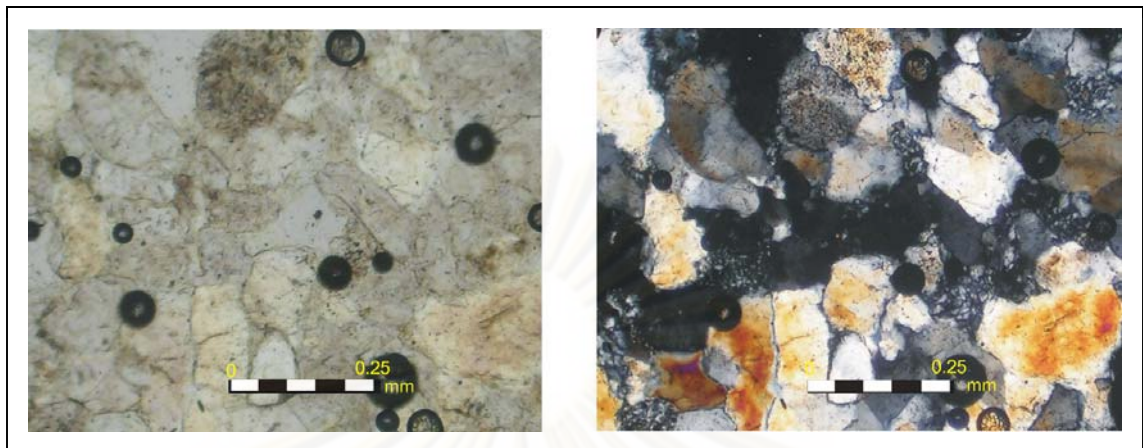


Figure C-3. Petrology characteristic of sample no. BB-03 (sandstone (CP_K)) at 0549946 E 1222098 N, Khao Kharm) is fine-medium grained (0.10-0.35 mm), mainly composed of quartz (40-50%), feldspar and rock fragments of chert, quartzite and quartzite; rarely of mica, opaque mineral and tourmaline, the cementing is silica, subangular-subrounded, fair sorting.

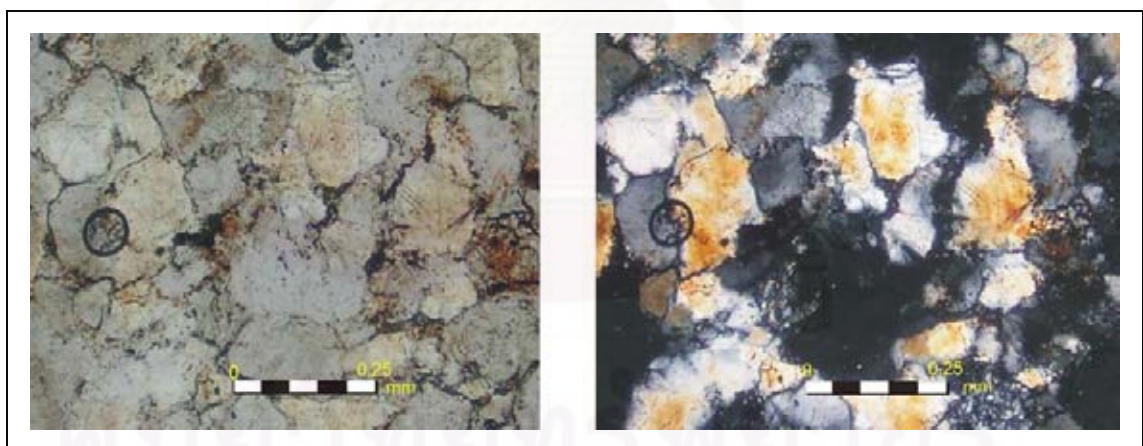


Figure C-4. Petrology characteristic of sample no. BB-04 (sandstone (JK_J)) at 0538928 E 1214922 N, Khao Phoe) is medium-grained (0.125-0.300 mm), mainly composed of quartz (40-50%), feldspar and rock fragments of chert and quartzite; rarely of muscovite and opaque mineral and tourmaline, the cementing is iron oxide, subrounded clasts, moderate-good sorting.

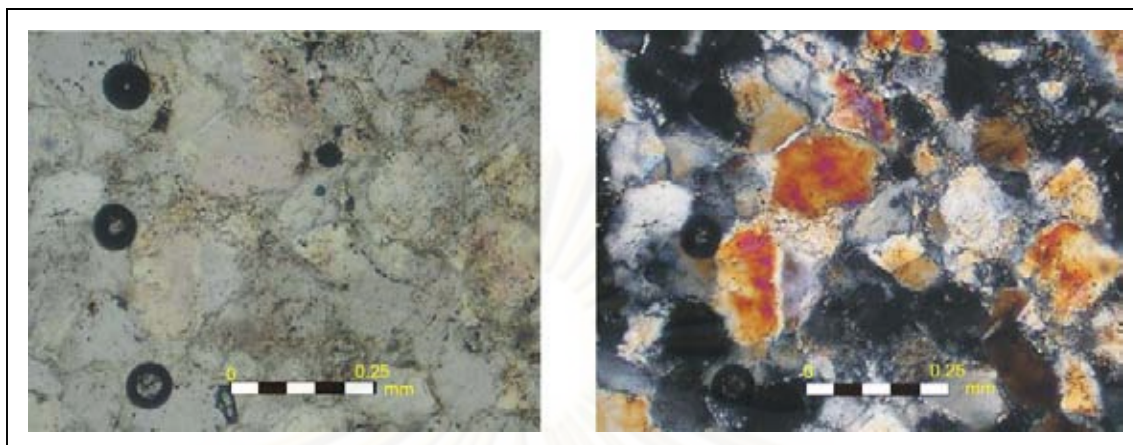


Figure C-5. Petrology characteristic of sample no.BB-05 (Sandstone (CP_{kp}) at 0537040 E 1217832 N) is fine- grained (0.10 mm), mainly composed of quartz (40-50%), feldspar and rock fragments of chert and quartzite ; rarely of muscovite and opaque mineral, the cementing is silica, quartz veins, subrounded clasts, good sorting.

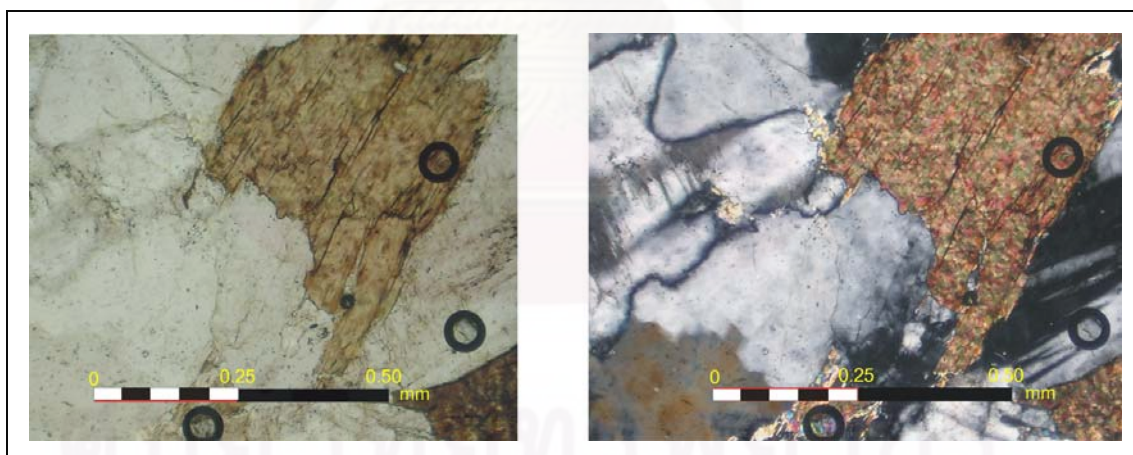


Figure C-6. Petrology characteristic of sample no.BB-06 (Granite (K_{gr}) at 0535154 E 1222290 N) is coarse grained (0.01-0.06 mm), mainly composed of quartz, K-feldspar (perthite and microcline) and plagioclase, granophyric texture.

APPENDIX D

RARE EARTH ANALYSIS (REE)

Sample no.	Location		RE ₂ O ₃ (%)	ThO ₂ (%)
	East	North		
BB-1-1	0554025	1207820	nil	< 0.05
BB-1-2	0554025	1207820	nil	< 0.05
BB-1-3	0554025	1207820	nil	< 0.05
BB-001	0554497	1207275	nil	< 0.05
BB-025	0554373	1218043	nil	< 0.05
BB-026	0553344	1214114	nil	< 0.05
BB-031	0553996	1214407	nil	< 0.05
BB-032	0554538	1214888	nil	< 0.05
BB-034	0552946	1210433	nil	< 0.05
BB-043	0553512	1210676	nil	< 0.05
BB-072	0553811	1213725	nil	< 0.05

Analysis by Mineral analysis and identification Division, 2009.

ศูนย์วิทยทรัพยากร
จุฬาลงกรณ์มหาวิทยาลัย

APPENDIX E

FREQUENCY DISTRIBUTION PLOT OF THE WIND DIRECTION
BETWEEN 1981-2009

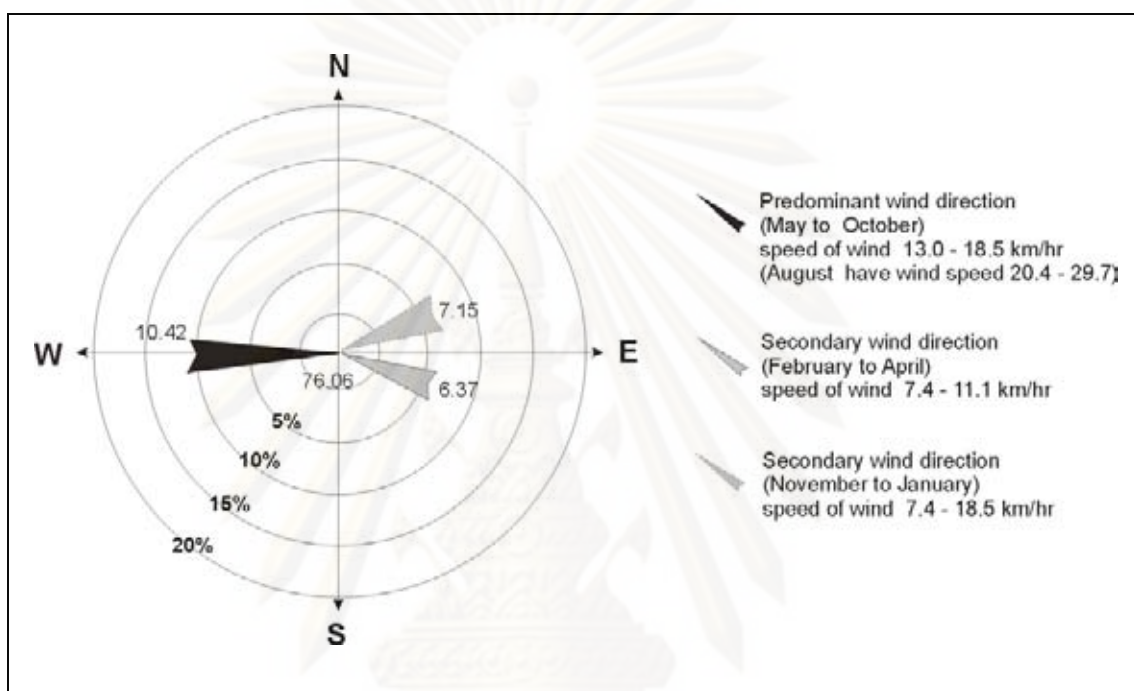


Figure E-1. Frequency distribution plot of the wind direction between 1981-2009. (Data from Meteorological Station at Changwat Chumphon, 2009)

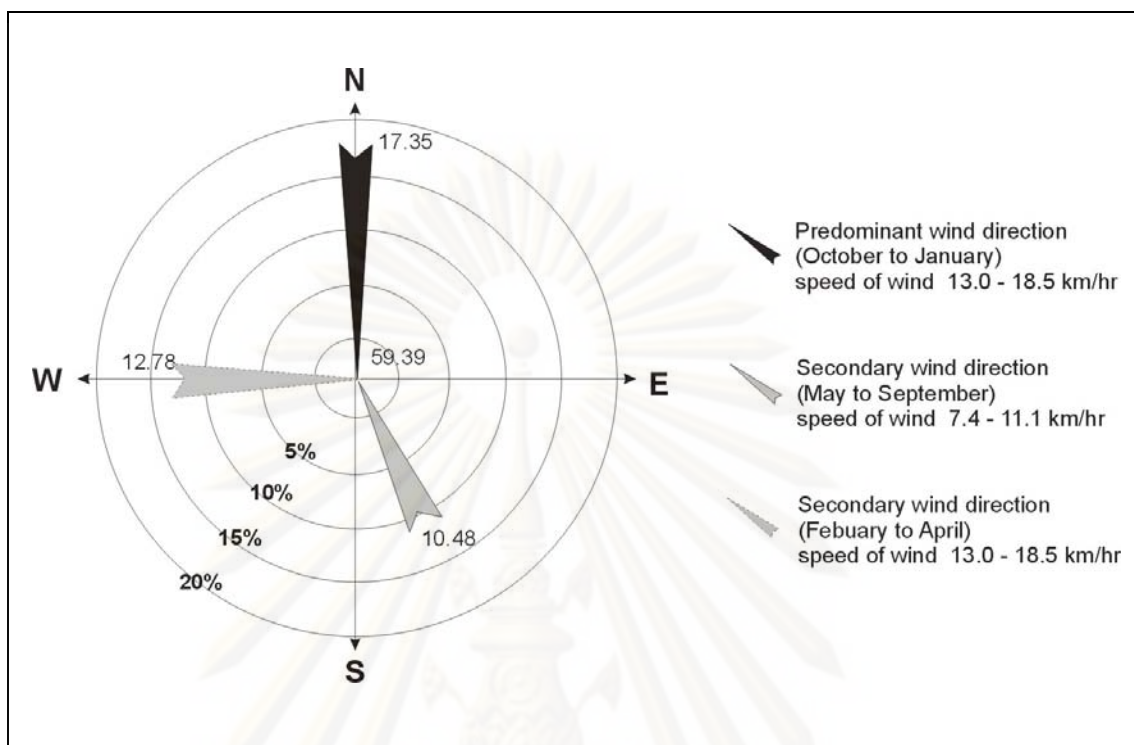


Figure E-2. Frequency distribution plot of the wind direction between 1981-2009. (Data from Meteorological Station at Changwat Prachuap Khiri Khan, 2009)

ศูนย์วิทยทรัพยากร
จุฬาลงกรณ์มหาวิทยาลัย

BIOGRAPHY

Miss Weeraya Lertnok was born in October 2, 1979, at Amphoe Muang, Changwat Nakhon Ratchasima. In 2001, she graduated in Geotechnology program from the Faculty of Technology, Khon Kaen University. After graduation, she became geologist at the Geological Survey Division, Department of Mineral Resources (DMR). In 2006, she transferred to the Geological Resources Conservation and Management Division, DMR. She has experienced in geological survey, geological mapping, geological resources management and geotechnical survey.



ศูนย์วิทยทรัพยากร
จุฬาลงกรณ์มหาวิทยาลัย